Superconductivity in iron compounds

G. R. Stewart

Department of Physics, University of Florida, Gainesville, Florida 32611-8440, USA

(published 13 December 2011)

Kamihara and coworkers' report of superconductivity at $T_c = 26$ K in fluorine-doped LaFeAsO inspired a worldwide effort to understand the nature of the superconductivity in this new class of compounds. These iron pnictide and chalcogenide (FePn/Ch) superconductors have Fe electrons at the Fermi surface, plus an unusual Fermiology that can change rapidly with doping, which lead to normal and superconducting state properties very different from those in standard electron-phonon coupled "conventional" superconductors. Clearly, superconductivity and magnetism or magnetic fluctuations are intimately related in the FePn/Ch, and even coexist in some. Open questions, including the superconducting nodal structure in a number of compounds, abound and are often dependent on improved sample quality for their solution. With T_c values up to 56 K, the six distinct Fe-containing superconducting structures exhibit complex but often comparable behaviors. The search for correlations and explanations in this fascinating field of research would benefit from an organization of the large, seemingly disparate data set. This review provides an overview, using numerous references, with a focus on the materials and their superconductivity.

CONTENTS

I. INTRODUCTION

The report of superconductivity at 26 K in LaFeAsO doped with F on the oxygen site in 2008 (Kamihara *et al.*, 2008) was not the first discovery of an iron-containing superconductor, nor even the first reported superconducting iron pnictide (LaFePO, $T_c \approx 5$ K, Kamihara *et al.*, 2006). Although iron has been considered deleterious to superconductivity due to its strong local magnetic moment, a number of superconducting

compounds containing iron in which the iron is nonmagnetic have long been known. Th_7Fe_3 ($T_c = 1.8$ K, Matthias, Compton, and Corenzwit, 1961), U_6Fe ($T_c = 3.9$ K Chandrasekhar and Hulm, 1958), $Lu_2Fe_3Si_5$ ($T_c = 6.1$ K, Braun, 1980), and β''-(bedt-ttf)$_4$[$(H_2O)Fe(C_2O_4)_3$] − PhCN ($T_c = 8.5$ K, Graham, Kurmoo, and Day, 1995) are all examples of Fe-containing superconductors. In fact, Fe itself under pressure is a superconductor, with $T_c \sim 1.8$ K at 20 GPa (Shimizu *et al.*, 2001, 2006).

However, the discovery of Kamihara *et al.* is ground breaking for a number of reasons. One is that just like the discovery of superconductivity at 35 K in Ba doped La_2CuO_4 (Bednorz and Müller, 1986) it led to the almost immediate further discovery of even higher T_c materials, with the current record ~ 56 K observed in $Gd_{0.8}Th_{0.2}FeAsO$ (C. Wang *et al.*, 2008), $Sr_{0.5}Sm_{0.5}FeAsF$ (G. Wu *et al.*, 2009) and $Ca_{0.4}Nd_{0.6}FeAsF$ (Cheng *et al.*, 2009). The path to this higher transition temperature was also similar to that in the high T_c cuprates, where pressure experiments (Chu *et al.*, 1987) first increased the T_c in Ba doped La_2CuO_4 from 35 to 53 K. This was followed by "chemical pressure" experiments where T_c was raised to 93 K (Wu *et al.*, 1987) by replacing La with the smaller Y to make a multiphase sample containing $YBa_2Cu_3O_{7-\delta}$. In the case of F doped LaFeAsO, Takahashi *et al.* (2008a) found that 4 GPa pressure increased the T_c from 26 to 43 K. This result then inspired researchers to use chemical pressure (replacing the La with the smaller rare-earth ions Gd, Sm, Nd, Pr, Ce), first reaching $T_c = 43$ K in $SmFeAsO_{0.85}F_{0.15}$ (X. H. Chen *et al.*, 2008) and then less than a month later $T_c = 55$ K in the oxygen deficient $SmFeAsO_{0.85}$ prepared by high pressure synthesis (Ren *et al.*, 2008a).

A second reason why the work of Kamihara *et al.* is so seminal is that it has led to a new *class* of high temperature superconductors, the so-called iron pnictides ("FePn," where Pn is As or P), which have already been extended to include iron chalcogenides ("FeCh," where Ch includes S, Se, and Te). The list of these compounds has expanded rapidly from the original LaFeAsO "1111" structure (of which there are over 150 rare earth/transition metal/pnictide/O examples, see Pöttgen and Johrendt, 2008 for a review) first explored by Kamihara *et al.* and successors for superconductivity. The next iron-containing superconductor structure includes members of the MFe_2As_2 ("122") family [of which there are over 450 distinct compounds, (Villars and Calvert, 1985)], where Rotter, Tegel, and Johrendt (2008) discovered $T_c = 38$ K in K doped $BaFe_2As_2$, $Ba_{0.6}K_{0.4}Fe_2As_2$. The MFeAs ("111") family (X. C. Wang *et al.*, 2008, $T_c = 18$ K), the iron chalcogenide FeSe ("11") family (Hsu *et al.*, 2008, $T_c = 8$ K), the Sr_2MO_3FePn, $M =$ Sc, V, Cr ("21311") family ($M =$ Sc and Pn = P, Ogino *et al.*, 2009, $T_c = 17$ K; $M =$ V and Pn = As, Zhu *et al.*, 2009b, $T_c = 37$ K) and the defect structure $A_{0.8}Fe_{1.6}Se_2$ ($T_c \approx 32$ K, $A =$ K, Rb, Cs, Tl) related to the 122 structure and called "122*" herein round out the established list. The last four families all exhibit superconductivity *without* doping an additional atom type and as yet have only a few members known, although this is changing. For example, Ogino *et al.* (2010c) reported an alteration of the 21311 structure and found $Ca_2(Mg_{0.25}Ti_{0.75})_{1.5}O_{\sim 4}FeAs$ to have $T_c^{onset} = 47$ K. As we will discuss, it is not just the

1111 structure whose initial T_c has been greatly enhanced by further work. For example, T_c of FeSe under 7 GPa pressure increases more than fourfold to 37 K (Margadonna *et al.*, 2009b) as discussed in Sec. II.D and Te doping [$Fe(Se_{1-x}Te_x)$] increases almost twofold to ~ 15 K (Yeh *et al.*, 2008), Sec. II.B.3.

A third, and perhaps the most interesting, aspect of these new iron-containing superconductors (the subject of over 2000 publications in just 3 years) from a basic physics point of view is that the superconducting pairing mechanism may be related to the coexistent magnetism in the phase diagram. Current thinking is that the pairing is not primarily phonon mediated, although due to the coupling of the magnitude of the Fe moments to the FePn/Ch bond length and the presence of an isotope effect (discussed in Sec IV.A), the magnetoelastic coupling is thought to be important for superconductivity; see, e.g., Cano *et al.* (2010) for a discussion of the magnetoelastic coupling. Theoretical alternatives to phonon coupling include various *electronic* excitations that could mediate the superconducting pairing, e.g., spin fluctuations (as is suggested by inelastic neutron scattering data) or interorbital pair hopping. If this is indeed the case, such a pairing mechanism may promise even higher temperature superconductivity since the transition temperature T_c would be proportional to a characteristic energy scale potentially significantly larger than the BCS scale dependence on the average phonon frequency, $T_c^{BCS} \propto \langle \omega \rangle$.

Fourth, as will be clear in this review, the properties of the FePn/Ch superconductors are fundamentally different both from those of a conventional electron-phonon coupled superconductor and from those of the cuprates.

In a clean conventional superconductor, the electronic excitations are (exponentially) suppressed in the superconducting state by the gap, while in unconventional superconductors such as the FePn/Ch there are many examples of compounds with nodal (gap zero) points or lines leading to finite electronic excitations remaining as $T \to 0$. Although the pairing symmetry in the superconducting state is still under debate, it is apparently not a conventional s wave in many of the FePn/Ch since neutron scattering measurements provide convincing (see, however, Onari, Kontani, and Sato, 2010) evidence for a sign change in the superconducting energy gap Δ on different parts of the Fermi surface in a number of compounds. In certain samples, neutron scattering data imply a direct coupling between the superconductivity and the magnetism, as seen in, for example, the unconventional heavy fermion superconductor UPt_3. As a more mundane comparison with conventional, e.g., elemental or A-15 superconductors, the discontinuity in the specific heat at T_c (ΔC) scales differently in the FePn/Ch superconductors: $\Delta C \propto T_c^3$ vs T_c^2 for conventional superconductors.

In comparing to the cuprates, it seems clear that although the FePn/Ch are unconventional superconductors, they are different in many respects from the cuprates. The cuprates have strong electron correlations, while the FePn/Ch show in general relatively weak correlations. For example, experiments by W.-L. Yang *et al.* (2009) found in representative 1111 and 122 FePn/Ch that the on-site Coulomb repulsion $U \leq 2$ eV versus a bandwidth for the Fe conduction band states of ~ 4 eV while theoretical discussion by Cvetkovic

and Tesanovic (2009) argued for the absence of strong local correlations in the FePn/Ch. Using thermoelectric power (TEP) measurements, Wang, Lei, and Petrovic (2011a) argued for relatively weak electronic correlations in 122* $K_xFe_{2-y}Se_2$, while Pourret *et al.*'s (2011) TEP data are interpreted as showing that 11 $FeTe_{0.6}Se_{0.4}$ [unique among the FePn/Ch and in agreement with DMFT calculations (Hirschfeld, Korshunov, and Mazin, 2011)] has electronic correlations comparable in strength to the cuprates. The cuprates are much more anisotropic and have *d* wave gap symmetry versus primarily *s* wave symmetry for FePn/Ch. The cuprates have a much different Fermiology that remains relatively constant (at least for hole doping) with doping versus the Fermiology in the FePn/Ch (whose Fermiology is believed key for the superconducting pairing; see Sec. IV). The cuprates have, barring some spin glass behavior [perhaps disorder induced (Andersen *et al.*, 2007)], no coexistent long range magnetic order and superconductivity as do at least the 122, 11 $FeSe_{1-x}Te_x$, the 122* and perhaps (Sefat *et al.*, 2010) the 21311. The cuprates exhibit a rapid decrease in T_c upon doping in the CuO planes versus the relative insensitivity of the FePn/Ch layer superconductivity to doping. Thus, doping and its effect on T_c, T_S, and T_{SDW} is an important tool for understanding the pairing mechanism in FePn/Ch. A comparison between the cuprates and FePn/Ch that is highlighted by the recent discovery of superconductivity in the defect-driven 122* structure $A_{0.8}Fe_{1.6}Se_2$ compounds is that, with the exception of the 122*s, FePn/Ch do not appear to have an insulating phase anywhere nearby in the phase diagram to the superconducting compositions, while the cuprates do. Last, it is well to remember that the FePn/Ch superconductors mechanically are metals, without the brittleness of the ceramic cuprates, making applications more tractable. The cuprates are in daily application (e.g., the SuperLink filters on cell phone towers) and researchers are actively investigating application (see Sec. V.B) of the FePn/Ch materials. For reviews of the high T_c cuprates, see Kastner *et al.* (1998), Basov and Timusk (2005), Lee, Nagaosa, and Wen (2006), Barzykin and Pines (2009), and Armitage, Fournier, and Greene (2010); for an early comparison of the cuprates with the FePn/Ch, see Sawatzky *et al.* (2009) and Mazin and Johannes (2009).

An important guiding organizational principle throughout this review is that despite a great diversity of behavior, the new iron superconductors have a number of properties in common. These common properties presumably hold the clue to understanding the relatively high temperature of the superconductivity. It is naturally hoped that achieving this understanding will help lead to discovery of even higher T_cs. A representative list of these common properties (together with the exceptions) would include:

- All six families of iron-containing superconductors have two-dimensional planes of FePn/Ch tetrahedra, and the angle of the bonds in the tetrahedra as well as the height of the Pn/Ch above the Fe are indicators of T_c.
- The Fe 3*d* electrons are (in contrast to the earlier superconductors containing Fe) at the Fermi energy, and clearly taking part in the superconductivity.
- In most FePn/Ch, the Fe 3*d* electrons are magnetic in some part of the phase diagram either close to or even

coexistent with superconductivity. Although there are examples of FePn/Ch superconductors without magnetism in their phase diagrams, e.g., LiFeAs, FeSe, and based on the limited data to date the 21311s (see the calculation of the susceptibility of Sr_2VO_3FeAs by Mazin, 2010 and data from Sefat *et al.*, 2010), it is arguably the case that the superconducting properties of this new class of superconductor are fundamentally influenced by the Fe and its magnetic fluctuations.

- Both hole and electron doping of the nonsuperconducting 1111 and 122 parent compounds cause superconductivity, with electron doping causing in general the higher T_cs in the 1111s while hole doping causes higher T_cs in the 122s.
- For the undoped 1111 and the 122 compounds, there are both a spin density wave (SDW) transition and a structural phase transition T_S (tetragonal to orthorhombic upon cooling). There is neither an SDW nor a structural transition in the Li 111 material but both occur in the Na 111, while superconducting FeSe displays a structural transition (tetragonal-orthorhombic) at 90 K (McQueen *et al.*, 2009b) but no magnetic transition. $Fe_{1+y}Se_xTe_{1-x}$, which is superconducting for $x \gtrsim 0.05$, has both a structural, tetragonal to monoclinic, and a coincident magnetic transition (at 72 K for $x = 0$) (Fruchart *et al.*, 1975, Martinelli *et al.*, 2010.) The spin density wave (antiferromagnetic) transition in the 1111 and 122 has a two sublattice structure with parallel "stripes" of parallel moments running along the orthorhombic *b* axis, versus a double stripe arrangement in FeTe. These parallel moments are aligned perpendicularly to the stripes with each successive stripe's moments opposite to those in the previous one, giving an antiferromagnetic moment in the *a* axis direction perpendicular to the stripes (Kitagawa *et al.*, 2008). In 122* there is a defect ordering temperature which changes the structure from one tetragonal symmetry to another a few tens of Kelvin above the antiferromagnetic transition which, unlike the other FePn/Ch structures, has the moment along the *c* axis.
- The two transitions are at different temperatures in the undoped 1111s [e.g., $T_S = 155$ K vs $T_{SDW} = 140$ K in CeFeAsO (Zhao *et al.*, 2008b) although this difference is shrinking with better sample quality (Jesche *et al.*, 2010)], but coincide in temperature in the undoped 122s (see Sec. II and Table I). T_S/T_{SDW} values for MFe_2As_2 are similar to those in 1111 and range from 140 to 205 K. This coincidence of the structural and magnetic transitions in 122 disappears with doping on the Fe and As sites, although the case of isoelectronic Ru doping of the Fe in $BaFe_2As_2$ is under debate (Rullier-Albenque *et al.*, 2010; Thaler *et al.*, 2010).
- Inelastic neutron scattering (INS) has found (similar to results in the cuprates) a spin-fluctuation resonance in the 1111, 122, 111, and 11 structure superconductors below T_c. These experiments may provide evidence that is still undergoing refinement for a causal link between the spin fluctuations (which are directionally in the Fermi surface pocket nesting direction) and the pairing that opens the superconducting gap.

TABLE I.   Structural and magnetic transition temperatures for undoped 1111, 122, 111, 11, and 122* parent compounds.

Material	T_S (K)	T_{SDW}(K)	Ref.
LaFeAsO	158	134	Luetkens *et al.* (2009)
PrFeAsO	154	135	Rotundu *et al.* (2009)
CeFeAsO	155	140	Zhao *et al.* (2008b)
	151	145	Jesche *et al.* (2010)
NdFeAsO	150	141	Qiu *et al.* (2008)/Y. Chen *et al.* (2008)
	143	137	Tian *et al.* (2010)
SmFeAsO	175	135	Martinelli *et al.* (2011); Drew *et al.* (2009); Sanna *et al.* (2009)
GdFeAsO	135		C. Wang *et al.* (2008)
SrFeAsF	180	133	Xiao *et al.* (2010)
CaFeAsF	134	114	Xiao *et al.* (2009a)
BaFe$_2$As$_2$	142	142	Huang *et al.* (2008)
SrFe$_2$As$_2$	205	205	Krellner *et al.* (2008)
CaFe$_2$As$_2$	171	171	Ronning *et al.* (2008)
EuFe$_2$As$_2$	190	190	Tegel *et al.* (2008b)
Na$_{1-\delta}$FeAs	50	40	S. Li *et al.* (2009a); Parker *et al.* (2009)
FeTe	72	72	Fruchart *et al.* (1975)
K$_{0.8}$Fe$_{2-y}$Se$_2$	578/551	559/540	Bao *et al.* (2011b); Liu *et al.* (2011)
Rb$_{0.8}$Fe$_{2-y}$Se$_2$	540	534	Liu *et al.* (2011)
Cs$_{0.8}$Fe$_{2-y}$Se$_2$	525	504	Liu *et al.* (2011)

- Measurement of angular resolved photoemission spectroscopy (ARPES) of FePn/Ch finds a Fermiology consisting typically of five separate pockets with varying degrees of interpocket nesting, ranging from very strong in the undoped 122 parent compounds to totally absent in overdoped but still superconducting BaFe$_{2-x}$Co$_x$As$_2$ and LiFeAs. The importance of the five Fe 3d bands at the Fermi energy in these materials is well established, with good agreement between measurement and calculation.

These common factors (with the exception of the fivefold Fermiology) have their analogs in the well-studied high T_c cuprates. All cuprate derivative structures have CuO planes in common, the Cu electrons are involved in the superconductivity, there is magnetism in the undoped, nonsuperconducting compound phase diagrams, both hole and electron doping cause superconductivity with hole doping being more effective in raising T_c, and pressure is known, as mentioned, to have a large effect on T_c.

There are, however, important differences between the new iron superconductors and the cuprates, as have been discussed above as one of the main points of interest for studying FePn/Ch. In the final analysis, although analogy with the large body of knowledge collected on the cuprates can be of help in choosing which investigations might yield essential insights, FePn/Ch appear to be (in much of their fundamental behavior) categorically different from the cuprates.

Effort has been made to make this review an organized whole, to provide easy navigation to topics of interest for the nonspecialist reader interested in understanding FePn/Ch superconductivity. Each of the succeeding main topics (Secs. II, III, IV, and V) begins with an introduction and summary, as do most of the major sections. The organization at the level of the presentation of detailed results is based on the six FePn/Ch structures, generally in the order of discovery (1111 ... 122*) presented above. There are numerous references to specialized reviews for further in-depth reading on selected topics. Several collections of papers on the field of FePn/Ch superconductors exist, including Superconductor

Science and Technology *23*, May 2010 (focus on electromagnetic properties), Physica C *469*, 313–674 (2009), Physica C *470* Supplement 1, S263–S520 (2010), New Journal of Physics *11*, February 2009, and J. Phys. Soc. Japan *77*, Supplement C, 1–159 (2008). The Journal of the Physical Society of Japan currently has a banner "Iron-Pnictide and Related Superconductors" on their home web page that links to an detailed index with links to 32 separate subject areas organizing all of the articles in the journal on this subject. Early reviews by Hosono (2008), Norman (2008), and Ishida, Nakai, and Hosono (2009) give a good overview of the beginning work and understanding thereof in this field. More recent reviews include those by Gasparov (2010), Lumsden and Christianson (2010) (magnetic properties), Mizuguchi and Takano (2010) (the iron chalcogenides), Mandrus *et al.* (2010) (BaFe$_2$As$_2$ and dopings thereof), Paglione and Greene (2010) (overview), Johnston (2010) (comprehensive overview, emphasis on normal state properties), Ivanovskii (2011) (the 122 defect structure superconductors), and Hirschfeld, Korshunov, and Mazin (2011) (theory). Last, in the modern multimedia age, there is a video of a slide presentation on this subject by Norman (2010).

II. STRUCTURAL AND ELECTRONIC PROPERTIES: T_c AND ITS DEPENDENCIES AND CORRELATIONS

As discussed in the Introduction, all of the iron pnictide and chalcogenide superconductors have structural and physical properties in common. The present section focuses on the superconductivity, its connection with the structural and magnetic phase transitions (phase diagrams), the important question of coexistence of magnetism and superconductivity, and the influences of pressure and magnetic field on T_c. First, the structure (Sec. II.A) of these materials is presented. The structure is crucial in any attempt to understand the superconductivity, particularly since there are aspects of the structure in FePn/Ch which influence T_c where similarities and correlations have been found. Then, the large body of data about the phase diagrams of these compounds (Sec. II.B) is

presented, with graphs of T_c, the structural phase transition temperature T_S, and T_{SDW} as a function of doping. There appear to be two distinct kinds of phase diagrams *vis-à-vis* whether the magnetism is suppressed by doping before superconductivity is induced. Further, in the "coexistent" kind of phase diagram, there are again two distinct types. These are distinguished by whether the magnetic transition temperature T_{SDW} ever sinks down to T_c at a given composition or whether T_{SDW} remains larger than T_c.

Section II.C considers the important topic of microscopic versus phase-separated coexistence of the magnetism and superconductivity after the experimental evidence for coexistence in Sec. II.B is established. Coexistence is a focus of interest for understanding the pairing mechanism. Finally, Secs. II.D and II.E discuss the pressure and field dependence of T_c and the insights therefrom for understanding the superconductivity.

A. Structure and T_c versus lattice spacing

The original discovery of superconductivity at 26 K by Kamihara *et al.* (2008) was in LaFeO$_{1-x}$F$_x$, which has the tetragonal, tP8 ("t" means tetragonal, "P" means "primitive" or no atoms in either the body or face centers, 8 atoms per unit cell) ZrCuSiAs (= prototypical compound) structure with 2D layers of FeAs shown in Fig. 1.

The second FePn/Ch structure discovered to be superconducting, also tetragonal with 2D FeAs planes, was K doped BaFe$_2$As$_2$, with the tetragonal tI10 ("I" means there is an atom at the center of the 10 atom unit cell, see Fig. 2) ThCr$_2$Si$_2$ structure (Fig. 2), and T_c = 38 K (Rotter, Tegel, and Johrendt, 2008). This is a well known and well studied structure in materials superconductivity and is the same structure as the first discovered heavy fermion superconductor, CeCu$_2$Si$_2$ (Steglich *et al.*, 1979.) The third and fourth FePn/Ch superconducting structures to be discovered, Figs. 3 and 4, also both with 2D planes (FeAs and FeSe respectively), were the MFeAs, "111," (X. C. Wang *et al.*, 2008, M = Li,

FIG. 2 (color online). Lattice structure of 122 BaFe$_2$As$_2$. From Shein and Ivanovskii, 2009a.

T_c = 18 K) with the tetragonal tP6 Cu$_2$Sb structure, and the iron chalcogenide FeSe ("11") family (Hsu *et al.*, 2008, T_c = 8 K) with the tetragonal tP4 PbO structure. The fifth structure with FePn planes to join this superconducting set of materials is the so-called 21311 (sometimes called the 42622) structure. The first member found, Sr$_2$ScO$_3$FeP (Ogino *et al.*, 2009) shown in Fig. 5 had a 17 K T_c. Replacement of Sc with Cr or V, and P with As, has increased T_c up to 37 K in Sr$_2$VO$_3$FeAs (Zhu *et al.*, 2009b), while Sr$_2$Mg$_{0.2}$Ti$_{0.8}$O$_3$FeAs has T_c = 39 K (Sato *et al.*, 2010). The structure in Fig. 5 can be visualized as layers of 122 SrFe$_2$P$_2$ alternating with perovskite Sr$_3$Sc$_2$O$_6$ layers. Intercalation of further layers of atoms between the FeAs
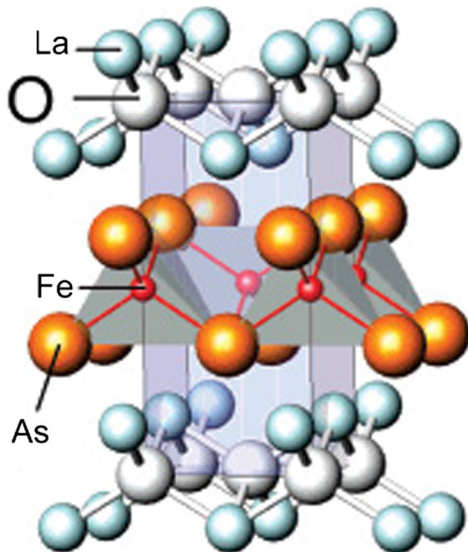
FIG. 1 (color online). Lattice structure of 1111 LaFeAsO. From Kamihara *et al.*, 2008.

FIG. 3 (color online). Lattice structure of 111 LiFeAs. From Deng *et al.*, 2009.
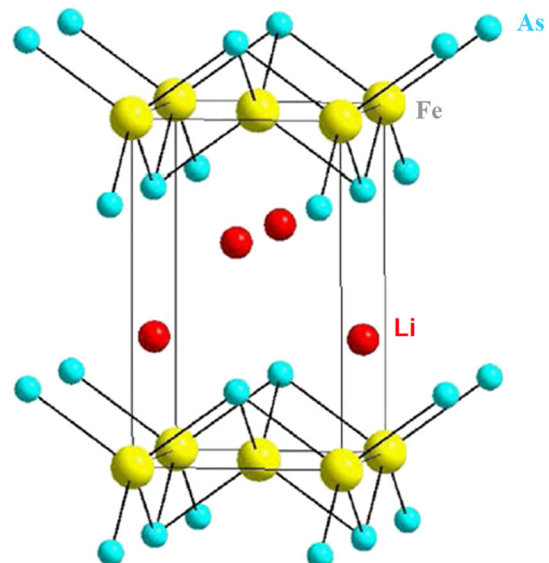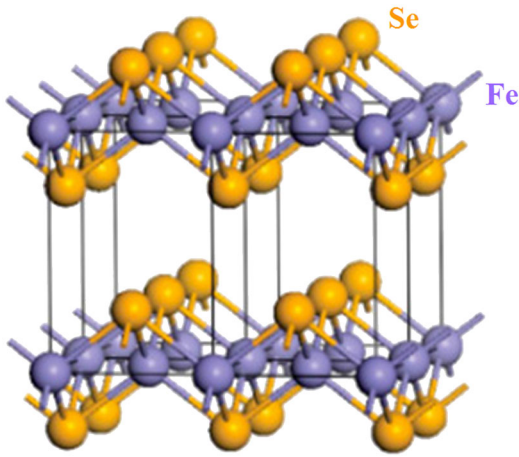
FIG. 4 (color online).   Lattice structure of FeSe. From Hsu *et al.*, 2008.

layers to try to increase T_c by expanding the c axis has so far (Ogino *et al.*, 2010c) (discussed in Sec. II.B.3.a) resulted in T_cs up to 47 K. The most recent FePn/Ch structure discovered (Fig. 6) with superconductivity ($T_c \approx 32$ K) is an ordered-defect alteration of the 122 $BaFe_2As_2$ structure (called the "122*" structure herein), written $A_{0.8}Fe_{1.6}Se_2$ or sometimes $A_xFe_{2-y}Se_2$ (A = K, Rb, Cs, Tl), where the ordered arrangement of Fe vacancies below T_S on the inequivalent Fe sites (in the ideal case Fe2 sites are fully occupied, Fe1 sites are fully unoccupied) has important influence (Bao *et al.*, 2011b; Ye *et al.*, 2011) on the measured properties, including superconductivity. Zavalij *et al.* (2011) state that below the ordering temperature T_S the Fe1 site may have nonzero (3.2%–7.8%) occupation, although they speculate that this could be due to small, fully Fe1 occupied domains. Another way to
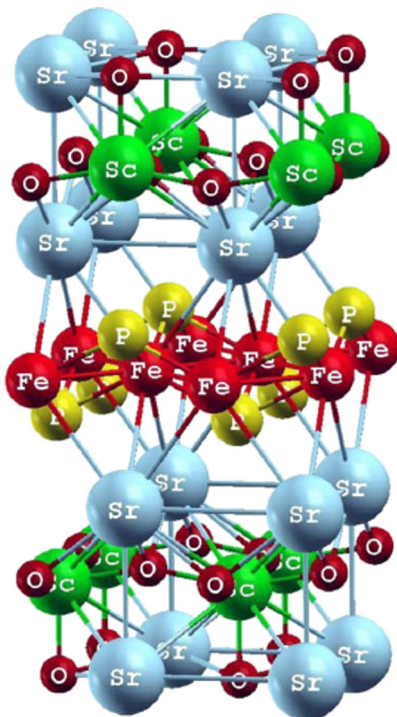

FIG. 5 (color online).   Lattice stucture of Sr_2ScO_3FeP. From Shein and Ivanovskii, 2009b.
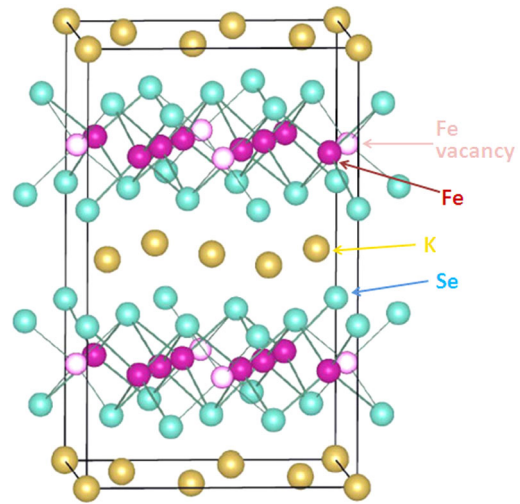

FIG. 6 (color online).   Lattice structure of $A_{0.8}Fe_{1.6}Se_2$. The Fe atoms (large solid circles arranged in diagonal rows), on the Fe2 site (16/unit cell), are all interior to the unit cell (marked with long solid lines) while the open circle Fe vacancies are on the Fe1 site (4/unit cell) and are all on faces, i.e., shared with neighboring unit cells. Note the enlarged unit cell with respect to the 122 structure in Fig. 2. From Bao *et al.*, 2011b.

interpret this structure is as FeSe intercalated with K, Rb, Cs, Tl, or combinations thereof. The unit cell for the tetragonal 122* ordered defect structure is larger than that for the tetragonal 122 by $\sqrt{5} \times \sqrt{5} \times 1$ in the a, b, and c axis directions, respectively; see Bao *et al.* (2011a; 2011b) for further diagrams.

Thus, all of the discovered FePn/Ch superconductors are tetragonal with planes of tetrahedra of Fe and either As or P (pnictogens) or S, Se, or Te (chalcogenides). The rather short [2.67 Å in the 11, 2.77 Å in the 122*, Guo *et al.* (2010), up to 2.84 Å in the 21311 and 2.85 Å in the 1111, Ishida, Nakai, and Hosono, 2009; Ogino *et al.*, 2009] Fe-Fe spacings insure that the $3d$ Fe electrons take part in band formation. Various calculations of the electronic structure result in the consensus that these Fe d bands dominate the rather large density of states near the Fermi energy [see Raghu *et al.* (2008) for a discussion of the basic features of a band model]. Together with nesting on the Fermi surface, these Fe bands can lead to magnetic ordering (Cao, Hirschfeld, and Cheng, 2008; J. Dong *et al.*, 2008; Cvetkovic and Tesanovic, 2009; Singh, 2009) as discussed in Sec. II.B. Four of the six structures have the same space group, $P4/nmm$, space group number 129. The exceptions are the 122, MFe_2As_2 structure, which has $I4/mmm$ (space group number 139) due to the body centered M atom shown in Fig. 2, and the ordered-defect 122* structure, $A_{0.8}Fe_{1.6}Se_2$. The 122* structure has the reduced $I4/m$ symmetry (space group 87) below the defect ordering transition T_S (vs $I4/mmm$ of the 122 structure at higher temperature) since as seen from Fig. 6 the ordered-defect 122* structure loses the mirror plane symmetries in the x and y directions of the 122 structure in Fig. 2 when the Fe1 sites are empty. In this symmetry notation, P and I mean primitive and body centered, respectively, just as in the structure notation, 4 means that the structure is identical under fourfold rotation (by 90°) around the c axis, mmm means that the structure is

identical when mirrored in planes perpendicular to all three of the orthogonal tetragonal axes, and *nmm* means symmetric about mirror planes perpendicular to the two equal tetragonal axes (*a* and *b*) and that for the third, unequal tetragonal axis (*c* axis) the symmetry operations that bring the crystal back to itself are called glide plane symmetry, where the *n* glide involves reflecting about a mirror plane parallel to the *c* axis followed by a translation along 1/2 of the face diagonal. These symmetry operations can be followed in Figs. 1–6. The space groups, numbered from 1 to 230, are all unique and describe all possible crystal symmetries.

The influence of lattice structure on T_c has been the focus of numerous researchers and is clearly an important issue. The $FeAs_4$ ($FeSe_4$) building blocks common to all structures form tetrahedra (see Figs. 1–6) that are ''regular'' (meaning the four faces are equilateral triangles) if the As-Fe-As bond angle α is 109.47°. Lee *et al.* (2008) pointed out that T_c plotted versus α for a wide range of doped 1111 and 122 Fe-Pn superconducting samples shows a sharp peak at the regular tetrahedron bond angle, indicating that local symmetry around Fe and As is decisive for the superconductivity. Putting this dependence of superconductivity on the lattice structure on a theoretical basis, Kuroki *et al.* (2009) discussed how nesting among pieces of the Fermi surface (see Sec. IV.A.2 for a discussion of the experimental determination of the Fermiology), which is determined by the lattice structure, determines not only the size of T_c but also the symmetry of the gap function (see also Kemper *et al.*, 2010 and Thomale *et al.*, 2011a). Thus, Kuroki *et al.* pointed out that the nature of the gap symmetry, nodal verus fully gapped (see Sec. IV for a discussion of the theory and experiments), is controlled by the height of the arsenic (or more generally the pnictogen or chalcogen) above the iron plane. Small pnictogen height favors nodal behavior (LaFePO) versus large pnictogen height which favors more fully gapped behavior ($LaFeAsO_{1-x}F_x$).

The correlation in the high T_c cuprates that T_c scales with the CuO interplanar spacing was at least part of the motivation for investigating the 21311 materials, e.g., Sr_2ScO_3FeP, but the resultant *c* axis spacing (15.543 Å vs 8.73 Å for $LaFeO_{1-x}F_x$), with the concomitant much larger Fe-Fe interlayer spacing, and relatively low (17 K) T_c indicates that other factors are also playing a role. For a discussion of the lattice parameters for the first four FePn/Ch structures, see Ishida, Nakai, and Hosono (2009); for the 21311, see Ogino *et al.* (2010b) and for the defect 122* structure, see Bao *et al.* (2011b) and Zavalij *et al.* (2011).

Within a given structure, various correlations between lattice spacing and T_c have been noted. Shirage *et al.* (2008) noted in electron doped, oxygen deficient $LnFeAsO_{1-x}$ and $La_{1-y}Y_yFeAsO_{1-x}$ that T_c scales with the *a* axis spacing (see Fig. 7). In terms of hole doping of 1111, this is somewhat of an open question as there have been conflicting reports since annealing of hole-doped samples to optimize the superconductivity can also lead to oxygen deficiency (equivalent to electron doping). Specifically, Wen *et al.* (2008) measured T_c as a function of doping in hole-doped $La_{1-x}Sr_xFeAsO$ and find that T_c remains unusually constant (within 10%) at ~25 K as a function of *x* between 0.1 and 0.2. Wu *et al.* (2008b) argued that Sr doping of
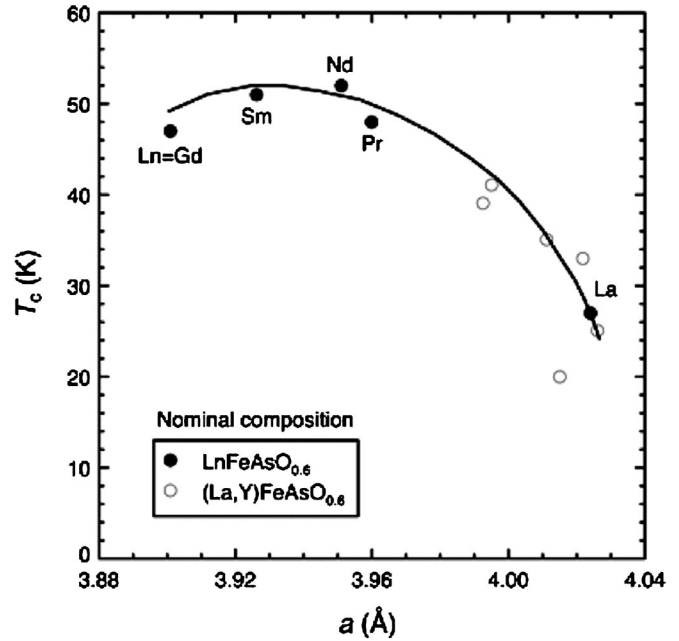

FIG. 7. T_c vs *a*-axis spacing in $LnFeAsO_{0.6}$ and $(La, Y)FeAsO_{0.6}$. See also Miyazawa *et al.* (2009) for a follow up work that includes Dy and Tb, $a = 3.86$ and 3.875 Å, respectively. Note the open circles corresponding to Y replacing La. From Eisaki *et al.*, 2008.

LaFeAsO does not cause bulk superconductivity, that only annealing which then produces an oxygen deficiency results in bulk behavior.

In the 122 materials, with decreasing transition metal electron doping (Canfield and Bud'ko, 2010) on the Fe site in $BaFe_2As_2$ [e.g. Co in $Ba(Fe_{1-x}Co_x)_2As_2$, $0 \leq x \leq 0.11$], the *c* axis increases (just as it does in electron doped LaFeAsO) while the ratio a/c falls (corresponding to an almost constant *a*-axis spacing), both monotonically as T_c falls with decreasing concentration [see Fig. 12 in Sec. II.B for T_c vs *x* in $Ba(Fe_{1-x}Co_x)_2As_2$]. With increasing doping (Rotter, Tegel, and Johrendt, 2008) of $BaFe_2As_2$ with K on the Ba site, the *a* axis shrinks while the *c* axis expands. Thus, the behavior of the *c* axis (proportional to the interlayer spacing) as doping concentration is varied from large electron (Co, $x \approx 0.11$) doping through $x = 0.00$ and further to increasing hole (K) doping is monotonically increasing, while T_c is approximately ''V shaped,'' i.e., has a minimum at $x = 0.00$ and rises approximately linearly with either electron or hole doping.

B. T_c, T_S, and T_{SDW} versus doping and phase diagrams

After the 2D layers common to the FePn/Ch superconductors, the search for other commonalities to explain the superconductivity focused on the magnetic behavior of the various systems as they were discovered. Using neutron scattering, de la Cruz *et al.* (2008) reported for the undoped parent compound LaFeAsO SDW antiferromagnetism at $T_{SDW} = 137$ K with a low temperature moment of $0.36\mu_B$/Fe atom, preceded by a structural distortion from tetragonal to orthorhombic (originally indexed as monoclinic, but corrected by Nomura *et al.*, 2008) at $T_S = 155$ K. Both these transitions are suppressed in the discovery compound of Kamihara *et al.* (2008), $LaFeAsO_{0.92}F_{0.08}$, $T_c = 26$ K. T_{SDW} and T_S are

depressed by intermediate doping at approximately the same rate, so that T_S remains greater than T_{SDW}, discussed below. LaFePO, which is superconducting at 5–6 K in the undoped state, is not magnetic (Carlo *et al.* 2009). Historically, the discovery of Kamihara *et al.* (2008) of superconductivity at 26 K in F-doped LaFeAsO was foreshadowed by the discovery of superconductivity around 5 K in LaFePO (Kamihara *et al.*, 2006) by more than just LaFePO having the same 1111 structure. The work in 2006 reported that T_c increased up to ≈ 10 K with 6% F doping on the O site in LaFePO.

Undoped BaFe$_2$As$_2$ was reported (Rotter *et al.*, 2008b) to have an SDW transition at 140 K, as well as a tetragonal-orthorhombic structural distortion at the same temperature. Later, neutron scattering work (Huang *et al.*, 2008) determined the low temperature moment to be $0.87 \mu_B$/Fe atom. Both this measured local moment and that for LaFeAsO ($0.36 \mu_B$/Fe atom) are significantly smaller than those calculated by density functional theory (DFT) band structure calculations (Mazin and Johannes, 2009). Since DFT calculations do not properly include electronic correlations [see Yin, Haule, and Kotliar (2011) for a comparison of DFT with DFT + DMFT (dynamical mean field theory) Fermi surface calculations], this difference in the determined magnetic moment implies that such correlations may be important in FePn/Ch. In the discovery work, upon doping with K, Ba$_{0.6}$K$_{0.4}$Fe$_2$As$_2$ became superconducting at 38 K with no structural transition down to at least 20 K (Rotter, Tegel, and Johrendt, 2008). Later work, discussed in Sec. II.B.2 on the 122 structure, delineated the decrease in T_{SDW} and the structural transition temperature T_S with doping on all three of the sites in MFe$_2$As$_2$. This later work found a clear consensus that there is a separation, with $T_S > T_{SDW}$, upon doping either the Fe (with the possible exception of Ru doping) or the As sites, but with some disagreement regarding doping on the *M* site. Thus, upon doping 122 on either the Fe or the Pn/Ch site, they are clearly comparable to the 1111 compounds in the separation of T_S and T_{SDW}, while there is only limited evidence in 122 for the splitting of T_S and T_{SDW} for doping on the *M* site.

The next 2D layered FePn superconductor discovered, LiFeAs, shows bulk superconductivity at $T_c = 18$ K but has neither a magnetic nor a structural transition, although there are very strong magnetic fluctuations (Jeglic *et al.*, 2010). The other known superconducting 111 material, Na$_{1-\delta}$FeAs, shows a broad (ΔT_c up to 15 K) resistive transition at $T_c = 23$ K, and shows two transitions above T_c (G. F. Chen *et al.*, 2009). The lower temperature transition had been earlier identified as a magnetic transition (~ 40 K, μSR (muon spin resonance) data from Parker *et al.*, 2009), with an estimate of the local moment of (0.1–$0.2 \mu_B$). A follow up work determined a local Fe moment of ($0.09 \pm 0.04) \mu_B$ [elastic neutron scattering data from S. Li *et al.* (2009a)] and a tetragonal to orthorhombic structural transition (at ~ 50 K) (S. Li *et al.*, 2009a). This low value of the local ordered moment is the lowest in the magnetically ordered parent FePn/Ch compounds. Whether Na$_{1-\delta}$FeAs is a bulk superconductor and the role of Na defects will be discussed in Sec. II.B.3. As will be discussed in several sections, LiFeAs is different from the other FePn/Ch superconductors in numerous ways, not just in its lack of structural or magnetic

transition in comparison to Na$_{1-\delta}$FeAs. The small Li ionic radius compared to that of Na (1.55 vs 1.90 Å) is presumably part of the reason; LiFeAs is already "precompressed" (see Sec. II.D on T_c as a function of pressure). The LiFeAs tetrahedral As-Fe-As bond angle α is 113.7° (Pitcher *et al.*, 2008), far from the regular tetrahedron value of 109.47° where Lee *et al.* (2008) pointed to a maximum in the T_cs of 1111.

The 11 structure FeSe$_{1-x}$, $T_c = 8$ K, shows a structural transition (just as the 1111 and 122 structures, tetragonal to orthorhombic) at 90 K (McQueen *et al.*, 2009b) with no magnetic transition (confirmed in McQueen *et al.*, 2009a who prefer "Fe$_{1+\delta}$Se") while FeSe$_x$Te$_{1-x}$, $T_c = 15$ K has both a structural (tetragonal to monoclinic) and magnetic transition (both at 72 K for $x = 0$) (Fruchart *et al.*, 1975, see also Viennois *et al.*, 2010.) The low temperature magnetic moment of nonsuperconducting Fe$_{1.068}$Te is $2.25 \mu_B$/Fe atom (S. Li *et al.*, 2009b). The physical properties of Fe$_{1+x}$Te depend on the amount of excess Fe, with the low temperature structure becoming orthorhombic rather than monoclinic below $T_S \sim 63$ K and the magnetic ordering becoming incommensurate for $x = 0.141$ (Bao *et al.*, 2009).

The 21311 structure, represented by Sr$_2$VO$_3$FeAs, $T_c = 37$ K, apparently does not have a structural transition but does show a transition (that is preparation dependent) consistent with magnetism at ~ 155 K with a moment less than $\sim 0.1 \mu_B$ (Sefat *et al.*, 2010; Cao *et al.*, 2010; Tegel *et al.*, 2010).

The ordered defect 122* K$_{0.8}$Fe$_{1.6}$Se$_2$ structure, $T_c \approx 32$ K, has (Bao *et al.*, 2011b) an Fe-sublattice order-disorder transition at $T_S \approx 578$ K, followed by antiferromagnetic order at $T_N \approx 559$ K with a low temperature ordered local moment of $3.31 \mu_B$/Fe atom. Both the high magnetic ordering temperature and the size of the local moment are records for the FePn/Ch superconductors. Liu *et al.* (2011), using resistivity ρ and magnetic susceptibility χ reported T_S and T_N for all of the superconducting A$_{0.8}$Fe$_{2-y}$Se$_2$, A = K, Cs, Rb, (Tl,K), and (Tl,Rb), and found T_N values between 540 K [A = K] and 496 K [A = (Tl, K)]. As a comparison, in insulating TlFe$_{1.6}$Se$_2$, Sales *et al.* (2011), using inelastic neutron scattering, found $T_N = 430$ K with the Fe sublattices slightly disordered (90% of the Fe2 sublattice and 30% of the Fe1 sublattice were occupied) below $T_S \approx T_N$. Sales *et al.* found that the ordered moment in the insulating compound peaks at $2.1 \mu_B$, significantly smaller than the Bao *et al.* (2011b) result of $3.31 \mu_B$ for the superconducting ordered 122* structure, at 140 K but then decreases to $1.3 \mu_B$ at low temperatures after two (still under investigation) phase transitions at 140 and 100 K.

Unlike 1111, 122, and the 11 structures, the low temperature crystal structure of the superconducting ordered defect 122* structure A$_{0.8}$Fe$_{1.6}$Se$_2$ remains tetragonal, although with a lower symmetry (see Fig. 6) than the high temperature structure ($I4/m$ vs $I4/mmm$, respectively) due to the Fe-sublattice ordering.

It is interesting to note that although both calculations (Subedi *et al.*, 2008) and ARPES measurements (Xia *et al.*, 2009) of the Fermi surfaces of the undoped 11 compounds indicate nesting similar to that of the undoped 1111 and 122 materials (see Sec. IV.B.2 for a discussion of the ARPES data), the ordered wave vector in 11 is different as
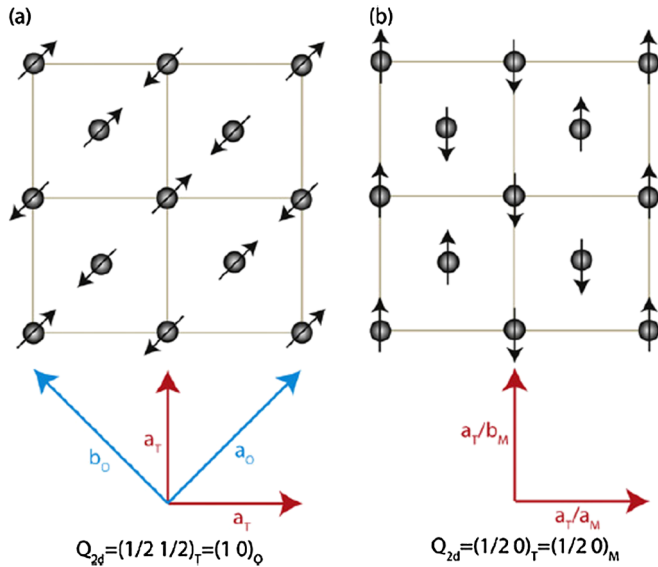
FIG. 8 (color online). In-plane magnetic spin arrangement for undoped 1111 and 122 materials, part (a) and for 11 materials, part (b). The colored vectors denote the tetragonal ("T"), ortho-rhombic ("O") and monoclinc ("M") structures. Note that some authors use tetragonal notation for the ordering wave vector $(\frac{1}{2}, \frac{1}{2})$ while others use orthorhombic (1,0). From Lumsden and Christianson, 2010.

shown in Fig. 8. [In 122*, the ordered moment is, instead of being in the ab plane, along the c axis (Bao $et\ al.$, 2011a.)]

Johannes and Mazin (2009), using linearized augmented plane wave calculations, calculated the stabilization energies for various magnetic configurations in the undoped 11 and 122 structures and found that the observed $(1/2, 1/2)_T$ wave vector in 122 is energetically favored while it is energetically approximately the same as the $(1/2, 0)_T$ wave vector observed in 11. Thus, they argued that, based on the calculated and observed difference in ordered wave vectors for 11 versus the 122 compounds despite the similar nesting, the magnetic ordering is not driven by the nesting in 122 (and, by exten-sion, in 1111). However, this logic can be inverted, since according to ARPES measurements there is no Fermi surface nesting in LiFeAs (Borisenko $et\ al.$, 2010) which is non-magnetic, $ergo$ one could argue that nesting is important for the magnetic ordering. Hsieh $et\ al.$ (2008), based on ARPES measurements in $SrFe_2As_2$, also argued that nesting is im-portant for the magnetic order. Johannes and Mazin (2009) concluded that instead of superexchange between neighbor-ing spins, the magnetic wave vector is due to a combination of local moments and long range itinerant interactions.

Based on the above discussion of local versus itinerant for the magnetic order in FePn/Ch, it is apparent that, as dis-cussed more thoroughly in the review of magnetism in Fe-based superconductors by Lumsden and Christianson (2010), this is still a topic of "considerable debate." There are a number of experimental and theoretical works on both sides of this question. For the experimental side, one of the main experimental probes is of course neutron scattering. See, e.g., neutron studies on $CaFe_2As_2$ by McQueeney $et\ al.$ (2008) and Zhao $et\ al.$ (2009) for conflicting points of view on the

itinerancy of the magnetism, as well as the review by Lumsden and Christianson (2010)). However, there are also results from other measurement techniques, see, e.g., ARPES work in $(Ba, Sr)Fe_2As_2$ of Yi $et\ al.$ (2009) and optical spectroscopy work on 122 parent compounds by Hu $et\ al.$ (2008). For discussion of the theory on both sides of this question, see, e.g., in addition to Johannes and Mazin (2009) discussions by Goswami $et\ al.$ (2011), M. J. Han $et\ al.$ (2009), and Knolle $et\ al.$ (2010).

There is an interesting theoretical argument by Fernandes and Schmalian based on the reentrant (magnetic $\rightarrow$ paramagnetic) behavior in the phase diagram of $Ba(Fe_{1-x}Co_x)_2As_2$ discussed in Sec. II.B.2.b (see also Fig. 12), that at least in some systems the magnetic order must be partially itinerant. There are also theoretical (Lee, Yin, and Ku, 2009; Lv, Wu, and Phillips, 2009; C.-C. Chen $et\ al.$, 2010; Kontani, Saito, and Onari, 2011) and experimen-tal (Akrap $et\ al.$, 2009; Dusza $et\ al.$, 2010; Shimojima $et\ al.$, 2010) works which propose that the observed magnetic order-ing and the structural phase transition are related to the orbital structure of the FePn/Ch (see also the discussions in Secs. II.B.2.b and III.A).

Moon $et\ al.$ (2010), in a combined optical spectroscopy and density functional calculation work, as well as Lumsden and Christianson (2010), argued in agreement with Johannes and Mazin for the best description being a combination of localized and itinerant magnetism. This is certainly in agree-ment with the thermodynamically determined entropy of ordering ΔS at T_{SDW} which, in the systems where high temperature specific heat data exist, is relatively small com-pared to that expected for full local moment ordering (5.76 J/mole K or $R\ln 2$ of entropy for a spin 1/2 local mo-ment.) On the other hand, for a fully itinerant magnetic moment, there would be essentially no entropy of ordering at the transition temperature as is observed, e.g., in the itinerant ferromagnet $ZrZn_2$, where $\Delta S \sim 0.02$ J/mole K (Yelland $et\ al.$, 2005). Values for ΔS at T_{SDW} for $BaFe_2As_2$ ($Ba_{0.8}K_{0.2}Fe_2As_2$), $SrFe_2As_2$, $EuFe_2As_2$, and $Fe_{1.1}Te$ (obtained by analyzing the published specific heat data) are respectively 0.85 (0.18 J/mole K) (Kant $et\ al.$, 2010), ≈ 1 J/mole K (Krellner $et\ al.$, 2008), 1.5 J/mole K (Jeevan $et\ al.$, 2008a), and 2.4 J/mole K (Westrum, Chou, and Gronvold, 1959). Further, this measured entropy of the magnetic moment ordering is intertwined with the entropy of structural ordering at the coincident T_S and thus is even smaller. It is interesting to note, however, that the neutron-scattering-determined local moments for these compounds (see Lumsden and Christianson, 2010) approximately scale with ΔS, since the moments for $BaFe_2As_2$ and $SrFe_2As_2$ are $\approx 1\mu_B$, while measured values for $Fe_{1.1}Te$ range between $1.96\mu_B$ and $2.25\mu_B$.

Leaving now the discussion of local versus itinerant mag-netic order, some aspects of the magnetic ordering and the spin excitations in the FePn/Ch, particularly in 122 where larger single crystal arrays are available (see the discussion in Sec. V.C), have in contrast been decided. The magnetic interactions determined by INS, in contrast to the 2D inter-actions in the cuprates (Kastner $et\ al.$, 1998), are 3D in nature, with some anisotropy. For example, the ratio of the spin wave velocity perpendicular to the plane ($v_\perp$) to that in

the plane ($v_\parallel$) is (McQueeney *et al.*, 2008) at least half in CaFe$_2$As$_2$, with similar values in BaFe$_2$As$_2$ ($v_\perp/v_\parallel \sim 0.2$, Matan *et al.*, 2009), SrFe$_2$As$_2$ ($v_\perp/v_\parallel \sim 0.5$, Zhao *et al.*, 2008d), and underdoped (before the ordering is suppressed) BaFe$_{1.92}$Co$_{0.08}$As$_2$ ($v_\perp/v_\parallel \sim 0.2$, Christianson *et al.*, 2009), versus $v_\perp/v_\parallel = 1$ for isotropic 3D and $v_\perp/v_\parallel = 0$ for purely 2D excitations. After the long range magnetic order in BaFe$_2$As$_2$ is suppressed with sufficient Co doping (optimally and overdoped samples), there is a significant decrease in *c*-axis spin correlations, moving toward more 2D behavior (Lumsden *et al.*, 2009). Whether the more 2D nature of the fluctuations at the highest T_c (optimally doped) part of the phase diagram is a significant consideration for understanding the superconductivity is at this point speculative. In CaFe$_2$As$_2$, measurements of INS to shorter wavelengths out to the zone boundary (Zhao *et al.*, 2009) have been able to determine the signs of the exchange coupling constants J_{1a} and J_{1b} in the plane, with the result that the former is antiferromagnetic and the latter is ferromagnetic. For a discussion of these data and the question of local versus itinerant magnetism and of the question of magnetic frustration, see Schmidt, Siahatgar, and Thalmeier (2010). Several theoretical works (Ma, Lu, and Xiang, 2008, Si and Abrahams, 2008, Yildirim, 2008) in the 1111 materials argue for the importance of frustration.

After this introduction, we now discuss the composition dependence of T_c (and T_S and T_{SDW} where they exist) for the FePn/Ch superconductors structure by structure (as each section in this review is organized) where doping has been used to vary the superconductivity. The response of T_c, T_S, and T_{SDW} to doping has been the subject of intense study in the search for understanding the basic mechanism of the superconductivity, and thus there is a mass of data to summarize below (much of it still waiting for unifying insight). For an example where this effort has made notable progress, see, e.g., the discussion of Ba(Fe$_{1-x}$Co$_x$)$_2$As$_2$ in Sec. II.B.2.b.

1. 1111 structure

The samples discussed in this section were all prepared in polycrystalline form unless otherwise stated. With the exception of SmFeAsO$_{1-x}$F$_x$, which is still under debate as discussed below, both T_S and T_{SDW} are suppressed by doping in 1111s before superconductivity appears. There are only a few examples of hole-doping-caused superconductivity in 1111, primarily in Ln$_{1-x}$Sr$_x$FeAsO, with Wu *et al.* (2008b) arguing for oxygen deficiency and thus effective electron doping in the Ln = La case. There is one example of "isoelectronic-doped," CeFeAs$_{1-x}$P$_x$O, where T_c remains zero (Luo *et al.*, 2010; de la Cruz *et al.*, 2010) for $0 \le x \le 1$ unlike P doping on the As site in BaFe$_2$As$_2$ discussed in Sec. II.B.2 below. Otherwise, the doping in 1111s has been electron doping, with T_cs found above 50 K.

This section on the T_c versus doping (Sec. II.B.1.a) and on the correlations between T_c, T_S, and T_{SDW} (Sec. II.B.1.b) in 1111 attempts to present a thorough review of all the data so that the reader can gain an overview. Table I and Figs. 9 and 10 are aids in this goal. Unfortunately, due to difficulty of preparation and sample quality questions, 1111 present a much less cohesive picture than 122 in Sec. II.B.2.
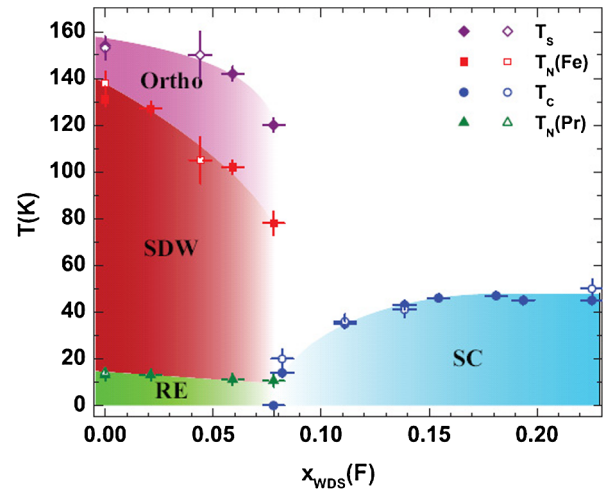
FIG. 9 (color online). The structural, magnetic, and superconducting phase diagram of electron doped PrFeAsO$_{1-x}$F$_x$, $0 \le x \le 0.225$ as determined from synchrotron x-ray powder diffraction, magnetization, and resistivity measurements (Rotundu *et al.*, 2009). T_{SDW} for $x = 0$ determined from ρ data is 140 K, while from ac susceptibility data is 130 K. Note that T_c is not a sensitive function of doping level for $x \ge 0.14$, i.e., the superconducting dome is relatively flat. This insensitivity of T_c to composition over a broad range is typical of the 1111s. "RE" in the diagram is the rare earth Pr antiferromagnetic ordering.

a. T_c versus doping

Electron doping LnFeAsO (Ln = La, Dy, Tb, Gd, Sm, Nd, Pr, Ce), via either the discovery method (F partially replacing O) of Kamihara *et al.* (2008) where superconductivity starts at 4% F doping or via oxygen deficiency achieved with high
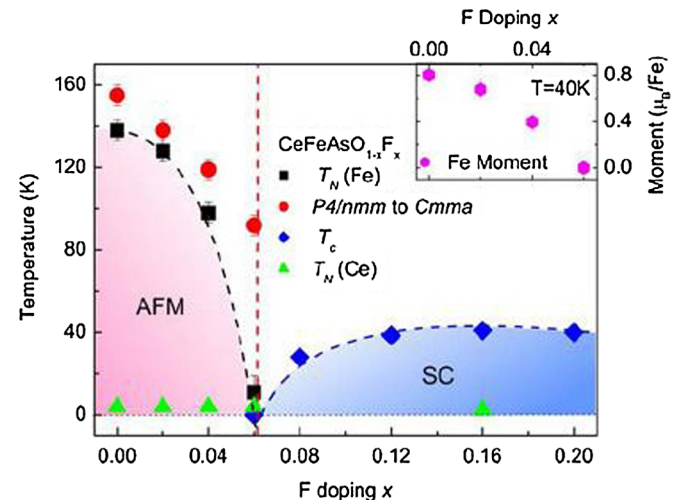
FIG. 10 (color online). Phase Diagram for CeFeAsO$_{1-x}$F$_x$. A recent phase diagram (not shown) for SmFeAsO$_{1-x}$F$_x$ (Martinelli *et al.*, 2011), using high resolution synchrotron powder diffraction to determine T_S, reports that T_S is only suppressed gradually with F doping, with the tetragonal to orthorhombic structural transition at ≈ 130 K for optimally doped $x = 0.2$ vs $T_S = 175$ K for $x = 0$. This work calls into question the accepted picture for the other LnFeAsO$_{1-x}$F$_x$, where as discussed here T_S is thought to vanish in the phase diagram at the beginning of the superconducting dome. From Zhao *et al.*, 2008b.

pressure synthesis, was the first focus of study in 1111 FePn superconductivity. The choice of smaller lanthanide elements (see Fig. 7) to increase T_c, as discussed in the Introduction, was inspired by the increase in T_c of LaFeAsO$_{1-x}$F$_x$, $x = 0.11$, from 26 to 43 K under pressure observed by Takahashi et al. (2008a). Eisaki et al. (2008) showed (Fig. 7) that T_c in LnFeAsO$_{1-y}$ was not actually a function of the electronic nature of the lanthanide element, but rather of the a-axis lattice spacing since they could achieve the same T_c progression by simply doping the smaller Y for La in LaFeAsO$_{1-y}$. Peak T_cs found for oxygen deficiency were in NdFeAsO$_{0.85}$, $T_c = 53.5$ K and in SmFeAsO$_{0.85}$, $T_c = 55$ K (Ren et al., 2008a, using high pressure synthesis) and for the fluorine doped SmFeAsO$_{0.9}$F$_{0.1}$, $T_c = 55$ K (Ren et al., 2008b).

Interestingly, Zhu et al. (2009a) found $T_c^{\text{onset}} \sim 32$ K in Sr$_{0.6}$La$_{0.4}$FeAsF (La provides electron doping of SrFeAsF, which has a positive Hall coefficient, Han et al., 2008). Further, G. Wu et al. (2009) found T_c in Sr$_{0.5}$Sm$_{0.5}$FeAsF at $\sim$56 K, and Cheng et al. (2009) found the same 56 K T_c in Ca$_{0.4}$Nd$_{0.6}$FeAsF, i.e., all three systems have no oxygen at all.

Next, electron and hole doped Ln$_{1-x}$M$_x$FeAsO was studied. Substitution of four-valent Th for three-valent Gd (i.e., electron doping) in Gd$_{0.8}$Th$_{0.2}$FeAsO leads to $T_c = 56$ K (C. Wang et al., 2008). Hole doping has been primarily studied in Ln$_{1-x}$Sr$_x$FeAsO, with Ln $=$ La ($T_c = 25$ K, Wen et al., 2008), Pr ($T_c = 15$ K, Mu et al., 2009b; Ju et al., 2009), and Nd ($T_c = 13.5$ K, Kasperkiewicz et al., 2009). Thus, at least from these few measurements, hole doping in 1111 structure FePn superconductors is much less effective at raising T_c than electron doping. The results for Ln$_{1-x}$Sr$_x$FeAsO, Ln $=$ Pr and Nd, seem to be undisputed. However, Wu et al. (2008b) argued for Ln$_{1-x}$Sr$_x$FeAsO, Ln $=$ La, in which T_c is reported (Wen et al., 2008) to be unusually constant with doping, that it is only superconducting with oxygen deficiency, which they achieved by annealing their La$_{0.85}$Sr$_{0.15}$OFeAs sample in vacuum. (Without the Sr, or other doping, pure 1111 materials with oxygen deficiency can be made superconducting only under high pressure.) Lin et al. (2011) investigated both electron and hole doping in one system, Pr$_{1-y}$Sr$_y$Fe$_{1-x}$Co$_x$AsO, and argued that the charge carrier density is a decisive factor in determining T_c.

In electron doped LnFe$_{1-x}$Co$_x$AsO, Sefat et al. (2008a) were the first to discover that, unlike the high T_c cuprate CuO planes, the superconducting FeAs planes can tolerate significant disorder (this is also the case for the 122 structure, discussed in Sec. II.B.2). This is a key point (and thus doping on the Fe site is thoroughly discussed here) in understanding the superconductivity in FePn/Ch and will be further discussed below. For Ln $=$ La and a Co concentration of $x \sim 0.05$, T_{SDW} is suppressed and T_c starts at $\sim$11 K, rising up to 14 K at $x = 0.11$ before falling back to $T_c = 6$ K at $x = 0.15$. Single crystal LaFe$_{0.92}$Co$_{0.08}$AsO had $T_c = 9$ K (Yan et al., 2009). See also Cao et al. (2009) who, besides LaFeAsO doped with Co, also studied SmFe$_{1-x}$Co$_x$AsO, with $T_c(x = 0.1) = 17$ K. Single crystal electron doped NdFe$_{0.95}$Co$_{0.05}$AsO has $T_c = 25$ K (S. K. Kim et al., 2010). Qi et al. (2009b) substituted Ir for Fe in LaFeAsO and found a maximum $T_c \sim 12$ K for 7.5% Ir. Co doping of SrFeAsF creates a maximum T_c of 4 K (Matsuishi et al., 2008a) while Co doping of the related CaFeAsF gives the

much higher T_c of 22 K for 10% replacement of Fe by Co (Matsuishi et al., 2008b). The higher T_c in Co-doped CaFeAsF versus SrFeAsF is argued by Nomura et al. (2009) to be due to Co doping causing the FeAs$_4$ tetrahedra to become more regular (angle approaches 109.47°) in CaFe$_{1-x}$Co$_x$AsF but more distorted in SrFe$_{1-x}$Co$_x$AsF.

Finally, "isoelectronic" doping (where Ru has the same valency as Fe) was studied (McGuire et al., 2009) in polycrystalline PrFe$_{1-x}$Ru$_x$AsO, with total suppression of the structural and magnetic transitions by $x = 0.67$. Possible distortion of the Fe-As tetrahedral by the larger Ru atom was suggested as an explanation for the lack of superconductivity down to 2 K. As will be seen in Sec. II.B.2.a and in Table II, Ru substitution does cause superconductivity when substituted for Fe in 122.

b. Correlation between T_c, T_S, and T_{SDW}

The progression of T_c, T_S, and T_{SDW} with fluorine doping in LnFeAsO$_{1-x}$F$_x$, Ln $=$ Pr, La, Ce, and Sm, varies in two distinct fashions, depending on the lanthanide atom. For Ln $=$ Nd, there have not been complete phase diagram studies as a function of fluorine doping as yet. Both van der Beek et al. (2010), for NdFeAsO$_{0.9}$F$_{0.1}$, $T_c \sim 36$ K, and Qiu et al. (2008), for NdFeAsO$_{0.8}$F$_{0.2}$, $T_c = 50$ K, reported no coexistence of magnetism and superconductivity at the superconducting compositions studied. For a list of the undoped 1111 T_S/T_{SDW} values, see Table I.

For Pr (Rotundu et al., 2009)/La (Luetkens et al., 2009) the two slightly different ordering temperatures—T_S (154/158 K for $x = 0$) for the tetragonal to orthorhombic lattice distortion and T_{SDW} ($\sim 135/134$ K for $x = 0$) for the ordering of the Fe ions—decrease gradually while T_c remains zero up to $x \sim 0.07/0.04$, and then T_S and T_{SDW} vanish to lowest temperature abruptly with further fluorine doping, $x = 0.08/0.05$, while at these compositions superconductivity appears at $\sim$20 K and rises in a rather flat dome shape to over 40 K, as shown in Fig. 9 for Ln $=$ Pr. Note that for Ln $=$ Pr, there is antiferromagnetic ordering of the Pr ions at low temperature, $T_N \sim 13$ K for $x = 0$, that is absent for the nonmagnetic Ln $=$ La. Otherwise, the two phase diagrams are comparable. In PrFeAsO the Fe local moment in the ordered SDW state is $0.48\mu_B$ and the Pr local ordered moment at 5 K is $0.84\mu_B$ (Zhao et al., 2008c).

For Ce (Fig. 10) and Sm, T_S and T_{SDW} vary more gradually with fluorine doping in LnFeAsO$_{1-x}$F$_x$, falling continuously to $T = 0$; for Ce (Zhao et al., 2008b), T_c becomes finite only after T_S and $T_{\text{SDW}} \to 0$. However, Sanna et al. (2010) used μSR data to argue for coexistence in CeFeAsO$_{0.938}$F$_{0.062}$, $T_c = 18$ K. For SmFeAsO$_{1-x}$F$_x$, the question of whether the magnetic order disappears before superconductivity appears with increasing electron doping is also not yet entirely resolved. Drew et al. (2009) used a microscopic probe, μSR, to determine that magnetism existed in at least 90% of their $x = 0.12$ and 0.13 samples ($T_{\text{SDW}} \sim 40$ and 30 K, respectively), with clear superconducting resistive transitions where $\rho \to 0$ at approximately 9 and 13 K, respectively. However, the diamagnetic indications of superconductivity in these two samples were weak, leading Drew et al. to leave open the possibility of phase separation between superconducting and magnetic regions.

TABLE II. T_c versus composition in $M_{1-x}A_x Fe_{2-y}TM_y As_{2-z}P_z$ T_cs given are the maxima versus composition. Only one site is doped at a time.

Material	M-site dopant	T_c (K) vs x, $y = z = 0$	Ref.	Fe-site dopant	T_c (K) vs y, $x = z = 0$	Ref.	As-site dopant	T_c (K) vs z, $x = y = 0$	Ref.
BaFe$_2$As$_2$	K	38/0.4	Rotter, Tegel, and Johrendt (2008)	Co	22/0.2	Sefat *et al.* (2008b)	P	30/0.7	Kasahara *et al.* (2010); Jiang *et al.* (2009)
	Rb	23/0.1	Bukowski *et al.* (2009)	Ni	20.5/0.1	L. J. Li *et al.* (2009)			
				Pd	19/0.11	Ni *et al.* (2009)			
				Rh	24/0.11	Ni *et al.* (2009)			
				Ru	21/0.9	Sharma *et al.* (2010)			
				Pt	25/0.1	Zhu *et al.* (2010); Saha *et al.* (2010b)			
SrFe$_2$As$_2$	K	36.5/0.5	Sasmal *et al.* (2008)	Co	20/0.2	Leithe-Jasper *et al.* (2008)	P	27/0.7	Shi *et al.* (2009)
	Na	35/0.5	Goko *et al.* (2009)	Ni	10/0.15	Saha *et al.* (2010a); Leithe-Jasper *et al.* (2008)			
	Cs	37/0.5	Sasmal *et al.* (2008)	Pd	9/0.15	F. Han *et al.* (2009)			
	La	22/0.4	Muraba *et al.* (2010)	Rh	22/0.25	F. Han *et al.* (2009)			
				Ru	13.5/0.7	Qi *et al.* (2009a)			
				Ir	22/0.5	F. Han *et al.* (2009)			
				Pt	16/0.16	Kirshenbaum *et al.* (2010)			
CaFe$_2$As$_2$	Na	33/0.66	K. Zhao *et al.* (2010) (see also Wu *et al.*, 2008a)	Co	17/0.06	Kumar *et al.* (2009b)	P	13/0.3	Shi *et al.* (2009)
				Ni	15/0.06	Kumar *et al.* (2009a)			
				Rh	18/0.1	Qi *et al.* (2011)			
EuFe$_2$As$_2$	K	32/0.5	Jeevan *et al.* (2008b), Anupam *et al.* (2009)				P	26/0.6	Ren *et al.* (2009); Jeevan *et al.* (2011)
	Na	35/0.3	Y. Qi *et al.* (2008)						

[a]Note: Cu substituted for Fe in BaFe$_2$As$_2$ suppresses T_S and T_{SDW} but does not induce superconductivity (Canfield *et al.*, 2009b) while Mn substituted for Fe in SrFe$_2$As$_2$ up to $x = 0.3$ is relatively ineffective in suppressing T_S and T_{SDW} (Kasinathan *et al.*, 2009).

Sanna *et al.* (2009), also using μSR, argued for a very narrow "virtually pointlike" region of coexistence in $SmFeAsO_{0.915}F_{0.085}$. Kamihara *et al.* (2010) presented resistivity data on $SmFeAsO_{1-x}F_x$ which showed the apparent coexistence of superconductivity and magnetism in only a very narrow composition range, with $T_{SDW} \sim 120$ K and T_c slightly below 1.8 K (lowest temperature of measurement) for $x = 0.037$ and no indications of magnetism from the resistivity for $x = 0.045$, where $\rho \to 0$ at ~ 22 K. Kamihara *et al.* presented Mössbauer data, which are a better measure of magnetic order, which showed clear lack of magnetic behavior to their lowest temperature of measurement (4.2 K) for $x = 0.069$, but do not report Mössbauer data for any lower x (e.g., 0.045) values except for $x = 0$. Kamihara *et al.* described their data around $x = 0.04$ in $SmFeAsO_{1-x}F_x$ as evidence for disorder and concluded that there is no coexistence of magnetism and superconductivity in $LnFeAsO_{1-x}F_x$, Ln = Sm.

Ignoring the compositional disagreement between the three Sm works as simply due to sample variation issues, what can be said is that none of the $LnFeAsO_{1-x}F_x$ are examples of coexistent magnetism and superconductivity over any appreciable compositional range, unlike all of the 122 materials to be discussed next.

In addition to these rather complete fluorine doping results there are data for electron doping via introducing oxygen deficiency in $LnFeAsO_{1-y}$, Ln = La, Nd, where T_c becomes finite at about $y = 0.08$ (Ishida *et al.*, 2010), a concentration (considering the respective valences) not inconsistent with the fluorine doping results. They argued for coexistence of magnetism (based on structure around 140 K in ρ) and superconductivity for $y = 0.08$ and 0.10. However, the structure in ρ is unusually constant in temperature versus the supposed monotonic increase in y, nor is there any investigation of possible microscopic phase separation.

Therefore, it may be that the 1111 materials, with respect to coexistence of superconductivity and magnetism, are fundamentally different from 122; see Sec. II.C for a summary discussion of coexistence in the FePn/Ch.

CeFeAsO, SmFeAsO, and NdFeAsO (phase diagram not shown, see Table I) show antiferromagnetic ordering of the rare earth ion moments below 4, 5, and 6 K, respectively. Below $T^* = 15$ K, Tian *et al.* (2010) report for the Nd compound, similar to results for Pr (Kimber *et al.*, 2008) and Ce (Zhao *et al.*, 2008b) but with more precise determination of T^*, that the c axis Fe ordering below $T_{SDW} = 141$ K changes from antiferromagnetic to ferromagnetic, indicating an interaction with the rare earth magnetic fluctuations and a delicate balance of the Fe c-axis exchange couplings.

In the case of Sm, the determination of T_{SDW} (Drew *et al.*, 2009; Sanna *et al.*, 2009) and the initial measurement of T_S (Margadonna *et al.*, 2009a) in separate works resulted in $T_{SDW} = 135$ K for undoped SmFeAsO and $T_S = 130$ K, i.e., reversed from the behavior seen in all other 1111 (Table I). However, Martinelli *et al.* (2011), using high resolution synchrotron powder diffraction, have now determined $T_S = 175$ K.

Since the work of Zhao *et al.* (2008b) on polycrystalline $CeFeAsO_{1-x}F_x$ shown in Fig. 10, higher quality samples of the undoped starting compound CeFeAsO in single crystal form have been prepared (Jesche *et al.*, 2010). The separation between T_S and T_{SDW} observed in the polycrystalline material (155 and 140 K, respectively) has shrunk by more than half, with values of 151 and 145 K, respectively. Thus, the question was posed (Jesche *et al.*, 2010) as to how much the separation of T_S and T_{SDW} in all undoped 1111 is intrinsic, and how much is due to defects. Recently, high quality single crystals of NdFeAsO have been prepared (Yan *et al.*, 2009), with $T_S = 142$ K and $T_{SDW} = 137$ K (Tian *et al.*, 2010) versus previous values on polycrystalline material of $T_S = 150$ K (Qiu *et al.*, 2008) and $T_{SDW} = 141$ K (Y. Chen *et al.*, 2008); see Table I. Thus, the shrinkage of the difference in T_S and T_{SDW} with increasing sample quality in 1111 suggested by Jesche *et al.* (2010) is borne out in NdFeAsO. It would be interesting to see if single crystals of SrFeAsF, where as shown in Table I the difference in polycrystalline material between T_S and T_{SDW} is 47 K (Xiao *et al.*, 2010) (the largest separation of any 1111), would also see a decrease in the difference $T_S - T_{SDW}$ with improved sample quality.

In their work on single crystal CeFeAsO, Jesche *et al.* (2010) analyzed the structural transition to be second order, and the magnetic transition to possibly be a broadened first order phase transition. Tian *et al.* (2010) identified the magnetic transition in their single crystal sample of NdFeAsO as being second order. These two 1111 compounds display different behavior than will be discussed below for undoped 122, where the question of the thermodynamic order of the two coincident-in-temperature transitions has been more of a focus.

2. 122 structure

Because of the ease by which 122 can be prepared in single crystal form (see Sec. V), a much larger variety of transition metal dopings (see Table II) on the Fe sites have been studied. In the properties discussed in this section, 122 are often unlike 1111: (1) T_S and T_{SDW} in general are the same in the undoped $122 M(TM)_2(Pn)_2$ compounds (as listed in Table I), but then do split upon doping upon the transition metal and the pnictide site, with some disagreement about splitting upon doping on the M site. (2) While a number of 1111 have magnetic ordering of the lanthanide site rare earth ion (Pr, Ce, Nd, Sm) in addition to the ordering of the Fe as discussed above, in the 122 undoped parent compounds there is only $EuFe_2As_2$ where, in addition to the Fe ordering at 190 K, the Eu orders antiferromagnetically below 19 K (Xiao *et al.*, 2009b). As an additional contrast, in $EuFe_2(As_{1-x}P_x)_2$, for $x \geq 0.22$, the Eu ordering becomes ferromagnetic (Jeevan *et al.*, 2011). (3) The structural transition in the undoped MFe_2As_2 compounds appears, based on hysteresis in the specific heat transition and on the jump in unit cell volume determined by neutron scattering or x-ray diffraction, to be first order in the following cases: M = Ba, $T_S = 142$ K (see early work by Huang *et al.*, 2008 and recent data on an annealed single crystal by Rotundu *et al.*, 2010); M = Sr, $T_S = 205$, (Krellner *et al.* (2008); Zhao *et al.* (2008a); M = Ca, $T_S = 171$ K (Ronning *et al.*, 2008; Goldman *et al.*, 2008; Kumar *et al.*, 2009a). This is consistent with Landau theory, which states that two simultaneous phase transitions that interact with each other (i.e., are not simultaneous due to coincidence) and break different symmetries result in a first

order transition. (See Secs. II.B.2.b and III.A for a discussion of the possible connection between the magnetic and structural phase transitions.) However, Wilson *et al.* (2009), in their neutron scattering experiments on a high quality single crystal of $BaFe_2As_2$, found that both the structural and magnetic transitions at 136 K are second order, with a possible weak first order transition within their error bar. Tegel *et al.* (2008b) argued from their measurements of the lattice order parameter $[P = (a - b)/(a + b)]$, where a and b are the orthorhombic axes' lengths] in $M = Sr$ ($T_S = 203$ K) and Eu ($T_S = 190$ K) that, despite their measured cell volume discontinuity at T_S in $SrFe_2As_2$, all of the MFe_2As_2 starting compounds undergo in fact second order structural phase transitions. Tegel *et al.* find that P in their data scales with $[(T_S - T)/T]^\beta$ where β, although small, remains finite; i.e., implying that the transition, despite its abruptness, remains second order. If this is the case, and in light of the prediction of Landau theory, then either the simultaneity of T_S and T_{SDW} are coincidental (see discussion in Secs. II.B.2.b and III.A) or there should be some higher temperature precursor of one of the transitions that breaks that transition's symmetry at a higher temperature. Yi *et al.* (2011), in an ARPES study of Co doped $BaFe_2As_2$ single crystals under uniaxial stress (which of course intrinsically provides symmetry breaking) to detwin the orthorhombic state, found electronic anisotropy well above the structural phase transition. In any case, the structural transitions in the samples that have been measured to date in 122 definitely show a more rapid variation of the lattice structure with temperature at T_S than those in 1111. (4) Unlike all the $LnFeAsO_{1-x}F_x$ except possibly for Ln = Sm, magnetism and superconductivity coexist quite generally in the lower ("underdoped") portion of the superconducting dome for 122. The question of whether this coexistence is at the microscopic or phase-separated level will be discussed. (5) Finally, hole doping raises T_c^{max} in 122 to a significantly higher value than electron doping, 38 vs 25 K.

a. T_c versus doping

The discovery of superconductivity in the 122 structure was via K doping (hole doping) of $BaFe_2As_2$ (Rotter, Tegel, and Johrendt, 2008). Three other nonsuperconducting MFe_2As_2 ($M = Sr$, Ca, Eu) host compounds were quickly also discovered, where both hole doping on the M site and electron doping on the Fe site, as well as more recently P doping on the As site, succeeded in causing superconductivity, see Table II for a complete listing. Clearly, the variety of dopants that achieve superconductivity in 122 is quite large. An exception is doping with Cu (Canfield and Bud'ko, 2010), three columns to the right of Fe in the periodic table, or Cr (Sefat *et al.*, 2009), two columns to the left of Fe, which do not induce superconductivity in $BaFe_2As_2$. In addition to doping-induced superconductivity, three Fe-containing 122 compounds superconduct without doping, KFe_2As_2 ($T_c \sim 3.8$ K, Rotter *et al.*, 2008a), $RbFe_2As_2$ ($T_c \sim 2.6$ K, Bukowski *et al.*, 2010), and $CsFe_2As_2$ ($T_c = 2.6$ K, Sasmal *et al.* (2008). KFe_2As_2 has been shown to be quite interesting in its properties, including evidence for nodal superconductivity, see Sec. IV; although according to the specific heat discontinuity at T_c, $\Delta C(T_c)$, KFe_2As_2 does not appear to belong with other FePn/Ch (Sec. III.B.3).

The so-called "isoelectronic" doping (substitution of P for As or Ru for Fe) in MFe_2As_2 causing quite respectable T_cs raises the issue of charge doping versus other effects. Since P is smaller than As, one might conclude that the T_c in $MFe_2As_{2-z}P_z$ is at least partly due to "chemical" pressure, analogous to the physical pressure discussed below in Sec. II.C. However, Ru is larger than Fe (although as Ru replaces Fe in $BaFe_2As_2$, the a axis grows as the c axis shrinks, Sharma *et al.*, 2010). Wadati, Elfimov, and Sawatzky (2010) using DFT calculations proposed that the transition metals Co and Ni when substituted for Fe in $BaFe_2As_2$ (as well as in FeSe) behave essentially isovalent with Fe, with their effect on superconductivity primarily due to their impurity and scattering nature affecting the Fermiology, "washing out" parts of the Fermi surface. Thus, rather than a rigid band shift due to adding electrons as would come from a naïve picture, the main effect is calculated to be an impurity-scattering-caused washing out of the more flat band contributions to the total Fermi surface. As stated in this section, T_c is strongly influenced by the structural properties of tetrahedron angle (Lee *et al.*, 2008) and pnictogen height (Kuroki *et al.*, 2009). Rotter, Hieke, and Johrendt (2010) concluded by a careful study of the crystal structure in $BaFe_2As_{2-z}P_z$ that P doping causes a slight reorganization of the crystal structure (not solely a change in the pnictogen height) that influences T_c via its effect on the bandwidth. Klintberg *et al.* (2010) compared the effect of pressure and P doping on the superconducting phase diagram of $BaFe_2As_2$, including the effect of pressure on $BaFe_2As_{2-z}P_z$, and concluded from the similarities between P doping and pressure that impurity scattering is not limiting T_c in the doped samples.

Thus, there are important details involved not only with the "isoelectronic" doping, but also with the other doping species. The simple "atomic" picture, where doping is described as simply adding or subtracting electrons, or isoelectronic doping with essentially no expected change, is definitely oversimplified.

b. Correlation between T_c, T_S, and T_{SDW}

In order to make the large set of numerical data of T_c, T_S, and T_{SDW} versus doping level in 122 more understandable, phase diagrams are shown here for selected dopants. Despite the hole doped $Ba_{1-x}K_xFe_2As_2$ being the discovery superconductor in 122 (Rotter, Tegel, and Johrendt, 2008), this phase diagram shown in Fig. 11 has received much less attention—perhaps due to K homogeneity issues (Ni *et al.*, 2008a; Johrendt and Pöttgen, 2009), where the concentration varies by $\pm 5\%$ so that "$Ba_{0.6}K_{0.4}Fe_2As_2$" has K concentrations between 0.35 and 0.45. Within the resolution of the early neutron scattering determinations of T_S and T_{SDW} (H. Chen *et al.*, 2009) and of the x-ray and Mössbauer determinations of T_S/T_{SDW} (Rotter *et al.*, 2009), the structural and magnetic transitions remained at the same temperature (see Fig. 11) until both transitions are suppressed in $Ba_{1-x}K_xFe_2As_2$. However, more recent measurements (Urbano *et al.*, 2010) found that there is clear evidence (distinct anomalies in both $d\rho/dT$ and specific heat) for splitting of T_S and T_{SDW} in an underdoped single crystal of $Ba_{0.86}K_{0.14}Fe_2As_2$, $T_c \approx 20$ K, and RRR ~ 8.5, with $T_S = 110$ K and $T_{SDW} = 102$ K.
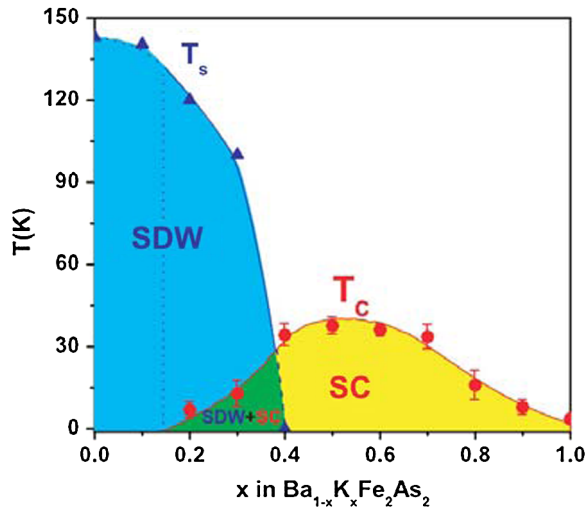
FIG. 11 (color online). T_S and T_{SDW} stay equal vs x. Johrendt and Pöttgen (2009) find that T_{SDW} is suppressed at $x = 0.3$, however both groups find that T_{SDW} does not join the superconducting dome. From H. Chen *et al.*, 2009.

FIG. 12 (color online). Note the factor of 2 between x in their notation vs the y used here and that T_S and T_{SDW} indeed intersect the superconducting dome. From Nandi *et al.*, 2010.

Although this sample was grown using Sn flux, Urbano *et al.* argued that improved methods resulted in a high quality sample with little or no effect from Sn-flux inclusion. This is an important result since, as will now be discussed, 122s in general (with one case, $BaFe_{2-x}Ru_xAs_2$, still under debate) all show such separation with doping. The exception for K doped $BaFe_2As_2$ was an important anomaly that needed clarification. For completeness it should be mentioned that this continues to be a subject of debate, with recent neutron scattering measurements (Avci *et al.*, 2011) on self-flux-grown samples of $Ba_{1-x}K_xFe_2As_2$ finding no separation at all dopings where T_S and T_{SDW} exist. The sample from Avci *et al.* that has the most comparable properties to the sample from the work of Urbano *et al.* (2010) has a nominal composition of $x = 0.21$ and a similar $T_c \approx 20$ K and ΔT_c as determined from susceptibility, i.e., the sample seems to be of comparable quality. Although Avci *et al.* found no separation in T_S and T_{SDW}, their apparent uncertainty in temperature seems to be at least 5 K due to the steep rise of the magnetic moment below $T_{SDW} \approx 80$ K. These samples should have their magnetic and structural transitions measured by some technique with a higher temperature resolution.

There still remain homogeneity issues in the K doped $BaFe_2As_2$ samples. For example, although superconducting samples achieved by doping on both the Fe and As sites in 122 show clear specific heat anomalies ΔC at T_c (see Sec. III.B.3) for the whole superconducting dome, as yet only samples near optimal doping ($x \sim 0.4$) show a measurable ΔC in $Ba_{1-x}K_xFe_2As_2$. For the Urbano *et al.* (2010) data on $x = 0.14$ and in the work of Rotter *et al.* (2009) for $x = 0.2$, no anomaly in the specific heat is observable in T_c (20 and 23.6 K, respectively).

Surprisingly, there are no other studies of doping on the M site in MFe_2As_2 (see Table II for a summary) that investigate the question of potential splitting of T_S and T_{SDW}, or the presence or absence of finite ΔC away from optimal doping.

In Fig. 12, the phase diagram for Co doped $BaFe_2As_2$ is shown, based on resistivity, magnetization, and specific heat
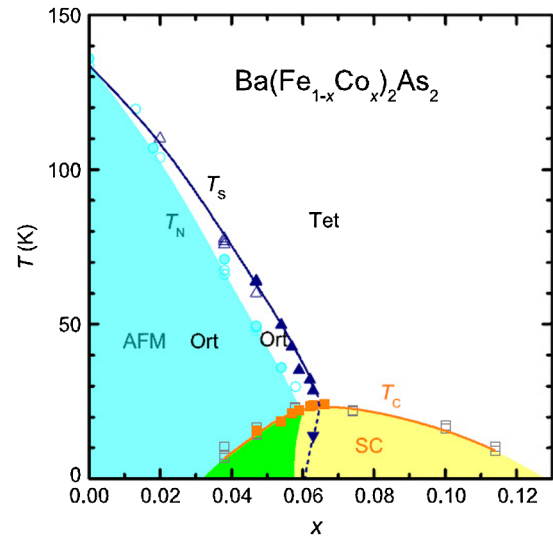
measurements. A common feature of doping the MFe_2As_2 materials on the Fe site has been the separation for finite doping of T_S from T_{SDW} (see results similar to those for Co doping for T_S/T_{SDW} splitting upon doping with TM = Ni and Rh in $BaFe_{2-y}TM_yAs_2$ by Canfield and Bud'ko, 2010). However, Thaler *et al.* (2010), in single crystal work, reported for isoelectronic Ru doping on the Fe site that no splitting is observable, using rather careful consideration of $d\rho/dT$ through the transition. In contradiction to this, another single crystal $BaFe_{2-x}Ru_xAs_2$ work, Rullier-Albenque *et al.* (2010) claimed to see features in their $d\rho/dT$ data indicative of two transitions (95 and 88 K, respectively) at $x = 0.3$. This discrepancy deserves further investigation.

The order of the structural phase transition in $BaFe_{1.906}Co_{0.094}As_2$ ($T_S = 60$ K) in the neutron scattering study of Pratt *et al.* (2009a), although there was slight hysteresis, could not be determined with certainty. However, the magnetic transition at $T_{SDW} = 47$ K is clearly second order. Ni *et al.* (2009) in their study of $BaFe_2As_2$ doped with Rh and Pd on the Fe site pointed out several comparisons in these $BaFe_{2-y}TM_yAs_2$ phase diagrams. Their T_c vs y for Rh falls on the same dome as shown in Fig. 12 for Co, which is isoelectronic with Rh. Their T_c vs y for Pd forms a narrower dome (T_c for Pd doping is finite for $y = 0.04$ to 0.16 vs 0.06 to 0.24 for Co) that only rises up to T_c^{max} of 19 K, but again coincides with the T_c vs y data of Ni (Canfield *et al.*, 2009b), isoelectronic to Pd. Doping with Cu suppresses T_S and T_{SDW}, but does not induce superconductivity (Canfield *et al.*, 2009b).

An interesting feature of the phase diagram in Fig. 12 for $Ba(Fe_{1-x}Co_x)_2As_2$ is the *reversal* of the phase boundary upon cooling through the superconducting dome at $x \sim 0.063$ (see similar work in Rh doped $BaFe_2As_2$, Kreyssig *et al.*, 2010). Thus, the sample at this composition transforms from orthorhombic back to tetragonal upon cooling below T_c. Nandi *et al.* (2010) discussed this in terms of a magnetoelastic coupling between nematic magnetic fluctuations (no static order is present at this composition) and the lattice. The

magnetic fluctuations are weakened by the superconductivity which competes with the magnetic order (Pratt *et al.*, 2009a), thus allowing reentry into the tetragonal lattice structure. In fact, neutron scattering work (Fernandes *et al.*, 2010a) for the magnetic composition $x = 0.059$ found not only a weakening of the magnetism by the superconductivity but actually a reversal from magnetically ordered back into the paramagnetic state below T_c. This reentrant behavior has been used as an argument by Fernandes and Schmalian (2010) that the magnetic order in at least $Ba(Fe_{1-x}Co_x)_2As_2$ must be partly itinerant in nature as discussed in Sec. II.B when the question of itinerant versus localized order was considered. INS studies (Lumsden *et al.*, 2009) of near optimally doped $BaFe_{1.84}Co_{0.16}As_2$ showed that the anisotropic 3D magnetic interactions in the ordered undoped $BaFe_2As_2$ become much more 2D with doping.

As an introduction to their work on the reentrant behavior around $x \approx 0.06$ in $Ba(Fe_{1-x}Co_x)_2As_2$, Nandi *et al.* (2010) discussed the link between magnetic fluctuations above T_{SDW}, i.e., for $x < 0.06$, and the orthorhombic lattice distortion. In their description, two antiferromagnetic sublattices have magnetizations $\mathbf{m}_1$ and $\mathbf{m}_2$ which are weakly coupled due to frustration caused by large next nearest neighbor interactions [see Chandra, Coleman, and Larkin (1990), for a discussion]. Below the magnetic ordering temperature, the time averaged order parameter $\langle \psi \rangle$, where $\psi = \mathbf{m}_1 \cdot \mathbf{m}_2$, and the time averaged sublattice magnetizations $\langle \mathbf{m}_1 \rangle$ and $\langle \mathbf{m}_2 \rangle$ are all finite, leading to static magnetic order. On the other hand, above T_S the time averaged order parameter $\langle \psi \rangle$, as well as $\langle \mathbf{m}_1 \rangle$ and $\langle \mathbf{m}_2 \rangle$, are zero, while nematic (but not static) ordering (where $\mathbf{m}_1$ and $\mathbf{m}_2$, which still time average to zero, are coupled to give a finite $\langle \psi \rangle$) sets in at T_S but still above T_{SDW}. Thus, in the view of Nandi *et al.* (2010), the nematic order above the magnetic transition (and even in the case where the magnetism is totally suppressed) drives the structural distortion. The relative importance of electronic nematic order, which breaks the tetragonal basal plane a–b axis symmetry, and its possible role in mediating the superconductivity in FePn/Ch is a subject of significant interest; see also Chuang *et al.* (2010), Chu *et al.* (2010), Fernandes *et al.* (2010b), Harriger *et al.* (2011), and Park *et al.* (2010).

Phase diagrams for other $MFe_{2-y}TM_yAs_2$ than $M = Ba$ are less thoroughly studied. Leithe-Jasper *et al.* (2008) studied $SrFe_{2-x}Co_xAs_2$ and found no superconductivity down to 1.8 K for $x \leq 0.15$ and $x \geq 0.5$, with $T_c^{max} = 19.2$ K at $x = 0.2$. Resistive indications of T_S/T_{SDW} were absent for $x > 0.15$. What is different in this $SrFe_{2-x}Co_xAs_2$ system from the $M = Ba$ data in Fig. 12 is the lack of the gradual ramp up of T_c on the underdoped side of the phase diagram for $M = Sr$. F. Han *et al.* (2009) reported phase diagrams based on the measurement of resistivity (i.e., they were unable to distinguish separation of T_S and T_{SDW}) for $SrFe_{2-x}TM_xAs_2$ for $TM = Rh$, Ir, Pd. Shown in Fig. 13 is the diagram for Rh, isoelectronic to Co just discussed. The behavior shown in Fig. 13 is similar to that seen for $BaFe_{2-x}TM_xAs_2$ discussed above. As shown in Table II, the T_c^{max} for $TM = Ir$, isoelectronic to Co and Rh, in $SrFe_{2-x}TM_xAs_2$ found by F. Han *et al.* (2009) is similar to that for Rh and Co, while that for $TM = Pd$ is significantly lower. Kasinathan *et al.* (2009) reported only weak
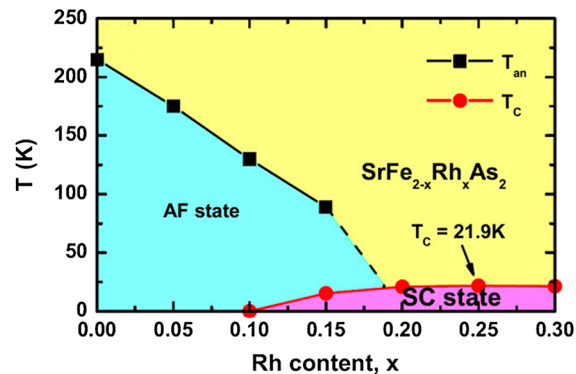
FIG. 13 (color online). The temperature of the anomaly in the resistivity, T_{an} is taken as T_{SDW}. The dashed line connecting the last measured T_{an}, at $x = 0.15$, to the superconducting dome is a guide to the eye. Note that no data for $x > 0.3$ are reported. From F. Han *et al.*, 2009.

suppression of T_S in $SrFe_{2-x}Mn_xAs_2$ up to $x = 0.3$, and no superconductivity.

In $CaFe_{2-x}TM_xAs_2$, Kumar *et al.* (2009a) studied $TM = Ni$ and found superconductivity only for $x = 0.053$ and 0.06, with $T_c = 15$ K and both the structural and magnetic transitions suppressed. Drops in the resistivity at 15 K (but not full transitions) were seen at $x = 0.027$, 0.030, and 0.075. This is a much narrower region of superconductivity with doping than the other Fe-site dopings in $M = Ba$ and Sr discussed above.

Finally, an example of a phase diagram for P doping is shown in Fig. 14, where data for $BaFe_2As_{2-x}P_x$ from Kasahara *et al.* (2010) are shown. Although the shading around $x = 0.3$ is drawn to indicate a gradual fall in T_S and T_{SDW}, the data suggest that in fact, just as seen for K doping in $BaFe_2As_2$ and Rh and Ir doping in $SrFe_2As_2$ (F. Han *et al.*, 2009), there is a region at the top of the superconducting dome where the T_S and T_{SDW} phase boundaries do not join the T_c dome phase boundary. This is also the case for the phase diagram of Shi *et al.* (2009) for $SrFe_2As_{2-x}P_x$, where T_c
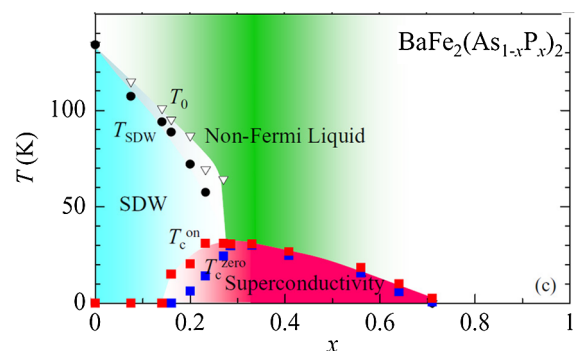
FIG. 14 (color online). Data for P-doped $BaFe_2As_2$. See Jiang *et al.* (2009) for a similar phase diagram. The open upside down triangles denote T_S, while the filled black circles denote T_{SDW} determined from resistivity. Two superconducting T_cs are shown, the upper points are the onset of the resistive transition, the lower ones are where $\rho \to 0$. Note the presence of non-Fermi liquid behavior in the resistivity for this compound, discussed in Sec. III. From Kasahara *et al.*, 2010.

becomes finite at $x = 0.5$ while T_{SDW} is still 140 K and disappears for higher P doping. For $EuFe_2As_{2-x}P_x$ (Jeevan *et al.*, 2011), the antiferromagnetic ordering in the Fe is suppressed before superconductivity occurs at $x = 0.4$; however, the superconductivity at $x = 0.4$ does coexist with the Eu antiferromagnetism. Such coexistence of antiferromagnetism and superconductivity in electrons from different atoms (in this case Eu and Fe) is well known in a variety of compounds; see, e.g., the review on the rare earth borocarbides by Gupta (2006).

3. 111, 11, 21311, and 122^* structures

Relatively less data exist for these structures, due to their more recent discovery and, in the case at least of the 11 structure, fewer possibilities for substitution.

a. T_c versus doping

111: Hole doping in LiFeAs by introducing Li vacancies has been calculated by Singh (2008). Experimentally, Pitcher *et al.* (2010) in polycrystalline material found that T_c falls rapidly with increasing Li deficiency in $Li_{1-y}Fe_{1+y}As$. Pitcher *et al.* also found that T_c falls with electron doping in $LiFe_{1-x}(Co, Ni)_xAs$, by approximately 10 K for every 0.1 doped electron independent of whether Co (one electron each) or Ni (two electrons each) is used as the dopant. This agrees fairly well with the T_c suppression measured in single crystal $LiFe_{0.95}Co_{0.05}As$, $T_c \approx 11$ K, reported by Aswartham *et al.* (2011). Based on the Fermiology reported by ARPES (Sec. IV.A.2), where there is no nesting in LiFeAs because the electron pockets are smaller than the hole pockets, it would be expected that electron doping in LiFeAs might improve the nesting and, if nesting were important for T_c in the 111, therefore T_c. The fact that the opposite effect is observed (especially since Co doping of the Fe site in $BaFe_{2-x}Co_xAs_2$ enhances T_c) may be confirmation that nesting is indeed not critical for the superconductivity in LiFeAs; see discussion of the theory in Sec. IV.A.2.

Before the doping in $Na_{1-\delta}FeAs$ is presented, the question of the superconductivity in the parent compound deserves discussion. In the early work on polycrystalline $Na_{1-\delta}FeAs$ material, Parker *et al.* (2009) reported only 10% diamagnetic shielding, i.e., not the more stringent field-cooled Meissner effect expulsion which is generally only a few percent at most due to pinning in the FePn/Ch superconductors. This 10% fraction of shielding, which is small compared to the typical behavior (≈ 100%) of the other FePn/Ch superconductors, in general argues for a small volume fraction of bulk superconductivity, perhaps a sheath of superconducting material or filaments. Others (Chu *et al.*, 2009) reported similarly weak shielding in polycrystalline material. Then self-flux-grown single crystals of $Na_{1-\delta}FeAs$ were characterized by G. F. Chen *et al.* (2009) via specific heat, and the lack of a ΔC anomaly at T_c was attributed to a small superconducting volume fraction. All of these works estimate a Na deficiency δ of 1%–2%, which is a kind of "self-doping."

In light of this discussion of the parent compound, the results of doping with Co in either polycrystalline or single crystal material are germane to understanding superconductivity in $Na_{1-\delta}FeAs$. Parker *et al.* (2010) doped Co and Ni

into polycrystalline $Na_{1-\delta}FeAs$, again with 1%–2% Na deficiencies. The fraction of diamagnetic shielding (zero field cooled susceptibility) grows from 5%–10% of full shielding for no Co doping (i.e., not bulk superconductivity) to 60% diamagnetic shielding for $Na_{1-\delta}Fe_{0.99}Co_{0.01}As$ to 100% diamagnetic shielding for $Na_{1-\delta}Fe_{0.975}Co_{0.025}$, $T_c = 21$ K. The superconducting dome ends at 10% Co doping. Within the error bar in the μSR measurement, the magnetism is suppressed at the 2.5% Co doping as is, determined via neutron scattering, the structural phase transformation (Parker *et al.*, 2010). Therefore it appears that, at least as thus far prepared, undoped $Na_{1-\delta}FeAs$ (presumably due to defects) is not a bulk superconductor but that slight electron doping brings it back to being equivalent to undoped 111 LiFeAs, $T_c = 18$ K. Since Li and Na are isoelectronic, comparable T_cs, as seen for the doped 122s in Table II, are expected. Xia *et al.* (2010) prepared single crystal $Na_{1-\delta}Fe_{0.95}Co_{0.05}As$ ($T_c = 19$ K) and $Na_{1-\delta}FeAs_{0.8}P_{0.2}$ ($T_c = 33$ K, a record high for P doping of an As pnictide superconductor), with resistive transition widths for both samples ~ 0.5 K. The resistivity measured up to room temperature in both compounds has no anomalies above T_c, confirming in the case of the Co doping the reported suppression of the magnetic transition by Parker *et al.* (2010).

11: McQueen *et al.* (2009a) performed a careful study of T_c in $Fe_{1+\delta}Se$ with Fe content variation and found that "stoichiometric" $Fe_{1+\delta}Se$, when made single phase, has $\delta = 0.01$ and $T_c = 8.5$ K, while for $\delta = 0.03$, T_c is below 0.6 K. Mizuguchi *et al.* (2009) studied FeSe doping with Te and S on the Se site and Co and Ni on the iron site. T_c rises from the initial ~ 8 K up to about 20% doping for both the S and Te, while Ni and Co both suppress T_c by 10% substitution. Replacing 10% of the Te in $Fe_{1+\delta}Te$ with S results in a depression of the magnetic transition from 72 to ~ 30 K and $T_c \sim 8.5$ K, i.e., coexistent magnetism and superconductivity (Hu *et al.*, 2009).

21311: As discussed in Sec. II.A, replacing Sc by V and P by As in Sr_2ScO_3FeP, $T_c = 17$ K, gives $T_c = 37$ K in Sr_2VO_3FeAs (Zhu *et al.*, 2009b). Replacing V by $Mg_{0.2}Ti_{0.8}$ increases T_c up to 39 K (Sato *et al.*, 2010), with a c axis spacing of 15.95 Å. A derivative structure of 21311 is the 2(1.5)411—doubled to preserve integer ratios, known as the "43822" structure (Kawaguchi *et al.*, 2010). This 43822 extension of the 21311 structure follows the idea (see, e.g., Ogino *et al.*, 2010a) of inserting or "doping" more layers between the FeAs planes to expand the c axis, based on the correlation that T_c and c axis spacing scale in the first four structures: $FeSe_{1-y}$ ($T_c = 8$ K, 5.49 Å), LiFeAs ($T_c = 18$ K, 6.36 Å), $Ba_{0.6}K_{0.4}Fe_2As_2$ ($T_c = 38$ K, 6.65 Å), $SmFeAsO_{1-x}F_x$ ($T_c = 55$ K, 8.44 Å). (Note that, within a given structure, T_c does not scale with c axis spacing, e.g., 1111 $LaFeAsO_{1-x}F_x$ has $T_c = 26$ K and $c = 8.73$ Å.) Ogino *et al.* (2010c) reported $Ca_2(Mg_{0.25}Ti_{0.75})_{1.5}O_{\sim 4}FeAs$ to have $T_c^{mid} = 47$ K, with a c axis spacing of 33.37 Å. This related structure is still tetragonal, but has space group $I4/mmm$, i.e., the same as the 122 structure which has an atom in the body center of the unit cell, and can be further expanded according to $Ca_{n+1}(M, Ti)_nO_{3n-1}Fe_2As_2$, $M =$ Sc, Mg (Ogino *et al.*, 2010a; Shimizu *et al.*, 2011), with n equal to the number of intercalated layers. As yet, only the discovery works discuss

this further progression of seeking higher T_c by stretching the c axis and the distance between the FePn/Ch layers so that understanding 21311 and derivative structures is still a work in progress.

122*: The discovery of superconductivity in this structure, before the correct stoichiometry as it presently is understood $(K_{0.8}Fe_{1.6}Se_2)$ was worked out, was in the nominal composition $K_{0.8}Fe_2Se_2$ by Guo *et al.* (2010), with a T_c^{onset} determined resistively in polycrystalline material of 30 K. Within weeks of the publication of Guo *et al.*, Krzton-Maziopa *et al.* (2011) reported superconductivity at $T_c = 27.4$ K in single crystals of $Cs_{0.8}Fe_2Se_2$. Fang *et al.* (2011b) then reported $T_c = 20$ K in $TlFe_{1.7}Se_2$ (nominal composition), and also—in order to affect the known (Zabel and Range, 1984) Fe-sublattice deficiency in the $TlFe_2Se_2$ compound—prepared single crystals of $Tl_{1-y}K_yFe_xSe_2$ ($1.50 \leq x \leq 1.88$, $0.14 \leq y \leq 0.57$) where the compositions were determined using energy dispersive x-ray spectrometry. For $1.78 \leq x \leq 1.88$, Fang *et al.* observed superconductivity in their samples, sometimes with multiple dips in ρ starting already at 40 K with decreasing temperature, with T_c ($\rho \rightarrow 0$) ≈ 30 K. It is interesting to note that Zhang and Singh (2009) *predicted* $TlFe_2Se_2$ as a possible parent compound for superconductivity. Rounding out the list of discovery of superconductivity in $A_{0.8}Fe_{1.6}Se_2$ ($A = $ K, Rb, Cs, Tl), C.-H. Li *et al.* (2011) reported superconductivity at $T_c^{onset} = 31$ K in single crystals of $Rb_{0.8}Fe_2As_2$ (nominal composition.)

Although the 122* structure is relatively new, some T_c versus doping information is available. The most important parameter for superconductivity is not the addition of an element to the parent compound (as is necessary for most of FePn/Ch and particularly 1111 and 122), but rather, as mentioned in Sec. II.A when the structure of 122* was first discussed, insuring the order of the Fe vacancies peculiar to the 122* structure. Bao *et al.* (2011b) (see also Ye *et al.*, 2011) reported that the metallic behavior (and the super-conductivity) in these materials is centered at the composition $K_{0.8}Fe_{1.6}Se_2$ (or $A_2Fe_4Se_5$) where the Fe2 sites (see Fig. 6, 16 per unit cell) can be completely occupied and the Fe1 sites (Fig. 6, 4 per unit cell) completely empty. In a contrasting work, Han *et al.* (2011) argued that their data are consistent with disorder being critical for the superconductivity, although they measured a degradation of superconductivity for samples left at room temperature over a time period of days that is unreported by others. Also, Z. Wang *et al.* (2011), in a transmission electron microscopy study of $K_{0.8}Fe_xSe_2$, concluded that the superconducting samples have Fe-vacancy disorder. This question continues to be of central interest in 122* materials.

Partially substituting the smaller S (i.e., effectively "chemical pressure") for Se in $K_{0.8}Fe_{1.7}SSe$, Guo *et al.* (2011a) found $T_c(\rho \rightarrow 0) = 24.8$ K, while both L. Li *et al.* (2011) and Wang, Lei, and Petrovic (2011b) found essentially no suppression in T_c when only 20% of the Se is replaced by S. T_c is fully suppressed by 80% substitution of Se by S (Lei *et al.*, 2011). Zhou *et al.* (2011) in a series of Co dopings in crystalline material found that T_c was suppressed below their lowest temperature of measurement (5 K) already in $K_{0.8}Fe_{1.70}Co_{0.01}Se_2$ (composition determined by inductively coupled plasma atomic emission spectroscopy). This result, if

it withstands scrutiny concerning possible alteration of the important-for-superconductivity Fe-sublattice vacancy ordering, would be a record in FePn/Ch for change of T_c with Co-for-Fe substitution.

b. Correlation between T_c, T_S, and T_{SDW}

Phase diagrams of T_c, T_S, and T_{SDW} do not exist in either the 111 or 21311 structures, since there are not enough data (e.g., only one indication of magnetism in 21311 to date, Sefat *et al.*, 2010). A phase diagram for $FeSe_xTe_{1-x}$ has been produced (Martinelli *et al.*, 2010) using neutron diffraction to determine the structural and magnetic transitions. T_S and T_{SDW} remain coincident and finite with increasing Se doping for $x \leq 0.075$—decreasing from 72 K at $x = 0$ down to 43 K at $x = 0.075$, whereas superconductivity is induced increasing Se for $x \geq 0.05$, i.e., there is a range of Se composition where long range magnetism and superconductivity coexist. Katayama *et al.* (2010) offered a competing phase diagram for $FeSe_xTe_{1-x}$, with spin glass behavior for $0.15 \leq x \leq 0.3$, with no range of Se composition with coexistence of long range magnetism and superconductivity. Further, these $FeSe_xTe_{1-x}$ phase diagrams are similar to those of K doped $BaFe_2As_2$ (Fig. 11), Ir and Rh doped $SrFe_2As_2$ (Fig. 13) and P doped $BaFe_2As_2$ (Fig. 14) and $SrFe_2As_2$ in that T_{SDW} does not coincide with or smoothly join T_c in the phase diagram. In the 122* structure, Bao *et al.* (2011b) presented a phase diagram for $K_xFe_{2-x/2}Se_2$ in which the magnetic transition versus x varies from ≈ 520 K determined by χ (559 K from neutron scattering) for $x \approx 0.8$ down to ≈ 475 K for $x \approx 1.0$, while T_c remains constant at around 30 K for $0.77 \leq x \leq 0.86$ and becomes abruptly 0 (insulating phase) for $x > 0.86$. The only structural transition in 122* materials is the ordering of the Fe atoms on the two sublattices (Fe1 and Fe2, see Fig. 6), changing the structure from the disordered tetragonal 122 structure ($I4/mmm$ symmetry) at high temperature with random defect occupation of the Fe1 and Fe2 sublattices to the ordered-defect tetragonal 122* structure (Fig. 6, $I4/m$ symmetry) where the vacancies are preferably on the Fe1 site, below T_S. Zavalij *et al.* (2011) gave an occupation of the Fe1 site in their ordered superconducting $K_{0.8}Fe_{1.6}Se_2$ and $Cs_{0.8}Fe_{1.6}Se_2$ of 3.2%–7.8% and held open the possibility that this Fe1 site occupation is only in isolated small domains. According to Bao *et al.* (2011b) the Fe-defect ordering transition occurs at 578 K for $x = 0.82$ and ≈ 500 K for $x = 0.99$. Liu *et al.* (2011), using resistivity and susceptibility measurements, found that the transition they associate with the vacancy ordering transition T_S is generally 10–20 K higher than T_N (see Table I), just as observed by Bao *et al.* (2011b), in all of the $A_{0.8}Fe_{1.6}Se_2$ systems they studied with the lowest $T_S = 512$ K for $A_{0.8} = Tl_{0.4}Rb_{0.4}$.

C. Coexistence of magnetism and superconductivity in FePn/Ch superconductors

From the discussion above, experimentally it is clear that superconductivity coexists with magnetism in a number of FePn/Ch superconductors, including $Ba_{1-x}M_xFe_2As_2$ (Fig. 11), a large number of different transition metal dopants (see Table II) in $BaFe_{2-y}TM_yAs_2$ (Fig. 12 for TM = Co), $SrFe_{2-y}TM_yAs_2$ (TM = Rh—Fig. 13, Ir, Pd), $MFe_2As_{2-z}P_z$

(M = Ba—Fig. 14, Sr), Na$_{1-\delta}$FeAs, FeTe$_{1-x}$Se$_x$ and the ordered-defect 122* structure $A_{0.8}$Fe$_{1.6}$Se$_2$ (A = K, Rb, Cs, Tl). Certainly other doped systems, e.g., Ca and Eu 122s, would likely show coexistence as well, when sufficient phase diagram data are gathered. On the other hand, it is equally clear that magnetism is suppressed by doping before the appearance of superconductivity in systems such as LnFeAsO$_{1-x}$F$_x$ (Ln = Pr—Fig. 9, La, Ce—Fig. 10, Nd, and possibly Sm).

The issue that researchers have considered is the following: when coexistence is indicated in the phase diagram, do magnetism and superconductivity evolve from the same conduction electrons on a microscopic scale?

Coexistent magnetism and superconductivity evolving from different bands, as is the case, for example, (see Gupta, 2006) in the quaternary borocarbides RENi$_2$B$_2$C, where RE is a rare earth, is simply magnetic ordering independent of (uncoupled from) the superconductivity, although the magnetically aligned spins can cause pair breaking and thus the superconductivity is coupled to the magnetism. Interestingly, this kind of negative influence of the magnetic rare earth ions on the superconductivity seen in the borocarbides has one comparison example in FePn/Ch, in EuFe$_2$As$_2$ under pressure, due to the antiferromagnetism on the Eu sublattice affecting the superconductivity on the Fe sublattice. In HoNi$_2$B$_2$C with decreasing temperature in an applied field of 0.2 T (Gupta, 2006) the resistivity ρ with decreasing temperature first goes to 0 at $T_c \approx 7.6$ K, followed by a finite value of ρ at somewhat lower temperature ≈ 5 K, where the magnetic Ho rare earth ions undergo an ordering transition followed by *reentrance* into the superconducting state again below 4.4 K. In EuFe$_2$As$_2$ under 3.1 GPa (Kurita *et al.*, 2011), $\rho \to 0$ at $T_c \approx 28$ K, then ρ reenters the normal state around the antiferromagnetic ordering temperature of T_N = 23 K, followed by $\rho \to 0$ again below 18 K.

However, this is the interaction of the *Eu* magnetic spins on the superconducting Fe electrons, i.e., not the sometimes observed positive interaction discussed in this review between the magnetism and superconductivity on the same Fe electrons (see, in particular, Sec. IV.A.1 on the spin resonance in INS below T_c). Thus, the question in FePn/Ch is whether there is coupling between the (antiferro)magnetic and superconducting order parameters, i.e., unconventional superconductivity.

Certainly some theories (see Sec. IV) suggest that the answer to this question is yes. There is also strong evidence experimentally for microscopic coexistence coming from the same Fe 3d electrons, particularly in Co doped BaFe$_2$As$_2$ which has excellent sample homogeneity. Prozorov *et al.* (2009), using magneto-optic imaging of Meissner screening, found homogeneous superconductivity on a scale of 2–4 μm in BaFe$_{2-x}$Co$_x$As$_2$ over the whole superconducting dome. Laplace *et al.* (2009 and 2010), using NMR, found lack of electronic inhomogeneity down to the nanometer scale in underdoped BaFe$_{1.88}$Co$_{0.12}$As$_2$. Julien *et al.* (2009), also using NMR, found homogeneous coexistence of magnetism and superconductivity in BaFe$_{1.90}$Co$_{0.10}$As$_2$ down to the sub-nanometer scale. Pratt *et al.* (2009a) found in their neutron scattering work that the integrated antiferromagnetic intensity in the underdoped, coexistent FePn superconductor

BaFe$_{1.906}$Co$_{0.094}$As$_2$ is "substantially" reduced when super-conductivity sets in at 17 K. This implies a direct coupling between the superconductivity and magnetism, as seen in, for example, the unconventional heavy fermion superconductor UPt$_3$ (Aeppli *et al.*, 1988) and is consistent with microscopic homogeneity such as reported by Prozorov *et al.* (2009) and inferred from thermodynamic and transport measurements (Ni *et al.*, 2008b).

However, there are contrary data. Shen *et al.* (2011) argued for phase separation (islands of superconductivity) in their single crystals of 122* K$_{0.8}$Fe$_{1.6}$Se$_2$ (approximate composition), although Shermadini *et al.* (2011) presented μSR data arguing for microscopic coexistence of superconductivity and magnetism in single crystal Cs$_{0.8}$Fe$_2$Se$_2$. There is certainly discussion about coexistence of superconductivity and magnetism for K doped BaFe$_2$As$_2$ where, as mentioned in Sec. II.B.2.b, there are sample homogeneity issues. For example, Park *et al.* (2009), using magnetic force microscopy and μSR measurements on Ba$_{1-x}$K$_x$Fe$_2$As$_2$, found the magnetic and superconducting regions to be mesoscopically separated, on a scale of ~65 nm. Using point contact Andreev reflection spectroscopy, Lu *et al.* (2009) in both K doped and Co doped BaFe$_2$As$_2$ found their results also consistent with mesoscopic-scale phase separation, and no true microscopic coexistence of magnetism and superconductivity in the same electrons.

Lu *et al.*, however, raised the issue of whether this phase separation in K doped BaFe$_2$As$_2$ could be due to crystalline inhomogeneity. This is the conclusion of Rotter *et al.* (2009) in the case of underdoped Ba$_{1-x}$K$_x$Fe$_2$As$_2$ (which, as discussed in this review, is known to have ±5% K inhomogeneity). Using Mössbauer spectra of their underdoped Ba$_{1-x}$K$_x$Fe$_2$As$_2$, Rotter *et al.* found at lower temperatures that all domains in the sample are antiferromagnetically ordered. Thus, the theorists' proposals (section IV), that superconductivity in FePn/Chs is intimately connected with magnetism and spin fluctuations, found at least partial support from experimental measurements. Sample quality issues (see Sec. V), particularly in the defect structure 122*s, still need to be resolved, however, to draw clear conclusions on this coexistence question.

D. T_c and T_S/T_{SDW} versus pressure

As discussed in the Introduction, the pressure dependence of the T_c of these FePn/Ch materials can be quite significant, and of interest for understanding the relative importance of various factors, e.g., lattice spacing or tetrahedral angle, that affect superconductivity. For example, as discussed above (see Fig. 7) T_c scales with the a axis spacing in REFeAsO$_{1-x}$. Thus, pressurizing REFeAsO$_{1-x}$ for the smaller rare earth ions Sm and Nd (which are at or below the peak in T_c versus the increasing a axis lattice parameter in Fig. 7), results in a monotonic decrease in T_c with increasing pressure as shown in Fig. 15. For the larger rare earth ions in REFeAsO$_{1-x}$ such as La that are to the right of the Fig. 7 peak in T_c with increasing a axis, pressure first increases T_c, followed thereafter by a decrease; see Figs. 15 and 16, which focus on T_c versus pressure for LaFeAsO$_{1-x}$F$_x$. Thus far, there is no evidence for pressure suppressing magnetism just at the point that superconductivity
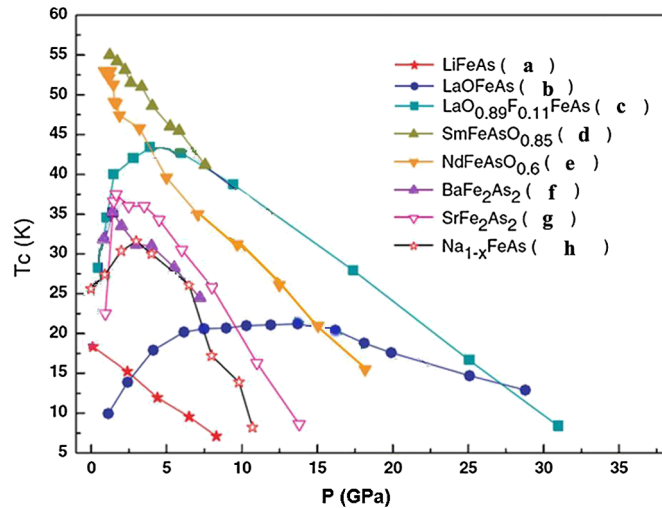
FIG. 15 (color online). T_c vs pressure in representative FePn/Ch superconductors. As shown, while some systems undergo an initial T_c increase vs pressure because pressure optimizes some controlling parameter (see discussion), a number of systems are already at their maximum T_c at zero pressure. Note the difference in the two 111 compounds. The basis for this figure is from Zhang et al. 2009a, whose data for $Na_{1-\delta}FeAs$ are shown (h). The other references are (a) Zhang et al., 2009b, (b) Okada et al., 2008, (c) Takahashi et al., 2008a, (d) Yi et al., 2008, (e) Takeshita et al., 2008, (f) Mani et al., 2009, and (g) Igawa et al., 2009. Note that for $BaFe_2As_2$ and $SrFe_2As_2$ T_c is zero until finite pressure. For an early review of the effect of pressure on the FePn/Chs, see Chu and Lorenz (2009). The effects of nonhydrostatic pressure can be quite significant, see discussions of $BaFe_2As_2$ and $CaFe_2As_2$.

appears in those samples (such as undoped 1111 and 122) where pressure induces T_c in a nonsuperconducting parent compound. In fact, several of underdoped 1111 and undoped $SrFe_2As_2$ show evidence under pressure for coexistence of magnetism and superconductivity.

Technically, pressure is typically applied in the 10 to 20 kbar range (1 to 2 GPa) via a metal (often BeCu alloy) clamp arrangement, while higher pressures use some form of diamond anvil cell. The metal clamp or diamond cell contains
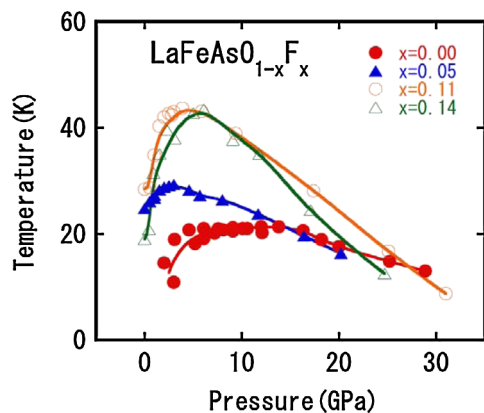

FIG. 16 (color online). T_c is plotted on the y axis vs pressure for electron doped $LaFeAsO_{1-x}F_x$ for various x. The data for $x = 0.0$ and 0.11 are reproduced in Fig. 15 for comparison with the other FePn/Ch superconductors. From Takahashi et al., 2008b.

some liquid pressure transmission medium (e.g., Daphne oil) that remains liquid (i.e., continues to give approximately hydrostatic conditions) to ~1 GPa upon application of pressure at room temperature. When the pressure medium solidifies upon cooling or at room temperature at higher pressures, shear strains can occur causing possible nonreproducibility of properties in samples where shear (see discussion of $CaFe_2As_2$ below) is important. For a comparison of the effects of pressure media on the effect of T_c vs P in $BaFe_2As_2$, see Duncan et al. (2010).

1. 1111 structure

The pressure response of T_c in electron doped $LaFeAsO_{1-x}F_x$ is positive, irregardless if the sample is underdoped, optimally doped, or overdoped as shown in Fig. 16. The initial slope $dT_c/dP|_{P=0} = +2$ K/GPa for $x = 0.05$ (Takahashi et al., 2008a). For optimally doped $LaFeAsO_{0.89}F_{0.11}$, Takahashi et al. measured the behavior of T_c with pressure all the way to 30 GPa [Fig. 15, data set (c), and Fig. 16]: initially T_c goes up to 43 K at 4 GPa as mentioned in the Introduction, with $dT_c/dP|_{P=0} = +3$ K/GPa, and then decreases monotonically to 9 K at the highest pressure. In a follow up work, Takahashi et al. (2008b) completed the T_c–P phase diagram, Fig. 16, showing that overdoped $LaFeAsO_{0.86}F_{0.14}$ behaves similarly to optimally doped material, while the pressure variation of T_c in undoped LaFeAsO is similar in sign but smaller in magnitude.

T_c versus P measurements for other 1111s have returned varied results. Lorenz et al. (2008) measured $SmFeAsO_{1-x}F_x$ up to 1.7 GPa and found, contrary to the behavior shown in Fig. 16 for the La analog, that T_c increases with pressure for undoped material, and decreases with pressure for an overdoped composition. Lorenz et al. also found that T_S/T_{SDW} decreases from ~100 K at an initial rate of 3.7 K/GPa (i.e., for a total suppression of only 6 K in the pressure range of measurement) in the underdoped $SmFeAsO_{0.95}F_{0.05}$. This is comparable to work on oxygen-deficient $NdFeAsO_{1-x}$ by Takeshita et al. (2008), where for an underdoped $x = 0.15$ sample they found that T_S/T_{SDW} decreases from ~140 K at an initial rate of 5 K/GPa. This decrease in T_S/T_{SDW} in $NdFeAsO_{0.85}$, which is difficult experimentally to determine from the resistivity measured under pressure for higher pressures, is not at a high enough rate to imply suppression of T_S/T_{SDW} by the time that an applied pressure of 10 GPa gives a drop in ρ (but not completely to 0) at around 15 K in this material. Thus, the question of whether pressure suppresses T_S/T_{SDW} in 1111 before superconductivity appears is answered in the negative, at least in these two underdoped cases where T_{SDW} could be measured.

The work of Takeshita et al. on optimally doped $NdFeAsO_{0.6}$ showed [see Fig. 15, data set (e)] a monotonic decrease in $T_c(P = 0) = 53$ K with increasing pressure up to their maximum pressure of 18 GPa since, as discussed, Nd is a smaller rare earth, versus Takahashi et al.'s (2008b) result (Fig. 16) of initial increase in T_c with applied pressure for the large La in optimally doped $LaFeAsO_{0.89}F_{0.11}$. Further, Takeshita et al. found that T_c for underdoped $NdFeAsO_{0.8}$ decreases from $T_c(P = 0) = 41$ K monotonically with increasing pressure, contrary to the Lorenz et al. (2008) result

that pressure increases T_c in underdoped $SmFeAsO_{1-x}F_x$ even though Sm is smaller than Nd.

2. 122 structure

Interestingly, the inducement of superconductivity via application of pressure in the undoped MFe_2As_2 mother compounds revealed important differences between $M =$ Ca and other MFe_2As_2, yet one further example of the richness and variety of behavior in FePn/Ch, that would perhaps have remained unknown without the application of pressure.

$BaFe_2As_2$ was reported (Alireza *et al.*, 2009) to become superconducting with T_c^{max} at ~ 29 K at $P = 4.5$ GPa with no superconductivity below 2.8 GPa versus Mani *et al.*, see Fig. 15, who reported $T_c^{max} \sim 35$ K at 1.5 GPa. Both works involved single crystals. Kimber *et al.* (2009) reported $T_c = 31$ K for $P = 5.5$ GPa, in somewhat better agreement with Mani *et al.* Interestingly, Kimber *et al.* (2009) found (using neutron powder diffractometry) that, just as Lee *et al.* (2008) pointed out at *zero* pressure for 1111 and 122 FePn superconductors as a function of doping, that the maximum T_c in their pressure work on $BaFe_2As_2$ corresponds to the pressure where the $FeAs_4$ tetrahedra are regular, with an angle of $109.47°$. At zero pressure, the irregular tetrahedra in undoped $BaFe_2As_2$ have a As-Fe-As bond angle of $108.5°$. Kimber *et al.* noted that the structural phase transition in $BaFe_2As_2$ appears to be suppressed with increasing pressure at ~ 1.3 GPa before superconductivity appears around 2.2 GPa. However, Fukazawa *et al.* (2008), using NMR measurements on polycrystalline material up to 2.5 GPa and resistivity measurements up to 9 GPa, argued that T_{SDW} is suppressed only slowly with pressure, about -6.7 K/GPa, and is still finite (> 70 K) over the entire pressure region (2.2–6 GPa) of the superconducting dome of Kimber *et al.*.

Thus, due to the difficulty of the experimental technique, pressure measurements sometimes return conflicting results. In the case of $BaFe_2As_2$ (see also the discussion of $CaFe_2As_2$ below), Yamazaki *et al.* (2010) used a quite hydrostatic cubic anvil apparatus up to 14 GPa on single crystals. They argued that the earlier results [including the data shown in Fig. 15, data set (f)] were strongly affected by a small uniaxial stress along the c axis under nonhydrostatic conditions, stabilizing islands of tetragonal phase and causing filamentary superconductivity. They found no coexistence of magnetism and superconductivity, and stated that T_{SDW} is suppressed only at 10 GPa (consistent with the NMR results of Fukazawa *et al.*, 2008), with superconductivity occurring between 11 and 14 GPa and $T_c^{max} = 13$ K (not > 30 K) at 11.5 GPa.

Alireza *et al.* (2009) further reported $T_c^{max} \sim 27$ K at $P = 3.2$ GPa for $SrFe_2As_2$, while Takahashi *et al.* (2008b) found T_c (~ 4 GPa) for $SrFe_2As_2$ to be 34 K, in agreement with Igawa *et al.* (2009) and Kotegawa, Sugawara, and Tou (2009), the former data being displayed in Fig. 15, data set (g). Kotegawa, Sugawara, and Tou (2009) were able, unlike most pressure works, to measure a fairly complete set of T_S/T_{SDW} values versus pressure and formed a phase diagram versus pressure where T_S/T_{SDW} was still finite (at ~ 105 K) after superconductivity was already induced at around 3.6 GPa. Thus, their phase diagram was similar to those with doping discussed above (e.g., $Ba_{1-x}K_xFe_2As_2$ or

$SrFe_{2-x}Rh_xAs_2$, Figs. 11 and 13, respectively) where T_S/T_{SDW} does not join or intersect the superconducting dome, and provides another example of coexistence of magnetism and superconductivity.

Uhoya *et al.* (2010) reported T_c versus pressure for $EuFe_2As_2$, with $T_c = 22$ K at 2 GPa rising up to $T_c^{max} = 41$ K at 10 GPa, the highest pressure-induced T_c of any of the undoped 122 parent compounds. Note that Eu undergoes a valence change to nonmagnetic Eu^{3+} between 3 and 9 GPa, the pressure region where T_c rises monotonically with increasing pressure.

Concerning $CaFe_2As_2$, first reports (Torikachvili *et al.*, 2008) for $T_c(P)$ for $CaFe_2As_2$ showed a superconducting dome that started at the much lower pressure, compared to $M =$ Ba, Sr, of 0.23 GPa, with a peak at only $T_c = 12$ K at 0.5 GPa. In addition, this pressure work on $CaFe_2As_2$ found a new, additional transition [identified later (Kreyssig *et al.*, 2008), as a "collapsed" tetragonal structure] at ~ 100 K that appeared at 0.55 GPa and moved to higher temperature with increasing pressure. Park *et al.* (2008) also found superconductivity in $CaFe_2As_2$, with $T_c \sim 13$ K at 0.69 GPa. After significant further work, the sensitivity of the structural transitions to different pressure conditions was solved (Canfield *et al.*, 2009a; Yu *et al.*, 2009) using helium gas as a more nearly perfect hydrostatic pressure medium [cf. the discussion of $T_c(P)$ in $BaFe_2As_2$ above]. The result is that, under improved hydrostatic conditions, there is actually no superconductivity in $CaFe_2As_2$ under pressure up to 0.6 GPa, i.e., the previous observations of superconductivity were due to shear stress from the pressure medium. The new structural phase transition (found in the hydrostatic helium to be at 0.4 GPa rather than the originally reported 0.55 GPa) is hysteretic in both temperature and pressure.

3. 111 structure

Gooch *et al.* (2009) reported a monotonic decrease of T_c with increasing pressure in LiFeAs at a rate of 1.5 K/GPa, in agreement with the data shown in Fig. 15 from Zhang *et al.* (2009b), data set (a). In $Na_{1-\delta}FeAs$, Zhang *et al.* (2009a) reported an increase of T_c from 26 K up to 31 K at 3 GPa, followed by a sharp decrease down to $T_c = 8$ K by 11 GPa, Fig. 15, data set (h). Presumably, LiFeAs under pressure behaves differently from $Na_{1-\delta}FeAs$ due to the smaller ionic radius of Li vs Na, i.e., LiFeAs is already "precompressed" (Zhang *et al.*, 2009b). The $T_c = 6$ K phosphorous analog of LiFeAs, LiFeP, discovered by Deng *et al.* (2009) has been studied under pressures up to 2.75 GPa by Mydeen *et al.* (2010). T_c declines monotonically with increasing pressure at a rate of 1.2 K/GPa, similar to the result for LiFeAs.

4. 11 structure

As mentioned in the Introduction, Margadonna *et al.* (2009b) found that 7 GPa increases the T_c of FeSe from 8 K at zero pressure up to 37 K, with T_c already 27 K at 2.6 GPa, followed by a decrease down to 6 K as pressure increases to 14 GPa. FeSe has a much larger compressibility (approximately twice that of LiFeAs, approximately three times that of 1111) than other FePn/Ch superconductors, at least partially explaining the large response of T_c to

pressure. However, the explanation of Kimber *et al.* (2009) for their observed maximum in T_c versus pressure for $BaFe_2As_2$ (which was called into question because of implied nonhydrostatic effects by Yamazaki *et al.*, 2010) that the tetrahedral bonding angle approached the optimal 109.47° at that pressure does not hold for the work of Margadonna *et al.* on FeSe. They observed rather that the tetrahedral bonding angle in FeSe, which starts around 111.5°, *increases* monotonically with pressure, leaving changes in the band structure with the much changed interatomic spacing with pressure (the c axis contracts by 7.3% at 7.5 GPa vs 4% at 6 GPa in $BaFe_2As_2$, Kimber *et al.*, 2009) as a possible explanation. Another possible explanation for the enhanced T_c with pressure of FeSe was pointed out by Imai *et al.* (2009), who found in an NMR study that applied pressure enhances spin fluctuations (proportional to $1/T_1T$) above T_c.

A positive enhancement of T_c with increasing pressure has also been found in $FeSe_{1-x}Te_x$ for $x = 0.43$ (Gresty *et al.*, 2009) and 0.50 (Horigane *et al.*, 2009) with an increase of T_c from ~15 K at zero pressure up to ~25 K at 2 GPa, while for $x = 0.75$ (Mizuguchi *et al.*, 2010b) the T_c enhancement at 1 GPa is only ~1.5 K [see Mizuguchi and Takano (2010) for an overview of FeCh].

5. 21311 structure

Sato *et al.* (2010) found that pressure monotonically increased the T_c of $Sr_2Mg_{0.3}Ti_{0.7}O_3FeAs$ from 37 K at $P = 0$ up to 43 K at 4.2 GPa. Kotegawa *et al.* (2009) showed that 4 GPa increased T_c of Sr_2VO_3FeAs from 36 K ($P = 0$) to 46 K, while the same pressure decreased the T_c of Sr_2ScO_3FeP from 16 K ($P = 0$) to 5 K. They discussed this difference in pressure effect as being due to the height of the pnictogen, as discussed in the theory of Kuroki *et al.* (2009) in Sec. II.A.

6. 122* structure

Guo *et al.* (2011b) reported that T_c in $K_{0.8}Fe_{1.7}Se_2$ remains constant with pressure at ≈ 32 K up to 1 GPa, and then falls monotonically to 0 at around 9.2 GPa. Seyfarth *et al.* (2011) reported that T_c in $Cs_{0.8}Fe_2Se_2$ is approximately constant at ≈ 30 K also up to 1 GPa, and then falls monotonically to $T_c^{onset} \approx 12$ K at 7.5 GPa.

E. T_c versus magnetic field

Measuring the upper critical field of a superconductor $H_{c2}(T)$ has impact not only on potential applications, but also helps the understanding of the superconductivity. The upward curvature of $H_{c2}(T) \parallel c$ axis with temperature in both the 1111 and 122 FePn superconductors has been interpreted as consistent with the existence of two superconducting gaps, while the size of $H_{c2}(T \to 0)$ (60–400 T in 1111, depending on sample and crystal orientation) is consistent with strong coupling (Jo *et al.*, 2009); see the following discussion. Two straightforward models are commonly used to fit the H_{c2} data and extract qualitative conclusions, sometimes followed by more intricate analysis involving, e.g., two-band models and more adjustable parameters. The weak coupling Werthamer, Helfand, and Hohenberg (1966) (WHH) model assumes that

H_{c2} is limited at higher fields and lower temperatures by spin orbit pair breaking in addition to spin paramagnetic effects (where alignment of the spins in the applied field breaks the pairs). When spin paramagnetism pair breaking effects dominate those from spin orbit coupling, then the Pauli paramagnetic limiting model is used. Qualitatively (see, e.g., the original paper by WHH), Pauli paramagnetic limiting being the dominant mechanism over spin orbit effects causes saturation ("flattening") of the upper critical field at lower temperatures and higher fields $[T_c(H)/T_c(H = 0) \lesssim 0.2$–$0.4]$. Because paramagnetic limiting is isotropic, a stronger effect is found in the higher critical field direction (H in plane in FePn/Ch) which reduces the anisotropy in the two field directions at lower temperatures (Putti *et al.*, 2010). As discussed below, this reduction in the $H_{c2}(\parallel ab)/H_{c2}(\perp ab)$ anisotropy at higher fields and lower temperatures is indeed often found in FePn/Ch. When the upper critical field data qualitatively show such saturation, but $H_{c2}(T = 0)$ exceeds the weak coupling BCS paramagnetic limit ($\mu_0 H_p^{BCS} = 1.84\ T_c$, where H_p^{BCS} is in units of T and T_c has units of K), which for the observed high values of $H_{c2}(0)$ in FePn/Ch is often the case, then enhancements of the weak coupling BCS paramagnetic limit due to strong coupling effects (proportional to $1 + \lambda$, where λ is the strength of the coupling) can be considered (Schlossmann and Carbotte, 1989). Thus, measurements of $H_{c2}(0)$ are often used as evidence for strong coupling effects being present (see, e.g., Jo *et al.*, 2009).

A more difficult measurement, that of the temperature and orientation dependence of the lower critical field (where flux first penetrates the superconductor), $H_{c1}(T)$ (~ 10 mT as $T \to 0$), of an underdoped, oxygen-deficient single crystal of $PrFeAsO_{0.9}$, $T_c = 35$ K, also was interpreted as consistent with multiple gap superconductivity (Shibauchi *et al.*, 2009).

1. 1111 structure

The excitement of the discovery of high T_cs in $LnFeAsO_{1-x}F_x$, where Ln started with La and then progressed rapidly to the smaller rare earth ions such as Sm and Nd, was fed by early measurements of very high upper critical fields $H_{c2}(T)$ required to extinguish superconductivity in these compounds. Using dc fields of up to 45 T, Jaroszynski *et al.* (2008) reported $H_{c2}(T)$ data for optimally doped polycrystalline $LaFeO_{0.89}F_{0.11}$ ($T_c = 28$ K), $SmFeAsO_{0.85}$ ($T_c = 53.5$ K), and $NdFeAsO_{0.94}F_{0.06}$ (50.5 K), finding already $H_{c2}(0)$ of 60 T for the lowest T_c sample. Jia *et al.* (2008), measuring single crystal $NdFeAsO_{0.82}F_{0.18}$, $T_c = 52$ K, at low (up to 9 T) fields found $dH_{c2}(T)/dT|_{T=Tc} = 9$ T/K for field in the ab plane, and 1.85 T/K for field in the c axis direction, i.e., an anisotropy of only about 5. Using the WHH formula $[H_{c2}(0) = -0.69 T_c dH_{c2}(T)/dT|_{T=Tc}]$ Jia *et al.* calculated $H_{c2}(0)$ in the two field directions of ~300 and 66 T. Using data up to 45 T on a similar crystal ($NdFeAsO_{0.7}F_{0.3}$, $T_c^{mid} = 47.4$ K), Putti *et al.* (2010) found the critical field slopes at T_c (10.1 and 2.1 T/K for $H \perp c$ and $H \parallel c$, respectively) to give a similar anisotropy, and calculated the coherence lengths in the ab plane and c axis directions to be 1.8 and 0.45 nm, respectively. These are quite short compared to the penetration depth, determined from various methods (see, e. g., Luan *et al.*, 2010) to be in the 100s of nm.
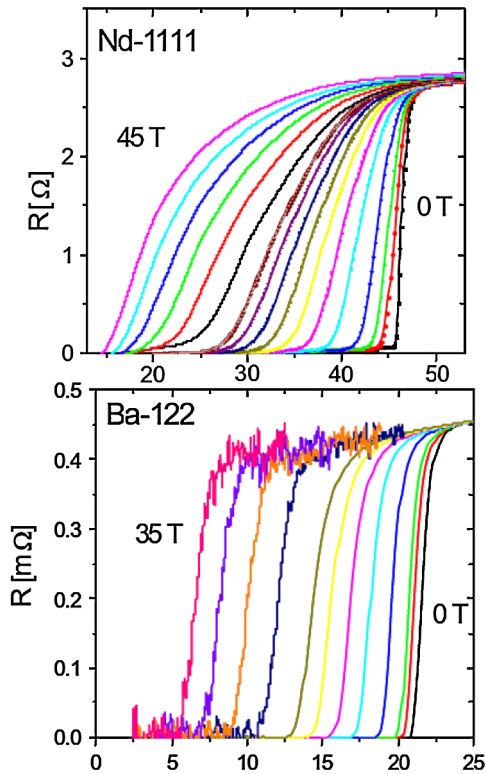
FIG. 17 (color online). Transitions into the superconducting state as measured by the resistivity as a function of field for single crystals of NdFeAsO$_{0.7}$F$_{0.3}$ (upper panel) and BaFe$_{1.8}$Co$_{0.2}$As$_2$, measured with field along the c-axis direction. From Putti *et al.*, 2010.

2. 122 structure

Critical field studies on single crystal Ba$_{0.6}$K$_{0.4}$Fe$_2$As$_2$ ($T_c = 29$ K) up to 45 T by Jo *et al.* (2009), on single crystal Ba$_{0.6}$K$_{0.4}$Fe$_2$As$_2$ ($T_c = 28$ K) up to 60 T by Yuan *et al.* (2009), on single crystal BaFe$_{2-x}$Co$_x$As$_2$ ($x = 0.076, 0.094, 0.116, 0.148, 0.20, 0.228$; $T_c = 7, 15, 23, 22, 17, 8$ K) up to 35 T by Ni *et al.* (2008b), and on single crystal BaFe$_{2-x}$Co$_x$As$_2$ ($x = 0.20$; $T_c = 22$ K) up to 35 T by Putti *et al.* (2010) allow several conclusions. Unlike 1111 but similar to 11 discussed below, the anisotropy for $H_{c2}(T)$ for 122 is only about 2–3 near T_c and essentially vanishes as $T \to 0$. The possible reasons for such isotropic $H_{c2}(0)$ values, which are in strong contrast to the cuprates, is still under discussion but include band warping in the cylindrical Fermi surfaces (see Sec. IV.A.2 which discusses ARPES measurements of the Fermiology) or multiband effects (Khim *et al.*, 2010). Also unlike 1111, whose resistive transitions broaden significantly with field presumably due to vortex depinning or dissipation, the transition widths in 122 remain fairly narrow with increasing field and merely shift downwards in temperature with increasing field. A comparison of $H_{c2}(T)$ graphs for 1111 NdFeAsO$_{0.7}$F$_{0.3}$ and 122 Co doped BaFe$_2$As$_2$ (Putti *et al.*, 2010) shown in Fig. 17 makes this latter comparison visually clear. The critical fields extrapolated to $T = 0$, whether via the WHH formula or via $H_{c2}(T) = H_{c2}(0)[1 - (T/T_c)^2]$, for 122 just as for 1111 exceed the weak-coupling Pauli paramagnetic limiting field, $H_P = 1.84k_BT_c$. Thus, the pair breaking effect of the magnetic field is qualitatively more dominated by orbital effects (WHH model) than by spin alignment effects (Pauli limit), although

consideration of the detailed interplay of the two scaled by the Maki parameter [$\alpha = \sqrt{2}H_{c2}^{WHH}(0)/H_P$] can bring more quantitative understanding (see, e.g., Kida *et al.*, 2009.)

3. 111 structure

Song *et al.* (2010) measured the critical fields up to 9 T in single crystal LiFeAs, $T_c = 19.7$ K, and found via the WHH formula $H_{c2}(0) = 83$ and 72 T for field in the ab plane and c axis directions, respectively. In addition to this small anisotropy, they found a lack of curvature in the measured $H_{c2}(T)$ curves where, as discussed, curvature in $H_{c2}(T)$ was discussed as consistent with multigap superconductivity. They also found significant broadening of the transition with increasing field, consistent with vortex dissipation. Sasmal *et al.* (2010) in their measurements of $H_{c1}(T)$ for single crystal LiFeAs found, on the other hand, evidence for a two-band gap scenario. G. F. Chen *et al.* (2009) measured the critical fields up to 14 T in a single crystal of Na$_{1-\delta}$FeAs, although T_c was only 15 K and there was no measurable ΔC anomaly at T_c. Using the WHH formula, they found $H_{c2}(0) = 60$ and 30 T for field in the ab plane and c axis directions, respectively.

4. 11 structure

Putti *et al.* (2010) measured $H_{c2}(T)$ of a single crystal of FeSe$_{0.5}$Te$_{0.5}$, $T_c = 15$ K, up to 32 T. Broadening of the transition with the field was observed, not as severe as in 1111 (Fig. 17) but much more than seen in 122. The critical field slope at T_c, $-dH_{c2}(T)/dT|_{T=T_c}$ was found to be the very high value of 25 T/K for the field in the ab plane, and 14 T/K for the field in the c axis direction, giving an anisotropy of 2 close to T_c. This anisotropy decreases at 32 T ($T_c \sim 11$ K) to $\sim$1 due to downward (not concave upwards) curvature for the ab plane field direction. $H_{c2}(T)$ measurements (Fang *et al.*, 2010; Braithwaite *et al.*, 2010) of a single crystal of Fe$_{1.11}$Se$_{0.4}$Te$_{0.6}$/FeSe$_{0.48}$Te$_{0.52}$, $T_c = 14/15$ K, in pulsed fields up to 60 T confirmed the decreasing anisotropy reported by Putti *et al.* (2010). In fact, the two curves for ab plane and c axis cross at about 40 T ($T_c = 3$–4 K) and $H_{c2}(T \to 0)$ for field in the ab plane is slightly *smaller* than for in the c axis direction, with both values for $H_{c2}(T \to 0)$ in the range 45–50 T (also exceeding the weak-coupling Pauli paramagnetic limiting field, $H_P = 1.84k_BT_c$, as just discussed for 122). This crossing of the H_{c2} curves for the ab and c directions was confirmed in dc measurements to 45 T in a single crystal of FeSe$_{0.4}$Te$_{0.6}$ by Khim *et al.* (2010).

5. 21311 Structure

Measurements (Sefat *et al.*, 2010) up to 10 T in Sr$_2$VO$_3$FeAs, $T_c \sim 33$ K, give a value of $-dH_{c2}/dT|_{T_c} = 9$ T/K. By using the WHH formula, this gives $H_{c2}(0) \approx 200$ T, comparable with values by Zhu *et al.* (2009b).

6. 122* structure

C.-H. Li *et al.* (2011) in single crystal Rb$_{0.8}$Fe$_2$Se$_2$, $T_c \approx 31$ K, reported $-dH_{c2}/dT|_{T_c}$ values of 6.78 T/K for field in the ab plane and 1.98 T/K for field along the c axis, resulting

(using the WHH formula) in $H_{c2}(0)$ values of 145 and 42 T, respectively.

Jiao *et al.* (2011) used pulsed fields up to 60 T and dc fields up to 14 T in single crystal $Tl_{0.58}Rb_{0.42}Fe_{1.72}Se_2$, $T_c = 33$ K, and reported $-dH_{c2}/dT|_{T_c}$ values of 12 T/K for field in the *ab* plane and 2 T/K for field along the *c* axis. This anisotropy decreases to 2 for $T_c \approx 20$ K, where the upper critical field is already 60 T for field in the *ab* plane. The superconducting transition temperature broadens strongly with increasing field, such as 1111 materials discussed above (see Fig. 17), again indicating strong thermal fluctuation effects in the superconducting state.

III. STRUCTURAL AND ELECTRONIC PROPERTIES: NORMAL STATE ρ, χ, C DOWN TO T_c

The present section focuses on the normal state from which the superconducting state forms, with the magnetic and structural transitions already discussed in Sec. II. Measurement of the resistivity and susceptibility, and to a lesser extent the specific heat, is often used to indicate, via anomalies in these parameters, the progression with doping of the structural and magnetic anomalies discussed in Sec. II, as shown in Fig. 18. Such measurements allow a more rapid estimate of the part of the phase diagram of particular interest in a given study, which can then be further examined with more microscopic measurement techniques (e.g., x-ray diffraction, neutron diffraction, μSR, and Mössbauer.)

In addition, the residual resistivity ratio (RRR), defined as $\rho(300 \text{ K})/\rho_0$ [$\rho_0 \equiv \rho(T \to 0)$, where the extrapolation to $T = 0$ is from the normal state above T_c if the sample is superconducting], serves as an important indicator of sample quality since scattering from impurities increases the residual resistivity ρ_0. Similarly, the sharpness and size of the specific heat anomaly at the superconducting transition $\Delta C(T_c)$
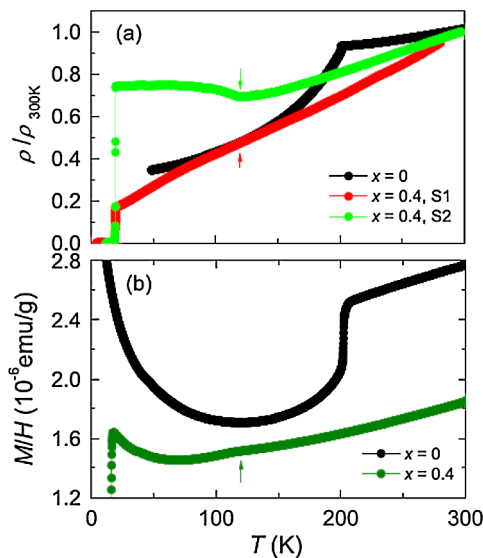
(discussed in Sec. III.B.3) also serves as a commonly used indicator of the quality of a sample.

A third use for these normal state measurements is that their temperature dependence can provide insights useful for understanding the superconductivity. For example, the temperature dependence of the resistivity in the normal state has been used in the study of FePn/Ch superconductors to determine nearness to quantum criticality in so far as ρ does not follow Fermi liquid behavior. Landau Fermi liquid behavior is $\rho = \rho_0 + AT^2$, with A a constant. Quantum critical behavior can occur (see Stewart, 2001; 2006; von Löhneysen *et al.*, 2007) at (or near) the point in a phase diagram where a second order phase transition, e.g., antiferromagnetism, has been suppressed to $T = 0$. In the case of FePn/Ch, T_{SDW} being suppressed to $T = 0$ by doping (Sec. II.B) is an obvious pathway to such quantum critical behavior, with the associated non-Fermi-liquid behavior at finite temperatures, including long range magnetic fluctuations potentially important for understanding superconductivity.

A. Resistivity and susceptibility

Some representative examples of the measurements are offered here to give an idea of the common behavior. The references given in Sec. II in the discussion of materials and their phase diagrams can also be followed to learn more about the various normal state properties of a particular compound.

In general, the resistivities of FePn/Ch superconductors are metallic in their temperature dependence ($d\rho/dT > 0$) as seen in Fig. 18 for pure and Co doped $SrFe_2As_2$ and for FeSe in Fig. 19, although $FeSe_{1-x}Te_x$, $x > 0.25$, provides counterexamples to this metallic behavior. Also, as a function of composition in 122*, there can (depending on whether the composition is optimized for metallic and superconducting behavior) be a "hump" in the resistivity peaked at around 150 K, where ρ rises over a large maximum when cooling from room temperature to T_c. For samples in the insulating composition range of the phase diagram in 122*, ρ continues to rise with decreasing temperature, while optimized samples near in composition to $A_{0.8}Fe_{1.6}Se_2$ show ρ decreasing

FIG. 18 (color online). Resistivity (upper panel) and magnetic susceptibility (lower panel) of single crystal $SrFe_{2-x}Co_x$, $x = 0$, and 0.4. Arrows mark anomalies for $x = 0.4$. 2×10^{-6} emu/g is 0.7 memu/mole. Note the sample dependence in ρ for $x = 0.4$, samples S1 and S2. From J. S. Kim *et al.*, 2009b.

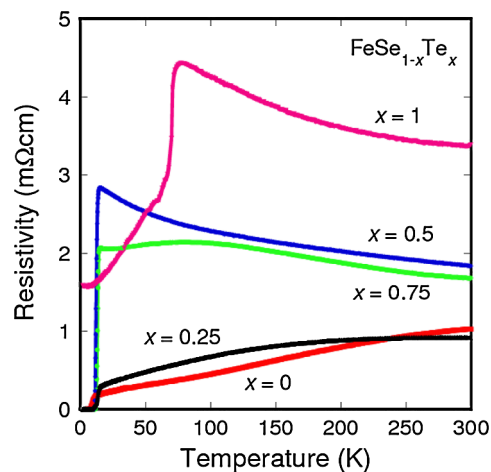FIG. 19 (color online). Resistivity vs temperature of polycrystalline $FeSe_{1-x}Te_x$. Note the anomaly at 72 K in pure FeTe (upper curve) at T_S/T_{SDW}. From Mizuguchi *et al.*, 2009.

monotonically (i.e., no hump) between room temperature and T_c (Bao *et al.*, 2011b), with decent RRR values (> 40, D. M. Wang *et al.*, 2011; ≈ 20, Luo *et al.*, 2011).

In all cases, the absolute values at room temperature for FePn/Ch are high, ≈ 1 mΩ cm (≥ 50 mΩ cm for 122*), where for a good metal (e.g., Cu or Ag) $\rho \sim 1$ $\mu\Omega$ cm. A band structure calculation (Singh, 2009) for FeSe results in small Fermi surface sections, resulting in a semimetallic classification, although in general FePn/Ch are called metallic. In the beginning of the study of FePn/Ch, the question of itinerant metal versus localized insulator (weak Coulomb repulsion U versus strong) was important for deciding how to understand the physics of these materials; see Tesanovic (2009). Rather early on, the x-ray measurements of W.-L. Yang *et al.* (2009), as discussed in the Introduction, indicated that 1111 and 122 FePn/Ch are actually similar to Fe metal, with relatively (compared to the bandwidth) small Coulomb correlation U, an even smaller Hund's coupling (diminishing the tendency to form large local moments), Fe 3d hybridized bands, and metallic behavior. Singh pointed out in general that for FePn/Ch materials, the small carrier density (which gives the high values of ρ), does not imply a small density of states $N(0)$ (in units of states/eV atom), at the Fermi energy, which in fact turns out [see discussion of the specific heat γ, proportional to $N(0)$, below] to be relatively high compared to the cuprates. This affects the scaling of $\Delta C/T_c$; see discussion in Sec. III.B.3.

The magnetic susceptibility χ shows a large anomaly at T_{SDW} in FePn/Ch structures (see Figs. 18, 20, and 21 for examples) where this transition exists (1111, 122, 122*, and some of 11). Perhaps more importantly, χ data when taken above T_{SDW} (not yet the case in 122* with their >500 K ordering temperature) give an idea about the magnetic fluctuations. As discussed in Sec. II, the structural transition occurs at higher temperature than T_{SDW} in 1111, and in 122
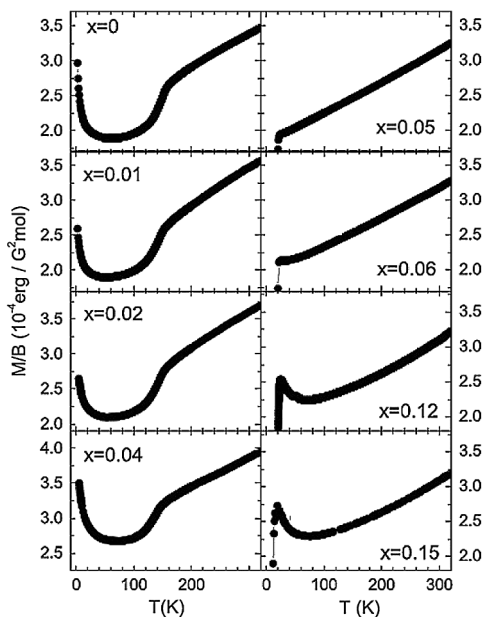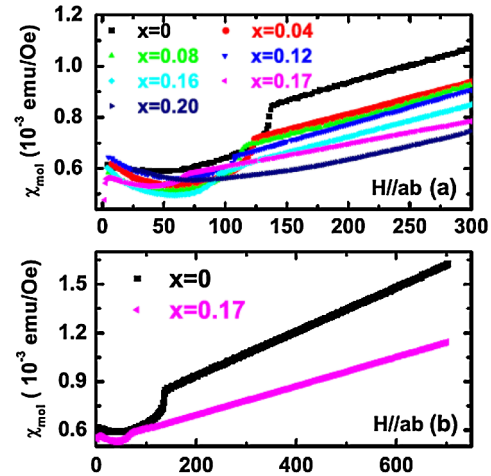

FIG. 21 (color online). Magnetic susceptibility for BaFe$_{2-x}$Co$_x$As$_2$. Note that the linearity with T, $\chi \sim T$, disappears abruptly for $x = 0.20$. From X. F. Wang *et al.*, 2009b.

after doping on the Fe or Pn sites splits the two transitions (Figs. 9, 10, 12, and 14). However, a number of early theories (Yildirim, 2008; Mazin and Johannes, 2009) suggested that the lower transition temperature magnetism causes the structural transition through a fluctuating magnetic state without long range order (see Singh, 2009 for a discussion). Profiting from development in understanding of the magnetic state, this argument was later refined (see, e.g., Nandi *et al.*, 2010, Fernandes *et al.*, 2010b) to note that the structural transition is caused by nematic magnetic fluctuations which break the tetragonal a–b axis symmetry as described in Sec. II.B.2.b where the reversal of the phase boundary in Ba(Fe$_{1-x}$Co$_x$)$_2$As$_2$, $x \approx 0.06$, was presented. Cano *et al.* (2010) discussed experiments from the point of view of their Ginzburg-Landau theory to further investigate whether magnetic fluctuations drive the structural transformation.

Instead of the above explanation for the cause of T_S, a number of theories (see, e.g., Lv, Wu, and Phillips, 2009; Turner, Wang, and Vishwanath, 2009; Lee, Yin, and Ku, 2009) as well as the experimental work of Martinelli *et al.* (2011) proposed instead that orbital ordering plays an important role for understanding the structural order. The five Fe d orbitals include two (the d_{xz} and d_{yz}) in directions that are asymmetric in the xy plane and thus could play a role in the tetragonal-orthorhombic distortion. If the orbitals in either of these two directions order, then the total energy is lowered, thus inducing the structural phase transition. ARPES (Shimojima *et al.*, 2010) and optical experiments (Akrap *et al.*, 2009; Dusza *et al.*, 2010) have been cited as consistent with orbital ordering below the magnetic transition. Yet another explanation for the structural transition involves a local Fe-moment picture described as the "Hund's rule correlation" model [see Ji, Yan, and Lu (2011) and references therein].

The other temperature range where the magnetic susceptibility and its temperature dependence might shed light on the underlying physics would be at low temperatures, where the resistivity for some systems indicates quantum criticality. There are known (Stewart, 2001; 2006; von Löhneysen *et al.*, 2007) temperature dependences in χ below ≈ 20 K

FIG. 20. Magnetic susceptibility for LaFeAsO$_{1-x}$F$_x$, $0 \leq x \leq 0.15$. Note the large anomalies at T_{SDW} up to $x = 0.04$. From Klingeler *et al.*, 2010.

that would be worthwhile to compare to the ρ data. Unfortunately, samples of the FePn/Ch appear almost uniformly to have at least some trace impurity phases that are magnetic, e.g., FeAs, Fe_3O_4, Fe (all of which also affect the low temperature specific heat discussed in Sec. II.B.3.b), which prevent the detailed analysis of the intrinsic low temperature dependence of χ.

1. 1111 structure

Kamihara *et al.* (2008) in their discovery of superconductivity in $LaFeAsO_{1-x}F_x$ reported that the undoped LaFeAsO resistivity was approximately temperature independent at 5 mΩ cm, with an anomaly at 150 K and an upturn below 100 K. Upon fluorine doping, the upturn in ρ below 100 K decreases and by $x = 0.11$ resistivity falls uniformly from room temperature (metallic behavior) with an RRR of $\sim$5.

Kamihara *et al.* (2008) reported that the susceptibility of LaFeAsO is about 0.4 memu/mole and roughly temperature independent below room temperature except for the 150 K anomaly and an upturn below $\sim$25 K. McGuire *et al.* (2008), with an expanded set of data for χ of LaFeAsO, showed that χ increases with increasing temperature above the anomaly up to room temperature by about 30%. Klingeler *et al.* (2010) extended χ for LaFeAsO up to 500 K, showing that χ continues to rise almost linearly up to the highest temperature of measurement. Klingeler *et al.* also found the same general behavior of χ increasing monotonically (see Fig. 20) starting at either T_{SDW} ($x < 0.05$) or T_c ($x \geq 0.05$) up to 300 K for seven additional compositions of $LaFeAsO_{1-x}F_x$, $0 \leq x \leq 0.15$. Note, however, that, as shown in Fig. 20, the linearity of χ with temperature does not hold for $x = 0.12$ and 0.15.

G. M. Zhang *et al.* (2009) considered the data in Fig. 20, along with similar data for MFe_2As_2 (M = Sr—see Fig. 18, Ca—Wu *et al.*, 2008a, and Ba) above the respective T_{SDW}s up to 300 K (the linearity of χ vs T for M = Sr extends up to 600 K—Mandrus *et al.*, 2010, and for M = Ba up to 700 K as shown in Fig. 21 above), as evidence for a "universal" $\chi \sim T$ dependence in FePn/Ch. They compared these results to the theory for a Heisenberg antiferromagnet (Chubukov and Sachdev, 1993) and to χ data for Cr which are approximately linear with T from 300 to 900 K (Fawcett *et al.*, 1994) as evidence for strong (antiferro)magnetic fluctuations above T_{SDW} (and indeed, as seen in Fig. 20 for $LaFeAsO_{1-x}F_x$, above T_c even after T_{SDW} is suppressed for $x > 0.04$) in FePn/Ch superconductors. Corroborating evidence for the universal $\chi \sim T$ behavior proposed by G. M. Zhang *et al.* (2009), but not remarked on by them, is the close to linear-in-temperature behavior of χ between $T_{SDW} = 180$ K and room temperature reported by Tegel *et al.* (2008a) in SrFeAsF. For further discussion of this $\chi \sim T$ behavior, see Korshunov *et al.* (2009) and Sales *et al.* (2010).

For oxygen-deficient $LnFeAsO_{1-x}$ polycrystalline samples prepared under high pressure (Miyazawa *et al.*, 2009), again $d\rho/dT$ is positive (metallic behavior), $\rho(300 K) \sim 2$ mΩ cm, and the RRR values range from $\sim$9 for La and $\sim$5 for Ce to over 20 for Sm, Gd, Pr, and Nd. For high-pressure-prepared single crystal $PrFeAsO_{0.7}$, $T_c = 35$ K, Kashiwaya *et al.* (2010) reported an anisotropy $\rho_c/\rho_{ab} = 120$ at 50 K, which is comparable to the transport anisotropies discussed below for single crystals of the other structures.

Hole doped $La_{1-x}Sr_xFeAsO$ shows metallic behavior in ρ vs T below 200 K, RRR $\sim$ 5 (Mu *et al.*, 2008a). Polycrystalline $Gd_{0.8}Th_{0.2}FeAsO$, $T_c = 56$ K, has RRR $\sim$ 5 and a magnetic susceptibility that increases below room temperature up to $\sim$0.27 emu/mole at T_c (C. Wang *et al.*, 2008).

2. 122 structure

Measurements of polycrystalline $BaFe_2As_2$ (Rotter, Tegel, and Johrendt, 2008) gave essentially constant ρ vs T from room temperature down to the T_S/T_{SDW} transition, followed by a monotonic fall off of ρ to lower temperatures with an RRR $\sim$ 5, while $Ba_{0.6}K_{0.4}Fe_2As_2$ is metallic in behavior ($d\rho/dT > 0$) down to T_c, with RRR $\sim$ 17. The same qualitative resistivity versus temperature behavior as seen in undoped $BaFe_2As_2$ is also seen in $SrFe_2As_2$, RRR = 3 (Saha *et al.*, 2009b) (see Fig. 18) and $EuFe_2As_2$ RRR = 3 (Jeevan *et al.*, 2008a). With single crystals, the anisotropy ρ_c/ρ_{ab} at 300 K in MFe_2As_2 for M = Ba, Sr, Ca, and Eu has been determined to be 150 (X. F. Wang *et al.*, 2009a), 80 (G. F. Chen *et al.*, 2008), $\geq$ 50 (Ronning *et al.*, 2008), and 7 (D. Wu *et al.*, 2009), respectively. Sample quality also plays an important role, Krellner *et al.* (2008) reported RRR = 32 for $SrFe_2As_2$ and Rotundu *et al.* reported RRR = 36 in single crystal $BaFe_2As_2$ after 30 days of annealing at 700 °C, versus the usual RRR = 5 for the unannealed sample. Krellner *et al.* (2008) also reported an increasing χ with decreasing temperature in their high quality $SrFe_2As_2$ as seen in 1111; see also Fig. 18. Undoped single crystal KFe_2As_2 has a wide range of RRR reported; see Fukazawa *et al.* (2009a) for RRR = 67, Dong and Li (2010) for RRR = 265, J. S. Kim *et al.* (2011b) for RRR = 650, and Hashimoto *et al.* (2010a) for RRR > 1200. (Samples without doping can in general be prepared with larger RRR due to the lack of any dopant-atom scattering.)

Dong *et al.* (2010b) reported that their KFe_2As_2 samples (RRR $\approx$ 90) show non-Fermi-liquid behavior, $\rho = \rho_0 + AT^{1.5}$ above $T_c \approx 3.5$ K up to 15 K in zero field or in a 5 T applied field to suppress T_c between 0.05 and 15 K. In contrast, Hashimoto *et al.* (2010a) reported that their (RRR > 1200) KFe_2As_2 sample shows Fermi liquid behavior, $\rho = \rho_0 + AT^2$, above T_c up to 10 K and Terashima *et al.* (2009), in KFe_2As_2 with RRR $\approx$ 90, reported $\rho = \rho_0 + AT^2$ between 4 and 45 K. Specific heat in field on a RRR = 650 crystal showed (J. S. Kim *et al.*, 2011b) a decreasing γ with decreasing temperature, i.e., consistent with Fermi liquid behavior. This controversy remains unresolved, although the non-Fermi-liquid result of Dong *et al.* is often cited as one proof of such behavior in FePn/Ch. Where a quantum critical point would be in the phase diagram of KFe_2As_2 to cause non-Fermi-liquid behavior is unclear, but there seems to be general agreement that KFe_2As_2 exhibits unconventional superconductivity (Fukazawa *et al.*, 2009a; Dong *et al.*, 2010b; Hashimoto *et al.*, 2010a).

Another interesting resistivity behavior seen in undoped MFe_2As_2 is that, for certain samples of M = Ba (Kim *et al.*, 2009a) and Sr (Saha *et al.*, 2009b), $\rho \rightarrow 0$ at $T_c^\rho \sim 22$ K but with no bulk indications of superconductivity (although Saha *et al.* saw diamagnetic zero-field-cooled shielding of 15% in one sample). Partial transitions in ρ at $\sim$10 K are seen in $CaFe_2As_2$ (Torikachvili *et al.*, 2009). The explanation for

these resistive transitions to superconductivity (including possible filamentary or planar defects) is still under investigation.

Considering now doped MFe$_2$As$_2$, Ahilan *et al.* (2008) pointed out that $\rho = \rho_0 + AT^1$ above $T_c = 22$ K in BaFe$_{1.8}$Co$_{0.2}$As$_2$ up to 100 K, a significant range of non-Fermi-liquid behavior. They discussed the nearness of BaFe$_{1.8}$Co$_{0.2}$As$_2$ to a magnetic instability and the possibility of this being linked to the superconductivity. Interestingly, X. F. Wang *et al.* (2009b) found that, as long as there is an SDW anomaly in the sample ($x \leq 0.17$, $T_{SDW} \sim 70$ K for $x = 0.17$), that χ for BaFe$_{2-x}$Co$_x$As$_x$ rises linearly with increasing T up to their highest temperature of measurement, generally 300 K (see Fig. 21). Ronning *et al.* (2008) reported $\chi \sim T$ for field both in the ab plane and in the c axis directions up to 350 K in CaFe$_2$As$_2$. Klingeler *et al.* (2010) reported the magnetic susceptibility for CaFe$_{2-x}$Co$_x$As$_2$ $0 \leq x \leq 0.25$ increases above T_{SDW} up to room temperature for all six compositions studied, with $\chi \sim T$ for as long as T_{SDW} remains finite (up to $x = 0.056$). For undoped BaFe$_2$As$_2$ and BaFe$_{1.83}$Co$_{0.17}$As$_2$, X. F. Wang *et al.* extended their range of measurement up to 700 K and χ is seen (Fig. 21) to rise linearly with increasing temperature for $T_{SDW} < T \leq 700$ K. These data are consistent with the arguments of G. M. Zhang *et al.* (2009), discussed above, for the existence of strong antiferromagnetic fluctuations above T_{SDW} and up to high temperature in these Co doped MFe$_2$As$_2$ alloys, $M =$ Ba and Ca. Note that the linearity in χ with T disappears when T_{SDW} is suppressed for $x = 0.20/0.065$ in the Co doped Ba [Fig. 21(a)]/CaFe$_2$As$_2$, while $\chi \sim T$ survives in LaFeAsO$_{1-x}$F$_x$, after T_{SDW} is suppressed for $x = 0.05$ and 0.06; see Fig. 20. Presumably this implies stronger fluctuations surviving in LaFeAsO$_{1-x}$F$_x$ after the magnetic transition is suppressed than in Co doped BaFe$_2$As$_2$, a point of potential interest for theorists and for neutron scattering (see Sec. IV.A.1) and NMR investigation of the fluctuations.

For further evidence for non-Fermi-liquid behavior in the resistivity of doped 122, $\rho = \rho_0 + AT$ above $T_c = 21$ K in SrFe$_{1.7}$Rh$_{0.3}$As$_2$ and in SrFe$_{1-x}$Ir$_x$As$_2$, $x > 0.4$, up to 300 K (F. Han *et al.*, 2009). Kasahara *et al.* (2010) found $\rho = \rho_0 + AT$ in single crystal BaFe$_2$As$_{1.4}$P$_{0.6}$ above $T_c = 30$ K up to 150 K, while Jiang *et al.* (2009) reported $\rho \sim T$ up to 300 K above T_c for BaFe$_2$As$_{2-x}$P$_x$, $0.6 \leq x \leq 0.9$.

3. 111 structure

Song *et al.* (2010) reported metallic behavior in the ρ of single crystal LiFeAs, with RRR ~ 35 and χ approximately (to within 10%) temperature independent from T_c to room temperature. G. F. Chen *et al.* (2009) also reported $d\rho/dT > 0$ for single crystal Na$_{1-\delta}$FeAs, but RRR was only 1.8. G. F. Chen *et al.* further reported that χ increases by about 40% approximately linearly with increasing temperature between 40 and 300 K, i.e., this would be consistent with the universal behavior proposal for $\chi \sim T$ of G. M. Zhang *et al.* (2009).

4. 11 structure

As an example of how measurements of resistivity offer a good overview of a phase diagram, Fig. 19 shows ρ up to room temperature of polycrystalline samples of FeSe$_{1-x}$Te$_x$ (Mizuguchi *et al.*, 2009). With the later advent of single crystals of FeSe the absolute value of ρ decreased by approximately a factor of 2 (Braithwaite *et al.*, 2009), but the temperature dependence (metallic, with rounding towards room temperature) remains qualitatively the same. An expanded view of ρ vs T in FeSe showed a linear temperature dependence (i.e., non-Fermi-liquid behavior as has been discussed above for 122) from $T_c \sim 8$ K up to almost 50 K (Masaki *et al.*, 2009; Sidorov, Tsvyashchenko, and Sadykov, 2009). Unlike the $\chi \sim T$ behavior reported above T_{SDW} for 1111, 122, and Na$_{1-\delta}$FeAs, χ for single crystal FeSe, which has no magnetic transition, increases faster than linearly with temperature by a factor of 3 above T_c up to ~ 180 K, at which point χ falls by about 20% by room temperature (Braithwaite *et al.*, 2009).

The magnetic susceptibility in FeTe$_{0.92}$ above T_{SDW} ~ 70 K *decreases* linearly with increasing temperature up to about 240 K (Iikubo *et al.*, 2009). Upon S doping (Hu *et al.*, 2009), this $\chi \sim -T$ behavior persists above the depressed T_{SDW} (~ 30 K for Fe$_{1+\delta}$Te$_{0.9}$S$_{0.1}$) up to room temperature. In FeSe$_{0.5}$Te$_{0.5}$, $T_c \sim 14$ K, χ increases linearly with temperature by about 15% between 100 and 250 K (highest temperature of measurement) (Sales *et al.*, 2009).

5. 21311 structure

Resistivity of polycrystalline Sr$_2$Mg$_{0.5}$Ti$_{0.5}$O$_3$Fe$_{1-x}$Co$_x$As shows metallic behavior from room temperature down to low temperature for $x = 0$, with RRR ~ 6, while ρ vs T shows a slight upturn in ρ with decreasing temperature above T_c caused by the Co doping (Sato *et al.*, 2010). Resistivity of polycrystalline Sr$_2$VO$_3$FeAs, $T_c \sim 33$ K (the superconductivity is sample dependent) is also metallic in behavior from 300 K down to T_c, with an extrapolated RRR of ~ 10. There appears to be no evidence for a structural ordering anomaly up to 300 K in this class of material. In the undoped parent compound Sr$_2$CrO$_3$FeAs, Cr orders antiferromagnetically at 31 K (Tegel *et al.*, 2009), while in Sr$_2$VO$_3$FeAs there is evidence in χ and specific heat (Sefat *et al.*, 2010) and ρ (Cao *et al.*, 2010) for a weak ($\sim 0.1 \mu_B$) magnetic transition at ~ 155 K. The magnetic susceptibility for Sr$_2$VO$_3$FeAs shows a definite anomaly at this temperature, as does the specific heat, while only the derivative of the resistivity reveals an anomaly. Investigations have not been reported above 50 K for any other of the superconducting examples of 21311 (Sr$_2$ScO$_3$FeP, $T_c = 17$ K; Sr$_2$Mg$_{0.2}$Ti$_{0.8}$O$_3$FeAs, $T_c = 39$ K) nor in the recently discovered example of 43822 [Ca$_2$(Mg$_{0.25}$Ti$_{0.75}$)$_{1.5}$O$_4$FeAs, $T_c = 47$ K].

6. 122* structure

As shown in Fig. 22, there is a wide range of resistivity (related to the effects of disorder on the iron Fe1 and Fe2 sublattices) behavior in A$_x$Fe$_y$Se$_2$ (the example given is for $A =$ Rb, data of Luo *et al.*, 2011), depending on the composition. However, as shown in Fig. 22, the magnetic susceptibility is relativity insensitive to the choice of A atom. Also, for varying compositions of Fe, Bao *et al.* (2011b) found relatively small variations in χ except for the most insulating sample.

Bao *et al.* (2011b) reported resistivity data for a range of insulating compositions (K$_{0.87}$Fe$_{1.57}$Se$_2$, K$_{0.94}$Fe$_{1.54}$Se$_2$, and
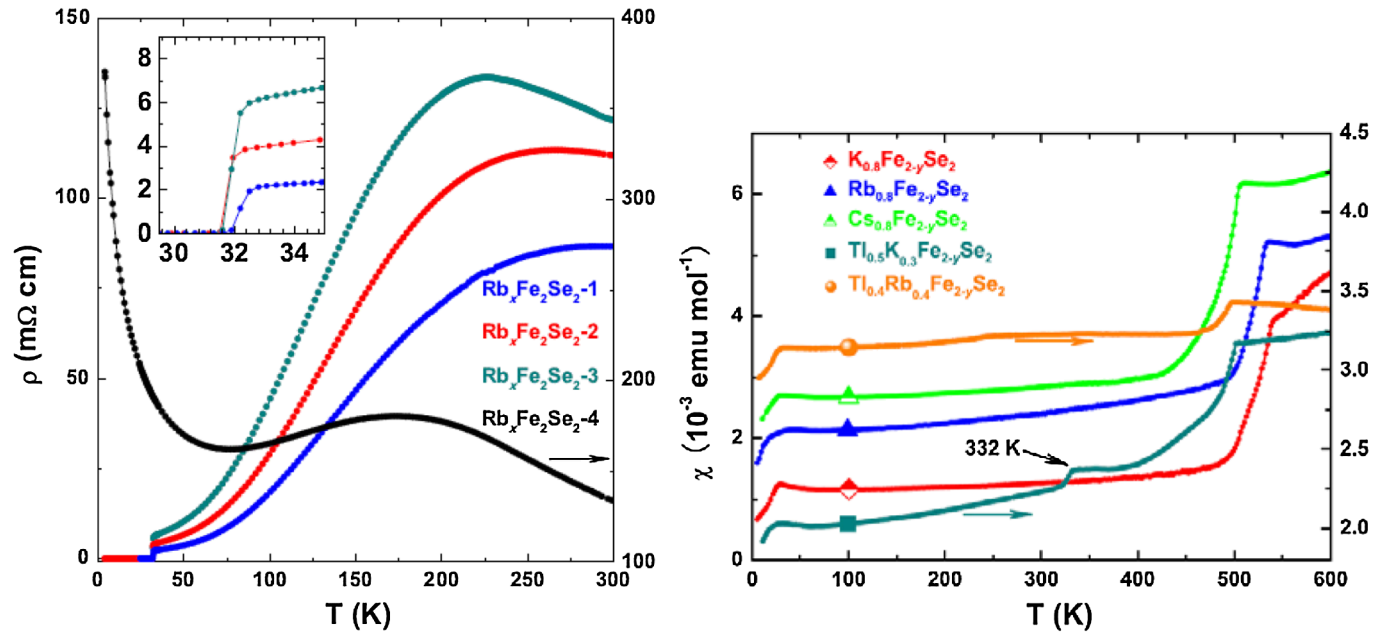
FIG. 22 (color online). Resistivity (left panel) (Luo *et al.*, 2011) for four samples of "$Rb_xFe_2Se_2$" (sample 1: $Rb_{0.75}Fe_{1.77}Se_2$ metallic, $d\rho/dT > 0$, behavior, 2: $Rb_{0.82}Fe_{1.67}Se_2$, 3: $Rb_{0.79}Fe_{1.64}Se_2$, 4: $Rb_{0.88}Fe_{1.54}Se_2$ insulating behavior) and magnetic susceptibility (right panel) (Liu *et al.*, 2011) for a selection of $A_{0.8}Fe_{2-y}Se_2$. Note the relative similarity in shape and even magnitude for all five compositions of the high temperature χ data. Susceptibility data by Bao *et al.* (2011b) for a similar K-based composition as that shown here are about 10% smaller and show about the same $\approx$ 40% decrease below T_N.

$K_{0.99}Fe_{1.48}Se_2$) where with decreasing Fe content the resistivity climbs more and more steeply than the one insulating Rb-based sample shown in Fig. 22 with decreasing temperature below 300 K. For the $K_{0.99}Fe_{1.48}Se_2$ composition, ρ can be fit to an exponential activation form, $\exp(-\delta/k_BT)$, with the energy gap $\delta \approx 85$ meV.

B. Specific heat

Measurements of the specific heat of superconductors in the normal state are generally of use to show higher temperature transitions, such as T_S and T_{SDW} in FePn/Ch superconductors. If T_c is low enough or if enough magnetic field can be applied to suppress T_c appreciably, C/T extrapolated to $T = 0$ from normal state data gives $C^{normal}/T|_{T\to0} = \gamma_n$. The parameter γ_n is proportional to the renormalized (by $1 + \lambda$, where λ can be a combination of electron-phonon and electron-electron interactions) bare electronic density of states at the Fermi energy $N(0)$, i.e., $\gamma_n \sim (1 + \lambda)N(0)$. The parameter γ_n is a useful parameter for various discussions including those of band structure calculations of $N(0)$ and dHvA(de Haas–van Alphen) measurements of the effective masses m^* of the various Fermi surface orbits since $\gamma_n \propto m^*$. Although there have been a few cases in the new FePn/Ch superconductors where γ_n has been either measured or estimated, extrapolating γ_n from above a superconducting transition of 10 K or higher is problematic. If the phonon contribution to the specific heat below T_c can be accurately estimated, e.g., via a neighboring composition (fortunately for this purpose Co doping of Fe involves almost the same molar mass) that is not superconducting, one can attempt to extrapolate the electronic specific heat below T_c by using the second order nature of the superconducting transition and matching entropies. Thus, the

measured superconducting state specific heat C_{sc} gives the superconducting state entropy at T_c, $S_{sc}(T_c) = \int(C_{sc}/T)dT$, by integrating the superconducting state data from $T = 0$ to T_c. Then, if the phonon contribution to the entropy (which is large) can be subtracted or accurately estimated, the extrapolated normal state electronic contribution C^{el}_{normal}/T must give, for a second order phase transition, a matching $S_{normal}(T_c)$ by integrating $\int(C^{el}_{normal}/T)dT$ and adding in the phonon contribution. Another possibility is if C/T in the superconducting state is proportional to H (from nodeless superconductivity, discussed in Sec. IV), then measurements of C/T up to some fraction of the upper critical field $H/H_{c2}(T \to 0)$ will give $C(H)/T$ in the superconducting mixed state equal to the product $\gamma_n^* H/H_{c2}(T \to 0)$. However, this is so far a rather rare measurement, since $H_{c2}(T \to 0)$ values are quite high, and this method of estimating γ_n is dependent on rather high applied fields to be of any accuracy.

1. γ_n (experiment)

A short list of those superconducting FePn/Ch materials for which estimated γ_n values in the normal ($T > T_c$) state exist consists of the following. Because of the higher T_cs and sample quality issues, most 1111 materials have unknown γ_n values. Kant *et al.* (2010) estimated γ_n for $Ba_{1-x}K_xFe_2As_2$ to be in the range 50–65 mJ/mole K^2 for x between 0 and 0.6. Popovich *et al.* (2010) found $\gamma_n = 50$ mJ/mole K^2 for $Ba_{0.68}K_{0.32}Fe_2As_2$, $T_c = 38.5$ K. Using 9 T C/T data which are proportional to H and extrapolating γ up to $H_{c2}(T \to 0)$ of 100 T (such a long extrapolation involves a large potential error), Mu *et al.* (2009a) estimated γ_n for $Ba_{0.6}K_{0.4}Fe_2As_2$ to be 63 mJ/mole K^2.

In a thorough study of the specific heat of $BaFe_{2-x}Co_xAs_2$ over the whole superconducting dome (see Fig. 12), Hardy

TABLE III. Specific heat γ_n and T_c for unannealed and annealed $BaFe_{2-x}Co_xAs_2$. Annealed values are designated with *.

$x =$	$T_c(K)$	$\gamma_n(mJ/mole\,K^2)$	Reference
0.08/0.09	5.8/5.6, 8.0*	14.9/13.7, 14*	Hardy *et al.* (2010a); Gofryk *et al.* (2011a, 2011b)
0.10	19.5	17.2	Hardy *et al.* (2010a)
0.11	21.5	19	Hardy *et al.* (2010a)
0.115	24.3	21.3	Hardy *et al.* (2010a)
0.15/0.16	22.9/20, 25*	22.1/18, 22*	Hardy *et al.* (2010a); Gofryk *et al.* (2011a, 2011b)
0.18	20.7	20	Hardy *et al.* (2010a)
0.22/0.21	11.1/11, 17.2*	17/23.2, 20*	Hardy *et al.* (2010a); Gofryk *et al.* (2011a, 2011b)
0.24	5.1	14.6	Hardy *et al.* (2010a)
0.31	0	16	Hardy *et al.* (2010a)

et al. (2010a) (see also Hardy *et al.*, 2010b) reported unannealed γ_n and T_c values versus composition (Table III), while values for three compositions ($x = 0.09$, 0.16, and 0.21) of both unannealed and annealed (2 weeks, 800 °C) material were reported by Gofryk *et al.* (2011a, 2011b). There is relatively good agreement between the annealed and unannealed γ_n values for comparable compositions (although note the differences in T_cs, discussed with $\Delta C/T_c$ later in Sec. III.B.4).

J. S. Kim *et al.* (2010) and Y. Wang *et al.* (2011), using superconducting state data to 15/35 T on a collage of single crystal $BaFe_2As_{1.4}P_{0.6}$, $T_c = 30$ K, estimated γ_n to be 16 mJ/mole K^2 by extrapolating to $H_{c2}(T \to 0)$ of 52 T. Zeng *et al.* (2011), using data to 9 T in $K_{0.8}Fe_{1.6}Se_2$ [$H_{c2}(0) \approx 48$ T, $T_c = 32$ K] offered the rough estimate that γ_n is roughly 6 mJ/mole K^2, or significantly smaller than found for the other FePn/Ch with comparable T_cs.

Low T_c compounds, such as $FeSe_{0.88}$, $T_c \approx 8$ K, LaFePO, $T_c \approx 5$–6 K, and KFe_2As_2, $T_c = 3.4$ K, have γ_ns that are more easily determined. For a polycrystalline sample of $FeSe_{0.88}$ Hsu *et al.* (2008) found that $C_{normal}/T = \gamma_n + \beta T^2$ with $\gamma_n = 9.2$ mJ/mole K^2. For a mosaic of single crystals of LaFePO, Analytis *et al.* (2008) found that $\gamma_n = 7$ mJ/mole K^2, while Fukazawa *et al.* (2009a) found $\gamma_n = 69$ mJ/mole K^2 for polycrystalline KFe_2As_2, RRR = 67. In a later work on KFe_2As_2, RRR > 1200, Hashimoto *et al.* (2010a) referenced an unpublished result for γ_n of 93 mJ/mole K^2, and J. S. Kim *et al.* (2011b) reported $\gamma_n = 102$ mJ/mole K^2 for single crystal KFe_2As_2 with RRR = 650, so clearly there is sample dependence of γ_n in KFe_2As_2 (and presumably in other FePn/Ch compounds).

2. γ_n (calculated)

It is also interesting to compare, where possible, the measured γ_n values to those calculated from band structure calculations. The normal state specific heat γ_n can be related to the calculated bare density of states $N(0)$ at the Fermi energy by $\gamma_n = \frac{1}{3}\pi^2 k_B^2 N(0)(1 + \lambda)$, where k_B is the Boltzmann constant and λ is the sum of the electron-phonon coupling parameters as well as the electron-electron coupling parameters, λ_{el-ph} and λ_{el-el}. If γ_n is in units of mJ/mole K^2 and $N(0)$ is in units of states/eV atom, then by combining the constants $\frac{1}{3}\pi^2 k_B^2$, we get $N(0)(1 + \lambda) = 0.42\gamma_n/n$. Usually the scaling between "mole" and "atom" is that the mole contains n atoms, e.g., $n = 5$ in the case of 122, without regard to whether the atoms are greater or lesser contributors

to $N(0)$, i.e., a mole of 122 is not considered to consist of just the two Fe atoms even though band structure calculations tell us that $N(0)$ comes mostly from the Fe bands. Most band structure calculations have been on the undoped parent compounds, which in the case of 1111 (with the exception of LaFePO) and 122 (excepting KFe_2As_2, $RbFe_2As_2$, and $CsFe_2As_2$) are not superconducting and thus not the focus here. Further, the 1111 and 122 parent compounds all undergo a spin density wave transition [which typically lowers $N(0)$] around 100–200 K, while in 21311 there is at least indication of magnetic order in Sr_2VO_3FeAs at 155 K (Sefat *et al.*, 2010) and 122* have magnetic order above 500 K. Therefore the measured low temperature γ_n will have a lower value than the calculations [which do not take into account the reduction in $N(0)$ due to magnetic order] predict in any case. Thus, in order to compare band structure calculations with experimental γ_n values, what is needed is either such a calculation on a nonmagnetic doped system or to compare the calculated and measured γ_n on a nonmagnetic 111 or 11 compound. We present here three disparate examples.

For FeSe, $T_c = 8$ K, Subedi *et al.* (2008) calculated $N(0) = 0.95$ states/eV atom. Based on the measured specific heat γ_n of Hsu *et al.* (2008), this implies, using $n = 2$, a $1 + \lambda$ of 2.05. A number of calculations exists for $N(0)$ in LaFePO, $T_c \approx 5$–6 K; see, e.g., Lebegue (2007), Lu *et al.* (2008), and Skornyakov *et al.* (2010). Using $\gamma_n = 10$ mJ/mole K^2 from Suzuki *et al.* (2009), the consensus for $1 + \lambda$ is 1.7. Considering these two values of $1 + \lambda$, it is interesting to note that those who perform such band structure calculations themselves note that their calculated band structures need to be a factor of ~2 narrower to correspond to the measured ARPES, e.g., Lu *et al.* (2008) renormalized their DFT band structure by narrowing it a factor of 2.2 to fit their ARPES data. Shein and Ivanovskii (2009c) calculated $N(0) = 1.11$ states/eV atom for $Ba_{0.5}K_{0.5}Fe_2As_2$, $T_c = 38$ K. However, they noted that the Fermi energy in the calculation lies on the slope of a sharp peak in the density of states, so that small changes in the Fermi energy would have a large effect on $N(0)$. Using the γ_n for this composition from Kant *et al.* (2010) of 54 mJ/mole K^2, and $n = 5$, leads to a $1 + \lambda$ of 4.1, clearly far larger than any possible $1 + \lambda_{el-ph}$ and perhaps indicative indeed that $N(0)$ has been underestimated.

The current theoretical understanding of the pairing mechanism (see also the discussion of the isotope effect in Sec. IV.A and the discussion of spin fluctuations below T_c in the discussion of inelastic neutron scattering in Sec. IV.A.1), it is clear that the pairing mechanism for the superconductivity in

FePn/Ch is not electron-phonon coupling (Subedi *et al.*, 2008; Boeri, Dolgov, and Golubov, 2009), but some other interaction that is presumably electronic, perhaps spin fluctuations.

If the so-called mass renormalization ($\propto 1 + \lambda$) were due to electron-phonon coupling in $FeSe_{1-x}$ or LaFePO, a standard estimate [e.g., the McMillan (1968) formula] in the BCS formalism would in fact, for $T_c = 8$ and 6 K and the lattice stiffnesses of FeSe and LaFePO as reported by Hsu *et al.* (2008) and Suzuki *et al.* (2009), require $\lambda_{el-ph} \sim 0.8$ and 0.6, respectively. This is not inconsistent with the $1 + \lambda$ values of $2.05/1.7$ derived from the ratio of the measured specific heat γ_n and calculated $N(0)$ discussed previously. However, Subedi *et al.* (2008) calculated $\lambda_{el-ph} = 0.17$ for FeSe, making it clear (see also the inelastic neutron scattering detected spin fluctuations below T_c discussed in Sec. IV.A.1) that even this low T_c FeCh is not an electron-phonon pairing superconductor.

Thus, it should be stressed that the ratio between measured γ_n values and band structure calculations for $N(0)$, even for such low T_c materials as FeSe, gives values for $1 + \lambda$ that either involve large contributions to λ from electron-electron mass renormalization or indicate errors in the calculations. For the higher T_c $Ba_{0.5}K_{0.5}Fe_2As_2$ it is clear that the derived $1 + \lambda$ of 4.1 implies a problem with the calculated $N(0)$. Such strong electron-electron interactions, if present, should strongly affect other measurements, for example, the low temperature resistivity.

3. $\Delta C/T_c$

An interesting correlation between ΔC and T_c has been proposed by Bud'ko, Ni, and Canfield (2009) (BNC), namely, that for 14 samples of various doped $BaFe_2As_2$ superconductors (including Co and Ni on the Fe site and K on the Ba site) $\Delta C/T_c = aT_c^2$ (see Fig. 23), where analyzing their graph gives $a \sim 0.056$ mJ/mole K^4. Zaanen (2009) proposed that this $\Delta C/T_c \sim T_c^2$ scaling behavior argues against a Fermi
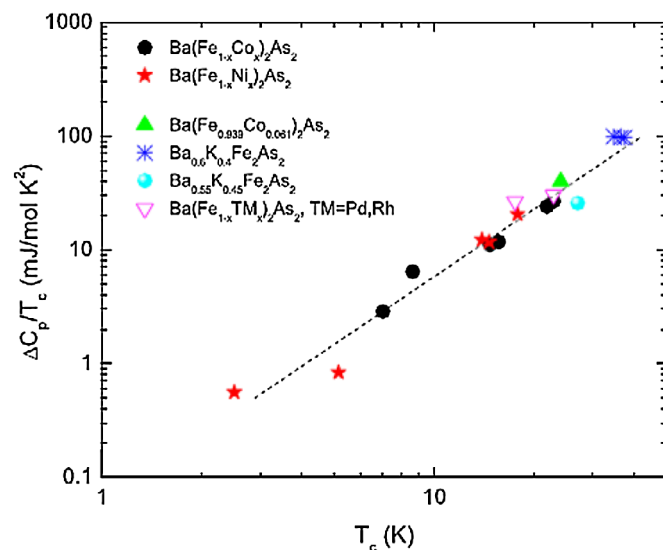
liquid picture, and instead discusses the idea that the superconductivity could be forming from a non-Fermi-liquid quantum critical metal. Rather than the usual quantum critical *point* in a phase diagram (see Stewart, 2001, 2006, and von Löhneysen *et al.*, 2007), Zaanen argued for a quantum critical *region* over some fraction of the superconducting dome in composition space. To explain the observed BNC scaling Kogan (2009 and 2010) considered instead that the FePn/Ch superconductors are weak coupled Fermi liquids with strong pair breaking, with the observed ΔCs and T_cs much reduced from those in hypothetical clean material. A third theory (Vavilov, Chubukov, and Vorontsov, 2011) calculated that $\Delta C/T_c \approx T_c^2$ below optimal doping in FePn/Ch for part of the underdoped dome as $T_c \to 0$ due to the coexistence of SDW magnetism and s_{+-} superconductivity. However, above optimal doping in the absence of coexistent magnetism, their work discusses a return to BCS behavior.

a. Possible errors in determining the intrinsic $\Delta C/T_c$

Before discussing this scaling of the discontinuity in the specific heat at T_c, a discussion of the determination of ΔC will help to establish the source of possible errors. Because of sample quality (disorder and strain) issues, these transitions can be quite broadened in temperature. One way to analyze and intercompare such broadened transitions is the so-called "equal area construction," sketched in Fig. 24. In this method, the low temperature superconducting state data up to the initial bend over in C/T at T_c^{low} are extrapolated linearly further as C^{ex}_{sc}/T; likewise, the normal state data are extrapolated linearly as C^{ex}_n/T to lower temperature. Then an ideally narrow discontinuity ΔC is constructed at a temperature approximately midway between T_c^{onset} and T_c^{low} at T_c^{mid} with the area (which is an entropy) between the linearly extrapolated C^{ex}_{sc}/T and the actual measured data below T_c^{mid} equal to the area (entropy) between the measured data above T_c^{mid} and the extrapolated C^{ex}_n/T from above T_c^{onset}. This then preserves the correct measured value of the superconducting state entropy at T_c in the new, idealized

FIG. 23 (color online).   Discontinuity in the specific heat ΔC at the superconducting transition in doped $BaFe_2As_2$ on a log-log plot showing $\Delta C/T_c$ proportional to T_c^2. From Bud'ko, Ni, and Canfield, 2009.
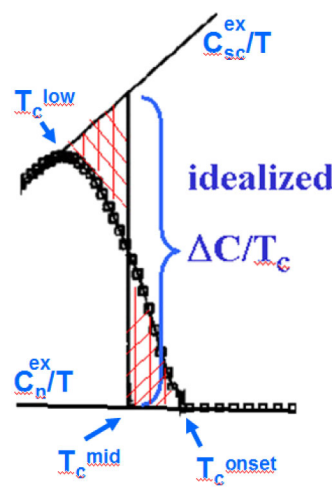
FIG. 24 (color online).   Sketch of the equal area construction method for determining $\Delta C/T_c$ in a broadened transition. Data points are denoted by squares. Red crosshatching marks the equal areas, which are entropies, discussed in the text.

transition. Sometimes, however, the transition is so broad [e.g., in $Sr(Fe_{0.925}Ni_{0.075})_2As_2$, $T_c^{onset} = 8.5$ K, $\Delta T_c \approx$ 3.5 K (Saha $et\ al.$ (2009a)] or even nonexistent [e.g., in underdoped $Ba_{1-x}K_xFe_2As_2$ (Rotter $et\ al.$, 2009; Urbano $et\ al.$, 2010), as discussed in Sec. II.B.2.b or in $Ca_{0.5}Na_{0.5}Fe_2As_2$, $T_c = 18$ K (J. K. Dong $et\ al.$, 2008)] that the equal area construction fails.

Further complicating the determination of $\Delta C/T_c$, for many samples of the FePn/Ch superconductors there is a finite γ in the superconducting state that is likely not intrinsic. How to distinguish if this residual γ_r is a sign of a part of the sample being nonsuperconducting (thus decreasing $\Delta C/T_c$ but not affecting T_c) or a sign of defects and gapless behavior (with both $\Delta C/T_c$ and T_c decreased, while the transition width ΔT_c is broadened) will now be discussed using examples from the FePn/Ch.

In KFe_2As_2, where γ_n extrapolated from above T_c is 69 mJ/mole K^2 in the data of Fukazawa $et\ al.$ (2009a) for an RRR = 67 sample as already mentioned, C/T in the superconducting state as $T \to 0$, γ_r, is ≈ 40 mJ/mole K^2 while in the data of J. S. Kim $et\ al.$ (2011b) down to 0.08 K for an RRR = 650 sample, $\gamma_n = 102$ mJ/mole K^2 and $\gamma_r \approx 0$. The fact that the sums of γ_n and γ_r in both samples are approximately the same gives credence to the idea that γ_r in the Fukazawa $et\ al.$ sample is simply from a non-superconducting fraction. Further, if one continues this logic, then the Fukazawa $et\ al.$ sample would, using their values for γ_n and γ_r, be approximately $\gamma_n/(\gamma_n + \gamma_r)$ (= 63%) super-conducting, and one would expect in this sample only this fraction of the $\Delta C/T_c$ observed in the fully superconducting ($\gamma_r \approx 0$) sample of J. S. Kim $et\ al.$ (2011b), or $\Delta C_{partially\ super}/T_c = [\gamma_n/(\gamma_n + \gamma_r)]\Delta C_{fully\ super}/T_c$. This is, within the error bars, borne out, since $\Delta C/T_c \approx$ 23 mJ/mole K^2 for the Fukazawa $et\ al.$ (2009a), RRR = 67 sample, or 56% of the $\Delta C/T_c \approx 41$ mJ/mole K^2 for the J. S. Kim $et\ al.$ (2011b), RRR = 650 sample with $\gamma_r \approx 0$.

In the Suzuki $et\ al.$ (2009) data for LaFePO, γ_n extrapolated from above $T_c = 5.8$ K is 10.1 mJ/mole K^2 whereas C/T extrapolated to $T = 0$ from their superconducting state data below T_c (between 2 and 4 K) gives a residual $\gamma_r \sim$ 7.5 mJ/mole K^2, seemingly similar to the results for KFe_2As_2.

Thus, in RRR = 67 KFe_2As_2 sample and possibly in LaFePO, a reasonable explanation is that only part of the sample is superconducting (since only part of the normal state γ_n is removed below T_c) and therefore for an ideal, 100% superconducting sample $\Delta C/T_c$ would be proportionately larger. Thus, in general, without high quality ($\Leftrightarrow$ low γ_r) samples it can be difficult comparing $\Delta C/T_c$ values and care must be taken.

As an aside, it should be stressed that such a large residual γ_r in the superconducting state as found in LaFePO, in early, low RRR samples of KFe_2As_2 or in unannealed nonoptimally doped $BaFe_{2-x}Co_xAs_2$ (where $\gamma_r > 10$ mJ/mole K^2 or roughly $\frac{1}{2}$ of γ_n) is a sample quality issue (see Sec. V), not a sign of nodal behavior. Since specific heat is a bulk measurement (versus resistivity and thermal conductivity which can be dominated by one dimensional pathways), even line nodes on a Fermi surface, if unsmeared due to defects, will have only a miniscule amount of normal Fermi surface

electronic density of states contribution to γ_r. Whether the extrinsic behavior is due to normal regions (as the conservation of $\gamma_r + \gamma_n$ in KFe_2As_2 with improving sample quality with no change in T_c but an increase in $\Delta C/T_c$ would imply), or defects on a microscopic, approximately homogeneous scale causing gapless behavior [where annealing of, e.g., $BaFe_{2-x}Co_xAs_2$ (Gofryk $et\ al.$, 2011a; 2011b) decreases γ_r markedly, down to 0.25 mJ/mole K^2 on one sample of optimally doped $x = 0.16$, and increases T_c while leaving γ_n (see Table III and discussion) approximately unchanged] has to be determined on a case by case basis. In any case, nodal behavior (line or point nodes) in a single crystalline (although no real material is ideal) superconductor cannot lead to over 30% of a Fermi surface being gapless and causing the large γ_r seen, e.g., in some KFe_2As_2 and LaFePO. As an example of a known d-wave superconductor with line nodes, $YBa_2Cu_3O_{6.99}$ (YBCO) has γ_r in a high quality sample (but presumably still with some defect broadening of the line nodes at the Fermi surface, as well as possible other contributions to γ_r) equal to 1.2 mJ/mole K^2 and $\gamma_n \approx$ 20 mJ/mole K^2 (Moler $et\ al.$, 1994). Further optimization of the YBCO samples could decrease γ_r even further, but the ratio 1.2/20 or 6% provides a useful "upper bound" estimate for the effect of nodal superconductivity on γ_r in well ordered single crystals.

If there are sufficient defects on a quasihomogeneous microscopic scale (rather than normal regions) to make a large γ_r, then T_c should be strongly affected (cf. Kogan, 2009; 2010). Although this is not the case in KFe_2As_2 (T_c seems to be fairly constant as a function of sample quality measured via RRR), in the annealing studies of $BaFe_{2-x}Co_xAs_2$, T_c increases with annealing by $\approx 50\%$ for the nonoptimally doped samples (Gofryk $et\ al.$, 2011a; 2011b) shown in Table III. How the $\Delta C/T_c$ results for the annealed and unannealed samples of $BaFe_{2-x}Co_xAs_2$ compare on the BNC plot will be discussed below.

In Sr_2VO_3FeAs, the status of the sample quality is that as yet no anomaly at T_c is visible in the specific heat (Sefat $et\ al.$, 2010), while the residual gamma in the superconducting state, $T \ll T_c$, is 25 mJ/mole K^2 for the sample with the largest fraction of superconductivity in the susceptibility ($\approx 10\%$ Meissner fraction, $\approx 50\%$ shielding) and $\gamma_n =$ 60 mJ/mole K^2 for the nonsuperconducting sample. In the defect 122^* superconductors, determinations of $\Delta C/T_c$ give about 10 mJ/mole K^2 (Luo $et\ al.$, 2011) to 12 mJ/mole K^2 (Zeng $et\ al.$, 2011), with $T_c \approx 31$ K, which is small compared to the BNC plot value expected for this T_c of about $\Delta C/T_c \approx 50$ mJ/mole K^2. Although γ_r was reported by Zeng $et\ al.$ to be small compared to γ_n (0.4 vs 6 mJ/mole K^2, respectively), another work (Shen $et\ al.$, 2011) by the same group on improved samples reported the possibility that these materials were made up of superconducting islands surrounded by insulating (i.e., $\gamma = 0$) material. Thus, for the 122^* samples evaluation of $\Delta C/T_c$ awaits homogeneous, single phase samples.

Now that potential sources of error in $\Delta C/T_c$ values in the FePn/Ch have been discussed, it is interesting to examine the error bars for several samples, with both large and small disagreements from the BNC scaling plot, shown in Fig. 23. First, $BaFe_{2-x}Ni_xAs_2$, $x = 0.144$, and $T_c \sim 5$ K has a very

broad, small, and hard to analyze transition in the specific heat, and the $\Delta C/T_c$ shown in Fig. 23 is likely underestimated, which would bring that point closer to the BNC fitted line. Another point which also lies too low versus the BNC $\Delta C/T_c \sim T_c^2$ trend (Ba$_{0.55}$K$_{0.45}$Fe$_2$As$_2$, $T_c \sim 28$ K) had $\Delta C/T_c \sim 25$ mJ/mole K^2 (versus 44 mJ/mole K^2 expected from the plot) estimated from a very broad, $\Delta T_c \sim 3$ K, transition in a Sn-flux grown single crystal (Ni *et al.*, 2008a), RRR ~ 3. The sample quality as well as the width of the transition again contribute to the possible error bar. Considering now a data point that lies on the BNC line, $\Delta C/T_c$ of a self-flux grown single crystal Ba$_{0.6}$K$_{0.4}$Fe$_2$As$_2$ ($\Delta C/T_c = 100$ mJ/mole K^2 at $T_c^{\text{mid}} = 34.7$ K), was idealized (Welp *et al.*, 2009) from a $\Delta T_c \sim 1$ K broad transition, rather high quality (RRR ~ 15) sample (Luo *et al.*, 2008). A more recent measurement on Ba$_{0.68}$K$_{0.32}$Fe$_2$As$_2$, $T_c = 38.5$ K, and a $\Delta T_c \sim 0.4$ K broad transition (not plotted in

the original BNC plot in Fig. 23) found $\Delta C/T_c = 125$ mJ/mole K^2 (Popovich *et al.*, 2010). Based on the square of the ratios of T_c ([38.5/34.7]^2), this $\Delta C/T_c$ value of Popovich *et al.* matches the BNC plot equally as well as the Welp *et al.* value. Thus, it is reasonable to conclude that the BNC scaling law fit, which was conceived for doped 122 FePns only, seems reasonably robust.

In order to supplement the BNC plot with data (and structures) not in the original version, as well as to introduce data that perhaps speak to the proposed theories, J. S. Kim *et al.* (2011a) considered $\Delta C/T_c$ values for several other FePn/Ch materials. In addition, they added $\Delta C/T_c$ data for conventional electron-phonon coupled superconductors (elements with $T_c > 1$ K and A-15 superconductors) and for several unconventional heavy fermion superconductors. This revised BNC plot, with $\Delta C/T_c \approx 0.083 T_c^{1.89}$ is shown in Fig. 25 and discussed here.
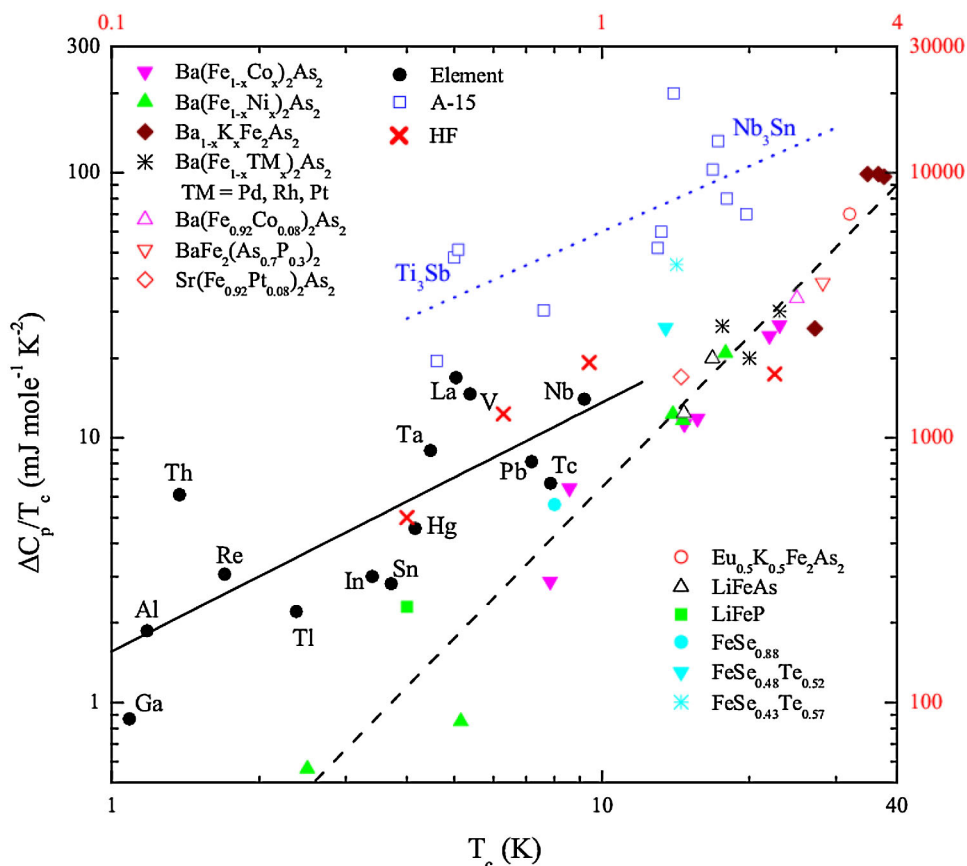
FIG. 25 (color online).   Expanded BNC plot based on the work by J. S. Kim *et al.* (2011a) with additional FePn/Ch data as discussed in the text, along with $\Delta C/T_c$ data for the elemental superconductors with $T_c > 1$ K as well as a selection of A-15 superconductors, both conventional, electron-phonon coupled, superconducting families. In these two kinds of superconductors the $\Delta C/\gamma_n T_c$ values, while they may deviate from the weak-coupling BCS value of 1.43, are generally between 1.3 (Re) and 2.7 (Pb), i.e., fairly constant compared to the wide range of $\Delta C/T_c$. Thus, the two groups of conventional superconductors lie at different places on the y axis in this $\Delta C/T_c$ plot since the γ_n values which would normalize the higher γ_n A-15s into rough agreement with the elements are not considered. In addition, four heavy fermion superconductors are shown. These materials, CeIrIn$_5$ ($T_c = 0.4$ K), CeCu$_2$Si$_2$ ($T_c = 0.63$ K), UBe$_{13}$ ($T_c = 0.94$ K), and CeCoIn$_5$ ($T_c = 2.25$ K), due to the different scale of their ΔC values, are plotted against the upper and right hand axes; all other points are plotted vs the left and lower axes. The slope of the elemental superconductor (solid circles) line gives $\Delta C/T_c \sim T_c^{0.94}$ and for the A-15 superconductors (which show a large spread in $\Delta C/T_c$ at the higher T_c end due to sample quality issues) the best fit (dotted) line gives $\Delta C/T_c \sim T_c^{0.75}$. The four heavy fermion superconductors, which are presumably nonconventional, surprisingly show $\Delta C/T_c$ vs T_c behavior similar to the conventional superconductors. Numerical values for T_c and $\Delta C/T_c$ for most of the plotted points are given in J. S. Kim *et al.* (2011a), while the others are given here in the text.

b. Additional examples of $\Delta C/T_c$ to discuss with respect to the BNC plot

1. KFe$_2$As$_2$

The disputed report of non-Fermi-liquid behavior in the resistivity (Dong *et al.*, 2010b) of the 3.4 K superconductor KFe$_2$As$_2$ discussed in Sec. III.A.2 makes this material perhaps germane for the quantum critical picture of Zaanen. The values for T_c and $\Delta C/T_c$ for KFe$_2$As$_2$ (Fukazawa *et al.*, 2009a) are T_c = 3.4 K and $\Delta C/T_c$ = 20–24 mJ/mole K^2, in a sample with RRR = 67. The lower value quoted for $\Delta C/T_c$ is from simply taking ΔC at the maximum in C_{sc}/T and the higher value is from the equal area construction method discussed above. This value for $\Delta C/T_c$ for an undoped 122 compound is approximately a factor of 40 larger than the 0.65 mJ/mole K^2 calculated from $\Delta C/T_c = aT_c{}^2$; see Fig. 23. Also, as discussed in the preceding section, due to the large value of C/T as $T \to 0$ in the superconducting state, $\Delta C/T_c$ for an improved sample [such as the RRR = 650 sample reported by J. S. Kim *et al.* (2011b)] of KFe$_2$As$_2$ is even larger, $\approx$ 41 mJ/mole K^2. J. S. Kim *et al.* (2011a) then concluded, in their updated BNC plot discussion, that this large positive discrepancy with $\Delta C/T_c \propto T_c{}^2$ is an indication that KFe$_2$As$_2$ does not belong to the class of superconductor represented by the BNC plot. Although not discussed by J. S. Kim *et al.* (2011a), RbFe$_2$As$_2$ with T_c = 2.6 K (Bukowski *et al.*, 2010), $\gamma_n \approx$ 110 mJ/mole K^2 and $\Delta C/T_c$ = 55 mJ/mole K^2 (Kanter *et al.*, 2011) is presumably also more comparable to a conventional, electron-phonon coupled superconductor.

2. BaFe$_2$(As$_{0.7}$P$_{0.3}$)$_2$/annealed Ba(Fe$_{0.92}$Co$_{0.08}$)$_2$As$_2$/ Sr(Fe$_{0.82}$Pt$_{0.08}$)$_2$As$_2$/Eu$_{0.5}$K$_{0.5}$Fe$_2$As$_2$/Ba(Fe$_{0.95}$Pt$_{0.05}$)$_2$As$_2$

Five additional 122 superconductors have been measured since the original BNC plot, and are included in the updated BNC plot, Fig. 25. J. S. Kim *et al.* (2011a) measured $\Delta C/T_c$ in a collage of single crystals of BaFe$_2$(As$_{0.7}$P$_{0.3}$)$_2$ and found a 1 K wide transition ΔT_c at $T_c{}^{\text{mid}}$ = 28.2 K and $\Delta C/T_c$ = 38.5 mJ/mole K^2, which lies slightly below the fit line in Fig. 25 for the FePn/Ch data. Chaparro *et al.* (2011), in an improved BaFe$_2$(As$_{0.7}$P$_{0.3}$)$_2$ sample with T_c = 29.2 K, report $\Delta C/T_c$ = 54 mJ/mole K^2 (not shown in Fig. 25) using an idealized equal area construction.

Since the original BNC plot, Gofryk *et al.* (2011a) and 2011b) have been the first to report specific heat on annealed (800 °C, 2 weeks) single crystals of Co doped BaFe$_2$As$_2$. For optimally doped Ba(Fe$_{0.92}$Co$_{0.08}$)$_2$As$_2$, T_c = 25 K, Gofryk *et al.* (2011a) reported $\Delta C/T_c$ = 33.6 mJ/mole K^2 for $\Delta T_c \sim$ 1 K, versus values for unannealed samples of approximately the same composition of $\approx$ 24 mJ/mole K^2, T_c = 22 K (Fukazawa *et al.*, 2009a) and T_c = 20 K (Gofryk *et al.*, 2011a; 2011b). As can be seen in Fig. 25, this T_c = 25 K point fits well with the other Co doped points of BNC to the general trend. For the other two compositions (x = 0.09, $T_c \approx$ 8 K and x = 0.21, $T_c \approx$ 17.2 K) annealed by Gofryk *et al.*, the $\Delta C/T_c$ values of $\approx$ 8.4 and 14 mJ/mole K^2, respectively, (not shown in Fig. 25) match fairly well values already in the original BNC plot; see Fig. 23. Annealing single crystal BaFe$_{2-x}$Co$_x$As$_2$ showed that annealing reduced the "residual" γ_r in the superconducting state by large amounts (from 10.5 to 1.3 mJ/mole K^2 for x = 0.09 and from 14.6 to 3.8 mJ/mole K^2 for x = 0.21) in the non-

optimally doped samples, versus a smaller reduction (from 3.6 to 1.3/0.25 mJ/mole K^2) for optimally doped, x = 0.16 (Gofryk *et al.*, 2011a; 2011b). [Values for γ_r in the unannealed samples of BaFe$_{2-x}$Co$_x$As$_2$ of Hardy *et al.* (2010a) are 9.8, 2.9, and 7.9 mJ/mole K^2 for the comparable compositions x = 0.08, 0.15, and 0.22, i.e., the γ_r values are, except for the overdoped case, in good agreement.] In contrast to the large changes in γ_r with annealing in BaFe$_{2-x}$Co$_x$As$_2$, Gofryk *et al.* (2011b) found (see Table III) that γ_n changed only by +0.3, +4, and −3.2 mJ/mole K^2 for their samples of x = 0.09, 0.16, and 0.21, respectively. Thus, in terms of the previous discussion about errors in determining $\Delta C/T_c$, the nonoptimally doped BaFe$_{2-x}$Co$_x$As$_2$ samples show a marked *decrease* in γ_r with γ_n approximately unchanged in comparison. This, along with the $\approx$ 50% increase in T_c with annealing (Table III) and rather broad transition widths ($\Delta T_c \approx 0.2T_c$) even after annealing for these two samples, x = 0.09 and 0.21, seems more consistent with defects and gapless behavior (cf. Kogan, 2009; 2010) rather than nonsuperconducting regions. However, the optimally doped annealed sample of Gofryk *et al.*, even though T_c increases 25% with annealing, has the same ΔT_c as the unannealed sample, as well as relatively small changes in γ_r, properties that are less consistent with a defect and or gapless picture.

Kirshenbaum *et al.* (2010) reported $\Delta C/T_c$ = 17 mJ/mole K^2, T_c = 14.5 K, and $\Delta T_c \sim$ 0.8 K for their single crystal Sr(Fe$_{0.92}$Pt$_{0.08}$)$_2$As$_2$. Jeevan and Gegenwart (2010) reported $\Delta C/T_c$ = 70 mJ/mole K^2, T_c = 32 K, and $\Delta T_c \sim$ 3 K for their polycrystalline Eu$_{0.5}$K$_{0.5}$Fe$_2$As$_2$. Finally, Saha *et al.* (2010b) reported $\Delta C/T_c \approx$ 20 mJ/mole K^2, $T_c{}^{\text{mid}}$ = 20 K in Ba(Fe$_{0.95}$Pt$_{0.05}$)$_2$As$_2$ for an addition to the original BNC (Fig. 23) Ba(Fe$_{1-x}$TM$_x$)$_2$As$_2$, TM = Pd, Rh points.

As may be seen in the updated BNC plot in Fig. 25, all five of these added 122 $\Delta C/T_c$ values agree rather well with the original BNC fit and support the robustness of their observation of $\Delta C/T_c \propto T_c{}^2$ for a broader range of 122s.

3. LiFeAs and LiFeP

These 111 structure superconductors have been well characterized by specific heat, and were not included in the original BNC plot. In particular, there are a number of works on the higher T_c LiFeAs (Chu *et al.*, 2009; B. S. Lee *et al.*, 2010; Stockert *et al.*, 2011; Wei *et al.*, 2010) and one on the $T_c \sim$6 K LiFeP (Deng *et al.*, 2009). Although the transition of Stockert *et al.* in their self-flux-grown crystal is sharp and their residual γ_r is essentially zero, their $\Delta C/T_c$ is only 12.4 mJ/mole K^2, T_c = 14.7 K, while the broader transition of Lee *et al.* in their Sn flux grown gives $\Delta C/T_c \sim$ 20 mJ/mole K^2, T_c = 16.8 K. The sample of Lee *et al.* has a residual gamma over half of the extrapolated normal state γ_n which, following the discussion above for KFe$_2$As$_2$, implies a larger $\Delta C/T_c$ in a sample where γ_r could be reduced. For LiFeP, Deng *et al.* (2009) found a broad transition, with $\Delta C/T_c \sim$ 2.3 mJ/mole K^2 at a midpoint T_c of 4 K. These values are plotted in the updated BNC plot in Fig. 25, and agree well with the trend of the 122 superconductors, $\Delta C/T_c \propto T_c{}^2$. Because of the lack of magnetism in these 111 samples (see also FeSe$_{0.88}$ below), the theory of Vavilov, Chubukov, and Vorontsov (2011) is not applicable to the comparison of these data with the BNC trend.

4. FeSe$_{0.88}$

Hsu *et al.* (2008) fitted their normal state data above $T_c \sim$ 8 K to a straight line on a C/T vs T^2 plot and arrived at $C^{ex}_n/T = 9.17 + 0.522$ T^2 (units of mJ/mole K^2) and $\Delta C/T_c$ of 5.6 mJ/mole K^2, which is somewhat large compared to the BNC plot value of 3.6 mJ/mole K^2; see Fig. 25. The superconducting $C/T(T \to 0) \approx 0$, implying a clean sample.

5. FeSe0.48Te$_{0.52}$

For this doped 11 compound, Braithwaite *et al.* (2010) found in single crystal material $T_c^{mid} = 13.5$ K, transition width $\Delta T_c \approx 3$ K, and $\Delta C/T_c = 20$–26 mJ/mole K^2 (where the larger value is from an equal area construction). In a later work [after J. S. Kim *et al.* (2011a), revised BNC plot] with improved single crystals of FeSe$_{0.43}$Te$_{0.57}$, $T_c^{mid} = 14.2$ K and $\Delta T_c \approx 2$ K, Hu *et al.* (2011) reported the much larger value of $\Delta C/T_c = 40$–51 mJ/mole K^2, with the upper value again from an idealized, sharp transition. In the Hu *et al.* sample there is an upturn above T_c in the normal state C/T [fit to a Schottky anomaly in comparable data by Tsurkan *et al.* (2011)] which makes the correct determination of $\Delta C/T_c$ more difficult. In any case, these values for $\Delta C/T_c$ for FeSe$_{0.48}$Te$_{0.52}$/FeSe$_{0.43}$Te$_{0.57}$ lie well above the modified BNC fit value in Fig. 25 of $\Delta C/T_c$ for $T_c = 14$ K of 12 mJ/moleK^2. The C/T data of Braithwaite *et al.* below 2.5 K show an upturn, as has been seen in the specific heat of other FePn/Ch superconductors (Kim, Kim, and Stewart, 2009). However, this upturn is likely due to some magnetic impurity rather than a fraction of the sample being normal, since C/T from above 2.5 K appears to extrapolate to approximately zero in this sample. The data of Hu *et al.* showed $\gamma_r \approx 2.3$ mJ/mole K^2 vs $\gamma_n \approx 27$ mJ/mole K^2. Therefore, both values of $\Delta C/T_c$ for FeSe$_{1-x}$Te$_x$ should *a priori* be approximately correct for intrinsic material. Why the two values are so disparate does not seem to be based on some obvious issue of sample quality.

In summary, most of the five additional 122 samples, two 111 examples, and two 11 examples, which are neither quantum critical nor show strong signs of pair breaking, seem approximately comparable to the 14 superconductors assembled by BNC for their proposed correlation between $\Delta C/T_c$ and T_c^2. However, the Hu *et al.* (2011) result for FeSe$_{0.43}$Te$_{0.57}$, similar to that for KFe$_2$As$_2$, lies well above the BNC trend.

One question that J. S. Kim *et al.* (2011a) addressed is how such a plot of $\Delta C/T_c$ vs T_c looks for conventional superconductors. The answer is not simply $\Delta C/\gamma_n T_c \propto$ const, therefore $\Delta C/T_c$ is also just a constant, independent of T_c. Such a plot, conventional superconductors together with the FePn/Ch data discussed above, was put forward by J. S. Kim *et al.* (2011a) and, together with the additional data for FePn/Ch, is the basis for Fig. 25. All the superconducting elements with $T_c > 1$ K are shown, as well as representative A-15 superconductors, in order to provide T_c values up to 20 K. The gamma values for the elemental superconductors are bounded by around 10 mJ/mole K^2 (V and La) (Stewart, 1983), while γ_n values for the A-15s are several times larger [see J. S. Kim *et al.* (2011a) and references within]. The slopes of the two $\Delta C/T_c$ vs T_c sets of data for the conventional superconductors are clearly quite close, and in strong contrast to that for the FePn/Ch.

Thus, this modified BNC plot from J. S. Kim *et al.* (2011a) makes clear that whatever the pairing mechanism in the superconducting state in FePn/Ch is, this superconductivity is different in a fundamental fashion from conventional superconductivity. Broadly speaking, the electron-phonon coupled elemental and A-15 superconductors have a $\Delta C/T_c$ that is dependent on three factors: the electronic density of states at the Fermi energy $N(0)$, the spectral density $\alpha^2 F(\omega)$, and the Coulomb pseudopotential μ^* (Carbotte, 1990). This dependence, using the slopes of the fits of $\Delta C/T_c$ to T_c^α in Fig. 25, says that for these superconductors (a) these three factors combine to give $\Delta C/T_c \sim T_c$ and (b) since in these superconductors $\Delta C/T_c$ roughly varies as γ_n, T_c then (again broadly speaking) must vary as $\gamma_n [\propto N(0)(1 + \lambda_{el-ph})]$. [In a less approximate fashion, in weak coupling BCS theory, $T_c \propto \exp[-1/N(0)V]$), where $(1 + \lambda_{el-ph})N(0) \propto \gamma_n$.] This dependence of T_c on the renormalized density of states in BCS superconductors derivable from Fig. 25 is of course the paradigm that drove the search for higher T_c in the A-15 superconductors, with some success. It is also the paradigm that Bednorz and Mueller ignored to discover high T_c superconductivity in the cuprates.

Now, the BNC plot suggests another paradigm, namely, that whatever instead of (or in addition to) $N(0)$, $\alpha^2 F(\omega)$, and μ^* determines $\Delta C/T_c$ for FePn/Ch, the result is that $\Delta C/T_c$ varies as T_c^2. As discussed in the next section, even for FePn/Ch, $\Delta C/T_c$, in so far as γ_n values are known, remains approximately proportional to γ_n. Also, the measured γ_ns (see Sec. III.B) combined with calculations imply that γ_n for FePn/Ch comes primarily from $N(0)(1 + \lambda_{el-el})$ since λ_{el-ph} is negligible. Thus, since for FePn/Ch $\Delta C/T_c \propto T_c^2$ and $\Delta C/T_c \propto \gamma_n \propto N(0)(1 + \lambda_{el-el})$, the BNC plot has implications for how the superconducting transition temperature T_c depends on the electron-electron interactions that are presumably involved in the superconducting pairing.

It is also interesting to note that, according to the quick look by J. S. Kim *et al.* (2011a) in Fig. 25 at the behavior for the heavy fermion superconductors CeIrIn$_5$, $T_c = 0.4$ K and $\Delta C/T_c = 500$ mJ/mole K^2, CeCoIn$_5$, $T_c = 2.25$ K, and $\Delta C/T_c = 1740$ mJ/mole K^2 as well as CeCu$_2$Si$_2$ and UBe$_{13}$, which include non-Fermi-liquid systems and unconventional superconductivity (*d*-wave gap for CeCoIn$_5$); see Pfleiderer (2009), FePn/Ch present another kind of unconventional superconductivity than the heavy fermion superconductors. The further question, what about $\Delta C/T_c$ vs T_c for the cuprates, runs into two difficulties in the cuprates: (a) ΔC is not easy to measure at such high transition temperatures due to the large phonon contribution to the total specific heat [e.g., ΔC in YBCO is just $\approx 1\%$ of $C_{Total}(T_c)$], just as is the case for the FePn/Ch and (b) determining ΔC is complicated by the pseudogap behavior for some compositions that affects the specific heat above T_c. If, however, one considers $\Delta C/T_c$ vs T_c for La$_{1-x}$Sr$_x$CuO$_4$, $x = 0.17, 0.22, 0.24$, T_cs from 17 to 25 K (other compositions can have similar T_cs and much different ΔCs) and YBa$_2$(Cu$_{0.98}$Zn$_{0.02}$)$_3$O$_7$, $T_c = 65$ K (Loram *et al.*, 2001), YBCO ($T_c = 91$ K, Junod *et al.*, 1997), HgBa$_2$Ca$_2$Cu$_3$O$_8$ ($T_c = 133$ K, Calemczuk *et al.*, 1994), and Bi$_{1.74}$Sr$_{1.88}$Pb$_{0.38}$CuO$_6$ ($T_c = 9.4$, Wen *et al.*, 2009), then for this choice of cuprate systems $\Delta C/T_c \sim T_c^{1.05}$.

Again, the FePn/Ch seem quite different in the behavior of ΔC with T_c.

In summary, the BNC plot provides a simple but insightful method for organizing data on the specific heat discontinuities at T_c. In addition, the BNC plot, *vis-a-vis* the discussion of KFe_2As_2, provides a simple test as to whether a material belongs to the FePn/Ch (magnetism and fluctuation dominated) class of superconductors. As with all the comparisons offered in this review, sample quality (e.g. in 122*) is definitely an issue for reaching correct conclusions. Whether the different dependence of $\Delta C/T_c$ with T_c for FePn/Ch versus that of elemental and A-15 superconductors (T_c^2 vs T_c) can provide a link between the superconductivity and related parameters such as $\lambda_{el\text{-}el}$ might be an interesting path for theoretical investigation.

4. $\Delta C/\gamma_n T_c$

In weak-coupling BCS theory $\Delta C/\gamma_n T_c = 1.43$ and serves as a traditional method to estimate the coupling strength of a superconductor, with larger values implying stronger coupling. In a d-wave superconductor, $\Delta C/\gamma_n T_c$ is [in the calculation of Won and Maki (1994)] about 0.9. For superconductors with multiple gaps (which ARPES data; see Sec. IV.A.2, as well as penetration depth, NMR, specific heat, tunneling, optical data, and a host of other measures, reveal for many of FePn/Ch), $\Delta C/\gamma_n T_c$ can be a wide variety of values from above 1.43 to significantly below. For example, in the canonical two gap electron-phonon mediated superconductor MgB_2, the normalized discontinuity at $T_c = 38.7/37$ K is $\Delta C/\gamma_n T_c = 1.3/0.9$ (Bouquet *et al.*, 2001; Wang *et al.*, 2003), where the disagreement is apparently due to sample differences with the higher T_c and $\Delta C/\gamma_n T_c$ coming from the sample with narrower ΔT_c.

Now that both $\Delta C/T_c$ and γ_n are accurately known for several FePn/Ch (believed to be unconventional) superconductors, with understood error bars, this ratio can be discussed in these specific cases. For $Ba_{0.6}K_{0.4}Fe_2As_2$, $T_c^{onset} = 37$ K, Kant *et al.* (2010) determined $\gamma_n = 49$ mJ/mole K^2 while Welp *et al.* (2009), with a sample with comparable T_c^{onset} (35.5 K) determined $\Delta C/T_c = 100$ mJ/mole K^2. Thus, for $Ba_{0.6}K_{0.4}Fe_2As_2$, $\Delta C/\gamma_n T_c = 2.04$. Using the value of $\Delta C/T_c = 125$ mJ/mole K^2 from Popovich *et al.* (2010) for $Ba_{0.68}K_{0.32}Fe_2As_2$ and the appropriate γ_n from Kant *et al.* (2010) of 53 mJ/mole K^2, this value of $\Delta C/\gamma_n T_c$ rises to 2.36, indicative of even stronger coupling. As discussed in Sec. IV, numerous measurement techniques (ARPES, penetration depth, NMR, tunneling, and others) imply that K doped $BaFe_2As_2$ has multiple superconducting energy gaps, i.e., a large value for $\Delta C/\gamma_n T_c$ is not a contraindication for multiple gaps in the FePn/Ch.

For annealed optimally doped $BaFe_{1.85}Co_{0.16}As_2$, Gofryk *et al.* (2011a and 2011b) determined $\gamma_n = 22$ mJ/mole K^2 and $\Delta C/T_c = 33.6$ mJ/mole K^2. This gives ~ 1.5 for $\Delta C/\gamma_n T_c$, a more weak coupled value and consistent with their fit of their data to a two gap model. Finally, taking $\Delta C/T_c = 24$ mJ/mole K^2 for KFe_2As_2 from the equal area construction as discussed above, and $\gamma_n = 69$ mJ/mole K^2 (Fukazawa *et al.*, 2009a, RRR = 67), we obtain $\Delta C/\gamma_n T_c = 0.35$, presumably indicative of sample quality issues. However, a sample of KFe_2As_2 with even higher quality

[J. S. Kim *et al.* (2011b), RRR = 650 with $\gamma_n = 102$ mJ/mole K^2] and $\Delta C/T_c \approx 41$ mJ/mole K^2 still only has $\Delta C/\gamma_n T_c \approx 0.40$, arguing perhaps for a two gap model.

IV. SUPERCONDUCTING PAIRING MECHANISM, THEORY AND EXPERIMENT; SYMMETRY AND STRUCTURE OF THE ENERGY GAP

Approximately eight years after the discovery of superconductivity in the cuprates (Bednorz and Müller, 1986), Tsuei *et al.* (1994) were able to show that the pairing symmetry was d wave. In less than half that time after the discovery of superconductivity in the iron pnictides (Kamihara *et al.*, 2008), thanks to the experience amassed studying the cuprates and heavy fermion superconductors plus significantly improved experimental and theoretical tools, the question of the pairing symmetry is being heavily studied. There is significant experimental evidence for some version of the so-called $s_\pm$ state, predicted first by Mazin *et al.* (2008) [see also Barzykin and Gorkov (2008); and Chubukov, Efremov, and Eremin (2008)] for the FePn superconductors, although predictions abound for other pairing states which may be dominant [e.g., the proposal for the s_{++} state mediated by orbital fluctuations; see Kontani and Onari (2010); Yanagi, Yamakawa, and Ono (2010); and Kontani, Saito, and Onari (2011)] or coexist in the $s_\pm$ materials. Fernandes and Schmalian (2010) [see also Vorontsov, Vavilov, and Chubukov (2010)] argued that, within their model for the magnetism and superconductivity (where the same electrons that form the superconducting pairs also cause the ordered moment), the observed coexistence of antiferromagnetism and superconductivity in, e.g., underdoped $BaFe_{2-x}Co_xAs_2$, implies a sign changing s_{+-} state and rules out s_{++} pairing. The discovery of superconductivity in 122* materials, with the large local moment ($3.3\mu_B/Fe$, Bao *et al.*, 2011a) and different Fermi surface (no hole pockets, Zhao *et al.*, 2011) seems at present to argue against the $s_\pm$ model being applicable to all FePn/Ch, but see Mazin (2011) for a discussion.

Predictions for the actual superconducting pairing mechanism are quite broad in scope, with some concentration on spin fluctuations due to, among other reasons, the nearness (sometimes coexistence) in the phase diagram of magnetism to the superconductivity and the inelastic neutron scattering evidence for at least some linkage between superconductivity and a spin fluctuation resonance peak below T_c (Sec. IV.A.1). Related ideas have been explored using phenomenological intraband and interband interaction parameters, leading to similar conclusions (Chubukov, 2009; F. Wang *et al.*, 2009).

A. Theory of superconductivity and some relevant experiments in FePn/Ch

Many have pointed out that the electron-phonon coupling is too weak (by about a factor of 5, Osborn *et al.*, 2009) in these materials to account for the >20 K T_cs. Boeri, Dolgov, and Golubov (2008) calculation of the Eliashberg $\alpha^2 F(\omega)$ produced an electron-phonon coupling parameter $\lambda_{el\text{-}ph} \sim 0.2$, with a follow-up work in the magnetic state by Boeri *et al.* (2010) finding $\lambda_{el\text{-}ph} \leq 0.35$. As examples of

experimental determinations, Rettig *et al.* (2010) found in the 122 parent compound $EuFe_2As_2$, using time resolved ARPES, that $\lambda_{el-ph} < 0.5$ while Mansart *et al.* (2010) found in $BaFe_{1.84}Co_{0.16}$, $T_c = 24$ K, using transient optical reflectivity that $\lambda_{el-ph} \approx 0.12$. However, there are several experimental works indicating an isotope effect (in BCS theory, $T_c \propto M^{-\alpha}$, $\alpha = 1/2$), indicating some role of the phonons in the superconductivity. In $SmFeAsO_{0.85}F_{0.15}$, $T_c = 41$ K, and $Ba_{0.6}K_{0.4}Fe_2As_2$, $T_c = 38$ K, R. H. Liu *et al.* (2009) found a conventional isotope effect, but only for the Fe: substitution of ^{54}Fe for ^{56}Fe results in an increase of T_c proportional to $M^{-0.35}$ with essentially no isotope effect due to substitution of ^{18}O for ^{16}O. Thus, phonon modes involving the Fe may through a magnetoelastic effect affect the magnetic fluctuations and therefore superconductivity, but the results of Liu *et al.* argued against an electron-phonon pairing mechanism. Shirage *et al.* (2010) in oxygen deficient $SmFeAsO_{1-y}$, $T_c = 54$ K, found essentially no isotope effect on the Fe site, with $\alpha = 0.02$. Shirage *et al.* (2009) in contradiction to R. H. Liu *et al.* (2009) found an *inverse* Fe isotope in $Ba_{1-x}K_xFe_2As_2$, $T_c = 38$ K, with $T_c \propto M^{+0.18}$. Khasanov *et al.* (2010b) found a conventional Fe-isotope effect in $FeSe_{1-x}$, $T_c = 8.2$ K, with, after some involved analysis (half of the change in T_c with ^{54}Fe isotopic enrichment is assigned to structural changes in the samples), $T_c \propto M^{-0.4}$. Khasanov *et al.* (2010a), following the same analysis as used in their $FeSe_{1-x}$ isotope effect work, argued that, when adjusted for structural changes, the results of Liu *et al.* and Shirage *et al.* are also consistent with a conventional $\alpha \approx 0.35$–0.4. Obviously, the possible partial role of the phonons in superconductivity in these materials is still not entirely decided but the evidence from the isotope measurements to date, with the possible exception of the low T_c $FeSe_{1-x}$, argues against electron-phonon coupling as the primary pairing mechanism.

Theorists, based on years of experience with the cuprate, heavy fermion, and other exotic superconductors and on the
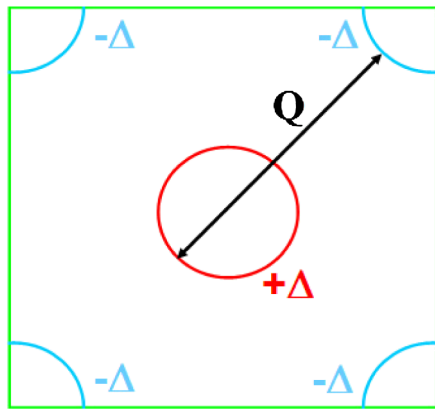

FIG. 26 (color online). Sketch of an idealized Fermi surface of undoped FePn/Ch with the hole pocket (full circle) in the center at the Γ point (0, 0) with energy gap $+\Delta$, the electron pockets (quarter circles) at the corner M (called "X" in some works' notation) points (π, π) with energy gap $-\Delta$, and the spin density wave momentum wave vector Q spanning the two nested pockets. This schematic Brillouin zone (BZ) follows the two Fe atoms/unit cell "folded" BZ notation. For a comparison with the "unfolded" BZ, one Fe/unit cell notation, see Chubukov (2009) or Hirschfeld, Korshunov, and Mazin (2011).

clear inability of the electron-phonon coupling to explain T_c, have proposed a number of electronic ("unconventional") pairing schemes (as opposed to the conventional, phononic, pairing) for the FePn/Ch materials. Beyond the short introduction to these ideas given here, see Boeri, Dolgov, and Golubov (2009), Chubukov (2009), Kuroki and Aoki (2009), Mazin and Schmalian (2009), Hirschfeld, Korshunov, and Mazin (2011), and references therein. For a discussion of the 122* superconductors, see Mazin (2011).

Many of these proposals for the pairing center around the early idea of Mazin *et al.* (2008), that even if the excitation (e.g., spin fluctuations) being exchanged to produce the coupling is repulsive it can still lead to attractive pairing if the excitation is being exchanged between parts of the Fermi surface with opposite signs of the order parameter. Simply put, if $\Delta_k = -\Delta_{k+Q}$ then a repulsive interaction with wave vector Q (Fig. 26) can be attractive due to the sign reversal in the order parameter Δ. This is a realization, specific to the FePn/Ch materials' Fermi surface with several small pockets separated by Q, of the general spin-fluctuation pairing mechanism (Berk and Schrieffer, 1966; Scalapino, 1995). See Sec. IV.A.2 for a discussion of the experimental work on the Fermiology of the FePn/Ch, which, such as the inelastic neutron scattering results discussed in Sec. IV.A.1, is mostly consistent with the proposed spin fluctuation, electronic-in-origin "pairing glue" picture. See also supporting evidence from optical conductivity measurements by J. Yang *et al.* (2009).

1. Spin resonance in INS below T_c

Early inelastic neutron scattering experiments in polycrystalline $Ba_{0.6}K_{0.4}Fe_2As_2$ (Christianson *et al.*, 2008) found evidence, a magnetic resonance below T_c, for a sign change [although see Onari, Kontani, and Sato (2010), for an opposing argument] in the superconducting energy gap Δ on different parts of the Fermi surface. Such a sign change in the order parameter is consistent with the s_{+-} model and the Fermiology of FePn/Ch sketched in Fig. 26. For a system such as $Ba_{0.6}K_{0.4}Fe_2As_2$, which experiments indicate are nodeless (see Sec. IV.B), d-wave pairing would be ruled out. This type of collective excitation/resonant mode below T_c is found in most of the cuprate superconductors [although with differences in, e.g., Sr-doped 214, see Tranquada *et al.* (2004)] as discussed by Eschrig (2006) and the experimental work (and references therein) of Dai *et al.* (2000). In the cuprates, the resonance mode, which is thought to be a triplet excitation of ground state singlet Cooper pairs, is centered in k space at the antiferromagnetic ordering wave vector and is 2D in behavior.

The first INS work on single crystals of $BaFe_{1.84}Co_{0.16}As_2$ (Lumsden *et al.*, 2009) found that the magnetic fluctuations associated with the resonance were, just as in the cuprates, also 2D in nature. Follow-up work on Ni doped $BaFe_2As_2$ found instead different resonant energies at (1/2, 1/2, L) depending on whether L was even or odd, indicating dispersion along the c axis (3D behavior). As shown in Table IV, this 3D character survives in overdoped $BaFe_{1.85}Ni_{0.15}As_2$ (M. Wang *et al.*, 2010). As well, Park *et al.* (2010) have been able to find this dispersive behavior of the resonance fluctuations in Co doped $BaFe_2As_2$.

TABLE IV. Spin resonance energies in the FePn/Ch. With the exception of the initial work and the work on the 1111, 111, and P doped 122 samples, all the experiments have been on single crystals in order to determine the wave vector(s) unambiguously.

Compound	$T_c(K)$	Resonance energy (meV)	$E_r/k_B T_c$	Ref.
$BaFe_{2-x}Co_xAs_2$ $x = 0.08$	11	4.5	4.9	Christianson *et al.* (2009)
$x = 0.094$	17	≈ 4.5	3.2	Pratt *et al.* (2009a)
$x = 0.13$	23	≈ 10	5.2	Lester *et al.* (2010)
$x = 0.148$	22.2	8.3	4.5	H.- F. Li *et al.* (2010)
$x = 0.15$	25	9.5	4.6	Inosov *et al.* (2010)
	25	9.6, 10.5[a]	4.6, 5.0	Park *et al.* (2010)
$x = 0.16$	22	8.6	4.7	Lumsden *et al.* (2009)
$BaFe_{2-x}Ni_xAs_2$ $x = 0.075$	12	5, 7[a]	5.0, 7.0	M. Wang *et al.* (2010)
$x = 0.09$	18	6.5, 8.8[a]	4.3, 5.9	Park *et al.* (2010)
$x = 0.1$	20	7.0, 9.1[a]	4.2, 5.5	Chi *et al.* (2009)
$x = 0.15$	14	6, 8[a]	5.1, 6.9	M. Wang *et al.* (2010)
$FeSe_{0.4}Te_{0.6}$	14/14.6	6.5/7.1	5.6	Qiu *et al.* (2009); Bao *et al.* (2010)
$FeSe_{0.5}Te_{0.5}$	14	6/6.5	≈ 5.6	Wen *et al.* (2010); Mook *et al.* (2010)
$LaFeAsO_{1-x}F_x$ $x = 0.057/0.082$	25/29	11	5.3/4.6	Wakimoto *et al.* (2010)
$Ba_{0.6}K_{0.4}Fe_2As_2$	38	14	4.4	Christianson *et al.* (2008)
$BaFe_2(As_{0.65}P_{0.35})_2$	30	12	4.8	Ishikado *et al.* (2011)
$LiFeAs$	17	≈ 8	$\approx 5–6$	Taylor *et al.* (2011)

[a]Resonances at *two* wave vectors: $\frac{1}{2}, \frac{1}{2}, 1$ and $\frac{1}{2}, \frac{1}{2}, 0$, with different energies.

Interestingly, INS studies (see Table IV) of $FeSe_{1-x}Te_x$ (Qiu *et al.*, 2009; Mook *et al.*, 2010; Wen *et al.*, 2010) found the wave vector of the resonance at the in-plane nesting vector between the electron and hole pockets (Fig. 26), or (1/2, 1/2, 0), as in the 122 single crystal work, and not at the 11 structure magnetic ordering wave vector (1/2, 0, 0) as sketched in Sec. II.B, Fig. 8). The case of nonmagnetic LiFeAs, in which ARPES data discussed in Sec. IV.A.2 indicate that there is, due to the size and shape of the Fermi surface pockets, no nesting is also interesting. Despite this lack of nesting and magnetism, INS studies of polycrystalline LiFeAs (Taylor *et al.*, 2011) also found antiferromagnetic spin fluctuations (and evidence for a spin resonance) in the same (1/2, 1/2) wave vector direction. NMR results also report evidence for antiferromagnetic fluctuations in LiFeAs (polycrystalline work, Jeglic *et al.*, 2010; single crystal work, Ma *et al.*, 2010).

Bao *et al.* (2010) and others found using unpolarized INS that the resonant spin correlations in $FeSe_{1-x}Te_x$ were quasi-2D, just as Lumsden *et al.* (2009) reported in the first work on single crystal Co doped $BaFe_2As_2$, in $BaFe_{1.84}Co_{0.16}As_2$. Whether this 2D characterization of the 11 FeCh survives further investigation is an open question.

A general feature of the resonance in optimally doped 122 $BaFe_{2-x}(Co, Ni)_xAs_2$ and $FeSe_{0.4}Te_{0.6}$ material is that its spectral weight comes from a spin gap that opens at even lower energy ($\leq \frac{1}{2}E_{resonance}$) as temperature is lowered below T_c [see, e.g., Chi *et al.* (2009), Qiu *et al.* (2009), and H.-F. Li *et al.* (2010)]. For underdoped 122 $BaFe_{1.92}Co_{0.08}As_2$, this spin gap is not observed down to 2 meV (Christianson *et al.*, 2009). Note that in 122 the underdoped samples all have coexistent magnetism and superconductivity (discussed with the phase diagrams in Sec. II.B.2.b), while in the optimally and overdoped materials T_{SDW} is suppressed. Indeed, Lumsden and Christianson (2010) pointed out that the spectral weight for the resonance in underdoped $BaFe_{2-x}Co_xAs_2$ may indeed come from the observed suppression of the spectral weight in the magnetic Bragg peaks below T_c.

In agreement with cuprate work, INS studies [see, e.g., Chi *et al.* (2009), H.-F. Li *et al.* (2010), and Inosov *et al.* (2010)] of the FePn/Ch superconductors found that the intensity associated with the spin-fluctuation resonance increases with decreasing temperature below T_c similar to the superconducting order parameter itself. Based on these results, one of the possible conclusions is that if the superconducting order parameter and the spin resonance are indeed linked in a causal fashion, then the order parameter, at least in Co and Ni doped $BaFe_2As_2$, is 3D and should depend sensitively on the c axis wave vectors; see, e.g., M. Wang *et al.* (2010) for further discussion of this.

When discussing the magnetic resonance in cuprates, it is common to point out that there is an approximately uniform scaling of the resonance energy with T_c, implying that the resonance is intimately connected to the superconductivity. In the cuprates, Hüfner *et al.* (2008) stated that $E_{resonance}$ is about $5k_B T_c$. Discussion of this scaling in FePn/Ch (see Table IV) is complicated by the dispersion of $E_{resonance}$ along the c axis, as discussed by M. Wang *et al.* (2010). As Table IV makes clear, there is in addition significant scatter in some of the values. This leads to a breadth in quoted values for the average $E_{resonance}/k_B T_c$ [~ 4.9, Lumsden and Christianson (2010); ~ 4.3, Park *et al.* (2010)]. In any case, the scaling argument made in the cuprates for the resonance appears to be valid in FePn/Ch as well, with the caveat that there may be differences between, e.g., 122 and 11.

Another method for investigating the resonance in the superconducting state of FePn/Ch is to measure its field dependence. If the applied field depresses the intensity and energy of the resonance similarly to its reduction of the superconducting energy gap Δ, this would provide a link between the two like the observed similar temperature dependence. In $BaFe_{1.9}Ni_{0.1}As_2$, $T_c = 20$ K, J. Zhao *et al.* (2010) found that a 14.5 T applied field suppresses $E_{resonance}$ and the associated neutron scattering intensity both by $\sim 20\%$, while T_c is also suppressed by 20% to 16 K. They argued that their data are evidence that the resonance is

related to the superconducting Δ. F. Wang *et al.* (2011), in a neutron scattering study of underdoped $BaFe_{1.92}Ni_{0.08}As_2$ ($T_c = 17$ K, $T_{SDW} = 44$ K) in zero and 10 T, found that the intensity of the INS resonance below T_c is reduced by field while the static antiferromagnetic order is enhanced. They argued that therefore the magnetic order competes with the superconducting order, similar to some of the cuprate superconductors.

A further use of magnetic field for probing the magnetic resonance below T_c in FePn/Ch has been the work of Bao *et al.* (2010). They applied 14 T to an optimized set of single crystals of $FeSe_{0.4}Te_{0.6}$ with a smaller mosaic spread than in previous INS works, and succeeded in their high resolution experiment in finding that the resonance peak splits into a set of three equal intensity peaks in field, a signature of a triplet excited state.

In another work that bears on the question of the triplet character of the resonance in FePn/Ch, Lipscombe *et al.* (2010) performed a polarized INS experiment (previous work discussed above in this section has been with unpolarized neutron sources) on a different material, $BaFe_{1.9}Ni_{0.1}As_2$. Their results are inconsistent with the usual understanding of the magnetic resonance in the cuprates (Eschrig, 2006) as being an isotropic triplet excited state of the ground state Cooper pair singlet, since their polarized neutron results are able to resolve an anisotropy in the resonance. In contrast to this, but in agreement with the magnetic field work of Bao *et al.*, Babkevich *et al.* (2011) found using polarized INS in $FeSe_{0.5}Te_{0.5}$ (comparable to the $FeSe_{0.4}Te_{0.6}$ sample of Bao *et al.*) a "quasi-isotropic" resonance consistent with the triplet excitation scenario.

These INS works on the magnetic resonance in the superconducting state of FePn/Ch indicate that the iron-containing superconductors have fundamental differences in their behavior. Although it is too early to reach a firm conclusion, certainly these resonance studies are of great interest since many theories posit that FePn/Ch superconductivity is mediated by spin fluctuations and/or magnetic excitations. In terms of actual calculations of the strength of the INS-detected fluctuation resonances and their wave vector, Maier and Scalapino (2008) calculated for which gap functions and for which wave vectors resonances in the dynamic spin susceptibility occur. They found for Mazin's predicted $s_\pm$ gap a predicted resonance in the $(1/2, 1/2)$ wave vector direction that matches the antiferromagnetic ordering vector, as well as resonances for two triplet p-wave gaps. Maier *et al.* (2009a), in a following calculation, found in addition to the prediction for the strongest resonance being for $q \parallel (1/2, 1/2)$ and an $s_\pm$ gap, two other weaker possible resonances for a non-sign-changing extended s-wave gap and a $d_{x^2-y^2}$ gap. They argued for further INS measurements along other wave vectors to distinguish which gap is causing the observed resonance.

As well from the experimental perspective, Wu *et al.* (2010), based on a strong similarity between their optical-conductivity-derived $\alpha^2 F(\omega)$ electron-boson spectral function and the INS-determined spin excitation spectrum in optimally doped $BaFe_{2-x}Co_xAs_2$, argue that the charge carriers in these superconductors are strongly coupled to the spin fluctuations. Thus, thorough studies of this resonance

continue to be one of the best approaches (see also experimental determination of the nodal structure in Sec. IV.B) in use to help elucidate the relation between magnetism and superconductivity in these new superconductors.

2. Fermiology in FePn/Ch: Theory and experiment

Theory: The calculated Fermi surfaces of undoped LaFeAsO (Singh and Du, 2008) have two electron cylinders around the tetragonal M point, plus two hole cylinders and a hole pocket around the Γ point. Similar results for the Fermiology of LaFePO, the first reported superconducting ($T_c \approx 5$ K) iron pnictide (Kamihara *et al.*, 2006, were obtained by Lebegue (2007). The calculation of Mazin *et al.* (2008) of the Fermiology for F-(electron) doped superconducting $LaFeAsO_{1-x}F_x$ resulted in a somewhat simplified Fermi surface, with the hole pocket filled. (See the experimental ARPES determinations of the Fermi surface of K doped $BaFe_2As_2$ in Figs. 27 and 28.)

Because of the nearness (even, in parts of the phase diagram in some samples, coexistence) of magnetism (Sec. II), Mazin *et al.* (2008) proposed spin-fluctuation-mediated pairing (weak coupling) for wave vectors connecting the electron and hole cylinders, the so-called s_{+-} pairing state, while rejecting the other possible spin-fluctuation-induced order parameter, i.e., triplet pairing.

Many have also discussed spin-fluctuation mediated pairing in FePn/Ch, with some theories stating that the s_{+-} (also known as "sign-reversing s wave" or "extended s wave") is the only pairing symmetry allowed (Chubukov, Vavilov, and Vorontsov, 2009, Maier *et al.*, 2009b, Y. L. Wang *et al.*,
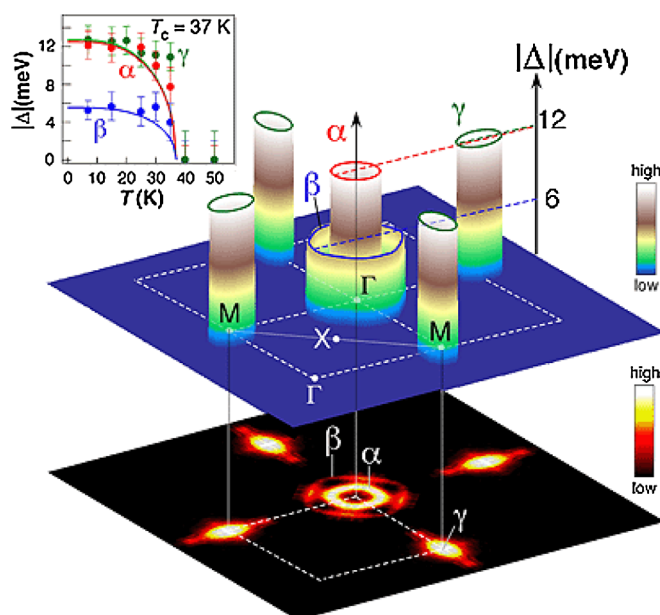
FIG. 27 (color online). Schematic picture of the Fermi surface in $Ba_{1-x}K_xFe_2As_2$ determined by ARPES measurements. The color bars denote the size of the energy gap, and the upper left inset displays the temperature dependence of the gaps on the three Fermi surface sheets (note the two different sized Δs). The α holelike pocket and β holelike sheet are both centered at the Brillouin zone center Γ while the electronlike γ Fermi sheet is centered at the M point. From Ding *et al.*, 2008.
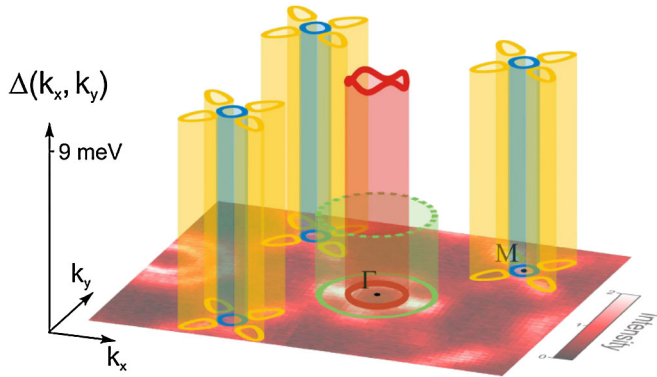
FIG. 28 (color online). ARPES determined Fermi surfaces in K doped $BaFe_2As_2$ (Evtushinsky *et al.*, 2009a). Note the propeller shaped five electron pockets at the M points.

2009), while some give *d*-wave pairing as the preferred state for particular values of the parameters chosen (Kuroki *et al.*, 2008, 2009, Graser *et al.*, 2009, Thomale *et al.*, 2009, Ikeda, Arita, and Kunes, 2010). "Nesting" between cylinders at a Fermi surface implies that one of the cylinders, when shifted over another, would be a close match in shape and size (see also Fig. 26 where the hole and electron pockets in the idealized sketch show perfect nesting). The nesting between the cylinders in Fig. 27 and concomitant measured susceptibility peak at this wave vector are the motivation for the spin-fluctuation pairing mechanism in several theories. A large amount of nesting of states at the Fermi energy is not necessary for the applicability of these theories (nesting changes with doping since the size of the cylinders changes with hole or electron addition to the respective pockets as discussed below when the ARPES data are reviewed). In fact, Platt, Thomale, and Hanke (2011), using a theory that takes into account orbital dependent interactions, proposed that LiFeAs, which as discussed in the experimental section just below has according to ARPES no nesting, also has an s_{+-} order parameter caused by antiferromagnetic fluctuations. As discussed above in Sec. IV.A.1, such fluctuations have now been experimentally found (Taylor *et al.*, 2011).

Some theories have posited that *p*-wave (triplet) pairing is possible (Lee and Wen, 2008; X.-L. Qi *et al.*, 2008; Brydon *et al.*, 2011). Theories of the FePn/Ch superconductors are further split into subgroups depending on whether they involve strong or weak coupling of the magnetic excitations and whether the predicted pairing states are nodal or have gaps. The predicted extended *s*-wave symmetry can be either nodeless or have nodes, depending on the interplay between intraband and interband interactions (Chubukov, Vavilov, and Vorontsov, 2009), which can be tuned by small changes in the electronic structure (Kemper *et al.*, 2010), e.g., by moderate hole doping in $Ba_{1-x}K_xFe_2As_2$ [for a discussion, see Thomale *et al.* (2011b)] or by adjustment of the pnictogen height by substituting P for As (Kuroki *et al.*, 2009). Upon further hole doping in $Ba_{1-x}K_xFe_2As_2$ to KFe_2As_2 Thomale *et al.* (2011b) argued that the modification of the Fermi surface by fully gapping the electron pockets leads to nodal d_{xy}-wave behavior. Interestingly, at the other end of the doping spectrum, the 122* $A_xFe_{2-y}Se_2$ [which, according to

ARPES data by Zhao *et al.* (2011) and references therein, have only electron pockets on the Fermi surface] are predicted (Maier *et al.*, 2011; F. Wang *et al.*, 2011) to have nodeless d_{x2-y2}-wave pairing symmetry [although see Fang *et al.* (2011a) and Mazin (2011) for counterarguments]. Indeed, the richness of the Fermiology in FePn/Ch involves more than just the large number of pockets (up to five) at the Fermi energy, their nesting, and their multiorbital (see the following experimental section for a discussion) character. The variation of the gap structure and superconducting transition temperature across a particular phase diagram with doping adds another dimension to this richness.

Experiment: ARPES on single crystals is a powerful tool that resolves both the Fermi surface structure in momentum space and the spectra of the electronic states near the Fermi energy. For an early review of ARPES investigations of FePn/Ch, see C. Liu *et al.* (2009).

ARPES can show the size, shape, and position in momentum space of the predicted Fermi surface pockets, allowing the verification of the extent of Fermi surface nesting, which is important as discussed above in numerous theories for the role of spin fluctuations in the superconducting pairing mechanism. As well, ARPES data can show the evolution of the Fermi surface pockets with doping, for example, the hole pocket at the Γ point in undoped $BaFe_2As_2/SrFe_2As_2$ expanding with K, i.e., hole, doping. This evolution is, to a first approximation, describable by a rigid band model (Liu *et al.*, 2008; Malaeb *et al.*, 2009; Y. Zhang *et al.*, 2009), although as discussed in Sec. II.B.2.a, the variation of T_c with isoelectronic doping makes clear that such a rigid band picture is oversimplified. Further, ARPES has been used to measure the *magnitudes* of the superconducting gap(s) in the FePn/Ch [see, for example, the inset in Fig. 27 for the two gaps found in K doped $BaFe_2As_2$ by Ding *et al.* (2008)]. Evtushinsky *et al.* (2009b) listed the magnitudes of the superconducting energy gaps determined via ARPES and other measurement techniques (for a discussion of some of these techniques, see Sec. IV.B), showing good agreement between the methods. For determining the *symmetry* of the gap in momentum space ARPES, due to the complexity and difficulty of the method as well as partially due to the inherent error bar [quoted to be ~20% in a work on 1111 material by Kondo *et al.* (2008)], is less used than other methods (Sec. IV.B). It is interesting to note that one of the puzzles of the research to date in the FePn/Ch is that ARPES measurements, despite their success in the cuprates is finding nodes (Damascelli, Hussain, and Shen, 2003) and despite there being (see Sec. IV.B) a wealth of other experimental evidence for nodal behavior in FePn/Ch, in general are interpreted as consistent with fully gapped behavior.

As with any measurement technique, ARPES measurements also have limitations, among them a resolution of at best several (sometimes as high as 15) meV, and a sensitivity to surface physics. For a discussion of some of these experimental limitations, see Yi *et al.* (2009) and van Heumen *et al.* (2011), as well as the theoretical discussion of Kemper *et al.* (2010) on the sensitivity of the surface band structure in FePn/Ch to small perturbations. Van Heumen *et al.* showed that the standard methods for preparing a clean surface for ARPES measurements (cleaving at low temperatures) in

$BaFe_{2-x}Co_xAs_2$ create surface states which broaden the ARPES spectra and also cause a surface related band (which can be annealed away by warming to 150 K, followed by recooling) not characteristic of the bulk. This is similar to ARPES results for 1111 (Liu *et al.*, 2010a). It should be noted that the surface in LiFeAs, due to the surface chemistry, does not (Lankau *et al.*, 2010) have such an influence on ARPES results.

There has been a large amount of ARPES work to characterize these new FePn/Ch superconductors. Work to date, because of the size and quality of the single crystals, has been focused in the 122 and 11 structures, which as an exception to the normal sequence in this review will be discussed first in this section, with some results in 1111 [where of course for undoped LaFePO sizeable crystals exist but also including work on $200 \times 200 \times 50~\mu$m crystals of $NdFeAsO_{0.9}F_{0.1}$, see Kondo *et al.* (2008)], 111, 21311, and 122* materials discussed afterwards. As will be seen, and as follows a recurring theme in this review, there are important differences in the ARPES-determined Fermiology for the various structures, particularly for the nesting, which is important for the theories of spin-fluctuation-mediated superconductivity. ARPES data for FePn/Ch, with their strong Fe conduction bands (width $\sim$4 eV) which have significant densities of states at the Fermi energy, strongly contrast with those for the cuprates [for a review of ARPES in the cuprates, see Damascelli, Hussain, and Shen (2003)].

122: In the early ARPES work of Ding *et al.* (2008) (Fig. 27), in K doped $BaFe_2As_2$ the general topology of five Fermi surface sheets (versus one in the cuprates) matching the calculations was clearly revealed. The schematic nature of the pockets, i.e., the cylindrical shape, in the 122 compounds has been refined by more recent work, e.g., Malaeb *et al.* (2009) in both $BaFe_2As_2$ and $BaFe_{1.86}Co_{0.14}$ to show significant variation of the size of the pocket in the k_x–k_y plane along the z axis, particularly around the Γ point, giving a 3D character. This 3D variation is seen even in the parent $BaFe_2As_2$ but is accentuated around both the Brillouin zone hole Γ center and electron M corner pockets in the doped compound. This 3D character in $BaFe_2As_2$ and its derivatives are consistent with ARPES work on the other 122s, see e.g. Hsieh *et al.* (2008) ($SrFe_2As_2$), Kondo *et al.* (2010) ($CaFe_2As_2$), and Zhou *et al.* (2010) ($EuFe_2As_2$) and with calculations, see, e.g., Ma, Lu, and Xiang (2010) for DFT calculations on MFe_2As_2, $M =$ Ba, Sr, Ca.

Another refinement of the Fermiology in K doped $BaFe_2As_2$ was carried out by Zabolotnyy *et al.* (2009), using improved energy resolution. They found (in disagreement with calculations and the early ARPES work), instead of the double walled electron pocket at the M point shown in Fig. 27, a central circular pocket surrounded by four "blade" shaped pockets, described as like the shape of a propeller. This result was refined by Evtushinsky *et al.* (2009a), see Fig. 28, who determined the superconducting gap in K doped $BaFe_2As_2$ in all of these pockets, with the result that the gap on the inner barrel at Γ and in the inner circular pocket and outer blades at M was approximately the same at 9 meV, while the gap on the outer barrel at Γ was only $\sim$4 meV.

The Fermiology in the parent compounds exhibits a temperature dependence due to the strong influence of the magnetic moment on the band structure below T_{SDW}. Yi *et al.* (2009) detailed the Fermi surface reconstruction below $\sim$135 K in $BaFe_2As_2$, with multiple new bands appearing. Below T_{SDW} their ARPES data show, in addition to two hole pockets centered at the Γ point, the appearance of four small surrounding "petal shaped" electron pockets while at the M point four holelike bands exist below T_{SDW} that merge into one above. Richard *et al.* (2010) using ARPES found the creation of "tiny Fermi surface pockets" below T_{SDW} in $BaFe_2As_2$ due to a Dirac cone in the electronic structure below T_{SDW}. In a follow-up ARPES work, Liu *et al.* (2010b) followed the evolution of the magnetic-order-induced additional holelike pockets of Yi *et al.* at the M point in $BaFe_{2-x}Co_xAs_2$ as a function of Co doping and found that they disappear at the point in the phase diagram where superconductivity appears. Liu *et al.* advanced the plausible (but not conclusive) argument that the pairing interaction due to spin fluctuations is suppressed by the long range magnetic order, which is indicated by the additional Fermi surface features. They also showed that there is no nesting between the Γ and M point Fermi surface pockets at $x = 0.114$ even though there is still superconductivity ($T_c = 12.8$ K), yet another argument that nesting is not necessary for superconductivity (see the discussion of ARPES in the 111 and 122* materials below for a similar result.)

Recent ARPES work with improved (~ 10 meV) resolution (Yoshida *et al.*, 2010a) on the strongly hole-doped end point of $Ba_{1-x}K_xFe_2As_2$, i.e., on pure KFe_2As_2, $T_c \sim 4$ K, revealed three hole pockets [versus two in earlier work, Sato *et al.* (2009)] at the zone center Γ point and, as expected from calculation, a small *hole* pocket (due to the strong hole doping) at the M points. The Fermi surface pockets, in contrast to the other 122 results discussed above, are nearly 2D in character and, due to the strong hole doping, have no electron pockets (no nesting.) An additional hole band near the hole center is seen in the ARPES data that is not in the calculation. Yoshida *et al.* (2010a) speculated this may due to surface states, again illustrating the difficulties of this very surface-sensitive measurement.

As mentioned in the introduction to this experimental ARPES section, ARPES data in general do not find nodal behavior in FePn/Ch. This is true, for example, in the prototypical (Sec. IV.B) nodal case, P doped $BaFe_2As_2$, where Yoshida *et al.* (2010b), using synchrotron radiation with an energy resolution of 15 meV, found no evidence of nodes.

11: ARPES studies of the 11 materials are to date more limited in number. In the parent compounds, Xia *et al.* (2009) found in $Fe_{1+x}Te$ a hole pocket at the Γ point and four electron pockets at the corner M points, similar to calculations (Subedi *et al.*, 2008) and to the experimental results for 1111 and 122 as sketched in Fig. 26. Unlike other magnetically ordered parent compounds, however, Xia *et al.* found no evidence for a SDW nesting-driven gap in the bands below T_{SDW}, $\sim$70 K, in $Fe_{1+x}Te$. This is consistent with the discussion in Sec. II.B (see Fig. 8) about the magnetic ordering wave vector in 11 $(1/2, 0)$ not being in the same direction $(1/2, 1/2)$ as links the nested electron and hole pockets. However, it is worth pointing out that, as discussed in Sec. IV.A.1, the INS-determined spin resonance below T_c in the doped 11 structure superconductors shows spin

fluctuations indeed in the electron-hole pocket nesting vector direction.

1111: As mentioned in the introduction to this section, ARPES data have been measured on NdFeAsO$_{0.9}$F$_{0.1}$, $T_c =$ 53 K, and LaFePO, $T_c = 5.9$ K. In NdFeAsO$_{0.9}$F$_{0.1}$ Kondo *et al.* (2008) reported the same Fermiology as reported for 122 and concentrate on measuring the magnitude of the superconducting gap. The gap at the Γ point is found to be 15 meV, with no measurable nodes or anisotropy within their error limits. Early ARPES work (Lu *et al.*, 2008) on LaFePO found reasonable agreement with local density approximation calculations and the usual five Fermi sheets, with hole pockets centered at the Γ point (based on d_{xz} and d_{yz} Fe orbitals for the inner pocket and based on Fe $d_{3z^2-r^2}$ states hybridized with P p orbitals and La orbitals for the outer pocket) and electron pockets at the M point.

111: Although the Fermi surface (Borisenko *et al.*, 2010) of 111 LiFeAs has qualitative similarities to the 122, 11, and 1111 topologies just discussed (i.e., the requisite five Fermi surface pockets corresponding to the five Fe 3d bands, with three holelike FSs around the Γ point and two electronlike ones at the corner of the Brillouin zone, with 3D character somewhat reduced versus the 122 structure), there is one important difference. As Borisenko *et al.* (2010) pointed out, the disparate sizes of these five pockets at Γ and M argues against any $(1/2, 1/2)$ nesting at all. This could be used as an argument for nesting being important for magnetism [see the counter arguments of Johannes and Mazin (2009), discussed in Sec. II.B] since LiFeAs is not magnetic. Borisenko *et al.* (2010) further reported an isotropic energy gap of $\sim$3 meV in the double walled electron cylindrical pocket at the M point in LiFeAs.

21311: Single crystals of a few tenths of a mm on a side of Sr$_2$VO$_3$FeAs have been measured using ARPES (Qian *et al.*, 2011). The results showed some nesting between the outer (β) of two circular hole pockets at the Γ point and the outer (δ) of two elliptical electron pockets at the M point, making 21311 similar to the 122, 11, and 1111 structures in their nesting.

122*: In the early ARPES work on these superconductors, there were sample quality issues. Zhao *et al.* (2011) reported unifying results on single crystals of K$_{0.68}$Fe$_{1.79}$Se$_2$ and (Tl$_{0.45}$K$_{0.34}$)Fe$_{1.84}$Se$_2$ (composition determined by energy dispersive x-ray spectroscopy), $T_c = 32$ and 28 K, respectively. In both materials they found at the zone center Γ two electron pockets, a small one they label α and a low intensity, larger pocket labeled β, and at the zone corner M an electron pocket labeled γ similar in size to the β pocket. The energy gaps for the γ pocket in both materials are $\approx$ 8–9 meV and fairly isotropic. These features are similar to those found in ARPES measurements on Tl$_{0.58}$Rb$_{0.42}$Fe$_{1.72}$Se$_2$ (Mou *et al.*, 2011, Γ and M pockets gaps of 15 and 12 meV, respectively) and in previous measurements of Tl$_{0.63}$K$_{0.37}$Fe$_{1.78}$Se$_2$ (X.-P. Wang *et al.*, 2011, Γ and M pockets gaps both $\approx$ 8 meV). Although all three of these ARPES works claim their results imply nodeless behavior in 122*, due to sensitivity and energy resolution issues this is not conclusive. X.-P. Wang *et al.* reported that there is a hole pocket approximately 50 meV below the Fermi energy at the Γ point which F. Wang *et al.* (2011) noted could have an important influence on the pairing interaction.

B. Experimental probes of the nodal structure

Understanding the pairing mechanism in the FePn/Ch superconductors is a central goal to the study of these materials. In a "conventional" superconductor, the superconducting gap, barring strong impurity effects, is nodeless, and the temperature dependence of a number of experimental probes is exponential, $\propto \exp(-\Delta/T)$. The nodal structure in the FePn/Ch superconductors is thus heavily studied deep in the superconducting state, $T \ll T_c$, for clues about the pairing symmetry and thus the pairing mechanism although defect scattering can play an important role in the nodal structure, e.g., gapped behavior may arise through intraband defect scattering (Mishra *et al.*, 2009a). In the discussion of the Fermiology above (Sec. IV.A.2), a number of theories and their predictions for the pairing symmetry were mentioned. The possible underlying pairing mechanisms are many and varied as discussed in the theory section above (in the introduction to Sec. IV and in Sec. IV.A) and in the several reviews cited there. While exchange of spin fluctuations as the pairing mechanism has at present somewhat more experimental support (see Secs. IV.A and IV.A.1), there is certainly no consensus within sight at this time. Thus, the experimental study of the nodal structure is important to provide further clues to the pairing mechanism responsible for the rather high T_c values found in FePn/Ch.

The generally accepted fact that the FePn/Ch superconductors have multiple bands at the Fermi surface (see, e.g., the ARPES data in Figs. 27 and 28) creates a variety of possibilities for the gap structure. As pointed out by Kemper *et al.* (2010), this multiplicity of nearly compensated electron and hole Fermi surfaces (excluding of course the 122* structure and KFe$_2$As$_2$) and the concomitant sensitivity of various properties, including the nodal structure, to small changes in atomic and/or electronic structure makes FePn/Ch "quite special." Further, Kemper *et al.* (2010) issued a warning that is important to remember during the remainder of this section: the sensitivity of the band structure may cause surface probes of the nodal structure to return evidence for a nodeless, fully gapped superconductor while the bulk behavior might in fact be nodal. More generally, measurements that probe primarily the surface are sensitive to small changes that in FePn/Ch can have important impact, see, e.g., the discussion of ARPES above (Sec. IV.A.2) and the work by van Heumen *et al.* (2011) on surface reconstruction effects. Thus, in order to experimentally determine the nodal structure, it is important to consider more than just one experimental method, preferably including at least one bulk probe. Even when such multiple results exist, it is important to note (Hirschfeld, 2011) that κ and λ, unlike the specific heat, are weighted by the Fermi velocity, v_F, and may be dominated by nodal behavior from a small, high v_F part of the Fermi surface, resulting in κ and/or λ measurements implying nodes in a system, while specific heat data imply a fully gapped superconductor. This may be more of an issue in the future as more specific heat data in field and as a function of angle become available.

Like ARPES just discussed, infrared optical spectroscopy [see, e.g., Dubroka *et al.* (2008); Li *et al.* (2008); Gorshunov *et al.* (2010); Tu *et al.* (2010); Cheng *et al.* (2011), and the review by Dressel *et al.* (2010)] is more used to determine the *size* of the gap rather than its symmetry [although see

Carbotte and Schachinger (2010), for theoretical modeling of how optics could provide more information about the nodes in the FePn/Ch]. The experimental probes used in the study of the nodal structure in FePn/Ch discussed here are penetration depth [$\Delta\lambda(T)$], NMR spin lattice relaxation time ($1/T_1$), specific heat $C/T(T \to 0)$ (γ), thermal conductivity (κ/T), Andreev spectroscopy, Josephson tunneling, and Raman scattering. The results to date of these experimental probes are both numerous and often self-contradictory. Reasons for these contradictions range from the trivial, including sample quality, to rather subtle. As an example of the latter, the complicated Fermiology and multiple bands return different results to probes that measure differing parts of the Fermi surface. Thus, measurement of the thermal conductivity κ (dominated by the light electron sheets on the Fermi surface) in P doped BaFe$_2$As$_2$ up to 12 T [$H_{c2}(0) = 52$ T] returns $\kappa \sim H^{1/2}$ which implies (Hashimoto *et al.*, 2009b) a gap with nodes. In contrast, the specific heat (dominated by the heavy hole sheets) on the same sample as a function of field up to 15 T appeared to result in $\gamma \sim H$ which implies (J. S. Kim *et al.*, 2010) fully gapped behavior. Recent measurements in P doped BaFe$_2$As$_2$ (Y. Wang *et al.*, 2011) focused on the low field γ (up to 4 T) does in fact reveal $\gamma \sim H^{1/2}$ and will be discussed below in the specific heat Sec. IV.B.3.

In order to provide a way to follow this involved discussion, it is useful to note that, despite all the disagreements, some compounds, as is discussed below, show mostly concurring evidence for nodes, and for some there is fairly good agreement for fully gapped behavior. As a short summary, a list of the *nodal* FePn/Ch superconductors and the supporting data would include LaFePO [$\Delta\lambda(T) \propto T$, analysis of $\kappa(T)$], KFe$_2$As$_2$ [$\Delta\lambda(T) \propto T$, large value of κ/T as $T \to 0$, $\kappa(H)/T \propto H^{1/2}$], P doped BaFe$_2As_2$ [$\Delta\lambda(T) \propto T$, $1/T_1 \propto T$, significant value of κ/T as $T \to 0$, $\kappa(H)/T \propto H^{1/2}$, $\gamma \propto H^{1/2}$ for $H < 0.1 H_{c2}$], and *overdoped* BaFe$_{2-x}$Co$_x$As$_2$ [$\kappa(H)/T \propto H^{1/2}$, $\gamma \propto H^{0.7}$]. It is interesting to note that the first two of these are low T_c materials, $T_c \approx 5$–6 and 3.4 K, respectively, and that KFe$_2$As$_2$ has, due to K being monovalent, a much different (Hashimoto *et al.*, 2010a) Fermiology (including no nesting and 2D behavior, as discussed in Sec. IV.A.2) than the other 122 FePn/Ch superconductors. In fact, as noted in Sec. III.B.3 in the discussion of $\Delta C/T_c$, KFe$_2$As$_2$ may be more comparable to an electron-phonon coupled superconductor. A list of the *fully gapped* materials would include Ba$_{1-x}$K$_x$Fe$_2$As$_2$ [analysis of $\Delta\lambda(T)$, $\gamma \propto H^1$, $\kappa/T \approx 0$ as $T \to 0$] and *underdoped* BaFe$_{2-x}$Co$_x$As$_2$ [analysis of $\Delta\lambda(T)$, $\kappa/T \approx 0$ as $T \to 0$].

Even within this short list, there are contradictions. For the supposed nodal systems, $\kappa/T \approx 0$ as $T \to 0$ (consistent with gapped behavior) for overdoped BaFe$_{2-x}$Co$_x$As$_2$. [However, note that nodes have been reported in c-axis thermal conductivity measurements for overdoped BaFe$_{2-x}$Co$_x$As$_2$ (Reid *et al.*, 2010; Mishra, Graser, and Hirschfeld, 2011)]. For the putative fully gapped systems, some NMR $1/T_1$ data for Ba$_{1-x}$K$_x$Fe$_2$As$_2$ indicate nodal behavior and specific heat in field data for underdoped BaFe$_{2-x}$Co$_x$As$_2$ gives $\gamma \propto H^{0.7}$ over a broad field range just as in the overdoped, believed-to-be-nodal material.

It is notable that these conclusions about nodal structure are not consistent within a given structure, nor sometimes

even within a given doping series, with underdoped BaFe$_{2-x}$Co$_x$As$_2$ different than overdoped (although not according to the $\gamma \propto H^{0.7}$ data).

Finally, before beginning the discussion of the experimental data, we list some caveats. In discussing systems where the experimental probes do not find exponential (fully gapped) temperature dependences, nodes caused by the underlying symmetry of the superconducting order parameter (of interest for understanding the superconducting pairing mechanism) should be distinguished from states in the superconducting gap caused by defects. In the case of realistic materials with unavoidable defects, states in the superconducting gap at the Fermi energy due to defects will of course cause a finite γ_r. Further, if these defect states are extended (offering a complete path in real space), then κ/T will also be finite. Nodes in the $s_\pm$ scenario are accidental if they exist, and are not symmetry driven. Note that deep minima in the gap [see, e.g., Tanatar *et al.* (2010a)] can mimic nodal behavior in measurements done as a function of temperature unless measurements are done to very low (dilution refrigerator) temperature. On the other hand, measurements in fields of several Tesla in materials with deep minima in the gap will mimic nodal behavior at low ($\leq$ several Kelvin) temperature, since the field energy scale is much larger than the milliKelvin gap scale.

1. Penetration depth measurements

The temperature dependence of the London magnetic field penetration depth below T_c can give information about the superconducting gap structure. Various measurement techniques are employed, including rf tunnel diode cavity oscillators, μSR, scanning tunneling microscopy, and small angle neutron scattering. For a fully gapped superconductor, $\Delta\lambda(T) \propto \exp(-\Delta/T)$. At sufficiently low temperatures ($T_c/T < 0.25$) the superfluid density of the superconducting electrons,

$$\rho_{SF} = \{1/[\lambda(T)/\lambda(0)]\}^2$$
$$= \{1/(1 + [\lambda(T) - \lambda(0)]/\lambda(0))\}^2$$
$$= \{1/[1 + \Delta\lambda(T)/\lambda(0)]\}^2,$$

can be approximated by just the leading correction term $[1 - 2\Delta\lambda(T)/\lambda(0)]$ in the expansion

$$\rho_{SF} = [1 + \Delta\lambda(T)/\lambda(0)]^{-2}$$
$$\approx 1 - 2\Delta\lambda(T)/\lambda(0) + 3[\Delta\lambda(T)/\lambda(0)]^2$$
$$- 4[\Delta\lambda(T)/\lambda(0)]^3 + \cdots, \tag{1}$$

where $\Delta\lambda(T)$ is the temperature dependent penetration depth $\lambda(T)$ minus the value of the penetration depth as $T \to 0$, $\lambda(0)$, i.e., $\Delta\lambda(T) = \lambda(T) - \lambda(0)$.

The temperature dependence of the superfluid density ρ_{SF}, which can be found by measurements of the penetration depth via Eq. (1), indicates the nodal gap structure. For a gap function with nodes, λ varies more rapidly with temperature, requiring higher order terms beyond the first correction term in Eq. (1) or measurements to lower temperature.

a. $\Delta\lambda(T) \propto T$ [or, equivalently, using this temperature dependence for $\Delta\lambda(T)$ and just the first term in the expansion in

(1) for the superfluid density, $\rho_{SF} \approx 1\text{-const} \times T$], for temperatures much smaller than T_c is clear indication of nodes (e.g., line nodes from d-wave pairing symmetry), with one proviso. Roddick and Stroud (1995) raised the possibility that $\Delta\lambda(T) \propto T$ could also be due to phase fluctuations, and estimated the magnitude of the effect on the coefficient C of the temperature in $\lambda(T) - \lambda(0) = CT$, as $C \approx k_B[8\pi\lambda(0)^3]/\xi_0\varphi_0^2$, where ξ_0 is the coherence length and $\varphi_0 = 2.07 \times 10^{-7}$ G cm^2 is the flux quantum. For $\lambda(0) = 2000$ Å and $\xi_0 = 10$ Å, Roddick and Stroud got $C \approx 1$ Å/K. Thus, any conclusions about nodal behavior in FePn/Ch from $\Delta\lambda(T) \propto T$ (or $\rho_{SF} \approx 1\text{-const} \times T$) should consider whether the slope $d\lambda/dT$ of the measured variation of the penetration depth with temperature is comparable to the estimate for C from phase fluctuation effects. For the materials considered here $C < 1$ Å/K [e.g., for LaFePO, $\lambda(0) \approx 2400$ Å, Fletcher *et al.* (2009), $\xi_0 \approx 60$ Å estimated from H_{c2}, Yamashita *et al.* (2009), giving $C \approx 0.3$ Å/K] and $d\lambda/dT$ is measured to be much larger. Thus, the conclusion that $\Delta\lambda(T) \propto T$ implies nodal behavior is valid in FePn/Ch. The clean, linear decrease with increasing temperature of ρ_{SF} for $T \ll T_c$ can be smeared by slight disorder (Hashimoto *et al.*, 2010b); see the following discussion for $\Delta\lambda(T) \propto T^2$.

b. $\Delta\lambda(T) \propto T^2$. At low temperatures for both d-wave parity in the presence of strong scattering (Hirschfeld and Goldenfeld, 1993) as well as for a fully gapped $s_\pm$ state also with strong impurity scattering (Vorontsov, Vavilov, and Chubukov, 2009). Thus, impurities and/or quality of sample can play an important role in being able to translate a "simple" temperature dependence of $\Delta\lambda(T)$ (or indeed any of the experimental probes of nodal structure discussed below) into a firm conclusion as to the gap structure. As a further example of the difficulty in interpretation, $\Delta\lambda(T) \propto T^2$ has also been interpreted (Einzel *et al.*, 1986) as evidence for axial spin triplet, p-wave pairing in the heavy fermion superconductor UBe$_{13}$.

Thus, as will be true of most of the experimental probes of the nodal structure discussed in this review, clear interpretation of a single probe may be difficult, particularly in the FePn/Ch superconductors with their complicated Fermiology whose implications for various measurements, including magnetic penetration depth, in the presence of scattering [see, e.g., Vorontsov, Vavilov, and Chubukov (2009)] is still in the process of being understood theoretically. For a review of magnetic penetration depth in unconventional superconductors, see Prozorov and Giannetta (2006), while Gordon *et al.* (2010) provided an overview of such measurements in the FePn/Ch.

(1.) 1111 Structure: Perhaps due to sample problems in the small (50 μm) single crystals available in the early investigation of the As-based 1111 FePn superconductors, or perhaps due to intrinsic differences between various rare earth 1111 compounds, there remains open discussion as to what to conclude about the gap structure in 1111 from penetration depth measurements. There are reports of fully gapped behavior (PrFeAsO$_{1-x}$, Hashimoto *et al.*, 2009b and SmFeAsO$_{1-x}$F$_x$, Malone *et al.*, 2009) and a report of $\Delta\lambda(T) \propto T^2$ behavior interpreted as consistent with unconventional two gap superconductivity (La/NdFeAsO$_{0.9}$F$_{0.1}$, Martin *et al.*, 2009b).

In the $T_c \approx 6$ K 1111 superconductor LaFePO, there is agreement (Fletcher *et al.*, 2009; Hicks *et al.*, 2009a) that $\Delta\lambda(T) \propto T$, with analysis of this evidence for nodal structure leaving both d-wave and multiband s-wave symmetry with nodes as possible explanations. Fletcher *et al.* found the slope of λ with temperature (with an exponent within 5% of T), proportional to the rate at which the gap grows away from the nodes, for their three samples to be 200–300 Å/K, while Hicks *et al.* [whose exponent n for $\Delta\lambda(T) \propto T^n$ data down to $0.06T_c$ varies between samples from 0.97 to 1.22] found $d\lambda/dT$ to be 143 ± 15 Å/K. Thus, since $d\lambda/dT$ is much greater than the Roddick and Stroud (1995) estimate for the contribution from phase fluctuations, the measured $\Delta\lambda(T) \propto T$ behavior in LaFePO is indicative of nodes in the gap.

(2.) 122 Structure: Although much larger crystals of 122 FePn superconductors were generally available than for the 1111 material (with the exception of LaFePO), there is a similar range of conflicting results on *a priori* similar samples. Hashimoto *et al.* (2009a), for their cleanest K doped BaFe$_2$As$_2$ crystal, found two band gaps, both fully gapped, consistent with ARPES data (Sec. IV.A.2). Khasanov *et al.* (2009a), using μSR, also found two gaps. Martin *et al.* (2009a) for their samples of K doped BaFe$_2$As$_2$ found $\Delta\lambda(T) \propto T^n$, with $n \approx 2$.

Work by the latter group on Co doped BaFe$_2$As$_2$ (Gordon *et al.*, 2009a; 2009b) found n ranges from ≈ 2 for underdoped to about 2.5 in overdoped samples, which was interpreted to imply either gapless regions or point nodes in the superconducting gap. Using magnetic force microscopy and scanning superconducting quantum interference device (SQUID) susceptometry, Luan *et al.* (2010) measured single crystal BaFe$_{1.90}$Co$_{0.10}$As$_2$ and described their data [$\Delta\lambda(T) \propto T^{2.2}$] using a clean two-band fully gapped model, consistent with the $s_\pm$ model.

Work on BaFe$_{2-x}$Ni$_x$As$_2$ found (Martin *et al.*, 2010) in overdoped material, $x = 0.144$, $T_c \approx 7$ K that λ in the c-axis direction behaved linearly with temperature (nodal), while $\lambda_{ab} \propto T^{1.6}$, i.e., anisotropy was present. In the underdoped, $x = 0.066$ and $T_c = 15$ K, and optimally doped regimes, $x = 0.092$ and $T_c = 19.4$ K, λ was isotropic, with the temperature exponent being 2 or larger. This opened up the possibility of a three dimensional nodal structure [see the 3D spin-fluctuation pairing calculations of Graser *et al.* (2010)] in the (over) Ni doped BaFe$_2$As$_2$, unlike what was seen in the Co doped and unlike the underdoped-with-Ni case, i.e., indicating a true richness of behavior in these materials. Upon irradiation of a nearly optimally doped BaFe$_{2-x}$Ni$_x$As$_2$ sample, $T_{c0} = 18.9$ K, as T_c decreases with irradiation (down to 15.9 K) the temperature exponent in $\lambda \propto T^n$ also decreases by about 15% (Kim *et al.*, 2010a). H. Kim *et al.* analyzed these results, where disorder increases, as consistent with a nodeless s_{+-} state in their optimally doped BaFe$_{2-x}$Ni$_x$As$_2$ and in agreement with the result for a similar composition by Martin *et al.* (2010).

μSR determination of λ in SrFe$_{1.75}$Co$_{0.25}$As$_2$, $T_c = 13$ K, (Khasanov *et al.*, 2009b) found 2 gaps. The size of the two gaps, when normalized as $2\Delta/k_BT_c$, agrees well with the general behavior of all FePn/Ch (with the large and small $2\Delta/k_BT_c \approx 7/2.5$) based on all the measurement techniques as reviewed by Evtushinsky *et al.* (2009b).

Measurements of $\Delta\lambda(T)$ (Hashimoto *et al.*, 2010a) in very clean (RRR $\approx$ 1200) crystals of KFe_2As_2, the $T_c = 3.4$ K end point of the $Ba_{1-x}K_xFe_2As_2$ phase diagram, resulted in linear with temperature dependence down to $0.1T_c$ with some admixture of T^2 due to impurity scattering below this temperature. They fitted $\Delta\lambda(T)$ to $T^2/(T + T^*)$ with $T^* \approx 0.3$ K. The slope $d\lambda/dT \sim 550$ Å/K (i.e., much greater than the phase fluctuation contribution, almost a factor of 4 larger than in LaFePO), implying line nodes. Thus, the non-nested Fermiology at the K end point in the $Ba_{1-x}K_xFe_2As_2$ phase diagram has perhaps surprisingly clear indication of nodal superconductivity. In a single crystal of $BaFe_2(As_{0.7}P_{0.3})_2$, $T_c = 30$ K, Hashimoto *et al.* (2010b) found $\Delta\lambda(T) \propto T^{1.1}$ [or $\propto T^2/(T + T^*)$, with $T^* = 1.3$ K or $0.04T_c$, comparable to the value for KFe_2As_2] between 0.2 and 6 K with $d\lambda/dT \approx 25$ Å/K. Using their NMR and thermal conductivity data, they concluded that there are line nodes in the gap of a relatively clean superconductor (*d* wave rather than impurity scattered $s_\pm$). The Roddick and Stroud (1995) phase fluctuation constant C is 0.4 Å/K, using $\lambda(0) \approx 2000$ Å, typical of FePn/Ch, and $H_{c2}(0) = 52$ T from Hashimoto *et al.* (2010b), which implies $\xi_0 = 25$ Å, i.e., negligible compared to the $d\lambda/dT$ of ≈ 25 Å/K from the penetration depth measurements of Hashimoto *et al.* (2010b).

It is important to reiterate that $\Delta\lambda(T)$ behaving approximately linearly with temperature [as discussed here for LaFePO, KFe_2As_2, and $BaFe_2(As_{0.7}P_{0.3})_2$] is not only consistent with nodal behavior. It is, at least according to current theoretical understanding and as long as the phase fluctuation contribution is minimal, a proof thereof. However, the other power law behaviors for $\Delta\lambda$ (e.g., T^2) can be interpreted as either due to nodes or due to an $s_\pm$ scenario with strong impurity scattering (Vorontsov, Vavilov, and Chubukov, 2009), as mentioned above.

(3.) 111 Structure: Measurements (Inosov *et al.*, 2010) of $\Delta\lambda(T)$ determined from the magnetic field dependence of the form factor in small angle neutron scattering in a large single crystal of LiFeAs, $T_c = 17$ K, imply a single isotropic superconducting gap. Imai *et al.* (2011), using microwave surface impedance, determined the in-plane penetration depth of single crystal LiFeAs, $T_c^{onset} = 19.0$ K, and found their data to be consistent with two nodeless isotropic gaps. H. Kim *et al.* (2011), using single crystals of LiFeAs, $T_c = 17.5$ K, found, via tunnel diode resonance, data in agreement with Imai *et al.*, i.e., two nodeless isotropic gaps.

(4.) 11 Structure: Measurements (Bendele *et al.*, 2010; Khasanov *et al.*, 2008) of $\Delta\lambda(T)$ using μSR data on $Fe_{1.045}Se_{0.406}Te_{0.594}/FeSe_{0.85}$ and $T_c = 14.6$ and 8.3 K, were fit by a fully gapped two gap $s_\pm$ model. Measurements (Kim *et al.*, 2010b) of $\Delta\lambda(T)$ using a tunnel diode oscillator on $Fe_{1.03}Se_{0.37}Te_{0.63}$ resulted in approximately T^2 behavior, which was interpreted as evidence for multigap superconductivity with scattering causing pair breaking and thus deviation from $\exp(-\Delta/T)$ behavior.

2. NMR and NQR measurements

Measurements of the temperature dependence of $1/T_1T$, where $1/T_1$ is the nuclear-spin-lattice relaxation rate, in the superconducting state of the FePn/Ch compounds have been used to infer the presence or absence of a residual density of states, "DOS", (gapless or nodal behavior). Coupled with other experimental probes, such data contribute to a more complete understanding. Although the applied magnetic field used to carry out the NMR measurements can introduce normal regions, i.e., vortex cores (and thus evidence for a finite DOS), the upper critical fields in these materials are high enough that this is generally not a problem. Methods to avoid the field induced DOS include NMR data on $1/T_1$ taken as a function of field and extrapolated to $H = 0$ and zero field nuclear quadrupole resonance (NQR) measurements of $1/T_1$. A peak in $1/T_1$ just below T_c, the Hebel-Schlichter coherence peak for a conventional isotropic gap open everywhere on the Fermi surface (simple *s*-wave symmetry), is in general not seen in the NMR or NQR measurements of all six structural families of the FePn/Ch superconductors. The lack of this coherence peak is discussed as theoretically consistent with the nodeless $s_\pm$ symmetry state by Parker *et al.* (2008). For spin singlet (*s* or *d* wave) pairing, the spin susceptibility part of the NMR Knight shift decreases to zero below T_c in all crystalline directions, thus ruling out triplet pairing. Thus, a strong decrease in the measured Knight shift below T_c, which as discussed below is sometimes seen in FePn/Ch, can be used to argue for singlet pairing. However, the *lack* of such a strong decrease in the total Knight shift need not be due to triplet pairing, since there are often large contributions, e.g., van Vleck (interband) susceptibility, not affected by the superconductivity which mask the spin susceptibility. For a discussion of this, see Joynt and Taillefer (2002) and their review of UPt_3, which is an example of an unconventional superconductor whose very small Knight shift below T_c has been interpreted as evidence for spin triplet pairing.

(a.) 1111 Structure: Grafe *et al.* (2008), Nakai *et al.* (2008), and Nakai *et al.* (2009) found $1/T_1 \sim T^3$ in $LaFeAsO_{0.9}F_{0.1}$, $T_c = 26$ K, which they analyzed as indicative of line nodes in the gap function. The lack of a significant residual density of states (no low temperature Korringa term in the NMR) was used by the latter authors to argue for *s*-wave pairing, since *d*-wave pairing in the presence of the scattering centers introduced by the F doping would be expected to introduce a significant residual DOS. Similar data ($1/T_1 \sim T^3$) and arguments have been put forward (Mukuda *et al.*, 2008) for $LaFeAsO_{0.6}$, $T_c = 28$ K. NMR $1/T_1$ data for $PrFeAsO_{0.89}F_{0.11}$ ($T_c = 45$ K) has been interpreted (Matano *et al.*, 2008) as "T^3-like" just below T_c, with evidence for a second gap at lower temperatures, i.e., two gaps with nodes, while the strong decrease in the Knight shift below T_c implied singlet pairing. Theory work by Chubukov, Efremov, and Eremin (2008) argued that the $1/T_1 \sim T^3$ fits over a wide temperature range by, e.g., Matano *et al.* (2008) and Nakai *et al.* (2008) are not evidence for nodes. Rather, they calculated that in the presence of impurity scattering $1/T_1 \sim T^3$ "as if the gap had nodes," even though the gaps are nodeless. NQR measurements (Kawasaki *et al.*, 2008) on $LaFeAsO_{0.92}F_{0.08}$, $T_c = 23$ K, were fit with a two gap model, where the gaps have either *d* wave or $s_\pm$ symmetry.

(b.) 122 Structure: NMR data by Fukazawa *et al.* (2009b) on $Ba_{1-x}K_xFe_2As_2$, $T_c = 38$ K, give $1/T_1 \sim T^{2.6}$ from 4 to 20 K, interpreted to mean that the sample's behavior is similar to the NMR data for the 1111s, i.e., with possible nodal behavior. In contrast, NMR data by Yashima *et al.* (2009) on

$Ba_{0.6}K_{0.4}Fe_2As_2$, $T_c = 38$ K, give $1/T_1 \sim T^5$ from about 7 to 20 K, interpreted to imply a multiple fully gapped $s\pm$ state. Yashima *et al.* noted that, based on the strong decrease of the Knight shift below T_c, their $Ba_{0.6}K_{0.4}Fe_2As_2$ is a spin singlet superconductor. Both measurements were on polycrystalline samples. NMR data on a single crystal of $Ba_{0.72}K_{0.28}Fe_2As_2$, $T_c = 31.5$ K found no simple power law behavior for $1/T_1$ and was interpreted (Matano *et al.*, 2009) as coming from two gaps, of either d wave or $s_{\pm}$ symmetry. NQR of single crystal, RRR = 67, KFe_2As_2 was analyzed (Fukazawa *et al.*, 2009a) to indicate multiple gaps, but was unable to distinguish (see the discussion of specific heat below) between nodal or fully gapped. Nakai *et al.* (2010) used NMR to measure $1/T_1$ of single crystal $BaFe_2(As_{0.7}P_{0.3})_2$ and found a linear-in-T response between 0.1 and 4 K, clear evidence for a residual DOS at zero energy. Together with penetration depth and thermal conductivity measurements, Nakai *et al.*, argued that their NMR data imply the existence of line nodes in the gap. Unfortunately, Nakai *et al.* could not separate the spin susceptibility part of the Knight shift, leaving the question of singlet versus triplet pairing open from the NMR point of view.

(c.) 111 Structure: Measurements (Z. Li *et al.*, 2010) of NMR and NQR on a polycrystalline sample of LiFeAs, $T_c = 17$ K, are fit to a two gap, $s_{\pm}$ model. Jeglic *et al.* (2010) found a Knight shift that went to zero as $T \rightarrow 0$, consistent with spin singlet pairing.

(d.) 11 Structure: NMR measurements (Michioka *et al.*, 2010) down to 2 K of $1/T_1$ on a single crystal of $Fe_{1.04}Se_{0.33}Te_{0.67}$, $T_c = 15$ K, resulted in a roughly T^3 temperature dependence, and were interpreted as consistent with spin singlet superconductivity.

(e.) 122* Structure: Ma *et al.* (2011) reported an approximately 50% drop in the Knight shift below $T_c \approx 32$ K in single crystals of $K_{0.8}Fe_{2-y}Se_2$, consistent with singlet pairing. In terms of the temperature dependence of $1/T_1$, they found an approximate T^2 dependence below $T_c/2$ which is unexplained. Torchetti *et al.* (2011) found a 60% decrease in their Knight shift measured in both crystalline directions in single crystal $K_xFe_{2-y}Se_2$ below T_c, consistent with spin singlet pairing, while Kotegawa *et al.* (2011) found an 80% decrease in Knight shift in their $K_xFe_{2-y}Se_2$ below T_c. Kotegawa *et al.* found that the best fit to their $1/T_1$ data below T_c matches an s_{+-} model.

3. Specific heat

Measurement of the specific heat C in the superconducting state can give information about the nodal structure in three ways. One way to probe the superconducting gap using specific heat is to determine if the temperature dependence of $C \propto T^2$, which implies line nodes in the gap. Although this is a well-known theoretical result (Sigrist and Ueda, 1991) it is extremely difficult to verify experimentally due to the large contributions from other temperature dependences; see the tour-de-force determination of $C \propto T^2$ in YBCO by Y. Wang *et al.* (2001).

A second way to use specific heat as a probe of the superconducting gap is to measure the low temperature, $T \ll T_c$, γ as a function of field, as long as the sample does not have a magnetic impurity phase (Kim, Kim, and Stewart, 2009) whose field response obscures that of γ. For a fully gapped superconductor with only one gap, γ will vary simply as H due to the localized Caroli–de Gennes–Matricon states in the vortex cores. Moler *et al.* (1994) observed $\gamma \sim H^{1/2}$ up to 9 T while investigating the gap structure on YBCO, $H_{c2}(0) \sim 120$ T. The theory of Volovik (1993) predicted $\gamma \sim H^{1/2}$ in a clean superconductor with lines of nodes for $H \ll H_{c2}$, while the theory of Kübert and Hirschfeld (1998) gives $\gamma \sim H \log H$ for a disordered superconductor with lines of nodes. The $H^{1/2}$ and $H \log H$ laws arise from the Doppler shift of the low-energy nodal quasiparticles in the superflow field of the vortex lattice. Another physical explanation for a pure power law, $\gamma \sim H^{\alpha}$, $\alpha < 1$, in a superconductor is due to vortex-vortex interactions changing the size of the vortex cores, giving $\gamma \sim H^{0.66}$ in the $T \rightarrow 0$ limit, as seen experimentally in the superconductor $NbSe_2$ up to about $0.3H_{c2}$ (Sonier *et al.*, 1999).

However, studies of γ vs H in superconductors are often more complicated than these simple, pure power law predictions. Although the Volovik theory is valid only in the low field limit, $\gamma \sim H^{1/2}$ has been found to higher field, e.g., up to H_{c2} in both $LuNi_2B_2C$ (Nohara *et al.*, 1997) and YNi_2B_2C (Park *et al.*, 2003). Another possible explanation for a sublinear variation of γ with H in the superconducting state is when the superconductor has two (or more) gaps (as found in all FePn/Ch due to their Fermiology), as reported experimentally, e.g., in the conventional superconductor $Na_{0.3}CoO_2{:}1.3H_2O$ (Oeschler *et al.*, 2008) and discussed theoretically, e.g., by Bang (2010) where both gaps have conventional s-wave symmetry. Thus, two gaps of differing magnitudes can, depending on the ratio of $\Delta_{min}/\Delta_{max}$ (possibly but not necessarily including the nodal case where $\Delta_{min} = 0$), mimic nonlinear behavior of γ with H due to nodes. As Nakai *et al.* (2004) pointed out, even in fully gapped superconductors the gap anisotropy (the ratio of $\Delta_{min}/\Delta_{max}$) can cause behavior similar to $\gamma \propto H^{1/2}$. Unfortunately, a rather large field range (to perhaps $H_{c2}/2$ or even higher) can be needed to distinguish between $\gamma \sim H$, $H \log H$, $H^{1/2}$ and the nonlinear field dependence H^{α}, $0.5 < \alpha < 1$, caused by have two separate band gaps, as would come from the $s_{\pm}$ model. Such high field work is in progress.

A third way to use specific heat as a probe of the superconducting gap structure is to measure γ in field as a function of angle in the nodal plane, see Fig. 29, where the minima indicate the nodal directions. For field perpendicular to the nodal plane, γ varies as $H^{1/2}$. Although this technique has been used for other unconventional superconductors [for a review see Park and Salamon (2004)], due to its technical difficulty and the precision required (the experimental variation between maximum and minimum in γ versus angle is typically only 2%–4%) such measurements are just beginning for the FePn/Ch superconductors.

Unlike thermal conductivity, discussed in Sec. IV.B.4, the residual gamma γ_r being finite is (as discussed in Sec. III.B.3 when $\Delta C/T_c$ was discussed) generally not useful as a definitive sign of nodal behavior.

(a.) 1111 Structure: Measurements (Mu *et al.*, 2008b) of C/T down to 1.8 K and up to 9 T on polycrystalline $LaFeO_{1-x}F_x$ were found to vary at $H^{1/2}$, implying either nodal superconductivity due to the inherent gap symmetry or possibly (Bang, 2010) two full band gaps with scattering.
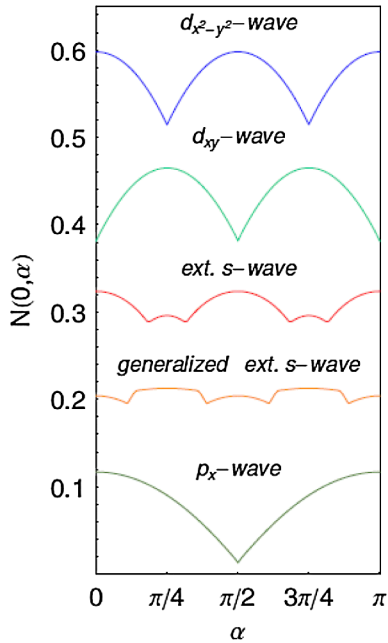
FIG. 29 (color online). Predictions for $\gamma(H)$ for field in the nodal plane of FePn/Ch superconductors of various pairing symmetries (Graser *et al.*, 2008). The direction chosen in their coordinates is that the Fe-Fe direction determines 100, whereas some works choose the Fe-As direction as defining 100, causing a $\pi/4$ shift in nomenclature for the angle.

The residual γ in the superconducting state in this work was 0.7 mJ/mole K^2, which is possibly consistent with nodes broadened by defects, but may be due to extrinsic (sample quality) effects.

(b.) 122 Structure: Measurements (Mu *et al.*, 2009a) of C/T down to 1.8 K and up to 9 T on single crystal K doped BaFe$_2$As$_2$, $T_c = 36.5$ K showed a linear dependence on field, implying fully gapped behavior. However, the quality of the crystals may not have been optimal since the residual γ in the superconducting state was 7.7 mJ/mole K^2 and the magnetic field below 4 K induced anomalies in C. Work (J. K. Dong *et al.*, 2008) on polycrystalline Ba$_{0.5}$K$_{0.5}$Fe$_2$As$_2$, $T_c = 36$ K, gave a residual γ of 9.1 mJ/mole K^2, which was described as possibly not intrinsic.

Unlike the status in K doped BaFe$_2$As$_2$, where sample quality has hindered progress, the quality of samples in Ni and Co doped BaFe$_2$As$_2$ has been gradually improved such that a consistent picture of intrinsic behavior has emerged. Early work in measuring the specific heat down to 2 K of both unannealed single crystal Ni and Co doped BaFe$_2$As$_2$ gave (Bud'ko, Ni, and Canfield, 2009) a residual $\gamma(T \to 0)$ of $\sim$10 mJ/mole K^2. Specific heat (Gofryk *et al.*, 2010) down to 0.4 K on a range of compositions in self-flux grown unannealed single crystals of BaFe$_{2-x}$Co$_x$As$_2$ gave comparable $\gamma(T \to 0)$ values ranging from 3.7 mJ/mole K^2 for optimally doped, $x = 0.16$, up to 14.6 mJ/mole K^2 for overdoped, $x = 0.21$. Gofryk *et al.* (2010), based on their specific heat data as well as magnetic susceptibility shielding data, assigned the large residual γ values as being due to nonsuperconducting volume fractions in their unannealed samples. Later these values were decreased markedly upon

annealing: for optimally doped BaFe$_{2-x}$Co$_x$As$_2$, $\gamma(T \to 0) = 1.3$ (0.25 on a second sample), and for overdoped $\gamma(T \to 0) = 3.8$ mJ/mole K^2 for samples annealed at 800 °C for 2 weeks (Gofryk *et al.*, 2011a; 2011b).

Low field γ vs H: Gofryk *et al.* (2010) measured (less than linear with) field dependence of γ up to 9 T in their unannealed BaFe$_{2-x}$Co$_x$As$_2$ samples. These results were analyzed to be consistent with a two gap model, as discussed theoretically by Bang (2010) for the $s_\pm$ model with impurity scattering, with the ratios of the gap sizes in their analysis being independent of the doping. Qualitatively, the amount of curvature in γ vs H up to 9 T was not markedly different in the annealed samples. Jang *et al.* (2011) measured $\gamma(H)$ up to 9 T on single crystals of unannealed overdoped BaFe$_{1.8}$Co$_{0.2}$As$_2$, $T_c = 19$ K, and fitted their data to a two gap model, an isotropic hole Fermi surface and an anisotropic nodal electron Fermi surface. They also found that $\gamma \propto H^{0.7}$ fit their data as well; cf. the high field γ vs H data from Kim *et al.* (2011b) discussed below. Mu *et al.* (2010) measured $\gamma(H)$ up to 9 T on optimally doped BaFe$_{2-x}$Co$_x$As$_2$ and found nonlinear behavior up to 1 T and essentially linear behavior above, too complicated a behavior to be analyzed by any of the simple existing models and in disagreement with the Gofryk *et al.* (2011b) $\gamma(H)$ results. The possibility that the low field, ≤ 1 T, behavior of Mu *et al.* (2010) was extrinsic was not discussed; Gofryk *et al.* (2010) only had one field point in that range.

High field γ vs H: Measurement of underdoped and overdoped, annealed single crystals of BaFe$_{2-x}$Co$_x$As$_2$ in fields up to $H_{c2} \sim 16$ and 27 T, respectively, showed $\gamma \sim H^{0.7}$ over the whole field range of measurement (J. S. Kim *et al.*, 2011c). The same measurements in underdoped BaFe$_{2-x}$Ni$_x$As$_2$ (J. S. Kim *et al.*, 2011c) also showed $\gamma \propto H^{0.5}$ up to $H_{c2} = 20$ T. The fact that γ vs H shows a relatively *pure* power law behavior all the way up to H_{c2} for several doping levels of BaFe$_{2-x}$(Co, Ni)$_x$As$_2$, such as observed in YB$_2$Ni$_2$C (Park *et al.*, 2003), in contrast to the Volovik effect, predicted to hold only for $H \ll H_{c2}$, requires modeling with at least two gaps [cf. Jang *et al.* (2011), discussed above] and variable anisotropy (ratio of $\Delta_{min}/\Delta_{max}$) therein as done by Bang (2010), Nakai *et al.* (2004), and Y. Wang *et al.* (2011).

In summary, the $\gamma(H)$ data for doped BaFe$_2$As$_2$ promise insights into the gap anisotropy. However, the sample quality is still being tuned with annealing, the data are still incomplete for the optimally doped composition and are still being analyzed with improved multigap models [see the discussion of the P doped BaFe$_2$As$_2$ γ vs H work, Y. Wang *et al.* (2011), below], leaving implications for the gap structure of these materials at present still open.

A rather large residual γ is found (Fukazawa *et al.*, 2009b) in a polycrystalline, RRR = 67 sample of KFe$_2$As$_2$, $T_c = 3.4$ K; analysis of the temperature dependence (two gap model) measured down to 0.4 K (not a large range of data below $T/T_c < 0.25$) of the superconducting specific heat is somewhat hampered by the >50% ratio of the residual γ_r versus the normal state extrapolation of C/T to $T = 0$, γ_n. In addition, there is evidence (J. S. Kim *et al.*, 2011b) that there is a magnetic transition in KFe$_2$As$_2$ at $\sim$0.7 K, further complicating the two gap model analysis.

Specific heat in fields to 15 T and down to 0.4 K of BaFe$_2$(As$_{0.7}$P$_{0.3}$)$_2$ gave (J. S. Kim *et al.*, 2010) $\gamma \sim H^1$, with a residual γ of 1.8 mJ/mole K^2. Since this field result indicated a fully gapped material, the residual γ was discussed as being not intrinsic. However, a follow-up work (Y. Wang *et al.*, 2011) showed that $\gamma \sim H^{1/2}$ in the low field, $H \leq 4$ T ($H \ll H_{c2} = 52$ T) limit, consistent with nodal or at least deep gap minimum behavior, so that this γ_r could be partially due to nodes with defect broadening.

(c.) 11 Structure: The specific heat (Zeng *et al.*, 2010a) as a function of angle $C(\Theta)$ of self-flux grown single crystals of FeSe$_{0.4}$Te$_{0.6}$ $T_c = 14.5$ K, was measured in the superconducting state ($T \sim 2.6$ K, or $\sim 0.2T_c$) in 9 T. Fourfold oscillations (minima at $\pm \pi/4$) with an amplitude of 0.25 mJ/mole K^2 were observed and could be interpreted, see Fig. 29, as either due to d_{xy} pairing or due to a strongly anisotropic s-wave nodeless gap, with deep minima at or near particular high-symmetry "hot spots." Based on thermal conductivity data (discussed in Sec. IV.B.4), they concluded that the second explanation is correct. However, theoretical work by Vorontsov and Vekhter (2006 and 2010) as well as experimental work on $C(\Theta)$ in field in the nodal superconductor CeCoIn$_5$ (An *et al.*, 2010) pointed out that the maxima and minima in $C(\Theta)$ *invert* upon going into the low temperature ($< 0.1T_c$) limit at low magnetic fields and only then show the correct nodal direction. Thus, the identification of the nodal directions from the $C(\Theta)$ data measured by Zeng *et al.* (2010a) in a 9 T field at $0.2T_c$ was questioned by Vorontsov and Vekhter (2010), who argued that the nodes will occur at $\pi/4$ away from the direction assigned by Zeng *et al.*, and are therefore consistent with d_{x2-y2} pairing. Zeng *et al.* (2010b), using improved data (sharper, more distinct minima) and correcting an error in their identification of the angular minima and maxima with respect to the crystallographic axes, reiterated their conclusion that an extended s-wave state ($s_\pm$ state) best fits their data. This work is the first report of $C(H, \Theta)$ in FePn/Ch, is a tour de force of measurement technique, and highlights the dynamic interaction of theory and experiment in this field. The measurement (Hu *et al.*, 2011) of the specific heat γ up to 9 T [$H/H_{c2}(0) = 0.2$)] on the high quality single crystal FeSe$_{0.43}$Te$_{0.57}$, $T_c^{\text{mid}} = 14.2$ K, shows $\gamma \propto H$, also consistent with nodeless behavior.

(d.) 122 Structure:* Zeng *et al.* (2011) reported γ vs H up to 9 T in single crystals of K$_x$Fe$_{2-y}$Se$_2$, $T_c = 32$ K, and $H_{c2}(0) = 48$ T, all fields in the c-axis direction. Their data showed a large change in slope at 3 T, with $\gamma \propto H$ both above and below this point. Wang, Lei, and Petrovic (2011b) reported γ vs H up to 9 T in single crystals of sulfur doped K$_{0.8}$Fe$_{2-y}$Se$_{1.68}$S$_{0.32}$ ($T_c = 31.4$ K and $H_{c2}(0) = 45$ T) and K$_{0.8}$Fe$_{2-y}$Se$_{1.01}$S$_{0.99}$ [$T_c = 21.4$ K and $H_{c2}(0) = 13$ T]. Both sets of data show $\gamma \propto H^1$ over the whole field range from 0 to 9 T which, at least in the lower critical field, higher S doped sample seems conclusive evidence for lack of nodes.

4. Thermal conductivity

Thermal conductivity κ is similar to specific heat in its probing of nodal structure. A zero κ/T as $T \rightarrow 0$ indicates a fully gapped superconductor, while a finite value can indicate either nodal structure due to the pairing symmetry, gapless

behavior due to scattering or nonintrinsic contributions connected throughout the sample. In the nodal case, the field dependence of κ/T ($\sim H \log H$) is also similar in cause to that of the specific heat ($H^{1/2}$). The specific heat residual γ in the FePn/Ch superconductors has not yet been reported to be smaller than 0.7 mJ/mole K^2 in a 1111 material (LaFeAsO$_{1-x}$F$_x$, Mu *et al.*, 2008b) or 0.25/1.78 mJ/mole K^2 in the 122s (in annealed optimally doped BaFe$_{1.84}$Co$_{0.16}$As$_2$, Gofryk *et al.*, 2011b/in unannealed P doped BaFe$_2$As$_2$, J. S. Kim *et al.*, 2010) and is typically 4–10 mJ/mole K^2. In contrast, several reports of $\kappa/T \sim 0$ within the error bar of the measurement (typically ≈ 1 μW/K^2 cm in the c-axis direction and ≈ 10–20 μW/K^2 cm in the a-axis direction, Reid *et al.*, 2010) are discussed below, taken as clear evidence for fully gapped behavior.

(a.) 1111 Structure: Thermal conductivity in Sn-flux grown single crystal LaFePO, $T_c = 7.4$ K, RRR = 28, was measured in the ab plane down to 0.46 K, with $\kappa(T \rightarrow 0)/T = 3000$ μW/K^2 cm, possibly at least partially due to extrinsic contributions (Yamashita *et al.*, 2009). The rather complex field dependence of the low temperature thermal conductivity was analyzed in a multiband model, with at least one band with nodal behavior.

(b.) 122 Structure: Measurements (Luo *et al.*, 2009) of the thermal conductivity κ in zero magnetic field result in a negligible residual linear term in κ/T as $T \rightarrow 0$ in self-flux-grown crystals of Ba$_{1-x}$K$_x$Fe$_2$As$_2$, $x = 0.25$ and 0.28, $T_c = 26$ and 30 K. This was interpreted as showing that there are no zero-energy quasiparticles and hence the superconducting gap has no nodes in the ab plane anywhere in this composition range. However, they found that a small magnetic field can induce a large κ/T, interpreted to imply that there is a deep minimum in the size of the gap somewhere on the Fermi surface. For a theoretical discussion of this scenario, see Mishra *et al.* (2009b). In BaFe$_{2-x}$Co$_x$As$_2$, $0.048 \leq x \leq 0.114$, measurements (Tanatar *et al.*, 2010a) of the thermal conductivity in zero magnetic field resulted in a negligible residual linear term in κ/T as $T \rightarrow 0$ at all x. This was interpreted just as in the results for K doped BaFe$_2$As$_2$: no zero-energy quasiparticles and hence the thermal currents in the ab plane are not carried by nodal quasiparticles. Also, a small magnetic field can induce a large κ/T, again implying that there is a deep minimum in the size of the gap somewhere on the Fermi surface.

Follow-up measurements in Co doped BaFe$_2$As$_2$, with $0.038 \leq x \leq 0.127$, by the same group (Reid *et al.*, 2010) found a finite residual κ/T as $T \rightarrow 0$ (implying states in the gap, or nodal behavior) with the thermal current along the c axis *away* from optimal doping, while in the ab plane κ/T, within the error bar, vanishes as $T \rightarrow 0$ for the whole composition range. A field of $H_{c2}/4$ induces a finite κ/T as $T \rightarrow 0$ along the a axis as well and brings the c and a axis data back into agreement. The field behavior of κ/T in the overdoped BaFe$_{2-x}$Co$_x$As$_2$, $x = 0.127$, where the sample has a residual κ/T (evidence for nodes) along the c axis, shows the same sublinear rise with H in both the c axis and ab-plane directions as does the d wave superconductor Tl$_2$Ba$_2$CuO$_{6-x}$. However, $\kappa(H)/T$ for the nearly optimally doped BaFe$_{2-x}$Co$_x$As$_2$, $x = 0.074$, where there was no

residual κ/T, shows $\kappa/T \sim H$ in both directions. The appearance of nodal quasiparticles carrying c axis thermal currents as composition is moved away from optimal doping is used (Reid *et al.*, 2010) to imply that the gapless behavior is "accidental", i.e., not imposed by symmetry but instead by scattering, and therefore consistent with, for example, $s_\pm$ symmetry. For a discussion of the theory, see Mishra, Graser, and Hirschfeld (2011). Thermal conductivity data (Dong *et al.*, 2010a) for overdoped $BaFe_{2-x}Co_xAs_2$, $x = 0.27$, in the *ab* plane also showed κ/T ($T \rightarrow 0$) equal to zero within their error bar, and $\kappa(H)/T$ behavior such as observed in d wave $Tl_2Ba_2CuO_{6-x}$.

Thermal conductivity of single crystal $BaFe_{1.9}Ni_{0.1}As_2$, $T_c = 20.3$ K, was measured (Ding *et al.*, 2009) down to 0.07 K. The results that the residual κ/T ($T \rightarrow 0$) was negligible, and $\kappa(H)/T \sim H^\alpha$, $\alpha > 1$, were interpreted as consistent with nodeless multiple gaps.

Thermal conductivity of single crystal $BaFe_2(As_{0.7}P_{0.3})_2$ was measured (Hashimoto *et al.*, 2010b) in zero and applied fields down to 0.1 K. A significant residual $\kappa/T(T \rightarrow 0)$ of 250 $\mu W/K^2$ cm and $\kappa(H)/T \sim H^{1/2}$ up to 12 T are found, analyzed to be consistent with nodal behavior. Thermal conductivity in the same material as a function of angle and field has been measured and found consistent with s-wave symmetry, with nodal structure on the electron pockets (Yamashita *et al.*, 2011).

Thermal conductivity of self-flux grown single crystal KFe_2As_2, RRR = 86, down to 0.07 K and up to H_{c2} was measured (Dong *et al.*, 2010b), resulting in a large residual $\kappa(T \rightarrow 0)/T = 2270$ $\mu W/K^2$ cm and a field dependence comparable to that of d wave $Tl_2Ba_2CuO_{6-x}$.

(c.) 111 Structure: Thermal conductivity of single crystal LiFeAs, $T_c \approx 18$ K, was measured (Tanatar *et al.*, 2011) down to 0.05 K in both $\perp c$-axis and $\parallel c$-axis directions. The residual $\kappa(T \rightarrow 0)/T \approx 0$ and the field dependence were interpreted to mean that LiFeAs has a 3D isotropic gap without nodes or deep minima.

(d.) 11 Structure: Thermal conductivity of vapor self-transport grown single crystal $FeSe_{\approx 1}$, $T_c = 8.8$ K, was measured (Dong *et al.*, 2009) in plane down to 0.12 K and up to 14.5 T ($\sim 0.75 H_{c2}$). The residual $\kappa(T \rightarrow 0)/T$ found was 16 $\mu W/K^2$ cm, only 4% of the normal state value. Together with a dependence on field similar to that of $NbSe_2$, these thermal conductivity data were interpreted as evidence for nodeless multigap s-wave superconductivity.

5. Andreev spectroscopy, tunneling, and Raman scattering

Point contact Andreev reflection spectroscopy applied to polycrystalline samples of the 1111 structure finds evidence for a conventional, single gap (T. Y. Chen *et al.*, 2008) or multiple gaps (Daghero *et al.*, 2009; Gonnelli *et al.*, 2009; Samuely *et al.*, 2009a, 2009b; Y. L. Wang *et al.*, 2009; Yates *et al.*, 2008) with possible unconventional behavior in one of the gaps. Work on Andreev spectroscopy on the 122 structure found a single gap in single crystal K doped $BaFe_2As_2$, but they suggested that their c-axis tunneling direction could be missing bands mostly in the *ab* plane (Lu *et al.*, 2009). Andreev spectroscopy by Szabo *et al.* (2009), also on single crystal $Ba_{0.55}K_{0.45}Fe_2As_2$, found two gaps in the *ab* plane. Early work on Co doped $BaFe_2As_2$ found (Samuely *et al.*,

2009a) a single gap while more recent work (Tortello *et al.*, 2010) found two gaps with no nodes in optimally doped material. Andreev spectroscopy on thin film Co doped $BaFe_2As_2$ (Sheet *et al.*, 2010) found evidence for unconventional pairing with fluctuations up to $1.3T_c$. For an early review on Andreev spectroscopy in the 122 superconductors, see Samuely *et al.* (2009a). For a general review on point contact spectroscopy in multiband superconductors, with one section on FePn/Ch, see Daghero and Gonnelli (2010).

C.- T. Chen *et al.* (2010) studied Josephson tunneling in a novel composite $Nb-NdFeAsO_{0.88}F_{0.12}$ superconducting loop and found evidence (1/2 integer quantum flux transitions) for a sign change in the superconducting order parameter on the Fermi surface. C.- T. Chen *et al.* (2010) then put forward arguments that this implies $s_\pm$ pairing. In a similar hallmark experiment, Hanaguri *et al.* (2010) in $FeSe_{1-x}Te_x$, $T_c \sim 14$ K, used scanning tunneling microscopy in 10 T to conclude $s_\pm$ pairing. Josephson tunneling has been used to infer s-wave pairing in K doped $BaFe_2As_2$ (X. Zhang *et al.*, 2009).

Scanning SQUID microscopy on polycrystalline $NdFeAsO_{0.94}F_{0.06}$, $T_c = 48$ K, detected (Hicks *et al.*, 2009b) no paramagnetic Meissner effect (Wohlleben effect). This was analyzed as consistent with s wave (including $s_\pm$) pairing or s wave with a slight admixture of d wave. Scanning tunneling microscopy on a similar composition, $NdFeAsO_{0.86}F_{0.14}$, with the same T_c by Jin *et al.* (2010) showed only a single gap, with $2\Delta(0)/k_BT_c \sim 4.3$. In general [see in addition, e.g., the work by Massee *et al.* (2009) on optimally doped $BaFe_{1.86}Co_{0.14}As_2$ and the review by Evtushinsky *et al.* (2009b)], scanning tunneling microscopy and scanning tunneling spectroscopy measurements of FePn/Ch only reveal one gap, in most cases the large, $2\Delta/k_BT_c \sim 7$, one. For a review of scanning tunneling microscopy and spectroscopy in the cuprates, see Fischer *et al.* (2007).

Muschler *et al.* (2009) measured $BaFe_{2-x}Co_xAs_2$ at two compositions around optimal doping using Raman spectroscopy, which is in principle sensitive to different Fermi surface sheets, and found evidence for nodes on the electron pockets. A follow-up theoretical paper (Boyd, Hirschfeld, and Devereaux, 2010) analyzed the results of Muschler *et al.* and found that Co functions primarily as an intraband scatterer.

In contrast to the results of Muschler *et al.*, Sugai *et al.* (2010) investigated the pairing symmetry of $BaFe_{2-x}Co_xAs_2$ using Raman scattering and argued that their similar data rather indicate nodes on the hole pockets. In the introduction to Sec. IV.B, it was stated that the experimental probes often give contradictory answers for the nodal structure and these Raman data provide a last example thereof.

Zhang *et al.* (2011a) performed Raman spectroscopy measurements on single crystals of $K_{0.8}Fe_{1.6}Se_2$, $T_c = 32$ K, and found a large number (14) of phonon modes which they analyzed as consistent with the Fe-vacancy ordering proposed by Bao *et al.* (2011a; 2011b). Interestingly, one of the observed phonon modes (with A_g symmetry) shows a change in frequency at $T = T_c$, indicating a connection between the superconductivity and a limited subset of the phonon modes. A follow-up work by Zhang *et al.* (2011b) also reported Raman data for $Tl_{0.5}K_{0.3}Fe_{1.6}Se_2$ ($T_c = 29$ K) and $Tl_{0.5}Rb_{0.3}Fe_{1.6}Se_2$ ($T_c = 31$ K) as well as for the insulating compound $KFe_{1.5}Se_2$. Consistent with the similar T_c values, they found that the alkali

metal substitution does not cause distortion (change the phonon frequencies) in the Fe-Se layers (where presumably the superconductivity occurs).

V. SAMPLE PREPARATION

The cornerstone on which the study of FePn/Ch rests is well prepared and well characterized samples. The discovery of superconductivity at 26 K by Kamihara *et al.* (2008) in LaFeAsO$_{1-x}$F$_x$ excited the imagination of the materials physics community, and led to concerted efforts by researchers worldwide to understand the new phenomena. However, it is not just the initial discovery of superconductivity in a given structure or at a particular composition that rewards insight and creativity in sample preparation, but very importantly the ensuing characterization drives the sample growers. Any hope of understanding the basic physics of these new materials depends strongly on the sample quality. The preceding sections discussed case after case where sample quality was key in deciding on the intrinsic behavior, the role of defects and disorder in discovering the true nodal behavior is just one example. Here we discuss a representative subset of the efforts in sample preparation, and the wide panoply of techniques being brought to bear, including budding efforts at producing materials for applications, certainly years ahead compared to the time frame required for application of the previous high T_c discovery in the cuprates; see Putti *et al.* (2010) for an overview of the FePn/Ch properties relevant for application.

Progress in the sample preparation of the FePn/Ch superconductors has been impressive. After the original discovery (Kamihara *et al.*, 2008) that F doped LaFeAsO was superconducting at 26 K, it was only several months until Ren *et al.* (2008b) succeeded in prepared electron-doped LaFeAsO without F via oxygen deficiency using high pressure synthesis. Single crystals of 122 Ba$_{1-x}$K$_x$Fe$_2$As$_2$ were produced and characterized (Ni *et al.*, 2008a) using Sn flux within two weeks of the original discovery (Rotter, Tegel, and Johrendt, 2008) of $T_c = 38$ K in polycrystalline Ba$_{1-x}$K$_x$Fe$_2$As$_2$. Faced with sample difficulties due to inclusions from the Sn flux, the community responded with creative flux alternatives that have led to larger and cleaner single crystals. Further work found systems where Sn-flux did not degrade the properties. Below is a small synopsis of these ongoing efforts in sample preparation, which is resulting in not only discovery of new systems but also improvement in quality to reveal the intrinsic physics in known systems.

A. Polycrystalline

The discovery work in the six structures discussed in this review was in each case using polycrystalline samples: Kamihara *et al.* (2008) in LaFeAsO$_{1-x}$F$_x$, Rotter, Tegel, and Johrendt (2008) in Ba$_{1-x}$K$_x$Fe$_2$As$_2$, X. C. Wang *et al.* (2008) in LiFeAs, Hsu *et al.* (2008) in FeSe, Ogino *et al.* (2009) in Sr$_2$ScO$_3$FeP, and Guo *et al.* (2010) in K$_{0.8}$Fe$_{2-y}$Se$_2$. The powder preparation techniques used are fairly standard, as an example consider the Kamihara *et al.* (2008) preparation of the discovery compound, LaFeAsO$_{1-x}$F$_x$. Polycrystalline samples were prepared by first mixing the appropriate stoichiometric amounts of lanthanum arsenide, iron arsenide, and dehydrated La$_2$O$_3$ powders, with LaF$_3$ and La added to achieve the proper fluorine content. Pressed pellets of the starting materials were then heated in a quartz tube under partial pressure of Ar gas at 1250 °C for 40 h. Certain polycrystalline preparation involves high pressures to keep in a volatile component during the sintering process, e.g., X. C. Wang *et al.* (2008) sintered their LiFeAs samples under 1 to 1.8 GPa for 1 h at 800 °C, with the starting material already containing prereacted (at 800 °C for 10 h) FeAs, so-called "precursor" material. High pressure polycrystalline synthesis is also used to achieve more homogeneous nonequilibrium concentrations, for example, in oxygen deficient LnFeAsO$_{1-x}$ by Ren *et al.* (2008a). Presintered LnAs powder, As, Fe, and Fe$_2$O$_3$ powders were mixed in the appropriate stoichiometric amounts, ground thoroughly, and pressed into small pellets. These were sealed in boron nitride crucibles and sintered under 6 GPa pressure at 1250 °C for 2 h.

Disadvantages of polycrystalline sintered material include the following: the contribution of grain boundary resistance to the determination of ρ (perhaps increasing the absolute value of ρ by a factor of 2 in some cases); the inability to determine direction dependence of properties (including, e.g., critical fields, resistivity, thermal conductivity); the inability to do elastic neutron scattering determinations which are useful, when sufficient single crystal mass is available, for example, to determine small magnetic moments; lack of homogeneity, important for determining the microscopic coexistence of superconductivity and magnetism; and potential increased reactivity of surfaces due to increased surface areas. For a recent study, and discussion of sample difficulties, of the intergranular current density of polycyrstalline sintered and hot isostatically pressed (HIPped) SmFeAsO$_{1-x}$F$_x$; see Yamamoto *et al.* (2011).

Polycrystalline sample preparation, on the other hand, is often easier, and, turning the small grain size into an advantage, can make samples where the diffusion of some component is the limiting factor so that powder winds up being more homogeneous than a large single crystal. Also, stoichiometry is often easier to control in a polycrystalline sample, as shown in the definitive work of Williams, Mcqueen, and Cava (2009) where the correct stoichiometry of superconducting FeSe (not deficient, but instead essentially 1:1 in stoichiometry) was determined in polycrystalline samples.

B. Superconducting thin films and wire and their possible application

Since these new superconductors are metals, since some of them are quite malleable (CaFe$_2$As$_2$ has a small bending radius, Canfield, 2009), and since modern thermoelectric coolers can reach 10 K quite efficiently, preparation of superconducting thin films or wires of FePn/Ch holds out the possibility of achieving applications of these materials. There has been a continuing effort in the superconducting thin film and application area almost since the initial discovery of Kamihara *et al.* in the 1111 structure.

Considering first thin films of FePn/Ch compounds which are known to be bulk superconductors, there is sufficient work to data to merit considering the results for the 1111, 122, and 11 materials in separate subsections.

1111: Backen *et al.* (2008) used pulsed laser deposition (PLD) onto room temperature LaAlO$_3$ and MgO substrates to prepare 600 nm thick films of LaFeAsO$_{1-x}$F$_x$. After a post-anneal of 4 h at 1030 °C the films shows $T_c^{\text{onset}} = 11.1$ K, but, possibly due to nonsuperconducting islands in the film, ρ did not fall entirely to zero. PLD work on epitaxial films of LaFeAsO using a target of LaFeAsO$_{0.9}$F$_{0.1}$ reported two weeks earlier by Hiramatsu *et al.* (2008b), despite postannealing, saw no superconductivity. Thus, it was clear in the beginning of this effort that conditions for producing superconducting films were not easy to achieve. More than a year later, the current state of the art of thin film preparation of 1111 superconductors has shown significant progress. Haindl *et al.* (2010), using PLD and postannealing, prepared homogeneous (pore free) polycrystalline films of LaFeAsO$_{1-x}$F$_x$ with T$_c^{\text{onset}} = 28$ K, $\rho(0) \sim 0.6$ mΩ cm, RRR ~ 4, and a 2 K critical current density around 2×10^3 A/cm^2. Kidszun *et al.* (2010), also using PLD and postannealing, succeeded in preparing 200 nm thick epitaxial films of LaFeAsO$_{1-x}$F$_x$ with $T_c = 25$ K and RRR = 6.8. T. Kawaguchi *et al.* (2010), using molecular beam epitaxy on GaAs substrates at 650 °C, now achieved $T_c^{\text{onset}} = 48$ K in NdFeAsO$_{1-x}$F$_x$ films, with $\rho = 0$ by 42 K, i.e., a complete transition, without, it should be stressed, the *ex situ* second annealing step necessary in the PLD works. The resistivity of their best films is ~ 1000 μΩ cm at room temperature.

122: Excellent progress has also been made in preparing thin films of doped 122 FePn/Ch superconductors, essentially getting to the point where applications are possible. Just as in the thin film work in 1111, much initial work was needed to improve the thin film quality. Hiramatsu *et al.* (2008a) succeeded early on using PLD in growing epitaxial, superconducting films of SrFe$_{2-x}$Co$_x$As$_2$ with no postannealing with $T_c \sim 20$ K, RRR ~ 1.5, and $\rho(0) \sim 300$ μΩ cm. This resistivity is comparable to that of polycrystalline material at the same temperature (270 μΩ cm, Leithe-Jasper *et al.*, 2008). This work, concurrent in time with the early, nonsuperconducting 1111 films reported by the same group (Hiramatsu *et al.*, 2008b), illustrates the relative ease with which 122 films can be grown versus 1111 films. Attacking the grain boundary and weak link problem [see Lee *et al.* (2009) for a discussion of this in Co doped BaFe$_2$As$_2$] to increase the critical current density, a number of groups including Choi *et al.* (2009) and Maiorov *et al.* (2009) continued using PLD to make thin (450–750 nm) SrFe$_{1.8}$Co$_{0.2}$As$_2$ films, $T_c = 18.9$ K, with one film of Maiorov *et al.* showing a critical current density of 0.510^6 A/cm^2.

N. H. Lee *et al.* (2010), using PLD of K doped BaFe$_2$As$_2$ onto single crystal Al$_2$O$_3$ substrates and postannealing at 700 °C for 6 h, achieved $T_c^{\text{onset}} = 40$ K (a new record for 122 T_cs) with $\rho = 0$ at 37 K, $\rho(300$ K$) = 2500$ μΩ cm, and RRR > 25 in 1 μm films of Ba$_{0.6}$K$_{0.4}$Fe$_2$As$_2$. The higher T_c^{onset} in the film versus bulk material is discussed as possibly due to strain in the *a*-axis direction. Strain as a way to increase T_c in Co doped BaFe$_2$As$_2$ thin films has been also investigated by Iida *et al.* (2009). Baily *et al.* (2009), in a study of upper critical magnetic field, reported the preparation of 180 nm thick SrFe$_{1.8}$Co$_{0.2}$As$_2$ epitaxial films on mixed perovskite (La, Sr)(Al, Ta)O$_3$ (LSAT) substrates at 670 °C, with $T_c^{\text{mid}} = 17.1$ K and $\rho_n(30$ K$) = 330$ μΩ cm. These

SrFe$_{1.8}$Co$_{0.2}$As$_2$ films were reported to have rough surfaces, granular morphology, and be unstable against reaction with the water vapor in the air. To improve on this, for increased critical current density and possible application, Katase *et al.* (2009) prepared, using PLD, 500 nm thick films of BaFe$_{2-x}$Co$_x$As$_2$ deposited at 700 °C. These films, with $T_c^{\text{onset}} = 20$ K, were optically flat, of better crystallinity, and much more resistant to reaction with water vapor than Co doped SrFe$_2$As$_2$ films. The room temperature resistivity $\rho(300$ K$)$ was 1300 μΩ cm, or about 4 times larger than that of a single crystal. The report did not address critical current questions for applications. However, in follow-up works T. Katase *et al.* (2010a) and S. Lee *et al.* (2010) were able to break through the 10^6 A/cm^2 barrier considered necessary for Josephson junctions by continuing the work with BaFe$_{2-x}$Co$_x$As$_2$. S. Lee *et al.* (2010) reported critical current densities of 4.5×10^6 A/cm^2 (~ 10 times that reported for single crystals, Yamamoto *et al.*, 2009) in epitaxial thin films of Co doped BaFe$_2$As$_2$, T_c ($\rho \rightarrow 0$) = 21.5 K, grown using PLD on single crystal intermediate layers of SrTiO$_3$ or BaTiO$_3$ between the single crystal perovskite substrate and the superconducting film. The residual resistivity in these ~ 350 nm films is $\rho(0) \approx 75$ μΩ cm, and the films are fully strain relaxed. T. Katase *et al.* (2010a) achieved critical currents of 4×10^6 A/cm^2 in thin films of BaFe$_{2-x}$Co$_x$As$_2$ using PLD, again on single crystal perovskite substrates but without the buffer layer of S. Lee *et al.* (2010).

Based on these PLD BaFe$_{2-x}$Co$_x$As$_2$ thin films, T. Katase *et al.* (2010b) succeeded in making initial thin film Josephson junctions across bicrystal grain boundaries, a critical step for potential application; see Sec. IV.B.5 for Josephson tunneling work on bulk specimens. Katase *et al.* (2010c) also succeeded in fabricating the first SQUIDs using this thin film technology, although the devices are still in the development stage with flux noise levels ~ 40 higher than in typical dc SQUIDs using epitaxial YBCO films.

In summary, the thin film work in the 122 FePn superconductors has now been brought, in under three years, to the application stage, with clear ideas on how to proceed and improve the process parameters to optimize performance.

11: FeSe thin films have been grown on semiconducting substrates for spintronic applications for over a decade (Takemura *et al.*, 1997 evaporation and molecular beam epitaxy on GaAs; Hamdadou, Bernede, and Khelil, 2002), without measurements below room temperature and without superconductivity being discovered. After the discovery of superconductivity in FeSe (Hsu *et al.*, 2008) M. J. Wang *et al.* (2009) reported the preparation of thin films of FeSe using PLD. Films of ~ 100 nm thickness grown on an MgO substrate at 500 °C exhibited superconducting resistive transitions starting around 9 K. According to Nie *et al.* (2009), FeSe films under tensile strain have their superconductivity suppressed. Jung *et al.* (2010) succeeded in growing high quality films of FeSe$_{0.9}$ using PLD with T_c onset above 11 K, RRR ~ 4, and $H_{c2}(0) \sim 50$ T. Huang *et al.* (2010), using PLD, prepared 400 nm films of FeSe$_{0.5}$Te$_{0.5}$, with the optimal $T_c^{\text{onset}} = 15$ K and $\rho = 0$ at 11 K achieved on 310 °C MgO substrates. Huang *et al.* varied the substrate temperature to vary the stress applied to their epitaxial films and thus to vary the lattice structure. They concluded that the chalcogenide

height is the controlling parameter for T_c in their films. Bellingeri *et al.* (2009), using PLD, prepared ~50 nm films of $FeSe_{0.5}Te_{0.5}$ and also found that they could control T_c on their $SrTiO_3$ substrates using substrate temperature, with their best T_c (17 K) occurring on a 450 °C substrate.

Now superconducting thin films of nonbulk superconducting material are summarized. As discussed in Sec. II, FeTe in the 11 structure has coincident T_S and T_{SDW} transitions at 72 K and is nonsuperconducting. Han *et al.* (2010), using PLD, prepared ~100 nm thick FeTe films under tensile stress on a variety of substrates at ~540 °C and achieved T_c^{onset} of 13 K. In order to compensate for Te losses, the targets used had the stoichiometry $FeTe_{1.4}$. The tetrahedral bond angles were changed from the nonsuperconducting bulk sample values, and the c-axis lattice parameter was uniformly decreased. Resistive, susceptibility, and Hall effect anomalies associated with the structural and magnetic transitions in the films were all broadened and occurred at slightly higher temperatures than in the bulk, indicating coexistence of magnetism and superconductivity but not necessarily on a microscopic scale. It was not clear from the description if the 20% superconducting fraction was a shielding or a Meissner expulsion fraction, but phase separation of the magnetic and superconducting domains is in any case a possibility. A second thin film work that achieved superconductivity in a material otherwise normal was by Hiramatsu *et al.* (2009). In that work (see also the discussion of the Co doped $SrFe_2As_2$ films above) they discovered that 200 nm films of $SrFe_2As_2$ grown using PLD on 700 °C LSAT single crystal substrates, displayed a full resistive superconducting transition at $T_c^{onset} = 25$ K, $\rho = 0$ at 21 K, after exposure to water vapor for 6 h. A more recent work in pressed pellets of $FeTe_{0.8}Se_{0.2}$ powder by Mizuguchi *et al.* (2010a) found an improvement in the temperature where $\rho \to 0$, the resistive transition width as well as an increase in the diamagnetic shielding, upon exposure to water vapor. The exact mechanism of the water exposure causing superconductivity is not yet clarified. However, the surface of the $SrFe_2As_2$ film [see also Katase *et al.* (2009)] after exposure to water has a Fe_2As impurity phase present after the reaction with the water vapor.

Wires: Gao *et al.* (2008) prepared $SmFeAsO_{0.65}F_{0.35}$ wires by filling 0.008 m diameter Ta tube, 0.001 m wall thickness, with stoichiometric amounts of the constituent reactant powders [powder-in-tube or (PIT) method]. The tube was then swaged down to 0.00225 m diameter and reacted at ~1170 °C for 45 h. The resultant wire had $T_c^{onset} = 52$ K, a global critical current density of 3.9×10^3 A/cm^2 at 5 K, and $H_{c2}(T \to 0) \approx 100$ T using the WHH formula. The rather low critical current in this early attempt at a practical FePn superconducting wire is affected by impurity phases and weak links between grains. Using the PIT method, Ozaki *et al.* (2011) prepared single and seven core $FeTe_xSe_{1-x}$ wires, $T_c^{onset} \approx 11$ K, with critical currents at 4 K of order 200 A/cm^2. As a comparison, although single crystals are not a practical form for a conductor, Kashiwaya *et al.* (2010) found a critical current density j_c in single crystal $PrFeAsO_{0.7}$, $T_c = 35$ K, in the c-axis direction of 2.9×10^5 A/cm^2. Prommapan *et al.* (2011) found j_c(2 K) in single crystals of LiFeAs of $\approx 2 \times 10^6$ A/cm^2. Ma *et al.* (2009) also discussed the PIT process, with Nb or Fe tubes in

addition to Ta. L. Wang *et al.* (2010) prepared $Sr_{0.6}K_{0.4}Fe_2As_2$, $T_c = 34$ K, in tape form with Ag sheathing with a critical current of 1.2×10^3 A/cm^2 at 4.2 K.

C. Single crystals

Although single crystals of 122 could be grown larger than those for 1111 for a few months, the surge of effort in making larger single crystals has now also extended to the 1111 structure, with a flux developed by Yan *et al.* (2009) achieving crystals of several mm in size, versus the old 50–100 μm size in the beginning. At present, five of the six discovered structures (1111, 122, 111, 11, and 122*) of the FePn/Ch superconductors can be grown in mm-sized single crystal form, and the 21311 structure has been prepared in 0.2×0.2 mm^2 crystals (Qian *et al.*, 2011). Some measurement techniques always can benefit from ever larger crystal mass: Goko *et al.* (2009) measured μSR of a collection of over 100 single crystals (each with a mass of ~10 mg) of $CaFe_2As_2$ prepared in Sn flux. Pratt *et al.* (2009b) measured inelastic neutron scattering under pressure of a collection of 300 single crystals (each with a mass of ~5 mg), again of Sn-flux grown $CaFe_2As_2$. However, it is important to understand that a "single crystal" is not a guarantee of a lack of impurities, perfect lattice order, lack of twinning [see Tanatar *et al.* (2010b) for strain detwinning of $CaFe_2As_2$ and $BaFe_2As_2$ below the tetragonal-orthorhombic structural phase transitions], or indeed of representative intrinsic behavior in the particular measurement of interest to a researcher. As discussed above in Sec. IV.B.3, annealing of single crystals of Co doped $BaFe_2As_2$ at 800 °C for 2 weeks has led to significant changes in their measured properties, including both an increase in T_c at a given composition and changes in the measured specific heat γ. Rotundu *et al.* (2010) found that the residual resistivity ratio in a single crystal of $BaFe_2As_2$ increased from 5 to 36 with 30 d of annealing at 700 °C. Starting with a short overview of flux growth, a summary of some of the various methods used to prepare single crystal FePn/Ch superconductors is given here, along with comparisons of sample quality.

1. Flux growth

In general, if the thermodynamics and stabilities of the various possible compounds involved are heeded, growing crystals via the flux method is straightforward; see reviews by Fisk and Remeika (1989) and Canfield and Fisk (1992) on the use of molten *metal* fluxes. (As will be seen below, fluxes for FePn/Ch need not be metallic.) The flux method consists of loading stoichiometric amounts of the elements desired in the final crystals into a ceramic crucible (perhaps alumina or MgO) with an excess of the material serving as the flux, with, for example, a molar ratio of 20–40 Sn flux: 1 $Ba_{0.6}K_{0.4}Fe_2As_2$. The crucible, sealed in quartz, or the more expensive welded Nb or Ta vessels to more securely contain the hazardous arsenic or volatile phosphorous or lithium, is then heated to some high temperature (typically 850–1150 °C) where all constituent elements are dissolved in the molten flux. The solubility of each of the constituents with the flux can be checked via compendia of binary phase diagrams if the flux is an element. The crucible is then slowly

cooled ($\sim 5\,°C/h$) and at some point the constituent elements form a supersaturated solution and crystals begin to nucleate out of the molten flux. Depending on the flux and the crystals, separation of the crystals from the flux is accomplished via dissolving of the flux (e.g., NaAs flux dissolves in water), decanting and/or centrifuging of the flux above the flux's melting point (T_M for Sn is 232 °C), harvesting of the crystals from the crucible on a hot plate (T_M for In is only 157 °C), mechanical separation, and others. For FePn/Ch, all of the activities performed when the material is not sealed away from the atmosphere in quartz or Nb/Ta are best done in an inert atmosphere glove box until the sensitivity to air (high, e.g., in LiFeAs) is determined.

2. Development of fluxes and progress in crystal growing

The first discovered FePn/Ch superconductor was in the 1111 structure (Kamihara *et al.*, 2008), and the search for higher sample quality and the ability to measure directionally dependent intrinsic properties such as resistivity, critical field, and penetration depth led to early efforts to produce single crystals. Zhigadlo *et al.* (2008) succeeded in growing single crystals of SmFeAsO$_{1-x}$F$_x$ in the 100 μm size regime using a NaCl/KCl flux technique at high (3 GPa) pressure. At about the same time, the first single crystals ($\sim 3 \times 3 \times 0.2$ mm^3) of the 122 superconducting compound Ba$_{1-x}$K$_x$Fe$_2$As$_2$ were grown using Sn flux (Ni *et al.*, 2008a), with an incorporation of ~1% Sn [see Su *et al.* (2009) for a report of up to 5% Sn] into the crystals, not just as inclusions but at least partly into the lattice as an impurity. It was clear in the Ni *et al.* work that Sn from the metal flux had an important influence on the properties of crystals of the parent compound, BaFe$_2$As$_2$, depressing T_S/T_{SDW} from the known polycrystalline value of 140 to 85 K. The Sn incorporated in Ba$_{1-x}$K$_x$Fe$_2$As$_2$ also affects the low-energy spin fluctuations in the NMR measurements (Baek *et al.*, 2008; Sun *et al.*, 2011) and causes a large upturn in the low temperature specific heat divided by temperature C/T (Kim *et al.*, 2009a). Rb doped BaFe$_2$As$_2$ crystals grown in Sn flux have as much as 9% Sn included (Bukowski *et al.*, 2009). Contrary to this experience of Sn
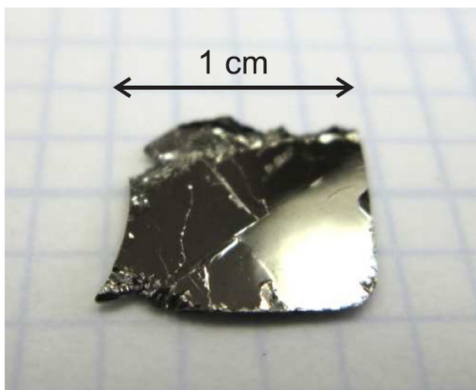

FIG. 30 (color online). As-grown single crystal of SrFe$_2$As$_2$ harvested from FeAs flux. Note the optically flat surfaces. The plane of the crystal is in the *ab* plane, while the *c* axis is perpendicular to the plane of the crystal. This is the typical growth habit for flux grown tetragonal 122 crystals. Size is limited by the size of the crucible. From Saha *et al.*, 2009a.

inclusion in the BaFe$_2$As$_2$ crystals, it became clear later that Sn-flux crystal growth was not in general detrimental to most FePn/Ch sample's intrinsic properties, and has been used quite successfully in the crystal growth of various other MFe$_2$As$_2$, 1111, and 111 compounds. In fact, a recent report (Urbano *et al.*, 2010) using a revised Sn-flux growth procedure finds little or no suppression of T_S/T_{SDW} in underdoped Ba$_{0.86}$K$_{0.14}$Fe$_2$As$_2$ from values in self-flux-grown samples. However, due to the initial experience with Sn a number of other fluxes were quickly tried.

One of these, somewhat unique to iron arsenide materials, is the so-called FeAs "self-flux." X. F. Wang *et al.* (2009a) grew BaFe$_2$As$_2$ crystals using prereacted FeAs powder as the flux, thus avoiding contamination from an extraneous element. An excess (factor of 2) of the FeAs precursor material is used with Ba, placed in an alumina crucible sealed in quartz, then heated to 700 °C to "soak" for 3 h, then to 1100 °C to react for ~30 h, then slowly cooled to 900 °C, then relatively rapidly cooled to room temperature. The $2 \times 2 \times 0.1$ mm^3 crystals were mechanically removed, since the compound FeAs melts at 1030 °C, and a T_S/T_{SDW} of 136 K is reported. Using FeAs self-flux is not without negative consequences, since FeAs, which is magnetic, can be contained in the crystals as an inclusion. In terms of magnetic properties, Sn-flux-grown crystals, on the other hand, can have elemental Sn inclusions (not just in the lattice atomically but as small regions) which superconduct at 3.7 K (Colombier *et al.*, 2009). A 1 cm crystal of SrFe$_2$As$_2$ grown in FeAs self-flux is shown in Fig. 30.

Other fluxes that have been used to grow 122 include In (Kim *et al.*, 2009a), where ~0.4 at percent In is included in BaFe$_2$As$_2$ crystals and $T_S/T_{SDW} = 137$ K (Kim, 2009) and Pb for growing BaNi$_2$As$_2$ (Ronning *et al.*, 2009) and BaRh$_2$As$_2$ (Singh *et al.*, 2008; Berry *et al.*, 2009). Before ending the discussion of single crystal growth of 122, it is instructive to compare T_{SDW} in various samples of undoped SrFe$_2$As$_2$ to gain an idea of how the properties can vary with differing preparation techniques. T_{SDW} was reported to be $201.5 \pm 0.25/198/200$ K in single crystals from self-flux, FeAs (H. Li *et al.*, 2009; Saha *et al.*, 2010a; Matsubayashi *et al.*, 2009), 203/205/220 K in polycrystalline material (Schnelle *et al.*, 2009; Kaneko *et al.*, 2008; Shi *et al.*, 2009), 198/200/220 K in single crystals from Sn flux (Yan *et al.*, 2008; G. F. Chen *et al.*, 2008; Zhao *et al.*, 2008a). Self-flux appears to give the most consistency in the result for T_{SDW}, while the values for Sn-flux single crystals and polycrystalline samples vary by 10%. In any case, Sn flux does not suppress T_{SDW} in SrFe$_2$As$_2$ as it does in BaFe$_2$As$_2$.

With all this effort in developing flux growth of single crystals in the 122 structure, workers had not lost focus on the more difficult, but higher T_c, 1111 FePn/Ch superconductors. Crystal size had grown from the initial 100 μm size to ~600 μm (CeFeAsO from Sn flux, Jesche *et al.*, 2009) when Yan *et al.* (2009) reported a breakthrough in crystal growth using NaAs flux for growing mm-sized crystals of LaFeAsO, LaFeAsO$_{1-x}$F$_x$, and LaFe$_{1-x}$Co$_x$AsO. Just as the case for the FeAs flux material, Na is prereacted with As, but in a sealed Ta tube at 600 °C for 12 h. For preparing LaFeAsO, the appropriate stoichiometric amounts of prefired LaFeAsO, LaAs, Fe$_2$O$_3$, and Fe are mixed in the molar ratio

of 20 NaAs:1 LaFeAsO (similar to the large molar ratio using Sn as a flux) and then sealed in a Ta tube. For the crystals containing F NaAs is partially replaced by NaF, for crystals containing Co the Co partially replaces the iron. The material is then reacted at 1150 °C for 24 h, and cooled at 3 °C down to 600 °C to allow the crystals to form out of the NaAs flux. Harvesting of the crystals, of typical size $3 \times 4 \times 0.05$–0.3 mm^3, from the flux is done by dissolving the NaAs flux in water.

Growth of single crystals in the more recently discovered 111 and 122* structures benefitted from the efforts in growing crystals of 1111 and 122 samples. Na$_{1-\delta}$FeAs crystals have been grown from self-flux (G. F. Chen *et al.*, 2009) while LiFeAs crystals have been grown by a Bridgman technique (Song *et al.*, 2010) and from both self-flux and Sn flux (Borisenko *et al.*, 2010). Both Bridgman and self-flux techniques were used to grow 122* beginning already in the discovery works [see, e.g., Fang *et al.* (2011b) and Krzton-Maziopa *et al.* (2011)] after the initial discovery work of Guo *et al.* (2010) in polycrystalline K$_{0.8}$Fe$_2$Se$_2$. FeSe$_{1-x}$ crystals have been grown using a vapor self-transport method, as iodine vapor transport was found to be ineffective (Patel *et al.*, 2009). FeSe$_{1-x}$Te$_x$ crystals have been grown by optical zone melting techniques (Yeh *et al.*, 2009) and a modified Bridgman technique (Sales *et al.*, 2009). For a review of single crystal growth in the 11 structure, see Wen *et al.* (2011). The 111 structure crystals can exceed 5 mm in lateral dimension, while the 11 structure crystals can exceed 10 mm.

D. Outlook

Much work remains to be done from a materials point of view. The thin film and wire application-oriented work is still just beginning. Superconducting transition widths are sometimes several Kelvin wide (in the case of Na$_{1-\delta}$FeAs, as much as 15 K wide), and residual resistivity ratios of undoped superconducting compounds are seldom over 10. Upon doping, the residual resistivity ratios, due to the scattering centers introduced by the doping, fall even further. Certainly greater homogeneity, possibly by long term annealing, may affect much that has been discussed herein, not least of the temperature dependences of various measures of nodal behavior. A study to reduce defects in certain systems, e.g., in Na$_{1-\delta}$FeAs, as was carefully done in FeSe by Williams, Mcqueen, and Cava (2009), would be useful. On the other hand, the controlled introduction of defects [see, e.g., Kim *et al.*, 2010a for $\Delta\lambda(T)$ measurements on superconducting doped BaFe$_2$As$_2$ irradiated with heavy ions] also is useful for understanding the influence of defects. After the initial rush to dope everything possible into 122, now is a good time to gain a perspective on what all these data mean for the fundamental physics and the mechanism of superconductivity. "Isoelectronic" doping, e.g., P for As or Ru for Fe, revealed interesting behavior (not found in the cuprates), and should be further pursued in more systems. Systems near a magnetic instability that show non-Fermi-liquid behavior are perhaps of critical importance to further understand FePn/Ch superconductivity. In the end, superconducting samples of new Fe-containing structures would also greatly help the search for commonality and therefore deeper understanding of the entire class of materials.

VI. SUMMARY AND CONCLUSIONS

The discovery of superconductivity in systems not just containing iron, but in systems where the magnetic behavior of iron appears to play a dominant role in the superconducting properties, has caused an "iron rush" of research. Up until this discovery of Kamihara *et al.* (2008) of $T_c = 26$ K in F doped LaFeAsO, the preponderance of superconductors seemed conventional, phonon-mediated-pairing types with a few unconventional, low T_c heavy fermion superconductors and the cuprates as exceptions. Now this new class of materials, with frequent examples of phase diagrams with clearly coexistent magnetism and superconductivity, makes the previously known unconventional superconductors seem to be less like exceptions and more like harbingers of what superconductivity is really like.

Much of this review presented evidence for magnetism and magnetic fluctuations being linked with the superconducting pairing mechanism in the FePn/Ch materials; see Secs. II.C and IV.A for partial overviews of the results pertaining to this central issue. Interesting goals, questions, and observations raised by this review for further understanding the superconductivity, the magnetism, and their possible "linkage" include the following.

- As discussed in Sec. III.A, G. M. Zhang *et al.* (2009) initially proposed that strong fluctuations in these materials cause $\chi \sim T$ based on data up to ~300 K for the LaFeAsO$_{1-x}$F$_x$ and MFe$_2$As$_2$, $M =$ Ba, Sr, and Ca. Susceptibility data varying linearly with temperature above T_c have also been measured in additional FePn/Chs (SrFeAsF, Co doped BaFe$_2$As$_2$, Na$_{1-\delta}$FeAs, FeSe$_{0.5}$Te$_{0.5}$) up to temperatures as high as 700 K. It would be useful if the lack of χ vs T data above 50 K in the three superconducting 21311 and in the reported 43822 FePn/Ch compounds, as well as the lack of χ vs T data above $T_N \approx 540$ K in the 122*, could be corrected. Presumably such χ data could serve as another metric for measuring the strength of the magnetic fluctuations in these materials, as well as to function as a potential differentiator in their fundamental behavior.

- The fact that this $\chi \sim T$ behavior persists in LaFeAsO$_{1-x}$F$_x$ even after T_{SDW} is suppressed with increasing F doping (Fig. 20) while $\chi \sim T$ behavior disappears upon the suppression of T_{SDW} for BaFe$_{2-x}$Co$_x$As$_2$ (Fig. 21) is intriguing. Does this indicate that 1111 have stronger magnetic fluctuations than 122? This would be consistent with their higher T_cs if indeed this linkage between superconductivity and magnetism is correct, and seems straightforward to further investigate by a more microscopic measure (e.g., INS) of the fluctuation strength.

- The idea of Jesche *et al.* (2009) discussed in Sec. II.B.1.b that T_S will coalesce with T_{SDW} with increasing sample quality in 1111 is certainly worth pursuing to see if 1111 in their undoped states are indeed intrinsically different from the undoped 122.

- The idea that quantum criticality can play a role in the FePn/Ch superconductivity has support from the resistivity data for several materials; see Sec. III.A. A typical scenario for a quantum critical point is that a second order magnetic transition (such as antiferromagnetism) has been suppressed to $T = 0$ at that point in a phase diagram. This is certainly a fertile field of investigation in these materials where there are so many examples of magnetism being suppressed by doping. Better quality samples, with attention to reducing magnetic impurities, need to be made so that possible non-Fermi-liquid behavior in the low temperature magnetic susceptibility, a mainstay of determining quantum criticality, can be investigated.

- In addition to aiding the investigation of intrinsic χ behavior, there are other areas where sample quality is central to understanding FePn/Chs. Knowledge of the nodal structure, as discussed in Sec. IV, is key to understanding the superconducting pairing mechanism. Presently, the consensus of the data indicates that several nodal FePn/Ch superconductors exist, while several fully gapped compounds also exist, with a larger number of disputed systems. Reduction of defects in the samples, e.g., to clarify the temperature dependences in penetration depth measurements, will advance this investigation markedly. Cleaner samples will help determine what the low temperature limiting values are for the specific heat γ and the thermal conductivity divided by temperature κ/T as well as allowing correct determination of the field dependences of γ (often made difficult by magnetic-impurity-phase-caused anomalies at ≈ 2 K) and κ/T at low temperature. Whether T_S remains equal to T_{SDW} in doping on the M site in 122 MFe$_2$As$_2$, unlike for most doping on the Fe and As sites, needs to be checked in homogeneous samples, which K doped BaFe$_2$As$_2$ is not.

- Specific heat was discussed in Secs. III.B and IV.B.3. Angle resolved specific heat in field to help determine the pairing symmetry, specific heat γ to fields greater than 9 T so that $H_{c2}(0)/2$ can be reached to look into two (or more) band anisotropy questions, as well as more high-precision low field data to try to distinguish $H^{1/2}$ from $H \log H$ (clean versus defects) Volovik effect would be interesting. Measuring ΔC in higher T_c 1111 compounds now that crystals of sufficient mass for such measurements are beginning to be available, as well as ΔC data for higher quality 122* samples would extend the check on the correlation $\Delta C \sim T_c^3$; see Sec. III.B.3.

- Although clearly difficult, it would be nice to settle the question of whether the isotope effect (Sec. IV.A) is positive or negative in some model FePn/Ch system.

- Pressure is an ideal method in these materials to scan the phase diagram, but only a few of the extant measurements have been able to track the T_S/T_{SDW} anomalies due to sample quality issues and perhaps strain broadening from nonideal pressure media.

- Crystals of LiFeAs are reportedly easily grown, and doping larger atoms on the Li site to expand the lattice and try to increase T_c, based on the monotonic suppression of T_c with pressure discussed in Sec. II.D, might provide interesting insights.

- Several routes to achieve higher T_c seem to offer promise. Introducing additional layers, or layers with different structure and/or chemistry, between the Fe$_2$As$_2$ layers (Ogino *et al.*, 2010a) and trying new compounds using theoretical insight are two such.

The central question of the relationship between magnetism and superconductivity in this new class of superconductor remains open, although the INS data on the spin fluctuations below T_c in particular are intriguing. There have been interesting suggestions for the key organizing parameter to link the known FePn/Ch materials and their T_cs, such as pnictide height or tetrahedral angle. As discussed, it appears that a single parameter will prove insufficient. Certainly understanding the FePn/Ch puzzle and how these structures interrelate could benefit from discovering more examples of this unusual form of superconductivity intertwined with magnetism. Faced with the large number of possible 1111, 122, and 21311/43822/? compounds containing magnetic ions and pnictides or chalcogenides as a starting point for such a search for new superconducting FePn/Ch, more theoretical input from band structure calculations, e.g., similar to Zhang and Singh (2009) prescient DFT work on TlFe$_2$Se$_2$ as a possible parent compound for superconductivity, would certainly be welcome. For example, Yan and Lu (2010) proposed that CaClFeP might exhibit high temperature superconductivity under doping or high pressure. The work underway to increase T_c by expanding the c axis, going from the 21311 to the 43822 structure and beyond, is another promising route.

In summary, hopefully researchers in the field can benefit from this review to help their future work. There seems much more to be done. For those not directly involved in FePn/Ch, the goal of this review was to introduce a rather complex set of results in an approachable fashion, with sufficient references to guide further study.

ACKNOWLEDGMENTS

REFERENCES

Aeppli, G., E. Bucher, C. Broholm, J. K. Kjems, J. Baumann, and J. Hufnagl, 1988, Phys. Rev. Lett. **60**, 615.

Ahilan, K., J. Balasubramaniam, F. L. Ning, T. Imai, A. S. Sefat, R. Jin, M. A. McGuire, B. C. Sales, and D. Mandrus, 2008, J. Phys. Condens. Matter **20**, 472201.

Akrap, A., J. J. Tu, L. J. Li, G. H. Cao, Z. A. Xu, and C. C. Homes, 2009, Phys. Rev. B **80**, 180502(R).

Alireza, P. L., Y. T. C. Ko, J. Gillett, C. M. Petrone, J. M. Cole, G. G. Lonzarich, and S. E. Sebastian, 2009, J. Phys. Condens. Matter 21, 012208.

An, K., T. Sakakibara, R. Settai, Y. Onuki, M. Hiragi, M. Ichioka, and K. Machida, 2010, Phys. Rev. Lett. 104, 037002.

Analytis, J. G., J.-H. Chu, A. S. Erickson, C. Kucharczyk, A. Serafin, A. Carrington, C. Cox, S. M. Kauzlarich, H. Hope, and I. R. Fisher, 2008, arXiv:0810.5368.

Andersen, B. M., P. J. Hirschfeld, A. M. Kampf, and M. Schmid, 2007, Phys. Rev. Lett. 99, 147002.

Anupam, P. L. P., H. S. Jeevan, C. Geibel, and Z. Hossain, 2009, J. Phys. Condens. Matter 21, 265701.

Armitage, N. P., P. Fournier, and R. L. Greene, 2010, Rev. Mod. Phys. 82, 2421.

Aswartham, S., et al., 2011, Phys. Rev. B 84, 054534.

Avci, S., et al., 2011, Phys. Rev. B 83, 172503.

Babkevich, P., B. Roessli, S. N. Gvasaliya, L.-P. Regnault, P. G. Freeman, E. Pomjakushina, K. Conder, and A. T. Boothroyd, 2011, Phys. Rev. B 83, 180506(R).

Backen, E., S. Haindl, T. Niemeier, R. Hühne, T. Freudenberg, J. Werner, G. Behr, L. Schultz, and B. Holzapfel, 2008, Supercond. Sci. Technol. 21, 122001.

Baek, S.-H., T. Klimczuk, F. Ronning, E. D. Bauer, J. D. Thompson, and N. J. Curro, 2008, Phys. Rev. B 78, 221509.

Baily, S. A., Y. Kohama, H. Hiramatsu, B. Maiorov, F. F. Balakirev, M. Hirano, and H. Hosono, 2009, Phys. Rev. Lett. 102, 117004.

Baker, P. J., S. R. Giblin, F. L. Pratt, R. H. Liu, G. Wu, X. H. Chen, M. J. Pitcher, D. R. Parker, S. J. Clarke, and S. J. Blundell, 2009, New J. Phys. 11, 025010.

Bang, Y., 2010, Phys. Rev. Lett. 104, 217001.

Bao, W., Q. Huang, G. F. Chen, M. A. Green, D. M. Wang, J. B. He, X. Q. Wang, and Y. Qiu, 2011a, Chin. Phys. Lett. 28, 086104.

Bao, W., G. N. Li, Q. Huang, G. F. Chen, J. B. He, M. A. Green, Y. Qiu, D. M. Wang, J. L. Luo, and M. M. Wu, 2011b, arXiv:1102.3674.

Bao, W., A. T. Savici, G. E. Granroth, C. Broholm, K. Habicht, Y. Qiu, J. Hu, T. Liu, and Z. Q. Mao, 2010, arXiv:1002.1617.

Bao, W., et al., 2009, Phys. Rev. Lett. 102, 247001.

Barzykin, V., and L. P. Gorkov, 2008, JETP Lett. 88, 131.

Barzykin, V., and D. Pines, 2009, Adv. Phys. 58, 1.

Basov, D. N., and T. Timusk, 2005, Rev. Mod. Phys. 77, 721.

Bednorz, J. G., and K. A. Müller, 1986, Z. Phys. B 64, 189.

Bellingeri, E., R. Buzio, A. Gerbi, D. Marre, S. Congiu, M. R. Cimberle, M. Tropeano, A. S. Siri, A. Palenzona, and C. Ferdeghini, 2009, Supercond. Sci. Technol. 22, 105007.

Bendele, M., et al., 2010, Phys. Rev. B 81, 224520.

Berk, N. F., and J. R. Schrieffer, 1966, Phys. Rev. Lett. 17, 433.

Berry, N., C. Capan, G. Seyfarth, A. D. Bianchi, J. Ziller, and Z. Fisk, 2009, Phys. Rev. B 79, 180502.

Boeri, L., M. Calandra, I. I. Mazin, O. V. Dolgov, and F. Mauri, 2010, Phys. Rev. B 82, 020506(R).

Boeri, L., O. V. Dolgov, and A. A. Golubov, 2008, Phys. Rev. Lett. 101, 026403.

Boeri, L., O. V. Dolgov, and A. A. Golubov, 2009, Physica C (Amsterdam) 469, 628.

Borisenko, S. V., et al., 2010, Phys. Rev. Lett. 105, 067002.

Bouquet, F., R. A. Fisher, N. E. Phillips, D. G. Hinks, and J. D. Jorgensen, 2001, Phys. Rev. Lett. 87, 047001.

Boyd, G. R., P. J. Hirschfeld, and T. P. Devereaux, 2010, Phys. Rev. B 82, 134506.

Braithwaite, D., G. Lapertot, W. Knaf, and I. Sheikin, 2010, J. Phys. Soc. Jpn. 79, 053703.

Braithwaite, D., B. Salce, G. Lapertot, F. Bourdarot, C. Marin, D. Aoki, and M. Hanfland, 2009, J. Phys. Condens. Matter 21, 232202.

Braun, H. F., 1980, Phys. Lett. A 75, 386.

Brydon, P. M. R., M. Daghofer, C. Timm, and J. Van den Beek, 2011, Phys. Rev. B 83, 060501.

Bud'ko, S. L., N. Ni, and P. C. Canfield, 2009, Phys. Rev. B 79, 220516.

Bukowski, Z., S. Weyeneth, R. Puzniak, J. Karpinski, and B. Batlogg, 2010, Physica C (Amsterdam) 470, S328.

Bukowski, Z., S. Weyeneth, R. Puzniak, P. Moll, S. Katrych, N. D. Zhigadlo, J. Karpinski, H. Keller, and B. Batlogg, 2009, Phys. Rev. B 79, 104521.

Calemczuk, R., C. Marcenat, J. L. Tholence, M. F. Gorius, and J. J. Capponi, 1994, Physica C (Amsterdam) 235–240, 1743.

Canfield, P. C., 2009 (private communication).

Canfield, P. C., and S. L. Bud'ko, 2010, Annu. Rev. Condens. Matter Phys. 1, 27.

Canfield, P. C., S. L. Bud'ko, N. Ni, A. Kreyssig, A. I. Goldman, R. J. McQueeney, M. S. Torikachvili, D. N. Argyriou, G. Luke, and W. Yu, 2009a, Physica C (Amsterdam) 469, 404.

Canfield, P. C., S. L. Bud'ko, N. Ni, J. Q. Yan, and A. Kracher, 2009b, Phys. Rev. B 80, 060501(R).

Canfield, P. C., and Z. Fisk, 1992, Philos. Mag. B 65, 1117.

Cano, A., M. Civelli, I. Eremin, and I. Paul, 2010, Phys. Rev. B 82, 020408(R).

Cao, C., P. J. Hirschfeld, and H.-P. Cheng, 2008, Phys. Rev. B 77, 220506.

Cao, G., C. Wang, Z. Zhu, S. Jiang, Y. Luo, S. Chi, Z. Ren, Q. Tao, Y. Wang, and Z. Xu, 2009, Phys. Rev. B 79, 054521.

Cao, G.-H., et al., 2010, Phys. Rev. B 82, 104518.

Carbotte, J. P., 1990, Rev. Mod. Phys. 62, 1027.

Carbotte, J. P., and E. Schachinger, 2010, Phys. Rev. B 81, 104510.

Carlo, J. P., et al., 2009, Phys. Rev. Lett. 102, 087001.

Chandra, P., P. Coleman, and A. I. Larkin, 1990, Phys. Rev. Lett. 64, 88.

Chandrasekhar, B. S., and J. K. Hulm, 1958, J. Phys. Chem. Solids 7, 259.

Chaparro, C., L. Fang, H. Claus, A. Rydh, G. W. Crabtree, V. Stanev, W. K. Kwok, and U. Welp, 2011, arXiv:1110.3075.

Chen, C.-C., J. Maciejko, A. P. Sorini, B. Moritz, R. R. P. Singh, and T. P. Devereaux, 2010, Phys. Rev. B 82, 100504.

Chen, C.-T., C. C. Tsuei, M. B. Ketchen, Z.-A. Ren, and Z. X. Zhao, 2010, Nature Phys. 6, 260.

Chen, G. F., W. Z. Hu, J. L. Luo, and N. L. Wang, 2009, Phys. Rev. Lett. 102, 227004.

Chen, G. F., Z. Li, J. Dong, G. Li, W. Z. Hu, X. D. Zhang, X. H. Song, P. Zheng, N. L. Wang, and J. L. Luo, 2008, Phys. Rev. B 78, 224512.

Chen, H., et al., 2009, Europhys. Lett. 85, 17006.

Chen, T. Y., Z. Tesanovic, R. H. Liu, X. H. Chen, and C. L. Chien, 2008, Nature (London) 453, 1224.

Chen, X. H., T. Wu, G. Wu, R. H. Liu, H. Chen, and D. F. Fang, 2008, Nature (London) 453, 761.

Chen, Y., J. W. Lynn, J. Li, G. Li, G. F. Chen, J. L. Luo, N. L. Wang, P. Dai, C. de la Cruz, and H. A. Mook, 2008, Phys. Rev. B 78, 064515.

Cheng, B., et al., 2011, Phys. Rev. B 83, 144522.

Cheng, P., B. Shen, G. Mu, X. Zhu, F. Han, B. Zeng, and H.-H. Wen, 2009, Europhys. Lett. 85, 67003.

Chi, S., et al., 2009, Phys. Rev. Lett. 102, 107006.

Choi, E.-M., S.-G. Jung, N. H. Lee, Y.-S. Kwon, W. N. Kang, D. H. Kim, M.-H. Jung, S.-I. Lee, and L. Sun, 2009, Appl. Phys. Lett. 95, 062507.

Christianson, A. D., M. D. Lumsden, S. E. Nagler, G. J. MacDougall, M. A. McGuire, A. S. Sefat, R. Jin, B. C. Sales, and D. Mandrus, 2009, Phys. Rev. Lett. **103**, 087002.

Christianson, A. D., *et al.*, 2008, Nature (London) **456**, 930.

Chu, C. W., F. Chen, M. Gooch, A. M. Guloy, B. Lorenz, B. Lv, K. Sasmal, Z. J. Tang, J. H. Tapp, and Y. Y. Xue, 2009, Physica C (Amsterdam) **469**, 326.

Chu, C. W., P. H. Hor, R. L. Meng, L. Gao, and Z. J. Huang, 1987, Science **235**, 567.

Chu, C. W., and B. Lorenz, 2009, Physica C (Amsterdam) **469**, 385.

Chu, J.-H., J. G. Analytis, K. De Greve, P. L. McMahon, Z. Islam, Y. Yamamoto, and I. R. Fisher, 2010, Science **329**, 824.

Chuang, T.-M., M. P. Allan, J. Lee, Y. Xie, N. Ni, S. L. Bud'ko, G. S. Boebinger, P. C. Canfield, and J. C. Davis, 2010, Science **327**, 181.

Chubukov, A. V., 2009, Physica C (Amsterdam) **469**, 640.

Chubukov, A. V., D. Efremov, and I. Eremin, 2008, Phys. Rev. B **78**, 134512.

Chubukov, A. V., and S. Sachdev, 1993, Phys. Rev. Lett. **71**, 169.

Chubukov, A. V., M. G. Vavilov, and A. B. Vorontsov, 2009, Phys. Rev. B **80**, 140515.

Colombier, E., S. L. Bud'ko, N. Ni, and P. C. Canfield, 2009, Phys. Rev. B **79**, 224518.

Cvetkovic, C., and Z. Tesanovic, 2009, Europhys. Lett. **85**, 37002.

Daghero, D., and R. S. Gonnelli, 2010, Supercond. Sci. Technol. **23**, 043001.

Daghero, D., M. Tortello, R. S. Gonnelli, V. A. Stepanov, N. D. Zhigadlo, and J. Karpinski, 2009, Phys. Rev. B **80**, 060502(R).

Dai, P., H. A. Mook, G. Aeppli, S. M. Hayden, and F. Dogan, 2000, Nature (London) **406**, 965.

Damascelli, A., Z. Hussain, and Z.-X. Shen, 2003, Rev. Mod. Phys. **75**, 473.

de la Cruz, C., *et al.*, 2010, Phys. Rev. Lett. **104**, 017204.

de la Cruz, C., *et al.*, 2008, Nature (London) **453**, 899.

Deng, Z., X. C. Wang, Q. Q. Liu, S. J. Zhang, Y. X. Lv, J. L. Zhu, R. C. Yu, and C. Q. Jin, 2009, Europhys. Lett. **87**, 37004.

Ding, H., *et al.*, 2008, Europhys. Lett. **83**, 47001.

Ding, L., *et al.*, 2009, New J. Phys. **11**, 093018.

Dong, J., *et al.*, 2008, Europhys. Lett. **83**, 27006.

Dong, J. K., L. Ding, H. Wang, X. F. Wang, T. Wu, X. H. Chen, and S. Y. Li, 2008, New J. Phys. **10**, 123031.

Dong, J. K., T. Y. Guan, S. Y. Zhou, X. Qiu, L. Ding, C. Zhang, U. Patel, Z. L. Xiao, and S. Y. Li, 2009, Phys. Rev. B **80**, 024518.

Dong, J. K., and S. Y. Li, 2010, Phys. Rev. Lett. **104**, 259702.

Dong, J. K., S. Y. Zhou, T. Y. Guan, X. Qiu, C. Zhang, P. Cheng, L. Fang, H. H. Wen, and S. Y. Li, 2010a, Phys. Rev. B **81**, 094520.

Dong, J. K., S. Y. Zhou, T. Y. Guan, H. Zhang, Y. F. Dai, X. Qiu, X. F. Wang, Y. He, X. H. Chen, and S. Y. Li, 2010b, Phys. Rev. Lett. **104**, 087005.

Dressel, M., D. Wu, N. Barisic, and B. Gorshunov, 2010, arXiv:1004.2962.

Drew, A. J., *et al.*, 2009, Nature Mater. **8**, 310.

Dubroka, A., K. W. Kim, M. Rössle, V. K. Malik, A. J. Drew, R. H. Liu, G. Wu, X. H. Chen, and C. Bernhard, 2008, Phys. Rev. Lett. **101**, 097011.

Duncan, W. J., O. P. Welzel, C. Harrison, X. F. Wang, X. H. Chen, F. M. Grosche, and P. G. Niklowitz, 2010, J. Phys. Condens. Matter **22**, 052201.

Dusza, A., A. Lucarelli, F. Pfuner, J.-H. Chu, I. R. Fisher, and L. Degiorgi, 2010, arXiv:1007.2543.

Einzel, D., P. J. Hirschfeld, F. Gross, B. S. Chandrasekhar, K. Andres, H. R. Ott, J. Beuers, Z. Fish, and J. L. Smith, 1986, Phys. Rev. Lett. **56**, 2513.

Eisaki, H., *et al.*, 2008, J. Phys. Soc. Jpn. **77**, Suppl. C, 36.

Eschrig, M., 2006, Adv. Phys. **55**, 47.

Evtushinsky, D. V., *et al.*, 2009a, Phys. Rev. B **79**, 054517.

Evtushinsky, D. V., *et al.*, 2009b, New J. Phys. **11**, 055069.

Fang, C., Y.-L. Wu, R. Thomale, B. A. Bernevig, and J. Hu, 2011a, Phys. Rev. X **1**, 011009.

Fang, M., H. Wang, C. Dong, Z. Li, C. Feng, J. Chen, and H. Q. Yuan, 2011b, Europhys. Lett. **94**, 27009.

Fang, M., J. Yang, F. F. Balakirev, Y. Kohama, J. Singleton, B. Qian, Z. Q. Mao, H. Wang, and H. Q. Yuan, 2010, Phys. Rev. B **81**, 020509(R).

Fawcett, E., H. L. Alberts, V. Yu Galkin, D. R. Noakes, and J. V. Yakhmi, 1994, Rev. Mod. Phys. **66**, 25.

Fernandes, R. M., *et al.*, 2010a, Phys. Rev. B **81**, 140501(R).

Fernandes, R. M., and J. Schmalian, 2010, Phys. Rev. B **82**, 014521.

Fernandes, R. M., L. H. VanBebber, S. Bhattacharya, P. Chandra, V. Keppens, D. Mandrus, M. A. McGuire, B. C. Sales, A. S. Sefat, and J. Schmalian, 2010b, Phys. Rev. Lett. **105**, 157003.

Fischer, O., M. Kugler, I. Maggio-Aprile, C. Berthod, and C. Renner, 2007, Rev. Mod. Phys. **79**, 353.

Fisk, Z., and J. P. Remeika, 1989, in *Handbook on the Physics and Chemistry of Rare Earth*, edited by K. A. Gschneidner, Jr., and L. Eyring (Elsevier, Amsterdam), Vol. 12, p. 53.

Fletcher, J. D., A. Serafin, L. Malone, J. Analytis, J.-H. Chu, A. S. Erickson, I. R. Fisher, and A. Carrington, 2009, Phys. Rev. Lett. **102**, 147001.

Fruchart, D., O. Convert, P. Wolfers, R. Madar, J. P. Senateur, and R. Fruchart, 1975, Mater. Res. Bull. **10**, 169.

Fukazawa, H., N. Takeshita, T. Yamazaki, K. Kondo, K. Hirayama, Y. Kohori, K. Miyazawa, H. Kito, H. Eisaki, and A. Iyo, 2008, J. Phys. Soc. Jpn. **77**, 105004.

Fukazawa, H., *et al.*, 2009a, J. Phys. Soc. Jpn. **78**, 083712.

Fukazawa, H., *et al.*, 2009b, J. Phys. Soc. Jpn. **78**, 033704.

Gao, Z., L. Wang, Y. Qi, D. Wang, X. Zhang, Y. Ma, H. Yang, and H.-H. Wen, 2008, Supercond. Sci. Technol. **21**, 112001.

Gasparov, V. A., 2010, JETP **111**, 313.

Gofryk, K., A. S. Sefat, M. A. McGuire, B. C. Sales, D. Mandrus, T. Imai, J. D. Thompson, E. D. Bauer, F. Ronning, 2011a, J. Phys. Conf. Ser. **273**, 012094.

Gofryk, K., A. S. Sefat, M. A. McGuire, B. C. Sales, D. Mandrus, J. D. Thompson, E. D. Bauer, and F. Ronning, 2010, Phys. Rev. B **81**, 184518.

Gofryk, K., A. B. Vorontsov, I. Vekhter, A. S. Sefat, T. Imai, E. D. Bauer, J. D. Thompson, and F. Ronning, 2011b, Phys. Rev. B **83**, 064513.

Goko, T., *et al.*, 2009, Phys. Rev. B **80**, 024508.

Goldman, A. I., D. N. Argyriou, B. Ouladdiaf, T. Chatterji, A. Kreyssig, S. Nandi, N. Ni, S. L. Bud'ko, P. C. Canfield, and R. J. McQueeney, 2008, Phys. Rev. B **78**, 100506(R).

Gonnelli, R. S., D. Daghero, M. Tortello, G. A. Ummarino, V. A. Stepanov, J. S. Kim, and R. S. Kremer, 2009, Phys. Rev. B **79**, 184526.

Gooch, M., B. Lv, J. H. Tapp, Z. Tang, B. Lorenz, A. M. Guloy, and P. C. W. Chu, 2009, Europhys. Lett. **85**, 27005.

Gordon, R. T., H. Kim, M. A. Tanatar, R. Prozorov, and V. G. Kogan, 2010, Phys. Rev. B **81**, 180501.

Gordon, R. T., C. Martin, H. Kim, N. Ni, M. A. Tanatar, J. Schmalian, I. I. Mazin, S. L. Bud'ko, P. C. Canfield, and R. Prozorov, 2009a, Phys. Rev. B **79**, 100506.

Gordon, R. T., *et al.*, 2009b, Phys. Rev. Lett. **102**, 127004.

Gorshunov, B., D. Wu, A. A. Voronkov, P. Kallina, K. Iida, S. Haindl, F. Kurth, L. Schultz, B. Holzapfel, and M. Dressel, 2010, Phys. Rev. B **81**, 060509(R).

Goswami, P., R. Yu, Q. Si, and E. Abrahams, 2011 Phys. Rev. B **84**, 155108.

Grafe, H.-J., *et al.*, 2008, Phys. Rev. Lett. **101**, 047003.

Graham, A. W., M. Kurmoo, and P. Day, 1995, J. Chem. Soc. Chem. Commun., 2061.

Graser, S., G. R. Boyd, Chao Cao, H.-P. Cheng, P. J. Hirschfeld, and D. J. Scalapino, 2008, Phys. Rev. B **77**, 180514.

Graser, S., A. F. Kemper, T. A. Maier, H.-P. Cheng, P. J. Hirschfeld, and D. J. Scalapino, 2010, Phys. Rev. B **81**, 214503.

Graser, S., T. A. Maier, P. J. Hirschfeld, and D. J. Scalapino, 2009, New J. Phys. **11**, 025016.

Gresty, N. C., *et al.*, 2009, J. Am. Chem. Soc. **131**, 16944.

Guo, J., X. Chen, G. Wang, T. Zhou, X. Lai, S. Jin, S. Wang, and K. Zhu, 2011a, arXiv:1102.3505.

Guo, J., *et al.*, 2011b, arXiv:1101.0092.

Guo, J., S. Jin, G. Wang, S. Wang, K. Zhu, T. Zhou, M. He, and X. Chen, 2010, Phys. Rev. B **82**, 180520(R).

Gupta, L. C., 2006, Adv. Phys. **55**, 691.

Haindl, S., *et al.*, 2010, Phys. Rev. Lett. **104**, 077001.

Hamdadou, N., J. C. Bernede, and A. Khelil, 2002, J. Cryst. Growth **241**, 313.

Han, F., B. Shen, Z.-Y. Wang, and H.-H. Wen, 2011, arXiv:1103.1347.

Han, F., *et al.*, 2009, Phys. Rev. B **80**, 024506.

Han, F., X. Zhu, G. Mu, P. Cheng, and H.-H. Wen, 2008, Phys. Rev. B **78**, 18503(R).

Han, M. J., Q. Yin, W. E. Pickett, and S. Y. Savrasov, 2009, Phys. Rev. Lett. **102**, 107003.

Han, Y., W. Y. Li, L. X. Cao, X. Y. Wang, B. Xu, B. R. Zhao, Y. Q. Guo, and J. L. Yang, 2010, Phys. Rev. Lett. **104**, 017003.

Hanaguri, T., S. Niitaka, K. Kuroki, and H. Takagi, 2010, Science **328**, 474.

Hardy, F., *et al.*, 2010a, Europhys. Lett. **91**, 47008.

Hardy, F., T. Wolf, R. A. Fisher, R. Eder, P. Schweiss, P. Adelmann, H. v. Löhneysen, and C. Meingast, 2010b, Phys. Rev. B **81**, 060501(R).

Harriger, L. W., H. Luo, M. Liu, T. G. Perring, C. Frost, J. Hu, M. R. Norman, and P. Dai, 2011, Phys. Rev. B **84**, 054544.

Hashimoto, K., *et al.*, 2010a, Phys. Rev. B **82**, 014526.

Hashimoto, K., *et al.*, 2010b, Phys. Rev. B **81**, 220501(R).

Hashimoto, K., *et al.*, 2009a, Phys. Rev. Lett. **102**, 207001.

Hashimoto, K., *et al.*, 2009b, Phys. Rev. Lett. **102**, 017002.

Hicks, C. W., T. M. Lippman, M. E. Huber, J. G. Analytis, Jiun-Haw Chu, A. S. Erickson, I. R. Fisher, and K. A. Moler, 2009a, Phys. Rev. Lett. **103**, 127003.

Hicks, C. W., T. M. Lippman, M. E. Huber, Z.-A. Ren, J. Yang, Z.-X. Zhao, and K. A. Moler, 2009b, J. Phys. Soc. Jpn. **78**, 013708.

Hiramatsu, H., T. Katase, T. Kamiya, M. Hirano, and H. Hosono, 2008a, Appl. Phys. Express **1**, 101702.

Hiramatsu, H., T. Katase, T. Kamiya, M. Hirano, and H. Hosono, 2008b, Appl. Phys. Lett. **93**, 162504.

Hiramatsu, H., T. Katase, T. Kamiya, M. Hirano, and H. Hosono, 2009, Phys. Rev. B **80**, 052501.

Hirschfeld, P. J., 2011 (private communication).

Hirschfeld, P. J., M. M. Korshunov, and I. I. Mazin, 2011, Rep. Prog. Phys. **74**, 124508.

Hirschfeld, P. J., and N. Goldenfeld, 1993, Phys. Rev. B **48**, 4219.

Horigane, K., N. Takeshita, C.-H. Lee, H. Hiraka, and K. Yamada, 2009, J. Phys. Soc. Jpn. **78**, 063705.

Hosono, H., 2008, J. Phys. Soc. Jpn. **77**, Suppl. C, 1.

Hsieh, D., Y. Xia, L. Wray, D. Qian, K. K. Gomes, A. Yazdani, G. F. Chen, J. L. Luo, N. L. Wang, and M. Z. Hasan, 2008, arXiv:0812.2289.

Hsu, F.-C., *et al.*, 2008, Proc. Natl. Acad. Sci. U.S.A. **105**, 14262.

Hu, J., T. J. Liu, B. Qian, A. Rotaru, L. Spinu, and Z. Q. Mao, 2011, Phys. Rev. B **83**, 134521.

Hu, R., E. S. Bozin, J. B. Warren, and C. Petrovic, 2009, Phys. Rev. **80**, 214514.

Hu, W. Z., J. Dong, G. Li, Z. Li, P. Zheng, G. F. Chen, J. L. Luo, and N. L. Wang, 2008, Phys. Rev. Lett. **101**, 257005.

Huang, Q., Y. Qiu, Wei Bao, M. A. Green, J. W. Lynn, Y. C. Gasparovic, T. Wu, G. Wu, and X. H. Chen, 2008, Phys. Rev. Lett. **101**, 257003.

Huang, S. X., C. L. Chien, V. Thampy, and C. Broholm, 2010, Phys. Rev. Lett. **104**, 217002.

Hüfner, S., M. A. Hossain, A. Damascelli, and G. A. Sawatzky, 2008, Rep. Prog. Phys. **71**, 062501.

Igawa, K., H. Okada, H. Takahashi, S. Matsuishi, Y. Kamihara, M. Hirano, H. Hosono, K. Matsubayashi, and Y. Uwatoko, 2009, J. Phys. Soc. Jpn. **78**, 025001.

Iida, K., J. Hänisch, R. Hühne, F. Kurth, M. Kidszun, S. Haindl, J. Werner, L. Schultz, and B. Holzapfel, 2009, Appl. Phys. Lett. **95**, 192501.

Iikubo, S., M. Fujita, S. Niitaka, and H. Takagi, 2009, J. Phys. Soc. Jpn. **78**, 103704.

Ikeda, H., R. Arita, and J. Kunes, 2010, Phys. Rev. B **81**, 054502.

Imai, T., K. Ahilan, F. L. Ning, T. M. McQueen, and R. J. Cava, 2009, Phys. Rev. Lett. **102**, 177005.

Imai, Y., H. Takahashi, K. Kitagawa, K. Matsubayashi, N. Nakai, Y. Nagai, Y. Uwatoko, M. Machida, and A. Maeda, 2011, J. Phys. Soc. Jpn. **80**, 013704.

Inosov, D. S., *et al.*, 2010, Nature Phys. **6**, 178.

Inosov, D. S., *et al.*, 2010, Phys. Rev. Lett. **104**, 187001.

Ishida, K., Y. Nakai, and H. Hosono, 2009, J. Phys. Soc. Jpn. **78**, 062001.

Ishida, S., *et al.*, 2010, Phys. Rev. B **81**, 094515.

Ishikado, M., *et al.*, 2010, Physica C (Amsterdam) **471**, 639.

Ivanovskii, A. L., 2011, arXiv:1104.3400.

Jang, D. J., *et al.*, 2011, New J. Phys. **13**, 023036.

Jaroszynski, J., *et al.*, 2008, Phys. Rev. B **78**, 064511.

Jeevan, H. S., and P. Gegenwart, 2010, J. Phys. Conf. Ser. **200**, 012060.

Jeevan, H. S., Z. Hossain, D. Kasinathan, H. Rosner, C. Geibel, and P. Gegenwart, 2008a, Phys. Rev. B **78**, 0052502.

Jeevan, H. S., Z. Hossain, D. Kasinathan, H. Rosner, C. Geibel, and P. Gegenwart, 2008b, Phys. Rev. B **78**, 092406.

Jeevan, H. S., D. Kasinathan, H. Rosner, and P. Gegenwart, 2011, Phys. Rev. B **83**, 054511.

Jeglic, P., *et al.*, 2010, Phys. Rev. B **81**, 140511(R).

Jesche, A., C. Krellner, M. de Souza, M. Lang, and C. Geibel, 2009, New J. Phys. **11**, 103050.

Jesche, A., C. Krellner, M. de Souza, M. Lang, and C. Geibel, 2010, Phys. Rev. B **81**, 134525.

Ji, W., X.-W. Yan, and Z.-Y. Lu, 2011, Phys. Rev. B **83**, 132504.

Jia, Y., P. Cheng, L. Fang, H. Luo, H. Yang, C. Ren, L. Shan, C. Gu, and H.-H. Wen, 2008, Appl. Phys. Lett. **93**, 032503.

Jiang, S., H. Xing, G. Xuan, C. Wang, Z. Ren, C. Feng, J. Dai, Z. Xu, and G. Cao, 2009, J. Phys. Condens. Matter **21**, 382203.

Jiao, L., *et al.*, 2011, arXiv:1106.2283.

Jin, R., *et al.*, 2010, Supercond. Sci. Technol. **23**, 054005.

Jo, Y. J., *et al.*, 2009, Physica C (Amsterdam) **469**, 566.

Johannes, M. D., and I. I. Mazin, 2009, Phys. Rev. B **79**, 220510.

Johnston, D. C., 2010, Adv. Phys. **59**, 803.

Johrendt, D., and R. Pöttgen, 2009, Physica C (Amsterdam) **469**, 332.

Joynt, R., and L. Taillefer, 2002, Rev. Mod. Phys. **74**, 235.

Ju, J., Z. Li, G. Mu, H.-H. Wen, K. Sato, M. Watahiki, G. Li, and K. Tanigaki, 2009, arXiv:0904.4613.

Julien, M.-H., H. Mayaffre, M. Horvatić, C. Berthier, X. D. Zhang, W. Wu, G. F. Chen, N. L. Wang, and J. L. Luo, 2009, Europhys. Lett. **87**, 37001.

Jung, S.-G., N. H. Lee, E.-M. Choi, W. N. Kang, S.-I. Lee, T.-J. Hwang, and D. H. Kim, 2010, arXiv:1005.0192.

Junod, A., M. Roulin, J.-Y. Genoud, B. Revaz, A. Erb, and E. Walker, 1997, Physica C (Amsterdam) **275**, 245.

Kamihara, Y., H. Hiramatsu, M. Hirano, R. Kawamura, H. Yanagi, T. Kamiya, and H. Hosono, 2006, J. Am. Chem. Soc. **128**, 10012.

Kamihara, Y., *et al.*, 2010, New J. Phys. **12**, 033005.

Kamihara, Y., T. Watanabe, M. Hirano, and H. Hosono, 2008, J. Am. Chem. Soc. **130**, 3296.

Kaneko, K., A. Hoser, N. Caroca-Canales, A. Jesche, C. Krellner, O. Stockert, and C. Geibel, 2008, Phys. Rev. B **78**, 212502.

Kant, Ch., J. Deisenhofer, A. Günther, F. Schrettle, A. Loidl, M. Rotter, and D. Johrendt, 2010, Phys. Rev. B **81**, 014529.

Kanter, J., Z. Shermadini, R. Khasanov, A. Amato, Z. Bukowski, and B. Batlogg, 2011 (unpublished).

Kasahara, S., *et al.*, 2010, Phys. Rev. B **81**, 184519.

Kashiwaya, H., *et al.*, 2010, Appl. Phys. Lett. **96**, 202504.

Kasinathan, D., A. Ormeci, K. Koch, U. Burkhardt, W. Schnelle, A. Leithe-Jasper, and H. Rosner, 2009, New J. Phys. **11**, 025023.

Kasperkiewicz, K., J. W. G. Bos, A. N. Fitch, K. Prassides, and S. Margadonna, 2009, Chem. Commun. (Cambridge), 707.

Kastner, M. A., R. J. Birgeneau, G. Shirane, and Y. Endoh, 1998, Rev. Mod. Phys. **70**, 897.

Katase, T., H. Hiramatsu, T. Kamiya, and H. Hosono, 2010a, Appl. Phys. Express **3**, 063101.

Katase, T., H. Hiramatsu, H. Yanagi, T. Kamiya, M. Hirano, and H. Hosono, 2009, Solid State Commun. **149**, 2121.

Katase, T., Y. Ishimaru, A. Tsukamoto, H. Hiramatsu, T. Kamiya, K. Tanabe, and H. Hosono, 2010b, Appl. Phys. Lett. **96**, 142507.

Katase, T., Y. Ishimaru, A. Tsukamoto, H. Hiramatsu, T. Kamiya, K. Tanabe, and H. Hosono, 2010c, Supercond. Sci. Technol. **23**, 082001.

Katayama, N., *et al.*, 2010, arXiv:1003.4525.

Kawaguchi, N., H. Ogino, Y. Shimizu, K. Kishio, and J. Shimoyama, 2010, Appl. Phys. Express **3**, 063102.

Kawaguchi, T., H. Uemura, T. Ohno, M. Tabuchi, T. Ujihara, K. Takenaka, Y. Takeda, and H. Ikuta, 2010, Appl. Phys. Lett. **97**, 042509.

Kawasaki, S., K. Shimada, G. F. Chen, J.L. Luo, N. L. Wang, and G.-Q. Zheng, 2008, Phys. Rev. B **78**, 220506(R).

Kemper, A.F., T. A. Maier, S. Graser, H.-P. Cheng, P. J. Hirschfeld, and D. J. Scalapino, 2010, New J. Phys. **12**, 073030.

Khasanov, R., M. Bendele, A. Bussmann-Holder, H. Keller, 2010a, Phys. Rev. B **82**, 212505.

Khasanov, R., M. Bendele, K. Conder, H. Keller, E. Pomjakushina, and V. Pomjakushin, 2010b, New J. Phys. **12**, 073024.

Khasanov, R., *et al.*, 2008, Phys. Rev. B **78**, 220510.

Khasanov, R., *et al.*, 2009a, Phys. Rev. Lett. **102**, 187005.

Khasanov, R., A. Maisuradze, H. Maeter, A. Kwadrin, H. Luetkens, A. Amato, W. Schnelle, H. Rosner, A. Leithe-Jasper, and H.-H. Klauss, 2009b, Phys. Rev. Lett. **103**, 067010.

Khim, S., J. W. Kim, E. S. Choi, Y. Bang, M. Nohara, H. Takagi, and K. H. Kim, 2010, Phys. Rev. B **81**, 184511.

Kida, T., T. Matsunaga, M. Hagiwara, Y. Mizuguchi, Y. Takano, and K. Kindo, 2009, J. Phys. Soc. Jpn. **78**, 113701.

Kidszun, M., S. Haindl, E. Reich, J. Hänisch, K. Iida, L. Schultz, and B. Holzapfel, 2010, Supercond. Sci. Technol. **23**, 022002.

Kim, H., *et al.*, 2010a, Phys. Rev. B **82**, 060518(R).

Kim, H., *et al.*, 2010b, Phys. Rev. B **81**, 180503.

Kim, H., M. A. Tanatar, Y. Jang Song, Y. S. Kwon, and R. Prozorov, 2011, Phys. Rev. B **83**, 100502(R).

Kim, J. S., 2009 (private communication).

Kim, J. S., T. D. Blasius, E. G. Kim, and G. R. Stewart, 2009a, J. Phys. Condens. Matter **21**, 342201.

Kim, J. S., P. J. Hirschfeld, G. R. Stewart, S. Kasahara, T. Shibauchi, T. Terashima, and Y. Matsuda, 2010, Phys. Rev. B **81**, 214507.

Kim, J. S., P. J. Hirschfeld, G. R. Stewart, S. Kasahara, T. Shibauchi, T. Terashima, and Y. Matsuda, 2011a, J. Phys. Condens. Matter **23**, 222201.

Kim, J. S., S. Khim, L. Yan, N. Manivannan, Y. Liu, I. Kim, G. R. Stewart, and K. H. Kim, 2009b, J. Phys. Condens. Matter **21**, 102203.

Kim, J. S., E. G. Kim, and G. R. Stewart, 2009, J. Phys. Condens. Matter **21**, 252201.

Kim, J. S., E. G. Kim, G. R. Stewart, X. H. Chen, and X. F. Wang, 2011b, Phys. Rev. B **83**, 172502.

Kim, J. S., G. R. Stewart, K. Gofryk, F. Ronning, A. S. Sefat, K. Y. Choi, and K. H. Kim, 2011c (unpublished).

Kim, S. K., M. E. Tillman, H. Kim, A. Kracher, S. L. Bud'ko, R. Prozorov, and P. C. Canfield, 2010, Supercond. Sci. Technol. **23**, 054008.

Kimber, S. A. J., *et al.*, 2008, Phys. Rev. B **78**, 140503(R).

Kimber, S. A. J., *et al.*, 2009, Nature Mater. **8**, 471.

Kirshenbaum, K., S. R. Saha, T. Drye, and J. Paglione, 2010, Phys. Rev. B **82**, 144518.

Kitagawa, K., N. Katayama, K. Ohgushi, M. Yoshida, and M. Takigawa, 2008, J. Phys. Soc. Jpn. **77**, 114709.

Klingeler, R., *et al.*, 2010, Phys. Rev. B **81**, 024506.

Klintberg, L. E., S. K. Goh, S. Kasahara, Y. Nakai, K. Ishida, M. Sutherland, T. Shibauchi, Y. Matsuda, and T. Terashima, 2010, J. Phys. Soc. Jpn. **79**, 123706.

Knolle, J., I. Eremin, A. V. Chubukov, and R. Moessner, 2010, Phys. Rev. B **81**, 140506(R).

Kogan, V. G., 2009, Phys. Rev. B **80**, 214532.

Kogan, V. G., 2010, Phys. Rev. B **81**, 184528.

Kondo, T., *et al.*, 2010, Phys. Rev. B **81**, 060507(R).

Kondo, T., *et al.*, 2008, Phys. Rev. Lett. **101**, 147003.

Kontani, H., and S. Onari, 2010, Phys. Rev. Lett. **104**, 157001.

Kontani, H., T. Saito, and S. Onari, 2011, Phys. Rev. B **84**, 024528.

Korshunov, M. M., I. Eremin, D. V. Efremov, D. L. Maslov, and A. V. Chubukov, 2009, Phys. Rev. Lett. **102**, 236403.

Kotegawa, H., Y. Hara, H. Nohara, H. Tou, Y. Mizuguchi, H. Takeya, and Y. Takano, 2011, J. Phys. Soc. Jpn. **80**, 043708.

Kotegawa, H., T. Kawazoe, H. Tou, K. Murata, H. Ogino, K. Kishio, and J. Shimoyama, 2009, J. Phys. Soc. Jpn. **78**, 123707.

Kotegawa, H., H. Sugawara, and H. Tou, 2009, J. Phys. Soc. Jpn. **78**, 013709.

Krellner, C., N. Caroca-Canales, A. Jesche, H. Rosner, A. Ormeci, and C. Geibel, 2008, Phys. Rev. B **78**, 100504(R).

Kreyssig, A., *et al.*, 2008, Phys. Rev. B **78**, 184517.

Kreyssig, A., *et al.*, 2010, Phys. Rev. B **81**, 134512.

Krzton-Maziopa, A., Z. Shermadini, E. Pomjakushina, V. Pomjakushin, M. Bendele, A. Amato, R. Khasanov, H. Luetkens, and K. Conder, 2011, J. Phys. Condens. Matter **23**, 052203.

Kübert C., and P. J. Hirschfeld, 1998, Solid State Commun. **105**, 459.

Kumar, N., S. Chi, Y. Chen, K. G. Rana, A. K. Nigam, A. Thamizhavel, W. Ratcliff II, S. K. Dhar, and J. W. Lynn, 2009a, Phys. Rev. B **80**, 144524.

Kumar, N., R. Nagalakshmi, R. Kulkarni, P.L. Paulose, A. K. Nigam, S. K. Dhar, and A. Thamizhavel, 2009b, Phys. Rev. B **79**, 012504.

Kurita, N., M. Kimata, K. Kodama, A. Harada, M. Tomita, H. S. Suzuki, T. Matsumoto, K. Murata, S. Uji, and T. Terashima, 2011, Phys. Rev. B **83**, 214513.

Kuroki, K., and H. Aoki, 2009, Physica C (Amsterdam) **469**, 635.

Kuroki, K., S. Onari, R. Arita, H. Usui, Y. Tanaka, H. Kontani, and H. Aoki, 2008, Phys. Rev. Lett. **101**, 087004.

Kuroki, K., H. Usui, S. Onari, R. Arita, and H. Aoki, 2009, Phys. Rev. B **79**, 224511.

Lankau, H., K. Koepernik, S. Borisenko, V. Zabolotnyy, B. Buchner, J. van den Brink, and H. Eschrig, 2010, Phys. Rev. B **82**, 184518.

Laplace, Y., J. Bobroff, F. Rullier-Albenque, D. Colson, and A. Forget, 2009, Phys. Rev. B **80**, 140501(R).

Laplace, Y., J. Bobroff, F. Rullier-Albenque, D. Colson, and A. Forget, 2010, Eur. Phys. J. B **73**, 161.

Lebegue, S., 2007, Phys. Rev. B **75**, 035110.

Lee, B. S., S. H. Khim, J. S. Kim, G. R. Stewart, and K. H. Kim, 2010, Europhys. Lett. **91**, 67002.

Lee, C.-C., W.-G. Yin, and W. Ku, 2009, Phys. Rev. Lett. **103**, 267001.

Lee, C.-H., A. Iyo, H. Eisaki, H. Kito, M. T. Fernandez-Diaz, T. Ito, K. Kihou, H. Matsuhata, M. Braden, and K. Yamada, 2008, J. Phys. Soc. Jpn. **77**, 083704.

Lee, N. H., S.-G. Jung, D. H. Kim, and W. N. Kang, 2010, arXiv:1004.4751.

Lee, P., and X.-G. Wen, 2008, Phys. Rev. B **78**, 144517.

Lee, P. A., N. Nagaosa, and X.-G. Wen, 2006, Rev. Mod. Phys. **78**, 17.

Lee, S., *et al.*, 2009, Appl. Phys. Lett. **95**, 212505.

Lee, S., *et al.*, 2010, Nature Mater. **9**, 397.

Lei, H., K. Wang, J. B. Warren, and C. Petrovic, 2011, Phys. Rev. Lett. **107**, 137002.

Leithe-Jasper, A., W. Schnelle, C. Geibel, and H. Rosner, 2008, Phys. Rev. Lett. **101**, 207004.

Lester, C., J.-H. Chu, J. G. Analytis, T. G. Perring, I. R. Fisher, and S. M. Hayden, 2010, Phys. Rev. B **81**, 064505.

Li, C.-H., B. Shen, F. Han, X. Zhu, and H.-H. Wen, 2011, Phys. Rev. B **83**, 184521.

Li, G., W. Z. Hu, J. Dong, Z. Li, P. Zheng, G. F. Chen, J. L. Luo, and N. L. Wang, 2008, Phys. Rev. Lett. **101**, 107004.

Li, H., W. Tian, J. L. Zarestky, A. Kreyssig, N. Ni, S. L. Bud'ko, P. C. Canfield, A. I. Goldman, R. J. McQueeney, and D. Vaknin, 2009, Phys. Rev. B **80**, 054407.

Li, H.-F., *et al.*, 2010, Phys. Rev. B **82**, 140503(R).

Li, L., Z. R. Yang, Z. T. Zhang, W. Tong, C. J. Zhang, S. Tan, and Y. H. Zhang, 2011, Phys. Rev. B **84**, 174501.

Li, L. J., *et al.*, 2009, New J. Phys. **11**, 025008.

Li, S., C. de la Cruz, Q. Huang, G. F. Chen, T.-L. Xia, J. L. Luo, N. L. Wang, and P. Dai, 2009a, Phys. Rev. B **80**, 020504(R).

Li, S., *et al.*, 2009b, Phys. Rev. B **79**, 054503.

Li, Z., Y. Ooe, X. C. Wang, Q. Q. Liu, C. Q. Jin, M. Ichioka, and G.-Q. Zheng, 2010, J. Phys. Soc. Jpn. **79**, 083702.

Lin, X., H. J. Guo, C. Y. Shen, Y. K. Luo, Q. Tao, G. H. Cao, and Z. A. Xu, 2011, Phys. Rev. B **83**, 014503.

Lipscombe, O. J., *et al.*, 2010, Phys. Rev. B **82**, 064515.

Liu, C., Y. Lee, A. D. Palczewski, J.-Q. Yan, T. Kondo, B. N. Harmon, R. W. McCallum, T. A. Lograsso, and A. Kaminski, 2010a, Phys. Rev. B **82**, 075135.

Liu, C., *et al.*, 2009, Physica C (Amsterdam) **469**, 491.

Liu, C., *et al.*, 2008, Phys. Rev. Lett. **101**, 177005.

Liu, C., *et al.*, 2010b, Nature Phys. **6**, 419.

Liu, R. H., *et al.*, 2009, Nature (London) **459**, 64.

Liu, R. H., *et al.*, 2011, Europhys. Lett. **94**, 27008.

Loram, J. W., J. Luo, J. R. Cooper, W. Y. Liang, and J. L. Tallon, 2001, J. Phys. Chem. Solids **62**, 59.

Lorenz, B., K. Sasmal, R. P. Chaudhury, X. H. Chen, R. H. Liu, T. Wu, and C. W. Chu, 2008, Phys. Rev. B **78**, 012505.

Lu, D. H., *et al.*, 2008, Nature (London) **455**, 81.

Lu, X., *et al.*, 2009, arXiv:0910.4230.

Luan, L., O. M. Auslaender, T. M. Lippman, C. W. Hicks, B. Kalisky, J.-H. Chu, J. G. Analytis, I. R. Fisher, J. R. Kirtley, and K. A. Moler, 2010, Phys. Rev. B **81**, 100501(R).

Luetkens, H.-H. Klauss, *et al.*, 2009, Nature Mater. **8**, 305.

Lumsden, M. D., and A. D. Christianson, 2010, J. Phys. Condens. Matter **22**, 203203.

Lumsden, M. D., *et al.*, 2009, Phys. Rev. Lett. **102**, 107005.

Luo, H., Z. Wang, H. Yang, P. Cheng, X. Zhu, and H.-H. Wen, 2008, Supercond. Sci. Technol. **21**, 125014.

Luo, X. G., *et al.*, 2009, Phys. Rev. B **80**, 140503(R).

Luo, X. G., *et al.*, 2011, New J. Phys. **13**, 053011.

Luo, Y., Y. Li, S. Jiang, J. Dai, G. Cao, and Z. Xu, 2010, Phys. Rev. B **81**, 134422.

Lv, W., J. Wu, and P. Phillips, 2009, Phys. Rev. **80**, 224506.

Ma, F., Z.-Y. Lu, and T. Xiang, 2008, Phys. Rev. B **78**, 224517.

Ma, F., Z.-Y. Lu, and T. Xiang, 2010, Front. Phys. China **5**, 150.

Ma, L., J. B. He, D. M. Wang, G. F. Chen, and W. Yu, 2011, Phys. Rev. Lett. **106**, 197001.

Ma, L., J. Zhang, G. F. Chen, and W. Yu, 2010, Phys. Rev. B **82**, 180501.

Ma, Y., Z. Gao, Y. Qi, X. Zhang, L. Wang, Z. Zhang, and D. Wang, 2009, Physica C (Amsterdam) **469**, 651.

Maier, T. A., S. Graser, P. J. Hirschfeld, and D. J. Scalapino, 2009a, Phys. Rev. B **79**, 134520.

Maier, T. A., S. Graser, P. J. Hirschfeld, and D. J. Scalapino, 2011, Phys. Rev. B **83**, 100515.

Maier, T. A., S. Graser, D. J. Scalapino, and P. J. Hirschfeld, 2009b, Phys. Rev. B **79**, 224510.

Maier, T. A., and D. J. Scalapino, 2008, Phys. Rev. B **78**, 020514(R).

Maiorov, B., S. A. Baily, Y. Kohama, H. Hiramatsu, L. Civale, M. Hirano, and H. Hosono, 2009, Supercond. Sci. Technol. **22**, 125011.

Malaeb, W., *et al.*, 2009, J. Phys. Soc. Jpn. **78**, 123706.

Malone, L., J. D. Fletcher, A. Serafin, and A. Carrington, N. D. Zhigadlo, Z. Bukowski, S. Katrych, and J. Karpinski, 2009, Phys. Rev. B **79**, 140501.

Mandrus, D., A. S. Sefat, M. A. McGuire, and B. C. Sales, 2010, Chem. Mater. **22**, 715.

Mani, A., N. Ghosh, S. Paulraj, A. Bharathi, and C. S. Sundar, 2009, arXiv:0903.4236.

Mansart, B., D. Boschetto, A. Savoia, F. Rullier-Albenque, F. Bouquet, E. Papalazarou, A. Forget, D. Colson, A. Rousse, and M. Marsi, 2010, Phys. Rev. B **82**, 024513.

Margadonna, S., Y. Takabayashi, M. T. McDonald, M. Brunelli, G. Wu, R. H. Liu, X. H. Chen, and K. Prassides, 2009a, Phys. Rev. B **79**, 014503.

Margadonna, S., Y. Takabayashi, Y. Ohishi, Y. Mizuguchi, Y. Takano, T. Kagayama, T. Nakagawa, M. Takata, and K. Prassides, 2009b, Phys. Rev. B **80**, 064506.

Martin, C., H. Kim, R. T. Gordon, N. Ni, V. G. Kogan, S. L. Bud'ko, P. C. Canfield, M. A. Tanatar, and R. Prozorov, 2010, Phys. Rev. B **81**, 060505(R).

Martin, C., *et al.*, 2009b, Phys. Rev. Lett. **102**, 247002.

Martin, C., *et al.*, 2009a, Phys. Rev. B **80**, 020501(R).

Martinelli, A., A. Palenzona, M. Tropeano, C. Ferdeghini, M. Putti, M. R. Cimberle, T. D. Nguyen, M. Affronte, and C. Ritter, 2010, Phys. Rev. B **81**, 094115.

Martinelli, A., A. Palenzona, M. Tropeano, M. Putti, C. Ferdeghini, G. Profeta, and E. Emerich, 2011, Phys. Rev. Lett. **106**, 227001.

Masaki, S., H. Kotegawa, Y. Hara, H. Tou, K. Murata, Y. Mizuguchi, and Y. Takano, 2009, J. Phys. Soc. Jpn. **78**, 063704.

Massee, F., Y. Huang, R. Huisman, S. de Jong, J. B. Goedkoop, and M. S. Golden, 2009, Phys. Rev. B **79**, 220517(R).

Matan, K., R. Morinaga, K. Iida, and T. J. Sato, 2009, Phys. Rev. B **79**, 054526.

Matano, K., Z. Li, G. L. Sun, D. L. Sun, C. T. Lin, M. Ichioka, and G.-Q. Zheng, 2009, Europhys. Lett. **87**, 27012.

Matano, K., Z. A. Ren, X. L. Dong, L. L. Sun, Z. X. Zhao, and G.-Q. Zheng, 2008, Europhys. Lett. **83**, 57001.

Matsubayashi, K., N. Katayama, K. Ohgushi, A. Yamada, K. Munakata, T. Matsumoto, and Y. Uwatoko, 2009, J. Phys. Soc. Jpn. **78**, 073706.

Matsuishi, S., Y. Inoue, T. Nomura, M. Hirano, and H. Hosono, 2008a, J. Phys. Soc. Jpn. **77**, 113709.

Matsuishi, S., Y. Inoue, T. Nomura, H. Yanagi, M. Hirano, and H. Hosono, 2008b, J. Am. Chem. Soc. **130**, 14428.

Matthias, B. T., V. B. Compton, and E. Corenzwit, 1961, J. Phys. Chem. Solids **19**, 130.

Mazin, I. I., 2010, Phys. Rev. B **81**, 020507(R).

Mazin, I. I., 2011, Physics **4**, 26.

Mazin, I. I., and M. D. Johannes, 2009, Nature Phys. **5**, 141.

Mazin, I. I., and J. Schmalian, 2009, Physica C (Amsterdam) **469**, 614.

Mazin, I. I., D. J. Singh, M. D. Johannes, and M. H. Du, 2008, Phys. Rev. Lett. **101**, 057003.

McGuire, M. A., *et al.*, 2008, Phys. Rev. B **78**, 094517.

McGuire, M. A., D. J. Singh, A. S. Sefat, B. C. Sales, and D. Mandrus, 2009, J. Solid State Chem. **182**, 2326.

McMillan, W. L., 1968, Phys. Rev. **167**, 331.

McQueen, T. M., *et al.*, 2009a, Phys. Rev. B **79**, 014522.

McQueen, T. M., A. J. Williams, P. W. Stephens, J. Tao, Y. Zhu, V. Ksenofontov, F. Casper, C. Felser, and R. J. Cava, 2009b, Phys. Rev. Lett. **103**, 057002.

McQueeney, R. J., *et al.*, 2008, Phys. Rev. Lett. **101**, 227205.

Michioka, C., H. Ohta, M. Matsui, J. Yang, K. Yoshimura, and M. Fang, 2010, Phys. Rev. B **82**, 064506.

Mishra, V., G. Boyd, S. Graser, T. Maier, P. J. Hirschfeld, and D. J. Scalapino, 2009a, Phys. Rev. B **79**, 094512.

Mishra, V., A. Vorontsov, P. J. Hirschfeld, and I. Vekhter, 2009b, Phys. Rev. B **80**, 224525.

Mishra, V., S. Graser, and P. J. Hirschfeld, 2011, Phys. Rev. B **84**, 014524.

Miyazawa, K., K. Kihou, P. M. Shirage, C.-H. Lee, H. Kito, H. Eisaki, and A. Iyo, 2009, J. Phys. Soc. Jpn. **78**, 034712.

Mizuguchi, Y., K. Deguchi, S. Tsuda, T. Yamaguchi, and Y. Takano, 2010a, Phys. Rev. B **81**, 214510.

Mizuguchi, Y., and Y. Takano, 2010, J. Phys. Soc. Jpn. **79**, 102001.

Mizuguchi, Y., F. Tomioka, K. Deguchi, S. Tsuda, T. Yamaguchi, and Y. Takano, 2010b, Physica C (Amsterdam) **470**, S353.

Mizuguchi, Y., F. Tomioka, S. Tsuda, T. Yamaguchi, and Y. Takano, 2009, J. Phys. Soc. Jpn. **78**, 074712.

Moler, K. A., D. J. Baar, J. S. Urbach, R. Liang, W. N. Hardy, and A. Kapitulnik, 1994, Phys. Rev. Lett. **73**, 2744.

Mook, H. A., *et al.*, 2010, Phys. Rev. Lett. **104**, 187002.

Moon, S. J., *et al.*, 2010, Phys. Rev. B **81**, 205114.

Mou, D., *et al.*, 2011, Phys. Rev. Lett. **106**, 107001.

Mu, G., L. Fang, H. Yang, X. Zhu, P. Cheng, and H.-H. Wen, 2008a, J. Phys. Soc. Jpn. **77**, Suppl. C, 15.

Mu, G., H. Luo, Z. Wang, L. Shan, C. Ren, and H.-H. Hu, 2009a, Phys. Rev. B **79**, 174501.

Mu, G., B. Zeng, P. Cheng, Z. Wang, L. Fang, B. Shen, L. Shan, C. Ren, and H.-H. Wen, 2010, Chin. Phys. Lett. **27**, 037402.

Mu, G., B. Zeng, X. Zhu, F. Han, P. Cheng, B. Shen, and H.-H. Wen, 2009b, Phys. Rev. B **79**, 104501.

Mu, G., X. Zhu, L. Fang, L. Shan, C. Ren, H.-H. Wen, 2008b, Chin. Phys. Lett. **25**, 2221.

Mukuda, H., *et al.*, 2008, J. Phys. Soc. Jpn. **77**, 093704.

Muraba, Y., S. Matsuishi, S.-W. Kim, T. Atou, O. Fukunaga, and H. Hosono, 2010, Phys. Rev. B **82**, 180512.

Muschler, B., W. Prestel, R. Hackl, T. P. Devereaux, J. G. Analytis, J.-H. Chu, and I. R. Fisher, 2009, Phys. Rev. B **80**, 180510.

Mydeen, K., E. Lengyel, Z. Deng, X. C. Wang, C. Q. Jin, and M. Nicklas, 2010, Phys. Rev. B **82**, 014514.

Nakai, N., P. Miranović, M. Ichioka, and K. Machida, 2004, Phys. Rev. B **70**, 100503.

Nakai, Y., K. Ishida, Y. Kamihara, M. Hirano, and Hideo Hosono, 2008, J. Phys. Soc. Jpn. **77**, 073701.

Nakai, Y., T. Iye, S. Kitagawa, K. Ishida, S. Kasahara, T. Shibauchi, Y. Matsuda, and T. Terashima, 2010, Phys. Rev. B **81**, 020503(R).

Nakai, Y., S. Kitagawa, K. Ishida, Y. Kamihara, M. Hirano, and H. Hosono, 2009, Phys. Rev. B **79**, 212506.

Nandi, S., *et al.*, 2010, Phys. Rev. Lett. **104**, 057006.

Ni, N., S. L. Bud'ko, A. Kreyssig, S. Nandi, G. E. Rustan, A. I. Goldman, S. Gupta, J. D. Corbett, A. Kracher, and P. C. Canfield, 2008a, Phys. Rev. B **78**, 014507.

Ni, N., A. Thaler, A. Kracher, J. Q. Yan, S. L. Bud'ko, and P. C. Canfield, 2009, Phys. Rev. B **80**, 024511.

Ni, N., M. E. Tillman, J.-Q. Yan, A. Kracher, S. T. Hannahs, S. L. Bud'ko, and P. C. Canfield, 2008b, Phys. Rev. B **78**, 214515.

Nie, Y. F., E. Brahimi, J. I. Budnick, W. A. Hines, M. Jain, and B. O. Wells, 2009, Appl. Phys. Lett. **94**, 242505.

Nohara, M., M. Isshiki, H. Takagi, and R. J. Cava, 1997, J. Phys. Soc. Jpn. **66**, 1888.

Norman, M., 2010, http://physics.aps.org/videos/2010-norman-ironage_superconductors.

Nomura, T., Y. Inoue, S. Matsuishi, M. Hirano, J. E. Kim, K. Kato, M. Takata, and H. Hosono, 2009, Supercond. Sci. Technol. **22**, 055016.

Nomura, T., S. W. Kim, Y. Kamihara, M. Hirano, P. V. Sushko, K. Kato, M. Takata, A. L. Shluger, and H. Hosono, 2008, Supercond. Sci. Technol. **21**, 125028.

Norman, M. R., 2008, Physics **1**, 21.

Oeschler, N., R. A. Fisher, N. E. Phillips, J. E. Gordon, M.-L. Foo, and R. J. Cava, 2008, Phys. Rev. B **78**, 054528.

Ogino, H., Y. Matsumara, Y. Katsura, K. Ushiyama, S. Horii, K. Kishio, and J.-I. Shimoyama, 2009, Supercond. Sci. Technol. **22**, 075008.

Ogino, H., S. Sato, K. Kishio, J. Shimoyama, T. Tohei, and Y. Ikuhara, 2010a, Appl. Phys. Lett. **97**, 072506.

Ogino, H., S. Sato, Y. Matsumura, N. Kawaguchi, K. Ushiyama, Y. Katsura, S. Horii, K. Kishio, J. Shimoyama, 2010b, Physica C (Amsterdam) **470**, S280.

Ogino, H., Y. Shimizu, K. Ushiyama, N. Kawaguchi, K. Kishio, and J.-I. Shimoyama, 2010c, Appl. Phys. Express **3**, 063103.

Okada, H., K. Igawa, H. Takahashi, Y. Kamihara, M. Hirano, H. Hosono, K. Matsubayashi, and Y. Uwatoko, 2008, J. Phys. Soc. Jpn. **77**, 113712.

Onari, S., H. Kontani, and M. Sato, 2010, Phys. Rev. B **81**, 060504 (R).

Osborn, R., S. Rosenkranz, E. A. Goremychkin, and A. D. Christianson, 2009, Physica C (Amsterdam) **469**, 498.

Ozaki, T., K. Deguchi, Y. Mizuguchi, Y. Kawasaki, T. Tanaka, T. Yamaguchi, S. Tsuda, H. Kumakura, and Y. Takano, 2011, arXiv:1103.0402.

Paglione, J., and R. L. Greene, 2010, Nature Phys. **6**, 645.

Park, J. T., *et al.*, 2009, Phys. Rev. Lett. **102**, 117006.

Park, J. T., *et al.*, 2010, Phys. Rev. B **82**, 134503.

Park, T., E. Park, H. Lee, T. Klimczuk, E. D. Bauer, F. Ronning, and J. D. Thompson, 2008, J. Phys. Condens. Matter **20**, 322204.

Park, T., and M. B. Salamon, 2004, Mod. Phys. Lett. B **18**, 1205.

Park, T., M. B. Salamon, E. M. Choi, H. J. Kim, and S.-I. Lee, 2003, Phys. Rev. Lett. **90**, 177001.

Parker, D., O. V. Dolgov, M. M. Korshunov, A. A. Golubov, and I. I. Mazin, 2008, Phys. Rev. B **78**, 134524.

Parker, D. R., M. J. Pitcher, P. J. Baker, I. Franke, T. Lancaster, S. J. Blundell, and S. J. Clarke, 2009, Chem. Commun. (Cambridge), 2189.

Parker, D. R., M. J. P. Smith, T. Lancaster, A. J. Steele, I. Franke, P. J. Baker, F. L. Pratt, M. J. Pitcher, S. J. Blundell, and S. J. Clarke, 2010, Phys. Rev. Lett. **104**, 057007.

Patel, U., J. Hua, S. H. Yu, S. Avci, Z. L. Xiao, H. Claus, J. Schlueter, V. V. Vlasko-Vlasov, U. Welp, and W. K. Kwok, 2009, Appl. Phys. Lett. **94**, 082508.

Pfleiderer, C., 2009, Rev. Mod. Phys. **81**, 1551.

Pitcher, M. J., *et al.*, 2010, J. Am. Chem. Soc. **132**, 10467.

Pitcher, M. J., D. R. Parker, P. Adamson, S. J. C. Herkelrath, A. T. Boothroyd, and S. J. Clarke, 2008, Chem. Commun. (Cambridge), 5918.

Platt, C., R. Thomale, and W. Hanke, 2011, arXiv:1103.2101.

Popovich, P., A. V. Boris, O. V. Dolgov, A. A. Golubov, D. L. Sun, C. T. Lin, R. K. Kremer, and B. Keimer, 2010, Phys. Rev. Lett. **105**, 027003.

Pöttgen, R., and D. Johrendt, 2008, Z. Naturforsch. B **63b**, 1135.

Pourret, A., L. Malone, A. B. Antunes, C. S. Yadav, P. L. Paulose, B. Fauqué, and K. Behnia, 2011, Phys. Rev. B **83**, 020504(R).

Pratt, D. K., W. Tian, A. Kreyssig, J. L. Zarestky, S. Nandi, N. Ni, S. L. Bud'ko, P. C. Canfield, A. I. Goldman, and R. J. McQueeney, 2009a, Phys. Rev. Lett. **103**, 087001.

Pratt, D. K., *et al.*, 2009b, Phys. Rev. B **79**, 060510.

Prommapan, P., M. A. Tanatar, B. S. Lee, S. H. Khim, K. H. Kim, and R. Prozorov, 2011, Phys. Rev. B **84**, 060509.

Prozorov, R., and R. W. Giannetta, 2006, Supercond. Sci. Technol. **19**, R41.

Prozorov, R., M. A. Tanatar, E. C. Blomberg, P. Prommapan, R. T. Gordon, N. Ni, S. L. Bud'ko, and P. C. Canfield, 2009, Physica C (Amsterdam) **469**, 667.

Putti, M., *et al.*, 2010, Supercond. Sci. Technol. **23**, 034003.

Qi, X. L., S. Raghu, Chao-Xing Liu, D. J. Scalapino, and Shou-Cheng Zhang, 2008, arXiv:0804.4332.

Qi, Y., Z. Gao, L. Wang, D. Wang, X. Zhang, and Y. Ma, 2008, New J. Phys. **10**, 123003.

Qi, Y., L. Wang, Z. Gao, D. Wang, X. Zhang, and Y. Ma, 2009a, arXiv:0903.4967.

Qi, Y., L. Wang, Z. Gao, D. Wang, X. Zhang, C. Wang, C. Yao, Y. Ma, 2011, New J. Phys. **13**, 033020.

Qi, Y., L. Wang, Z. Gao, D. Wang, X. Zhang, Z. Zhang, and Y. Ma, 2009b, Phys. Rev. B **80**, 054502.

Qian, T., *et al.*, 2011, Phys. Rev. B **83**, 140513(R).

Qiu, Y., *et al.*, 2008, Phys. Rev. Lett. **101**, 257002.

Qiu, Y., *et al.*, 2009, Phys. Rev. Lett. **103**, 067008.

Raghu, S., X.-L. Qi, C.-X. Liu, D. J. Scalapino, and S.-C. Zhang, 2008, Phys. Rev. B **77**, 220503(R).

Reid, J.-Ph., M. A. Tanatar, X. G. Luo, H. Shakeripour, N. Doiron-Leyraud, N. Ni, S. L. Bud'ko, P. C. Canfield, R. Prozorov, and L. Taillefer, 2010, Phys. Rev. B **82**, 064501.

Ren, Z., Q. Tao, S. Jiang, C. Feng, C. Wang, J. Dai, G. Cao, and Z. Xu, 2009, Phys. Rev. Lett. **102**, 137002.

Ren, Z.-A., *et al.*, 2008a, Europhys. Lett. **83**, 17002.

Ren, Z.-A., *et al.*, 2008b, Chin. Phys. Lett. **25**, 2215.

Rettig, L., R. Cortés, S. Thirupathaiah, P. Gegenwart, H. S. Jeevan, T. Wolf, U. Bovensiepen, M. Wolf, H. A. Dürr, and J. Fink, 2010, arXiv:1008.1561.

Richard, P., *et al.*, 2010, Phys. Rev. Lett. **104**, 137001.

Roddick, E., and D. Stroud, 1995, Phys. Rev. Lett. **74**, 1430.

Ronning, F., E. D. Bauer, T. Park, N. Kurita, T. Klimczuk, R. Movshovich, A. S. Sefat, D. Mandrus, and J. D. Thompson, 2009, Physica C (Amsterdam) **469**, 396.

Ronning, F., T. Klimczuk, E. D. Bauer, H. Volz, and J. D. Thompson, 2008, J. Phys. Condens. Matter **20**, 322201.

Rotter, M., C. Hieke, and D. Johrendt, 2010, Phys. Rev. B **82**, 014513.

Rotter, M., M. Pangerl, M. Tegel, and D. Johrendt, 2008a, Angew. Chem., Int. Ed. **47**, 7949.

Rotter, M., M. Tegel, and D. Johrendt, 2008, Phys. Rev. Lett. **101**, 107006.

Rotter, M., M. Tegel, D. Johrendt, I. Schellenberg, W. Hermes, and R. Pöttgen, 2008b, Phys. Rev. B **78**, 020503.

Rotter, M., M. Tegel, I. Schellenberg, F. M. Schappacher, R. Pöttgen, J. Deisenhofer, A. Günther, F. Schrettle, A. Loidl, and D. Johrendt, 2009, New J. Phys. **11**, 025014.

Rotundu, C. R., *et al.*, 2010, Phys. Rev. B **82**, 144525.

Rotundu, C. R., D. T. Keane, B. Freelon, S. D. Wilson, A. Kim, P. N. Valdivia, E. Bourret-Courchesne, and R. J. Birgeneau, 2009, Phys. Rev. B **80**, 144517.

Rullier-Albenque, F., D. Colson, A. Forget, P. Thuéry, and S. Poissonnet, 2010, Phys. Rev. B **81**, 224503.

Saha, S. R., N. P. Butch, K. Kirshenbaum, and J. Paglione, 2009b, Phys. Rev. Lett. **103**, 037005.

Saha, S. R., N. P. Butch, K. Kirshenbaum, and J. Paglione, 2010a, Physica C (Amsterdam) **470**, S379.

Saha, S. R., T. Drye, K. Kirshenbaum, N. P. Butch, P. Y. Zavalij, and J. Paglione, 2010b, J. Phys. Condens. Matter **22**, 072204.

Saha., S. R., N. P. Butch, K. Kirshenbaum, and J. Paglione, 2009a, Phys. Rev. B **79**, 224519.

Sales, B. C., M. A. McGuire, A. F. May, H. Cao, B. C. Chakoumakos, and A. S. Sefat, 2011, Phys. Rev. B **83**, 224510.

Sales, B. C., M. A. McGuire, A. S. Sefat, and D. Mandrus, 2010, Physica C (Amsterdam) **470**, 304.

Sales, B. C., A. S. Sefat, M. A. McGuire, R. Y. Jin, and D. Mandrus, 2009, Phys. Rev. B **79**, 094521.

Samuely, P., Z. Pribulová, P. Szabó, G. Pristáš, S. L. Bud'ko, and P. C. Canfield, 2009a, Physica C (Amsterdam) **469**, 507.

Samuely, P., P. Szabo, Z. Pribulova, M. E. Tillman, S. Bud'ko, and P. C. Canfield, 2009b, Supercond. Sci. Technol. **22**, 014003.

Sanna, S., R. De Renzi, G. Lamura, C. Ferdeghini, A. Palenzona, M. Putti, M. Tropeano, and T. Shiroka, 2009, Phys. Rev. B **80**, 052503.

Sanna, S., *et al.*, 2010, Phys. Rev. B **82**, 060508(R).

Sasmal, K., B. Lv, B. Lorenz, A. M. Guloy, F. Chen, Y.-Y. Xue, and C.-W. Chu, 2008, Phys. Rev. Lett. **101**, 107007.

Sasmal, K., B. Lv, Z. Tang, F. Y. Wei, Y. Y. Xue, A. M. Guloy, and C. W. Chu, 2010, Phys. Rev. B **81**, 144512.

Sato, S., H. Ogino, N. Kawaguchi, Y. Katsura, K. Kishio, J. Shimoyama, H. Kotegawa, and H. Tou, 2010, Supercond. Sci. Technol. **23**, 045001.

Sato, T., *et al.*, 2009, Phys. Rev. Lett. **103**, 047002.

Sawatzky, G. A., I. S. Elfimov, J. van den Brink, and J. Zaanen, 2009, Europhys. Lett. **86**, 17006.

Scalapino, D. J., 1995, Phys. Rep. **250**, 329.

Schlossmann, M., and J. P. Carbotte, 1989, Phys. Rev. B **39**, 4210.

Schmidt, B., M. Siahatgar, and P. Thalmeier, 2010, Phys. Rev. B **81**, 165101.

Schnelle, W., A. Leithe-Jasper, R. Gumeniuk, U. Burkhardt, D. Kasinathan, and H. Rosner, 2009, Phys. Rev. B **79**, 214516.

Sefat, A. S., A. Huq, M. A. McGuire, R. Jin, B. C. Sales, D. Mandrus, L. M. D. Cranswick, P. W. Stephens, and K. H. Stone, 2008a, Phys. Rev. B **78**, 104505.

Sefat, A. S., R. Jin, M. A. McGuire, B. C. Sales, D. J. Singh, and D. Mandrus, 2008b, Phys. Rev. Lett. **101**, 117004.

Sefat, A. S., D. J. Singh, V. O. Garlea, Y. L. Zuev, M. A. McGuire, L. van Bebber, and B. C. Sales, 2010, arXiv:1009.4911.

Sefat, A. S., D. J. Singh, L. H. VanBebber, Y. Mozharivskyj, M. A. McGuire, R. Jin, B. C. Sales, V. Keppens, and D. Mandrus, 2009, Phys. Rev. B **79**, 224524.

Seyfarth, G., D. Jaccard, P. Pedrazzinib, A. Krzton-Maziopa, E. Pomjakushina, K. Conder, Z. Shermadini, 2011, Solid State Commun. **151**, 747.

Sharma, S., A. Bharathi, S. Chandra, R. Reddy, S. Paulraj, A. T. Satya, V. S. Sastry, Ajay Gupta, and C. S. Sundar, 2010, Phys. Rev. B **81**, 174512.

Sheet, G., et al., 2010, Phys. Rev. Lett. **105**, 167003.

Shein, I. R., and A. L. Ivanovskii, 2009a, Solid State Commun. **149**, 1860.

Shein, I. R., and A. L. Ivanovskii, 2009b, Phys. Rev. B **79**, 245115.

Shein, I. R., and A. L. Ivanovskii, 2009c, JETP Lett. **88**, 107.

Shen, B., B. Zeng, G. F. Chen, J. B. He, D. M. Wang, H. Yang, and H. H. Wen, 2011, Europhys. Lett. **96**, 37010.

Shermadini, Z., et al., 2011, Phys. Rev. Lett. **106**, 117602.

Shi, H. L., H. X. Yang, H. F. Tian, J. B. Lu, Z. W. Wang, Y. B. Qin, Y. J. Song, and J. Q. Li, 2009, arXiv:0909.4600.

Shibauchi, T., K. Hashimoto, R. Okazaki, and Y. Matsuda, 2009, Physica C (Amsterdam) **469**, 590.

Shimizu, K., K. Amaya, N. Suzuki, and Yoshichika Ōnuki, 2006, Physica B (Amsterdam) **378–380**, 632.

Shimizu, K., T. Kimura, S. Furomoto, K. Takeda, K. Kontani, Y. Onuki, and K. Amaya, 2001, Nature (London) **412**, 316.

Shimizu, Y., H. Ogino, N. Kawaguchi, K. Kishio, and J.-I. Shimoyama, 2010, Supercond. Sci. Technol. **24**, 085020.

Shimojima, T., et al., 2010, Phys. Rev. Lett. **104**, 057002.

Shirage, P. M., K. Kihou, K. Miyazawa, C.-H. Lee, H. Kito, H. Eisaki, T. Yanagisawa, Y. Tanaka, and A. Iyo, 2009, Phys. Rev. Lett. **103**, 257003.

Shirage, P. M., K. Miyazawa, K. Kihou, H. Kito, Y. Yoshida, Y. Tanaka, H. Eisaki, and A. Iyo, 2010, Phys. Rev. Lett. **105**, 037004.

Shirage, P. M., K. Miyazawa, H. Kito, H. Eisaki, and A. Iyo, 2008, Phys. Rev. B **78**, 172503.

Si, Q., and E. Abrahams, 2008, Phys. Rev. Lett. **101**, 076401.

Sidorov, V. A., A. V. Tsvyashchenko, and R. A. Sadykov, 2009, arXiv:0903.2873.

Sigrist, M., and K. Ueda, 1991, Rev. Mod. Phys. **63**, 239.

Singh, D. J., 2008, Phys. Rev. B **78**, 094511.

Singh, D. J., 2009, Physica C (Amsterdam) **469**, 418.

Singh, D. J., and M. H. Du, 2008, Phys. Rev. Lett. **100**, 237003.

Singh, Y., Y. Lee, S. Nandi, A. Kreyssig, A. Ellern, S. Das, R. Nath, B. N. Harmon, A. I. Goldman, and D. C. Johnston, 2008, Phys. Rev. B **78**, 104512.

Skornyakov, S. L., N. A. Skorikov, A. V. Lukoyanov, A. O. Shorikov, and V. I. Anisimov, 2010, Phys. Rev. B **81**, 174522.

Song, Y. J., J. S. Ghim, B. H. Min, Y. S. Kwon, M. H. Jung, and J. S. Rhyee, 2010, Appl. Phys. Lett. **96**, 212508.

Sonier, J. E., M. F. Hundley, J. D. Thompson, and J. W. Brill, 1999, Phys. Rev. Lett. **82**, 4914.

Steglich, F., J. Aarts, C. D. Bredl, W. Lieke, D. Meschede, W. Franz, and H. Schaefer, 1979, Phys. Rev. Lett. **43**, 1892.

Stewart, G. R., 1983, Rev. Sci. Instrum. **54**, 1.

Stewart, G. R., 2001, Rev. Mod. Phys. **73**, 797.

Stewart, G. R., 2006, Rev. Mod. Phys. **78**, 743.

Stockert, U., M. Abdel-Hafiez, D. V. Evtushinsky, V. B. Zabolotnyy, A. U. B. Wolter, S. Wurmehl, I. Morozov, R. Klingeler, S. V. Borisenko, and B. Büchner, 2011, Phys. Rev. B **83**, 224512.

Su, Y., et al., 2009, Phys. Rev. B **79**, 064504.

Subedi, A., L. Zhang, D. J. Singh, and M. H. Du, 2008, Phys. Rev. B **78**, 134514.

Sugai, S., Y. Mizuno, K. Kiho, M. Nakajima, C. H. Lee, A. Iyo, H. Eisaki, and S. Uchida, 2010, Phys. Rev. B **82**, 140504(R).

Sun, G. L., D. L. Sun, M. Konuma, P. Popovich, A. Boris, J. B. Peng, K.-Y. Choi, P. Lemmens, and C. T. Lin, 2011, J. Supercond. Novel Magnetism **24**, 1773.

Suzuki, S., S. Miyasaka, S. Tajima, T. Kida, and M. Hagiwara, 2009, J. Phys. Soc. Jpn. **78**, 114712.

Szabo, P., Z. Pribulova, G. Pristas, S. L. Bud'ko, P. C. Canfield, and P. Samuely, 2009, Phys. Rev. B **79**, 012503.

Takahashi, H., K. Igawa, K. Arii, Y. Kamihara, M. Hirano, and H. Hosono, 2008a, Nature (London) **453**, 376.

Takahashi, H., H. Okada, K. Igawa, K. Arii, Y. Kamihara, S. Matsuishi, M. Hirano, H. Hosono, K. Matsubayashi, and Y. Uwatoko, 2008b, J. Phys. Soc. Jpn. **77**, Suppl. C, 78.

Takemura, Y., H. Suto, N. Honda, K. Kakuno, and K. Saito, 1997, J. Appl. Phys. **81**, 5177.

Takeshita, N., T. Yamazaki, A. Iyo, H. Eisaki, H. Kito, T. Ito, K. Hirayama, H. Fukazawa, and Y. Kohori, 2008, J. Phys. Soc. Jpn. **77**, Suppl. C, 131.

Tanatar, M. A., J.-Ph. Reid, H. Shakeripour, X. G. Luo, N. Doiron-Leyraud, N. Ni, S. L. Bud'ko, P. C. Canfield, R. Prozorov, and L. Taillefer, 2010a, Phys. Rev. Lett. **104**, 067002.

Tanatar, M. A., et al., 2010b, Phys. Rev. B **81**, 184508.

Tanatar, M. A., et al., 2011, Phys. Rev. B **84**, 054507.

Taylor, A. E., M. J. Pitcher, R. A. Ewings, T. G. Perring, S. J. Clarke, and A. T. Boothroyd, 2011, Phys. Rev. B **83**, 220514(R).

Tegel, M., F. Hummel, S. Lackner, I. Schellenberg, R. Pöttgen, and D. Johrendt, 2009, Z. Anorg. Allg. Chem. **635**, 2242.

Tegel, M., S. Johansson, V. Weiß, I. Schellenberg, W. Hermes, R. Pöttgen, and D. Johrendt, 2008a, Europhys. Lett. **84**, 67007.

Tegel, M., M. Rotter, V. Weiss, F. M. Schappacher, R. Poettgen, and D. Johrendt, 2008b, J. Phys. Condens. Matter **20**, 452201.

Tegel, M., T. Schmid, T. Stürzer, M. Egawa, Y. Su, A. Senyshyn, and D. Johrendt, 2010, Phys. Rev. B **82**, 140507(R).

Terashima, T., M. Kimata, H. Satsukawa, A. Harada, K. Hazama, S. Uji, H. Harima, G.-F. Chen, J.-L. Luo, and N.-L. Wang, 2009, J. Phys. Soc. Jpn. **78**, 063702.

Tesanovic, Z., 2009, Physics **2**, 60.

Thaler, A., N. Ni, A. Kracher, J. Q. Yan, S. L. Bud'ko, and P. C. Canfield, 2010, Phys. Rev. B **82**, 014534.

Thomale, R., C. Platt, W. Hanke, and B. A. Bernevig, 2011a, Phys. Rev. Lett. **106**, 187003.

Thomale, R., C. Platt, W. Hanke, J. Hu, and B. A. Bernevig, 2011b, Phys. Rev. Lett. **107**, 117001.

Thomale, R., C. Platt, J. Hu, C. Honerkamp, and B. A. Bernevig, 2009, Phys. Rev. B **80**, 180505.

Tian, W., et al., 2010, Phys. Rev. B **82**, 060514(R).

Torchetti, D. A., M. Fu, D. C. Christensen, K. J. Nelson, T. Imai, H. C. Lei, and C. Petrovic, 2011, Phys. Rev. B **83**, 104508.

Torikachvili, M. S., S. L. Bud'ko, N. Ni, and P. C. Canfield, 2008, Phys. Rev. Lett. **101**, 057006.

Torikachvili, M. S., S. L. Bud'ko, N. Ni, P. C. Canfield, and S. T. Hannahs, 2009, Phys. Rev. B **80**, 014521.

Tortello, M., D. Daghero, G. A. Ummarino, V. A. Stepanov, J. Jiang, J. D. Weiss, E. E. Hellstrom, and R. S. Gonnelli, 2010, Phys. Rev. Lett. **105**, 237002.

Tranquada, J. M., C. H. Lee, K. Yamada, Y. S. Lee, L. P. Regnault, and H. M. Ronnow, 2004, Phys. Rev. B **69**, 174507.

Tsuei, C. C., J. R. Kirtley, C. C. Chi, Lock-See Yu-Jahnes, A. Gupta, T. Shaw, J. Z. Sun, and M. B. Ketchen, 1994, Phys. Rev. Lett. **73**, 593.

Tsurkan, V., J. Deisenhofer, A. Günther, Ch. Kant, H.-A. Krug von Nidda, F. Schrettle, and A. Loidl, 2011, Eur. Phys. J. B **79**, 289.

Tu, J. J., J. Li, W. Liu, A. Punnoose, Y. Gong, Y. H. Ren, L. J. Li, G. H. Cao, Z. A. Xu, and C. C. Homes, 2010, Phys. Rev. B **82**, 174509.

Turner, A. M., F. Wang, and A. Vishwanath, 2009, Phys. Rev. B **80**, 224504.

Uhoya, W., G. Tsoi, Y. K. Vohra, M. A. McGuire, A. S. Sefat, B. C. Sales, D. Mandrus, and S. T. Weir, 2010, J. Phys. Condens. Matter **22**, 292202.

Urbano, R. R., E. L. Green, W. G. Moulton, A. P. Reyes, P. L. Kuhns, E. M. Bittar, C. Adriano, T. M. Garitezi, L. Bufai, and P. G. Pagliuso, 2010, Phys. Rev. Lett. **105**, 107001.

van der Beek, C. J., *et al.*, 2010, Phys. Rev. B **81**, 174517.

van Heumen, E., *et al.*, 2011, Phys. Rev. Lett. **106**, 027002.

Vavilov, M. G., A. V. Chubukov, and A. B. Vorontsov, 2011, Phys. Rev. B **84**, 140502.

Viennois, R., E. Giannini, D. van der Marel, and R. Cerny, 2010, J. Solid State Chem. **183**, 769.

Villars, P., and L. D. Calvert, 1985, *Pearson's Handbook of Crystallographic Data for Intermetallic Phases* (American Society for Metals, Metals Park, Ohio).

Volovik, G. E., 1993, JETP Lett. **58**, 469.

von Löhneysen, H., A. Rosch, M. Vojta, and P. Wölfle, 2007, Rev. Mod. Phys. **79**, 1015.

Vorontsov, A. B., M. G. Vavilov, and A. V. Chubukov, 2009, Phys. Rev. B **79**, 140507(R).

Vorontsov, A. B., M. G. Vavilov, and A. V. Chubukov, 2010, Phys. Rev. B **81**, 174538.

Vorontsov, A. B., and I. Vekhter, 2006, Phys. Rev. Lett. **96**, 237001.

Vorontsov, A. B., and I. Vekhter, 2010, Phys. Rev. Lett. **105**, 187004.

Wadati, H., I. Elfimov, and G. A. Sawatzky, 2010, Phys. Rev. Lett. **105**, 157004.

Wakimoto, S., *et al.*, 2010, J. Phys. Soc. Jpn. **79**, 074715.

Wang, C., *et al.*, 2008, Europhys. Lett. **83**, 67006.

Wang, D. M., J. B. He, T.-L. Xia, and G. F. Chen, 2011, Phys. Rev. B **83**, 132502.

Wang, F., F. Yang, M. Gao, Z.-Y. Lu, T. Xiang, and D.-H. Lee, 2011, Europhys. Lett. **93**, 57003.

Wang, F., H. Zhai, Y. Ran, A. Vishwanath, and D.-H. Lee, 2009, Phys. Rev. Lett. **102**, 047005.

Wang, K., H. Lei, and C. Petrovic, 2011a, Phys. Rev. B **83**, 174503.

Wang, K., H. Lei, and C. Petrovic, 2011b, Phys. Rev. B **84**, 054526.

Wang, L., Y. Qi, D. Wang, X. Zhang, Z. Gao, Z. Zhang, Y. Ma, S. Awaji, G. Nishijima, and K. Watanabe, 2010, Physica C (Amsterdam) **470**, 183.

Wang, M., H. Luo, M. Wang, S. Chi, J. A. Rodriguez-Rivera, D. Singh, S. Chang, J. W. Lynn, and P. Dai, 2011, Phys. Rev. B **83**, 094516.

Wang, M., *et al.*, 2010, Phys. Rev. B **81**, 174524.

Wang, M. J., J. Y. Luo, T. W. Huang, H. H. Chang, T. K. Chen, F. C. Hsu, C. T. Wu, P. M. Wu, A. M. Chang, and M. K. Wu, 2009, Phys. Rev. Lett. **103**, 117002.

Wang, X. C., Q. Q. Liu, Y. X. Lv, W. B. Gao, L. X. Yang, R. C. Yu, F. Y. Li, and C. Q. Jin, 2008, Solid State Commun. **148**, 538.

Wang, X. F., T. Wu, G. Wu, H. Chen, Y. L. Xie, J. J. Ying, Y. J. Yan, R. H. Liu, and X. H. Chen, 2009a, Phys. Rev. Lett. **102**, 117005.

Wang, X. F., T. Wu, G. Wu, R. H. Liu, H. Chen, Y. L. Xie, and X. H. Chen, 2009b, New J. Phys. **11**, 045003.

Wang, X.-P., T. Qian, P. Richard, P. Zhang, J. Dong, H.-D. Wang, C.-H. Dong, M.-H. Fang, and H. Ding, 2011, Europhys. Lett. **93**, 57001.

Wang, Y., F. Bouquet, I. Sheikin, P. Toulemonde, B. Revaz, M. Eisterer, H. W. Weber, J. Hinderer, and A. Junod, 2003, J. Phys. Condens. Matter **15**, 883.

Wang, Y., J. S. Kim, G. R. Stewart, P. J. Hirschfeld, S. Graser, S. Kasahara, T. Terashima, Y. Matsuda, T. Shibauchi, and I. Vekhter, 2011, Phys. Rev. B **84**, 184524.

Wang, Y., B. Revaz, A. Erb, and A. Junod, 2001, Phys. Rev. B **63**, 094508.

Wang, Y. L., L. Shan, P. Cheng, C. Ren, and H.-H. Wen, 2009, Supercond. Sci. Technol. **22**, 015018.

Wang, Z., Y. J. Song, H. L. Shi, Z. W. Wang, Z. Chen, H. F. Tian, G. F. Chen, J. G. Guo, H. X. Yang, and J. Q. Li, 2011, Phys. Rev. B **83**, 140505.

Wei, F., F. Chen, K. Sasmal, B. Lv, Z. J. Tang, Y. Y. Xue, A. M. Guloy, and C. W. Chu, 2010, Phys. Rev. B **81**, 134527.

Welp, U., R. Xie, A. E. Koshelev, W. K. Kwok, H. Q. Luo, Z. S. Wang, G. Mu, and H. H. Wen, 2009, Phys. Rev. B **79**, 094505.

Wen, H.-H., G. Mu, L. Fang, H. Yang, and X. Zhu, 2008, Europhys. Lett. **82**, 17009.

Wen, H.-H., G. Mu, H.-Q. Luo, H. Yang, L. Shan, C. Ren, P. Cheng, J. Yan, and L. Fang, 2009, Phys. Rev. Lett. **103**, 067002.

Wen, J., G. Xu, G. Gu, J. M. Tranquada, and R. J. Birgeneau, 2011, Rep. Prog. Phys. **74**, 124503.

Wen, J., G. Xu, Z. Xu, Z. W. Lin, Q. Li, Y. Chen, S. Chi, G. Gu, and J. M. Tranquada, 2010, Phys. Rev. B **81**, 100513(R).

Werthamer, N. R., E. Helfand, and P. C. Hohenberg, 1966, Phys. Rev. **147**, 295.

Westrum, E. F., C. Chou, and F. Gronvold, 1959, J. Chem. Phys. **30**, 761.

Williams, A. J., T. M. Mcqueen, and R. J. Cava, 2009, Solid State Commun. **149**, 1507.

Wilson, S. D., Z. Yamani, C. R. Rotundu, B. Freelon, E. Bourret-Courchesne, and R. J. Birgeneau, 2009, Phys. Rev. B **79**, 184519.

Won, H., and K. Maki, 1994, Phys. Rev. B **49**, 1397.

Wu, D., N. Barisic, M. Dressel, G. H. Cao, Z-A. Xu, E. Schachinger, and J. P. Carbotte, 2010, Phys. Rev. B **82**, 144519.

Wu, D., *et al.*, 2009, Phys. Rev. B **79**, 155103.

Wu, G., H Chen, T. Wu, Y. L. Xie, Y. J. Yan, R. H. Liu, X. F. Wang, J. J. Ying, and X. H. Chen, 2008a, J. Phys. Condens. Matter **20**, 422201.

Wu, G., H. Chen, Y. L. Xie, Y. J. Yan, T. Wu, R. H. Liu, X. F. Wang, D. F. Fang, J. J. Ying, and X. H. Chen, 2008b, Phys. Rev. B **78**, 092503.

Wu, G., *et al.*, 2009, J. Phys. Condens. Matter **21**, 142203.

Wu, M. K., J. R. Ashburn, C. J. Torng, P. H. Hor, R. L. Meng, L. Gao, Z. J. Huang, Y. Q. Wang, and C. W. Chu, 1987, Phys. Rev. Lett. **58**, 908.

Xia, T.-L., J. B. He, D. M. Wang, and G. F. Chen, 2010, arXiv:1001.3311.

Xia, Y., D. Qian, L. Wray, D. Hsieh, G. F. Chen, J. L. Luo, N. L. Wang, and M. Z. Hasan, 2009, Phys. Rev. Lett. **103**, 037002.

Xiao, Y. Y. Su, R. Mittal, T. Chatterji, T. Hansen, C. M. N. Kumar, S. Matsuishi, H. Hosono, and Th. Brueckel, 2009a, Phys. Rev. B **79**, 060504(R).

Xiao, Y., *et al.*, 2009b, Phys. Rev. B **80**, 174424.

Xiao, Y., *et al.*, 2010, Phys. Rev. B **81**, 094523.

Yamamoto, A., J. Jiang, F. Kametani, A. Polyanskii, E. Hellstrom, D. Larbalestier, A. Martinelli, A. Palenzona, M. Tropeano, and M. Putti, 2011, Supercond. Sci. Technol. **24**, 045010.

Yamamoto, A., *et al.*, 2009, Appl. Phys. Lett. **94**, 062511.

Yamashita, M., N. Nakata, Y. Senshu, S. Tonegawa, K. Ikada, K. Hashimoto, H. Sugawara, T. Shibauchi, and Y. Matsuda, 2009, Phys. Rev. B **80**, 220509(R).

Yamashita, M., *et al.*, 2011, Phys. Rev. B **84**, 060507(R).

Yamazaki, T., N. Takeshita, R. Kobayashi, H. Fukazawa, Y. Kohori, K. Kihou, C.-H. Lee, H. Kito, A. Iyo, and H. Eisaki, 2010, Phys. Rev. B **81**, 224511.

Yan, J. Q., *et al.*, 2009, Appl. Phys. Lett. **95**, 222504.

Yan, X.-W., and Z.-Y. Lu, 2010, arXiv:1010.0342.

Yan, J.-Q., *et al.*, 2008, Phys. Rev. B **78**, 024516.

Yanagi, Y., Y. Yamakawa, and Y. Ono, 2010, Phys. Rev. B **81**, 054518.

Yang, J., D. Hüvonen, U. Nagel, T. Room, N. Ni, P. C. Canfield, S. L. Bud'ko, J. P. Carbotte, and T. Timusk, 2009, Phys. Rev. Lett. **102**, 187003.

Yang, W.-L., *et al.*, 2009, Phys. Rev. B **80**, 014508.

Yashima, M., H. Nishimura, H. Mukuda, Y. Kitaoka, K. Miyazawa, P. M. Shirage, K. Kiho, H. Kito, H. Eisaki, and A. Iyo, 2009, J. Phys. Soc. Jpn. **78**, 103702.

Yates, K. A., L. F. Cohen, Z.-A. Ren, J. Yang, W. Lu, X. L. Dong, and Z.-X. Zhao, 2008, Supercond. Sci. Technol. **21**, 092003.

Ye, F., S. Chi, Wei Bao, X. F. Wang, J. J. Ying, X. H. Chen, H. D. Wang, C. H. Dong, and M. Fang, 2011, Phys. Rev. Lett. **107**, 137003.

Yeh, K.-W., *et al.*, 2008, Europhys. Lett. **84**, 37002.

Yeh, K.-W., C. T. Ke, T. W. Huang, T. K. Chen, Y. L. Huang, P. M. Wu, and M. K. Wu, 2009, Cryst. Growth Des. **9**, 4847.

Yelland, E. A., S. J. C. Yates, O. Taylor, A. Griffiths, S. M. Hayden, and A. Carrington, 2005, Phys. Rev. B **72**, 184436.

Yi, M., *et al.*, 2009, Phys. Rev. B **80**, 174510.

Yi, M., *et al.*, 2011, Proc. Natl. Acad. Sci. U.S.A. **108**, 6878.

Yi, W., *et al.*, 2008, Europhys. Lett. **83**, 57002.

Yildirim, T., 2008, Phys. Rev. Lett. **101**, 057010.

Yin, Z. P., K. Haule, and G. Kotliar, 2011, arXiv:1104.3454.

Yoshida, T., *et al.*, 2010a, arXiv:1007.2698.

Yoshida, T., *et al.*, 2010b, arXiv:1008.2080.

Yu, W., A. A. Aczel, T. J. Williams, S. L. Bud'ko, N. Ni, P. C. Canfield, and G. M. Luke, 2009, Phys. Rev. B **79**, 020511(R).

Yuan, H. Q., J. Singleton, F. F. Balakirev, S. A. Baily, G. F. Chen, J. L. Luo, and N. L. Wang, 2009, Nature (London) **457**, 565.

Zaanen, J., 2009, Phys. Rev. B **80**, 212502.

Zabel, M., and K. J. Range, 1984, Rev. Chim. Miner. **21**, 139.

Zabolotnyy, V. B., *et al.*, 2009, Nature (London) **457**, 569.

Zavalij, P., *et al.*, 2011, Phys. Rev. B **83**, 132509.

Zeng, B., G. Mu, H. Q. Luo, T. Xiang, H. Yang, L. Shan, C. Ren, I. I. Mazin, P. C. Dai, and H.-H. Wen, 2010a, arXiv:1004.2236.

Zeng, B., G. Mu, H. Q. Luo, T. Xiang, H. Yang, L. Shan, C. Ren, I. I. Mazin, P. C. Dai, and H.-H. Wen, 2010b, Nature Commun. **1**, 112.

Zeng, B., Bing Shen, G. Chen, J. He, D. Wang, C. Li, and H.-H. Wen, 2011, Phys. Rev. B **83**, 144511.

Zhang, A. M., K. Liu, J. H. Xiao, J. B. He, D. M. Wang, G. F. Chen, B. Normand, and Q. M. Zhang, 2011a, arXiv:1101.2168.

Zhang, A. M., K. Liu, J. H. Xiao, J. B. He, D. M. Wang, G. F. Chen, B. Normand, and Q. M. Zhang, 2011b, arXiv:1105.1198.

Zhang, G. M., Y. H. Su, Z. Y. Lu, Z. Y. Weng, D. H. Lee, and T. Xiang, 2009, Europhys. Lett. **86**, 37006.

Zhang, L., and D. J. Singh, 2009, Phys. Rev. B **79**, 094528.

Zhang, S. J., *et al.*, 2009a, Europhys. Lett. **88**, 47008.

Zhang, S. J., *et al.*, 2009b, Phys. Rev. B **80**, 014506.

Zhang, X., Y. S. Oh, Y. Liu, L. Yan, K. H. Kim, R. L. Greene, and I. Takeuchi, 2009, Phys. Rev. Lett. **102**, 147002.

Zhang, Y., *et al.*, 2009, Phys. Rev. Lett. **102**, 127003.

Zhao, J., D. T. Adroja, D.-X. Yao, R. Bewley, S. Li, X. F. Wang, G. Wu, X. H. Chen, J. Hu, and P. Dai, 2009, Nature Phys. **5**, 555.

Zhao, J., W. Ratcliff II, J. W. Lynn, G. F. Chen, J. L. Luo, N. L. Wang, J. Hu, and P. Dai, 2008a, Phys. Rev. B **78**, 140504(R).

Zhao, J., L.-P. Regnault, C. Zhang, M. Wang, Z. Li, F. Zhou, Z. Zhao, C. Fang, J. Hu, and P. Dai, 2010, Phys. Rev. B **81**, 180505(R).

Zhao, J., *et al.*, 2008b, Nature Mater. **7**, 953.

Zhao, J., *et al.*, 2008c, Phys. Rev. B **78**, 132504.

Zhao, J., *et al.*, 2008d, Phys. Rev. Lett. **101**, 167203.

Zhao, K., Q. Q. Liu, X. C. Wang, Z. Deng, Y. X. Lv, J. L. Zhu, F. Y. Li, and C. Q. Jin, 2010, J. Phys. Condens. Matter **22**, 222203.

Zhao, L., *et al.*, 2011, Phys. Rev. B **83**, 140508(R).

Zhigadlo, N. D., S. Katrych, Z. Bukowski, S. Weyeneth, R. Puzniak, and J. Karpinski, 2008, J. Phys. Condens. Matter **20**, 342202.

Zhou, B., *et al.*, 2010, Phys. Rev. B **81**, 155124.

Zhou, T., X. Chen, J. Guo, G. Wang, X. Lai, S. Wang, S. Jin, and K. Zhu, 2011, arXiv:1102.3506.

Zhu, X., F. Han, P. Cheng, G. Mu, B. Shen, L. Fang, and H.-H. Wen, 2009a, Europhys. Lett. **85**, 17011.

Zhu, X., F. Han, G. Mu, P. Cheng, B. Shen, B. Zeng, and H.-H. Wen, 2009b, Phys. Rev. B **79**, 220512(R).

Zhu, X., F. Han, G. Mu, P. Cheng, J. Tang, J. Ju, K. Tanigaki, and H.-H. Wen, 2010, Phys. Rev. B **81**, 104525.